METAL VAPOUR SYNTHESIS OF STABILIZED TRANSITION METAL NANOPARTICLES: CHARACTERIZATION, STUDIES ON FACTORS AFFECTING PARTICLE SIZE AND CATALYTIC APPLICATIONS

PhD Thesis in Chemistry

Scuola Normale Superiore
2005-2007

Candidate

Dr Patrizio Raffa

Supervisor

Prof. Piero Salvadori

Referees

Prof. Wolfgang A. Herrmann
Prof. Ulrich Zenneck
Prof. Martin Bennett

to my mother, Renata, and my brother, Mauretto

to the memory of my father, Alfonso (17/01/1948 – 6/07/2001)

to all my friends

“Ho cercato me stesso. Non si cerca che questo”

Cesare Pavese

“Science cannot solve the ultimate mystery of nature. And that is because, in the last analysis, we ourselves are a part of the mystery that we are trying to solve”

Max Planck

“A good gulp of hot whiskey at bedtime - it's not very scientific, but it helps”

Alexander Fleming

This work was carried out at Scuola Normale Superiore of Pisa and at Department of Chemistry and Industrial Chemistry of University of Pisa, with the partial financial support of the european project FP6-STRP GSOMEN, which is acknowledged. HRTEM analysis were performed in collaboration with prof. Giammario Martra and Luca Bertinetti, at department of Chemistry of University of Torino, which are also acknowledged. I wish also to acknowledge prof. Gloria Uccello-Barretta, Federica Balzano and Samuele Nazzi for NMR and NMR-DOSY analysis, Elisabetta Pitzalis at CNR for A.A.S. analysis, Dr. Giovanni Vitulli and Dr. Claudio Evangelisti, which gave a great contribution to this work and carefully followed all my experiments. Finally, I would like to acknowledge all my other lab mates, in particular Dr. Francesco Mazzini, that contributed to make this last three years less hard, more funny and full of wisdom.

Abstract

This PhD thesis is focused on the synthesis, characterization and evaluation of catalytic activity of stabilized platinum and gold nanoparticles, generated by use of the metal vaporization technique. Metal vapour synthesis allows to obtain platinum and gold particles with diameters in the range of few nanometers. The introduction of suitable organic molecules at various stage of the synthesis has proven to be useful in order to control the final size of the produced particles. The metal nanoparticles obtained by this new approach are very stable and can be easily handled and characterized in solution. In particular, NMR based measurement of diffusion parameters has proven to be useful for the quick determination of particles size in solution. The choice of organic stabilizing ligand is crucial in determining both the particle size and the catalytic activity and selectivity of the system. Platinum particles characterized by small diameters and good catalytic performances are obtained using vinylsiloxanes and aromatic solvents while, in the synthesis of gold particles, branched thiols and alkylamines demonstrated to be a better choices over linear alkylthiols if catalytic activity is required. A new application of gold nanoparticles in catalytic silane alcoholysis reaction has also been discovered.

CONTENTS

GENERAL INTRODUCTION AND AIM OF THE WORK

"Le véritable voyage de découverte ne consiste pas à chercher de nouveaux paysages mais à avoir de nouveaux yeux."

Marcel Proust

"This paper will no doubt be found interesting by those who take an interest in it."

John Dalton

"The best way to have a good idea is to have a lot of ideas."

Linus Pauling

Words such as nanoscience, nanotechnology, nanoparticles, nanodevices and similar, are nowadays, in the 21st century, of rather common use in our society. The research in nanostructured materials involve all the scientific community, sharing knowledge between chemistry, physics, material science and biology. Nanoscience is now often considered as a new emerging science, with very promising and revolutionary technological applications in several fields[1] such as optics, electronics, computer science, catalysis, medicinal chemistry, genetic engineering and others and his interest is exponentially increasing in academic research as well as in technological development (Figure 1).

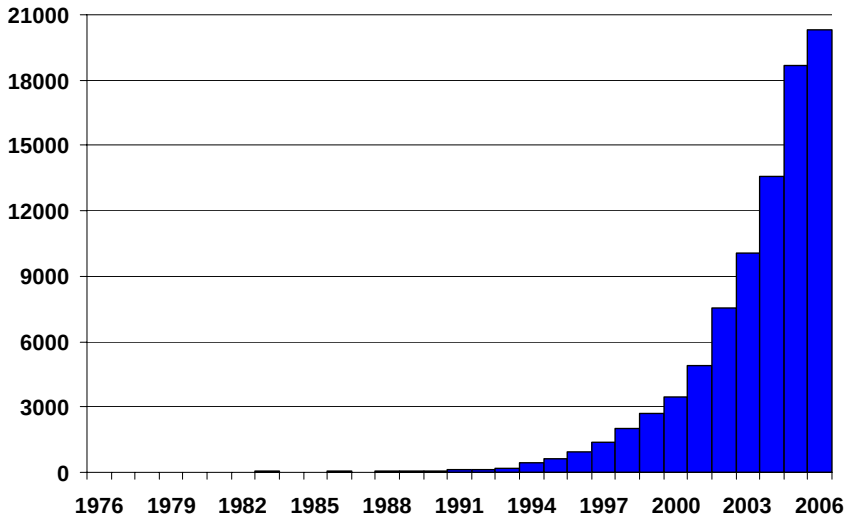

Figure 1. Histogram of scientific papers and patents containing the keyword "nanoparticles" published until 2006

The interest in nanoparticles arise from the unique properties that matter shows in the size range located between atoms and bulk material. In this nanoscale regime, neither quantum chemistry nor classical laws of physics hold (Figure 2)[1b]. In materials where strong chemical bonding is present, delocalization of valence electrons can be extensive, and the extent of delocalization can vary with the size of the system. This effect, coupled with structural changes with size variation, can lead to different chemical and physical properties, depending on size. Indeed, it has now been demonstrated that a host of properties depend on the size of such nanoparticles, including optical and magnetic properties, melting points, specific heats and surface reactivity. Furthermore, when such ultrafine particles are consolidated into macroscale solids, these bulk materials sometimes exhibit new properties (e.g., enhanced plasticity).

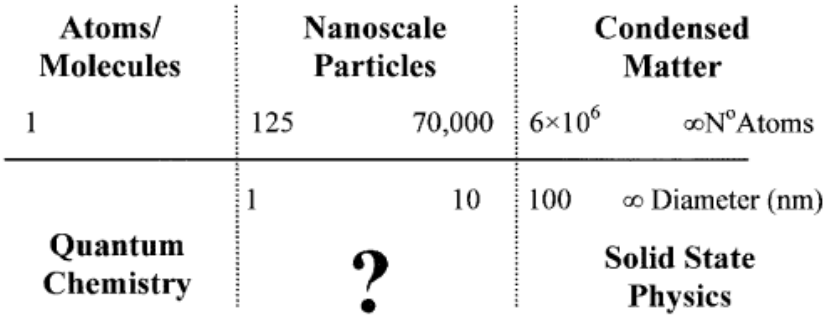

Figure 2 Size relationships of chemistry, nanoscience and condensed matter physics

Despite the lack of a their complete understanding, nanoparticles have a long history. It is not clear when humans first began to take advantage of nanosized materials. It is known that in the 4th century A.D. Roman glassmaker were fabricating glasses containing nanosized metals. An artefact from this period, the Lycurgus cup, is made from soda lime glass containing silver and gold nanoparticles and his colour change from green to deep red when a light source is placed inside it. The great varieties of beautiful colours of the windows of medieval cathedrals are due to the presence of metal nanoparticles in the glass.

The first scientific report on nanoparticles was presented in 1857, exactly 150 ago, by Michael Faraday, in a lecture to the Royal Society of London[2]. Faraday prepared his colloidal dispersions of gold by a two-phase preparation, reducing an aqueous solution of a gold salt, such as sodium tetrachloroaurate ($Na[AuCl_4]$), with a solution of phosphorus in carbon disulfide, since phosphorus as regarded as "a very favourable agent". The reduction proceeds rapidly at room temperature and the bright yellow colour of the $Na[AuCl_4]$ solution is replaced within minutes of mixing by the deep ruby coloration characteristic of colloidal gold. Faraday concluded that the gold was dispersed in the liquid in a very finely divided form, the presence of which could be detected by the reddish opalescence when a narrow intense beam of light is passed through the liquid (an anticipation of the Tyndall effect). Of course, he had no means of determining the size of the particles that he produced. The term "colloid" to describe stable dispersion of finely divided particles was introduced some year later, in 1861, by Graham[3]. During the 20th Century, substantial progress

has been obtained in colloids chemistry and physics. The purple-red colour of gold colloids stimulate Mie to formulate his classical theory of scattering[4]; Ostwald, La Mer and Turkevich works[5] have allowed understanding better the nucleation processes, growing and agglomeration linked up to the preparation of nanoparticles. In more recent times, a great acceleration in nanoscience research is surely due to the development of several characterization techniques which allows to investigate matter in the nanoscale region: high resolution transmission electron microscopy (HRTEM); scanning tunnelling microscopy (STM) and related atomic force microscopy (AFM); X-ray based methods (XRD, XPS, EXAFS, XANES) and mass spectroscopy (MALDI-TOF) are relevant examples.

This PhD Thesis is focused on transition metal nanoparticles (TMNPs). The main field of interest of such particles is catalysis, but they find use in several of the above mentioned applications.[1] Metal colloids are very efficient catalysts because of a great ratio of atoms remaining at the surface, and so available to chemical transformation of substrates (Figure 3).

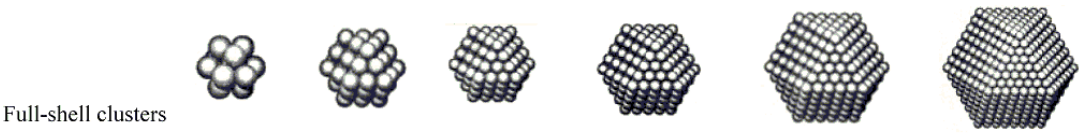

Full-shell clusters	1 shell	2 shells	3 shells	4 shells	5 shells	7 shells
Total number of atoms	13	55	147	309	561	1415
surface atoms (%)	92	76	63	52	45	35

Figure 3. Relation between number of shells and surface atoms of full-shell metal clusters

Reproducible synthesis of TMNPs is a not so simple task, because the bulk metal is thermodynamically more stable than small aggregates and a careful kinetic control during preparation is required. However, nanoparticles of all transition metal present in the periodic table of elements has been prepared and deeply investigated from different point of view by a large number of research groups. The idea of the present work follows the outlines of the european project GSOMEN (*Growth and Supra-Organization of noble and transition MEtal Nanoparticles*), in which our research group is involved since its beginning in 2005, and intend to investigate the factors which influence particles nucleation and growth, starting from single atoms in the vapour phase to the formation of kinetically stable nanoclusters in solution. This PhD work was conceived with a double aim: (i) an improvement in the understanding of the nucleation and growth processes of TMNPs, also with some theoretical support from partners of the GSOMEN project, and a technological advancement in the preparation of systems with tailored dimensions; (ii) a preliminary investigation of catalytic activity of the prepared systems in some useful reactions.

Since clustering process in MVS of TMNPs shows to happens gradually, it seemed to us possible to quench the particles growth during the various stages, by adding a

strong stabilizing ligand at the appropriate time, in order obtain DLVO stabilized systems (see Chapter 1) characterized by different particle size (Scheme 1). This could represent a new way to achieve a size-selective synthesis of TMNPs, giving at the same time information about the growth processes during MVS which are, at present, scarcely investigated.

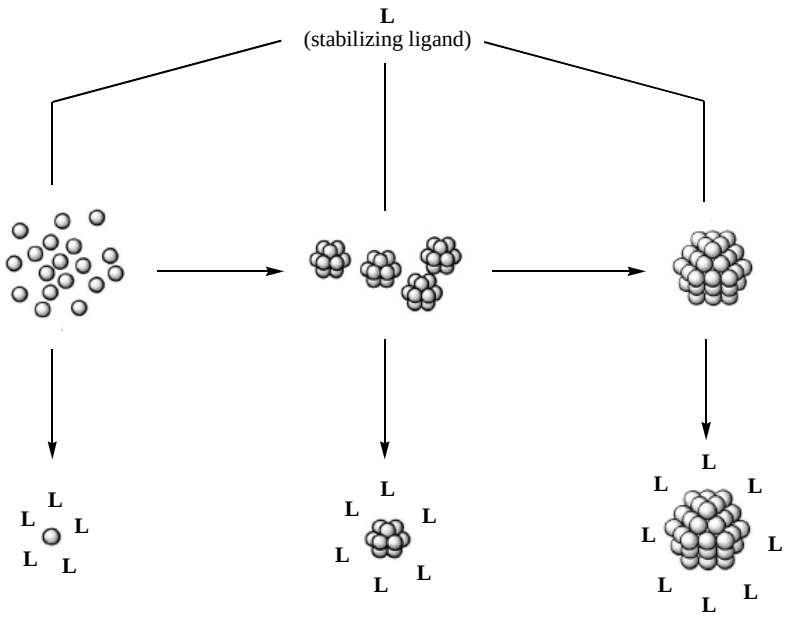

Scheme 1

We focused our attention in preparation of solvated metal atoms dispersion (SMAD) by means of metal vapour synthesis (MVS) route, choosing two different metals of interest: platinum and gold. As we will show, the choice of the additional stabilizing ligand is a crucial point in order to achieve both control over particles size and good catalytic performance of the obtained particles. The use of strong stabilizing agent in synthesis of TMNPs, is often required to achieve good control over particles size and narrow size-distribution (see Chapter 1), but this often leads to a loss of catalytic activity because of the poisoning effect of the ligand itself. This problem has sometimes been resolved for particular cases by deposition of the obtained particles on an inert support, followed by calcination in air at high temperature, in order to decompose the ligand,[6] but still remains an important challenge for the study of size-dependent activities and selectivities of transition metal heterogeneous catalysts.

The utilization of MVS in metal colloids preparation was firstly developed in 70s principally by Klabunde[7] and their applications in catalysis were extensively studied also in our labs until recent times.[8] Among the various methods generally employed for synthesis of TMNPs, that will be reviewed in Chapter 1, MVS seems to be feasible for the study of particles growth, because the so obtained product (called SMAD) can be considered as solution or suspension of weekly stabilized (or "naked") clusters, in which agglomeration phenomena can be eventually observed during time. Additionally, in MVS procedure the presence of pollutants (halides, reductants) can be minimized, because only bulk metal, solvent and, in some case, stabilizing organic ligands, are used as starting materials.

A survey of characterization method will be also given in Chapter 1, with particular attention to the emerging utilization of NMR-based techniques, namely DOSY (*Diffusion Ordered SpectroscopY*), that in those cases in which is feasible, provide a fast and cheap method of characterization of nanoparticles directly in solution, whereas other methods can be useful very often only in the solid state. Chapter 1 ends with a brief survey of the main application of TMNPs in catalysis, both as dissolved stabilized particles and as heterogeneous supported systems.

Subsequently, in Chapter 2, attention will be focused on the central task of nucleation and growth of TMNPs. The already mentioned importance of particle size in determining the properties of materials is object of several studies, which are reviewed in this Chapter. In order to achieve a size-selective, reproducible synthesis of monodisperse systems, a general mechanism of agglomeration processes of metal atoms to stable nanoparticles has to be elucidated and this is currently a very difficult and exciting challenge.[9]
In chemistry applications, the most important field in which control over particle size is a crucial task, is catalysis. As already mentioned, the most important TMNPs catalyzed organic reaction are summarized on the last part of Chapter 1 but several examples of the great influence that particles size distribution can have in activity and selectivity of various transition metal catalyzed reaction will be described in last section of Chapter 2.

Chapters 3 and 4 will describe the original works made in this PhD Thesis in synthesis, characterization and study in factors affecting nucleation and growth of stabilized Pt and Au nanoparticles obtained by metal vaporization, with some preliminary observation in size-dependent catalytic activity. Platinum metal is a really important catalyst in lab scale preparations as well as in fine chemistry both in homogeneous and in heterogeneous phase. Several platinum catalyst of general use are nanostructured and the importance of particle size and distribution in activity and selectivity is widely studied. For this reason the understanding of growth processes of Pt clusters for the preparation of size-controlled particles is a very active and important task. Control over Pt particle size can generally be achieved in several ways. In chapter 3 we illustrate synthesis and growth study of mesitylene solvated Platinum nanoparticles stabilized in solution with an appropriate ligand, namely 1,3-divinyl-1,1,3,3-tetramethyldisiloxane (DVTMDS) and their employ in selective hydrogenation and hydrosilylation reactions.
Chapter 4 is focused in gold nanoparticles preparation and study. Gold nanoparticles was the first investigated and probably the more studied nanoparticles. This metal shows very marked size-dependent properties, starting from surface plasmon resonance, where intensity and frequency of maximum absorption change considerably with size, to catalytic activity, which is present only if the gold has nanometric size, while bulk gold is completely inactive as catalyst.
In the case of gold we used several solvents and ligand in order to find the appropriate conditions to follow growth of metallic clusters, with some interesting results. The appropriate choice of ligand and preparation conditions, allow to obtain catalitically active systems for reactions of hydrosilanes with various substrate, even if in these cases the catalyst has to be deposited on inert support before it can successfully be used.

REFERENCES OF GENERAL INTRODUCTION

[1] (a) *Introduction to Nanotechnology*: Edited by Poole, C.P., Jr. and Owens, F.J., 2003, New York: Wiley-Interscience; (b) *Handbook of nanoscience, engineering and technology*, Edited by W. A. Goddard III, D. W. Brenner, S. E. Lyshevski, G. J. Iafrate, 2002, CRC Press,; (c) *Nanoscale Materials in Chemistry*. Edited by Kenneth J. Klabunde, 2001, John Wiley & Sons, Inc.; (d) Freund, H.-J. *Surf. Sci*. **2002**, *500*, 271–299

[2] Faraday, M. *Philos. Trans. R. Soc.* **1857**, *147*, 145; Edwards, Thomas, Angew. Chem. Int. Ed. 2007, 46, 5480 – 5486

[3] Graham, T. Philos. Trans. R. Soc. **1861**, 151, 183.

[4] Mie, G. *G. Ann. Phys.* **1908**, *25*, 377.

[5] Ostwald, W. *Colloid-Z.* **1907**, *1*, 291; LaMer, V. K.; Dinegar, R. H. *J. Am. Chem. Soc.* **1950**, *72*, 4847; Turkevich, J.; Stevenson, P. C.; Hillier, J. *Faraday Discuss.Chem. Soc.* **1951**, *11*, 55.

[6] Zeng, N.; Stuchy, G. D. *J. Am. Chem. Soc.* **2006**, *128*, 14278-14280.

[7] (a) S.-T. Lin, M. T. Franklin, K. J. Klabunde *Langmuir*, **1986**, *2*, 259-260; (b) Y.-X. Li, K. J. Klabunde, J. Catal. **1990**, *126*, 173-186; (c) B. J. Tan, P. M. A. Sherwood, K. J. Klabunde *Langmuir*, **1990**, *6*, 105-113 (d) B. J. Tan, K. J. Klabunde, P. M. A. Sherwood, *J. Am. Chem. Soc.* **1991**, *113*, 855-861; (e) S. I. Stoeva, B. L. V. Prasad, S. Uma, P. K. Stoimenov, V. Zaikovski, C. M. Sorensen, K. J. Klabunde, *J. Phys. Chem. B* **2003,** *107,* 7441-7448. (f) A. A. Ponce, K. J. Klabunde, J. Mol. Cat. A, **2005**, *225*, 1–6; (g) A. B. Smetana, K. J. Klabunde, C. M. Sorensen; Journal of Colloid and Interface Science, **2005**, *284*, 521–526

[8] (a) Vitulli, G.; Verrazzani, A.; Pitzalis, E.; Salvadori, P., Capannelli, G.; Martra, G., C*atal. Lett.* **1997**, *44*, 205-210; (b) Vitulli, G.; Evangelisti, C. Pertici, P.; Caporusso, A. M.; Panziera, N.; Salvadori, P.;Faga, M. G.; Manfredotti, C.; Martra, G.; Coluccia, S.; Balerna, A.;Colonna, S.; Mobilio S. J. Organomet. Chem. **2003,** *681* 37-50; (c) Evangelisti, C.; Vitulli, G.; Schiavi, E.; Vitulli, M.; Bertozzi, S.; Salvadori, P.; Bertinetti, L.; Martra, G. Catal. Lett. **2007**, *116*, 57-62; (d) Vitulli, G.; Evangelisti, C.; Ciardelli, F.; Salvadori, P.; Rocchi, F. European Patent Application, EP 1 797 949, (2007); (e) G. Vitulli, C. Evangelisti, A.M. Caporusso, P. Pertici, N. Panziera, S. Bertozzi, P. Salvadori, in *Metal nanoclusters in catalysis and materials science: the issue of size-control*, Edited by B. Corain, G. Schmid, N. Toshima, Elsevier, (2007), *in press.*

[9] Finney, E. E.; Finke, R. G. *J. Coll. Interf. Sci.* **2008**, *317*, 351-374.

CHAPTER 1

TRANSITION METAL NANOPARTICLES STABILIZED IN SOLUTION: A SURVEY ON SYNTHETIC METHODS, CHARACTERIZATION AND APPLICATION IN CATALYSIS

"One never notices what has been done; one can only see what remains to be done."

Marie Curie

1.1 INTRODUCTION

Before beginning a description of synthetic methods, we will briefly consider a general yet crucial aspect of colloid chemistry and that is the means by which the metal particles are stabilized in the dispersing medium, since small metal particles are unstable with respect to agglomeration to the bulk. The particles formation process then basically consists of a nucleation step followed by particle growth stages. Generally, there are three kinds of nucleation processes: homogeneous nucleation, heterogeneous nucleation, and secondary nucleation. Homogeneous nucleation occurs in the absence of a solid interface by combining solute molecules to produce nuclei. Homogeneous nucleation happens due to the driving force of the thermodynamics because the supersaturated solution is not stable in energy. The free energy of formation, ΔG_i, of a cluster from i monomers in the vapour phase is:

$$\Delta G_i = -i(\Delta\mu) + \sum_n \gamma_n A_n \qquad 1.1$$

Where A is the surface area and γ is the surface free energy per unit surface area. Two terms contribute to the free energy of the system with opposite sign: the aggregation is favoured by the formation of new bonds between atoms (negative term), but a work is required against the surface energy of the new forming phase (positive term). For spherical particles equation 1.1 becomes:

$$\Delta G_i = -\frac{4\pi r^3}{3v_c}(\Delta\mu) + 4\pi r^2\gamma \qquad 1.2$$

where r is the radius of cluster and v_c is the molecular (or atomic) volume of the cluster. A graph of ΔG_i verus r shows a maximum for a particular value of radius (Fig. 1.1), which can be obtained differentiating the free energy with respect to r in equation 1.2 and equating to 0:

$$r^* = \frac{2\gamma v_c}{\Delta\mu} \qquad 1.3$$

This is one of the forms of the Gibbs-Thomson equation and is generally valid in vapour phase as well as in solution.

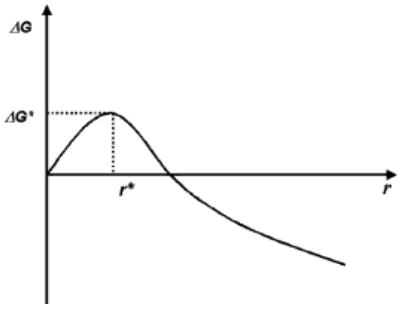

Figure 1.1. Illustration of the overall free energy ΔG as a function of the particle size r.

Figure 1 shows that particles with r > r* will grow indefinitely and particles with r < r* will dissolve. The value r* is the radius of a so-called critical nucleus and is a function of temperature, nature of solute, solvent and saturation ratio S. For particles precipitation from solutions, we have:

$$\Delta G = -\frac{4}{v_c}\pi r^3 k_B T \ln S + 4\pi r^2 \gamma \qquad 1.4$$

So, for this particular case, the critical radius r* become:

$$r^* = \frac{2 v_c \gamma}{3 k_B T \ln S} \qquad 1.5$$

At short interparticle distances, the Van Der Waals forces will attract two metallic particles to each other. These forces vary inversely as the sixth power of the distance between their surfaces. In the absence of repulsive forces opposed to the Van Der Waals forces, the colloidal metal particles will aggregate. Consequently, the use of a stabilizing agent able to induce a repulsive force opposed to the Van Der Waals forces is necessary to provide stable nanoparticles in solution. The general stabilization mechanisms of colloidal materials have been described in Derjaguin-Landau-Verwey-Overbeek (DLVO) theory. The two basic modes of stabilization which have been distinguished are electrostatic and steric (Fig. 1.2). Electrostatic stabilization (see Fig. 1.2a) involves the coulombic repulsion between the particles caused by the electrical double layer formed by ions adsorbed at the particle surface and the corresponding counterions. By coordinating sterically demanding organic molecules that act as protective shields on the metallic surface, steric stabilization (Fig. 1.2b) is achieved. A combination of the two effect, a so-called electrosteric stabilization, is often proposed.

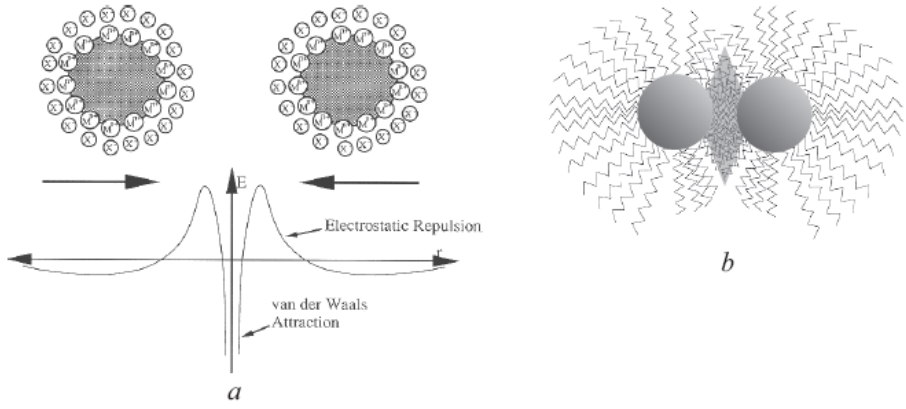

Figure 1.2. Schematic representation of electrostatic (a) and steric (b) stabilization of metal nanoparticles

It has occasionally been reported that nanoparticles can be stabilized only by solvent molecules.[1,2] However, proof of the absence of stabilizing agents such as anions or cations is lacking. Sometimes, elemental analysis shows that potentially coordinating bromide or chloride anions still remain.
In metal vapour synthesis (MVS) technique (see below) the TMNPs are prepared starting only from bulk metal and organic solvent, so in this case stabilization by weakly coordinated molecules of the solvent is claimed.[3] However, solvent-only stabilization is still object of scientific debate.[4]

1.2 SYNTHESIS OF TRANSITION METAL NANOPARTICLES STABILIZED IN SOLUTION

Dispersions of metallic nanoparticles can be obtained by two main strategies (Figure 1.3): mechanic subdivision of metallic aggregates (top-down, or physical methods) or nucleation and growth of metallic atoms (bottom-up, or chemical methods). Top-down methods reduce macroscopic particles to the nano size scale. This route is usually not very well suited to preparing uniformally shaped particles; very small sizes are especially difficult to realize. Advanced examples of top-down methods are nanolithography[5] and laser ablation.[6]
Bottom-up methods start with atoms that aggregate in solution or even in the gas phase to form particles of definite size, if appropriate experimental conditions are applied. Bottom-up procedures are much better suited to generating uniform particles, often of distinct size, shape and structure and will be discussed in more detail. A general approach to the synthesis of supported TMNPs catalysts involve the direct interaction between forming nanoparticles and the support[7] (metal oxide, activated carbon or insoluble polymer), without using further stabilizing agents. We will focus only in preparation of TMNPs stabilized in solution by means of suitable ligands.

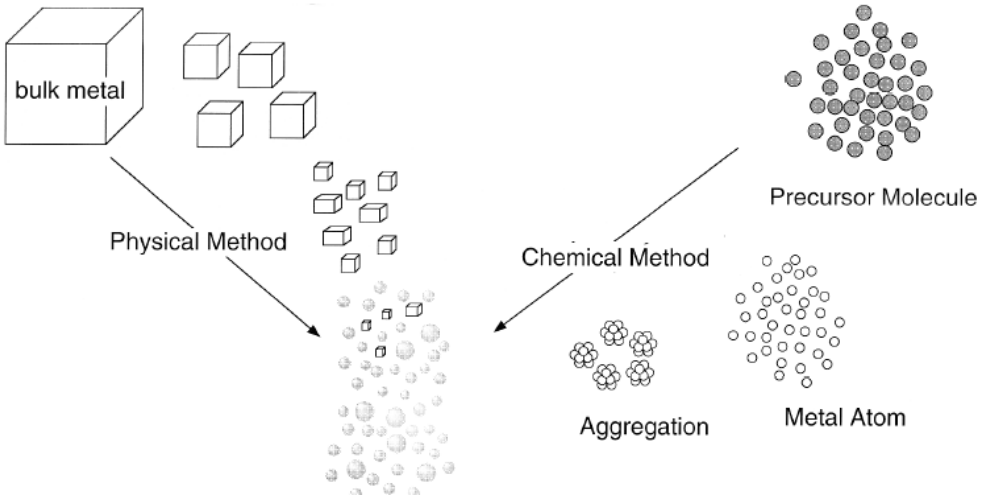

Figure 1.3. Schematic representation of preparative methods of metal nanoparticles

1.2.1 CHEMICAL REDUCTION OF SALTS

The reduction of transition metal salts in solution is the most widely used method to generate colloidal suspensions of metals. In fact, this method is generally very simple to implement. This synthetic route start with the reduction of positively charged metal ions, either as simple cations or as centers of complexes in solution. As already mentioned, in any case it is essential to generate the particles in the presence of suitable molecules that will cover the surface. This is an essential, but also the most serious and complicated step in cluster formation: if the ligand molecules are already present when reduction starts, formation of larger particles can be prevented by blocking of growth. If the ligands are added subsequently, it is difficult to determine the right moment for stopping cluster growth; in practice it involves the interplay between the generation of metallic precipitates or mirrors in the one hand and the formation of mono- or oligonuclear complexes on the other hand.[8] Figure 1.4 shows a highly simplified scheme of the principal steps of nanosized particle formation in solution.

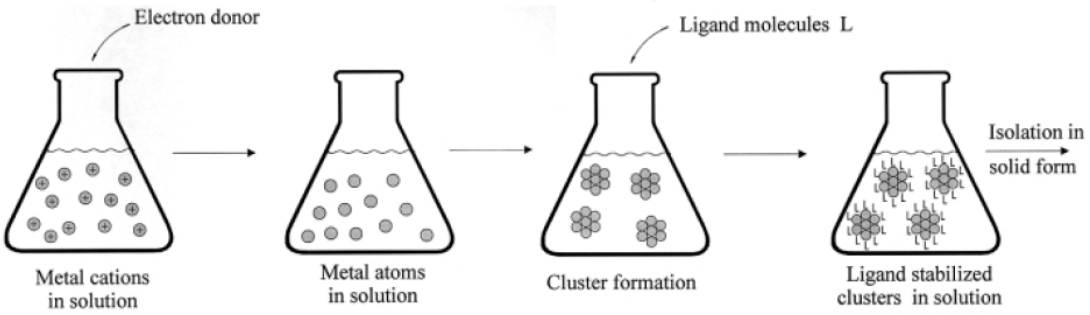

Figure 1.4. Schematic procedure of cluster synthesis

A large variety of combination of solvents, stabilizing ligand and reducing agents has been successfully employed. The main classes of protective groups selected from the literature are[9,10]: polymers and block copolymers; P, N, S, C, O donors (e.g.,

phosphines, amines, thiols, carbon monoxide, long chain alcohols); tetraalkylammonium salts and other surfactants and also dendrimers and cyclodextrins. In general, lipophilic protective agents give metal colloids that are soluble in organic media ("organosols") while hydrophilic agents yield water-soluble colloids ("hydrosols"). Silanes have also found use in colloid preparation. An interesting example for the use of organosilanes in the formation of organosols of transition metals is the reduction of platinum (II) complexes, especially cyclooctadieneplatinum dichloride, to colloidal platinum by trialkoxysilanes and trialkylsilanes. This was reported by Lewis and co-workers[11] who demonstrate that the presumably homogeneous hydrosilylation catalysts formed from platinum compound in the presence of silanes were in fact colloidal in nature, and raised the prospect for colloid activity in many homogeneous catalyst system. The same reduction method with organosilanes has been used for the preparation of colloids of rhodium and palladium.[12]
Composition, size and morphology of the final product are strictly dependent on the nature of the precursors. Water soluble sodium salts of phosphines, such as sulfonated triphenylphosphine, are examples of surfactants which function as stabilizers for hydrosols of colloidal rhodium prepared by hydrogen reduction of aqueous $RhCl_3 \cdot 3H_2O$ in the presence of the surfactant.[13] The description of the colloidal material as a polyhydroxylated rhodium particles implies considerable oxidation of the rhodium surface to Rh(I), and stabilization occurs through the interaction of the anionic heads of the surfactant with the Rh(I) sites at the colloidal surface. Conversely, if the rhodium sol is prepared by aqueous borohydride reduction of $RhCl_3 \cdot 3H_2O$, the colloidal particles are thought to contain only zerovalent rhodium metal and the stabilization occurs through the interaction with the hydrophobic alkyl groups on the surfactant.[14]

1.2.1.1 Nanoparticles synthesis by reduction in water

The salt reduction method has the main advantage that in the liquid phase it is reproducible and it allows colloidal nanoparticles with a narrow size distribution to be prepared on the multigram scale. The classical Faraday route via the reduction of $[AuCl_4]^-$ with sodium citrate for example, extensively investigated by Turkevich, is still used to prepare standard 20-nm gold sols for histological staining applications.[9]
Wet chemical reduction procedures have been applied in the last 20 years or so to combine practically all transition metals with different types of stabilizers, and the whole range of chemical reducing agents has successfully been applied. In 1981, Schmid et al. established the "diborane-as-reductant route" for the synthesis of $Au_{55}(PPh_3)_{12}Cl_6$ (1.4 nm, Figure 1.5a), a full shell ("magic number") nanocluster stabilized by phosphine ligands.[15] Clusters of Au_{55} were uniformly formed when a stream of B_2H_6 was carefully introduced into a Au(III) ion solution. The "diborane route" for $M_{55}L_{12}Cl_n$ nanoclusters was recently reviewed by Finke et al.[16]
Hydrogen has been used as an efficient reducing agent for the preparation of electrostatically stabilized metal sols and of polymer-stabilized hydrosols of Pd, Pt, Rh, and Ir.[10] Moiseev's giant Pd cluster (Fig. 1.5b), Finke's polyoxoanion $P_2W_{15}Nb_3O_{62}^{9-}$ (Fig. 1.5c), and tetrabutylammonium stabilized transition metal nanoclusters were also prepared by the hydrogen reduction pathway.[10,16]

Using CO, formic acid or sodium formate, formaldehyde, and benzaldehyde as reductants, colloidal Pt in water was obtained.[10] Duff, Johnson, and Baiker et al. have successfully introduced tetrakis(hydroxymethyl)phosphoniumchloride (THPC) as a reducing agent, which allows the size- and morphologyselective synthesis of Ag, Cu, Pt, and Au nanoparticles from their corresponding metal salts[17]. Further, hydrazine,[18] hydroxylamine,[19] and electrons trapped in, for example, $K^+[(crown)_2K]^-$,[20] have also been successfully applied as reductants.

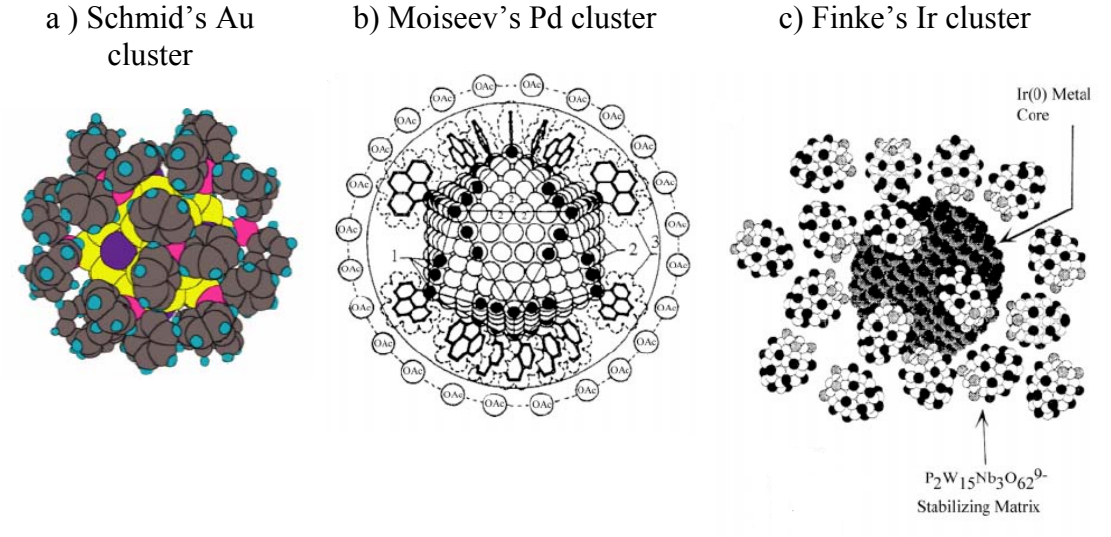

Figure 1.5. Idealized representations of a) Schmid's, b) Moiseev's, c) Finke's metallic clusters

The borohydrides ($NaBH_4$ or KBH_4) reduction of transition metal salts is the most widely used hydride reduction method of generating aqueous suspensions of metals.[21] The stabilizing agents used in these cases are generally surfactants or water-soluble polymers. With this method Cu nanoparticles were generated by Hirai in the presence of PVP, PVE, PVA, or various polysaccharides.[22] Pt colloids were also stabilized by PVP with this method. Mayer and co-workers have studied extensively the stabilizing polymer on the reduction of aqueous suspension of Ag, Au, Pt, or Pd by KBH_4.[23] They investigated cationic polyelectrolytes, polyacides, nonionic polymers, and block copolymers. Recently, $NaBH_4$ reduction was used to obtain Au, Ag, Pt, Pd, or Cu nanoparticles stabilized by dendrimers (polyamidoamine or PAMAM).[24] These macromolecules allow one to obtain nearly monodispersed particles. Dimethylamineborane has been also used to prepare gold nanoparticles stabilized by hydrophobically modified PAMAM in toluene or chloroform. Surfactants are generally used as stabilizers of aqueous colloidal suspensions of transition metal reduced by $NaBH_4$ or KBH_4. They can be cationic, anionic, or nonionic. In fact, Nakao and co-workers described the preparation of Ru, Rh, Pd, Pt, Ag, or Au nanoparticles stabilized by quaternary ammonium, sulfates, or poly(ethylene glycol).[25] A disadvantage, however, in the use of borohydrides as reductant, is that transition metal borides are often found along with the nanometallic particles.[10,21]

1.2.1.2 Nanoparticles synthesis by reduction in organic media

Several authors applied the reduction of transition metal salts to the preparation of colloidal suspensions of transition metal in organic media. The first approach consists of reducing a metallic salt in aqueous phase by $NaBH_4$. The water is then evaporated and the solid obtained is redispersed in an organic solvent. The classical approach consists of reducing transition metal salts in an organic phase.[10,21]
Some recent reports in which trialkylborohydrides were used are of particular interest. Bonnemann and co-workers have used tetraalkylammonium hydrotriorganoborates[26] in THF solution to reduce a wide range of group 6-11 metal halide salts (Scheme 1.1). The reductant [BEt_3H^-] is combined with the stabilizing agent (e.g. NR_4^+) in this case. The surface-active NR_4^+ salts are formed immediately at the reduction center at high local concentration and prevent particle aggregation. The advantages of this system include the large-scale preparation and the wide range of metal nanoclusters available, but the main disadvantage is a lack of exact compositional characterization of the resultant colloid materials. Indeed, boron from the initial BEt_3H^- reductant is found as a 1-2% impurity in the resultant colloids.[21] Most recently it has been demonstrated that the chain length of the alkyl group in the tetraalkylammonium plays a critical role in the stabilization of various metal colloids.[27]

$$MX_\nu + NR_4(BEt_3H) \longrightarrow M_{colloid} + \nu\, NR_4X + \nu\, BEt_3 + \nu/2\, H_2 \uparrow$$

Scheme 1.1. Bonnemann's route to TMNPs

The reported particle sizes are generally between 1 and 5 nm, and by using appropriately substituted (R = $C_{4\text{-}20}$) tetralkylammonium salts, the colloidal metal particles can be stabilized in the organic solvent. Organic solutions with metal concentration of up to 1 M can be obtained by these reactions. The remarkable solubility of these materials is undoubtedly due to the absorption of the tetralkylammonium cations at adsorbed anion sites on the colloidal metal surface, implying the presence of an oxidized layer of metal cations at the surface.
In a refinement of the Bonnemann method[9] a long chain tetralkylammonium cation is added to a solution of the precursor transition metal salt with subsequent reduction by conventional means. An example of this is the treatment of $Pd(OAc)_2$ in THF with tetraoctylammonium bromide followed by reaction with hydrogen, trialkylborane, formic acid, or simply by thermolysis, which leads to stable organosols of palladium with a lower ratio of the long chain ammonium surfactant then was necessary for the original method.

In aqueous systems the reducing agent must be added or generated *in situ*, but in non-aqueous systems the solvent and the reducing agent can be one at the same. Easily oxidized solvents such as alcohols can thus function both as reducing agents and as the colloid diluent, and they have been used widely in colloid preparations. Generally, the alcohols, which are useful reducing agents, contain α-hydrogen. Thus, methanol, ethanol, or 2-propanol are good reducing agents, whereas *tert*-butyl alcohol is not effective. During the reduction, the alcohols are oxidized to the corresponding carbonyl compounds (Scheme 1.2). The formation of the organic

carbonyl compound was ascribed to the intermediacy of an oxonium complex, followed by deprotonation to an alkoxyde, and finally an hydride elimination to give the carbonyl compound with subsequent elimination of HX. The presence of a base (often water) with sufficient strength to deprotonate the oxonium intermediate is required, especially in the case of methanol. The use of additional base can be avoided by using metallic acetate as precursor, which act as base himself.

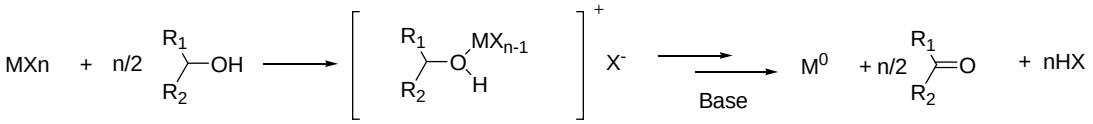

Scheme 1.2. Formation of metallic nanoparticles in alcoholic media

Hirai and more recently Delmas have extensively used aqueous alcohols as reducing agents in the synthesis of colloidal transition metals such as Rh, Pt, Pd, Os, or Ir.[10,21] All these colloidal suspensions were stabilized by organic polymers or oligomers such as polyvinylic alcohol (PVA), polyvinylpyrrolidinone (PVP), polyvinylic ether (PVE), or cyclodextrins. Other kinds of polymers were used for the stabilization of colloids formed during the metallic salt reduction. The use of various polyacides, polyelectrolytes, or block copolymers to stabilize Pd, Pt, and Au nanoparticles has been largely studied. In the same way, after reduction in aqueous alcohol Pt colloids were stabilized by poly(*N*-isopropylacrylamide) (PNIPAAm), poly(*N*-sulfonatopropyl-*p*-benzamide), or PVA/PVP copolymers.
Recently, it has been demonstrated that through the appropriate choice of reduction temperature and acetate ion concentration, ruthenium nanoparticles prepared by the reduction of $RuCl_3$ in a liquid polyol could be monodispersely prepared with sizes in the 1–6 nm range.[28]

1.2.1.3 Nanoparticles synthesis by reduction in biphasic systems

A range of methods for the phase transfer of particles has been also reported, with most studies focusing on the transfer from aqueous to organic media.[10,21]
A classical approach to such stabilization is exploited in the reduction of $[AuCl_4]^-$ with hydrazine or of $[PtCl_6]^{2-}$ with aqueous formaldehyde after extraction of the metal salts into such organic liquid as chloroform or cyclohexane with surfactant cations like dodecylpyridinium, trioctylmethylammonium, or dioctadecyldimethylammonium. The resulting colloidal metal particles are stabilized by the surfactant cations in the essentially nonpolar organic phase.
Surfactant stabilized organosols have been prepared by extraction of the colloidal metal into an immiscible organic liquid from a preformed hydrosol. Reduction of H_2PtCl_6 by $NaBH_4$ in water containing cetyltributylphosphonium bromide followed by extraction into toluene gave a stable organosol of platinum. Colloidal silver particle (8 nm) were displaced from water into cyclohexane, or benzene, by extraction with sodium oleate. Phase transfer resulted in no change in the particle size distribution.
Another promising approach is developed by Caruso who describes the spontaneous phase transfer of nanoparticles from organic to aqueous media. $HAuCl_4$ or Na_2PdCl_4 were reduced by $NaBH_4$ in the presence of tetraoctylammonium bromide in toluene

and the rapid and complete transfer without no signs of degradation or aggregation were performed by the use of aqueous DMAP (4-(dimethylamino)pyridine) solution.[29]

1.2.1.4 The Brust-Schiffrin method

A real breakthrough in biphasic synthesis of transition metal organosols was the procedure developed by Brust and Schiffrin and published in 1994.[30]
The Brust-Schiffrin method for AuNPs synthesis has had a considerable impact on the overall field in less than a decade, because it allowed the facile synthesis of thermally stable and air-stable AuNPs of reduced dispersity and controlled size for the first time (ranging in diameter between 1.5 and 5.2 nm).[31] Indeed, these AuNPs can be repeatedly isolated and redissolved in common organic solvents without irreversible aggregation or decomposition, and they can be easily handled and functionalized just as stable organic and molecular compounds. The technique of synthesis is inspired by Faraday's two-phase system[32] and uses the thiol ligands that strongly bind gold due to the soft character of both Au and S.[30] $AuCl_4^-$ is transferred to toluene using tetraoctylammonium bromide as the phase-transfer reagent and reduced by $NaBH_4$ in the presence of dodecanethiol (Scheme 1.3). The organic phase changes colour from orange to deep brown within a few seconds upon addition of $NaBH_4$

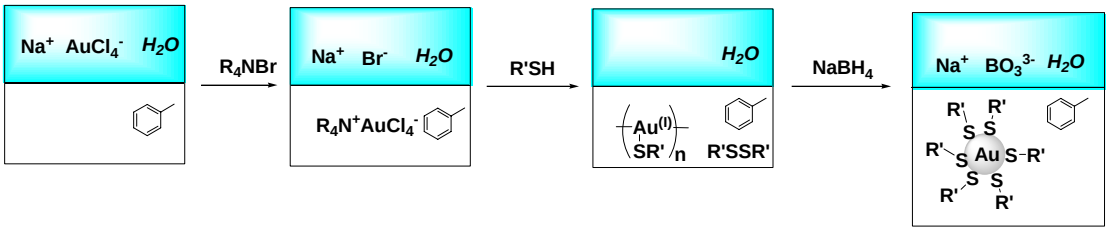

Scheme 1.3. Graphical representation of the Brust-Schiffrin method

The TEM photographs showed that the diameters were in the range 1-3 nm, with a maximum in the particle size distribution at 2.0-2.5 nm, with a preponderance of cuboctahedral and icosahedral structures. Larger thiol/gold mole ratios give smaller average core sizes, and fast reductant addition and cooled solutions produced smaller, more monodisperse particles. A higher abundance of small core sizes (< 2 nm) is obtained by quenching the reaction immediately following reduction or by using sterically bulky ligands.[33] Brust et al. extended this synthesis to *p*-mercaptophenol-stabilized AuNPs in a single phase system, which opened an avenue to the synthesis of AuNPs stabilized by a variety of functional thiol ligands. Subsequently, many publications appeared describing the use of the Brust-Schiffrin procedure for the synthesis of other stable AuNPs, also sometimes called monolayer-protected clusters (MPCs), of this kind that contained functional thiols.[34] The proportion thiol:$AuCl_4^-$ used in the synthesis controls the size of the AuNPs (for instance, a 1:6 ratio leads to the maximum average core diameter of 5.2 nm, i.e., ca. 2951 Au atoms and ca. 371 thiolate ligands; core diameter dispersity of ~ ±10%). Murray et al. reported and studied the "place exchange" of a controlled proportion of

thiol ligands by various functional thiols (Figure 1.5) and the subsequent reactions of these functional AuNPs.[35]

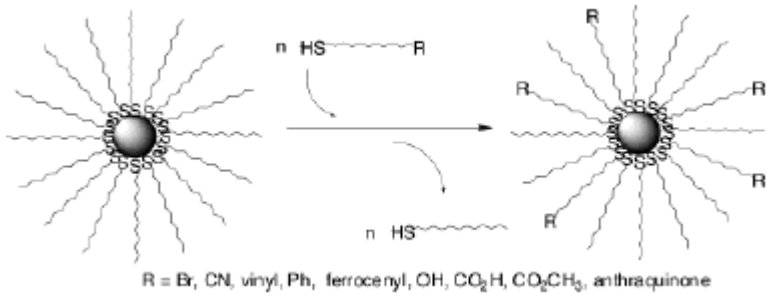

Figure 1.5 ligand exchange for AuNPs

1.2.1.5 Nanoparticles synthesis by reduction in micelles

The reduction of physically constrained metal precursors offers the potential for restricting the growth of the metal particles either by limiting the amount of metal particle precursor accessible to a growing nucleus or by restricting the motion of the precursor species and the growing nuclei, thus diminishing the rate of productive collisions. This tactic has found wide application, for example, in the preparation of small metal particles in zeolite cages. In an analogous approach, liquid phase colloidal metals have been prepared in surfactant micelles, reverse micelles (water-in-oil microemulsions), and vescicles (Figure 1.6) which act as microreactors for the preparation and stabilization of metal colloids.[36,37]

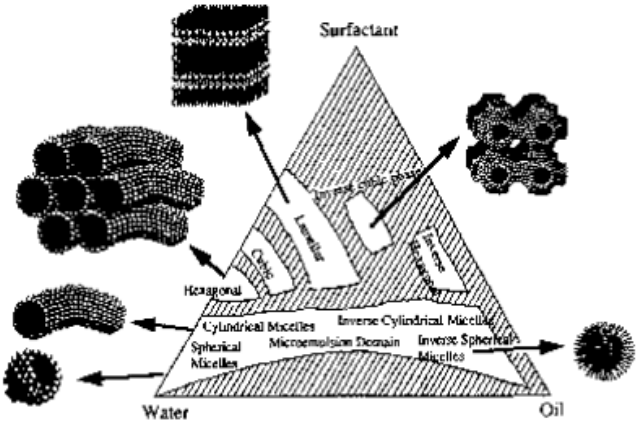

Figure 1.6 Schematic phase diagram of surfactant-oil-water systems showing a variety of self-assembled structures.

These encapsulating organic particles are formed from the self-assembly of surfactant molecules in nonpolar solvents, such that water is trapped in the intraparticle space. Although the terms micelle and microemulsion are often used interchangeably, a useful distinction between the two can be made on the basis of size (aggregates containing less than about 50 molecules are micelles, whereas bigger aggregates, containing several hundred or more molecules are referred to as microemulsions). Bilayered vescicles can reach size of 10 – 100 nm. These different

types of nanocapsules can contain various amounts of water, and this has allowed surfactant micelles, reverse micelles and vescicles to be used as highly dispersed reaction vessels for metal precursors solution in metal colloid preparations. Such synthesis of metal nanoparticles was first reported by Boutonnet et al. in the early 1980s.[38] There are two main ways of preparation in order to obtain nanoparticles from microemulsions: by mixing two microemulsions, one containing the precursor and the other the precipitating agent (Scheme 1.4a); by adding the precipitating agent directly to the microemulsion containing the metal precursor (Scheme 1.4b).

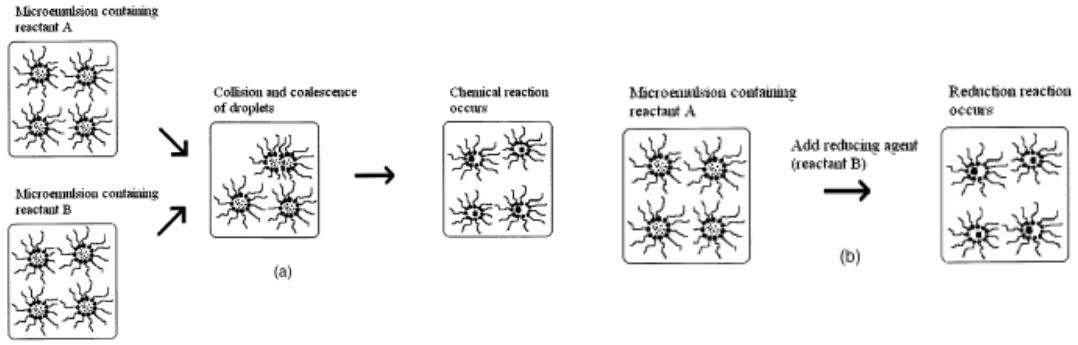

Scheme 1.4. Modes of particle preparation from microemulsion: (a) mixing of two microemulsions; (b) direct addition of precipitating (reducing) agent to the microemulsion.

The most studied systems for TMNPs synthesis in microemulsions are reverse micelles. Reverse micelles can be formed by ionic surfactants with double-long alkyl chains alone, such as diethyl sulfosuccinate (DES) or a mixture of ionic and nonionic surfactants with a short oxyethylene chain dissolved in organic solvents. Reverse micelles are usually thermodynamically stable mixtures of four components: surfactant, cosurfactant, organic solvent, and water. The surfactants used include sodium bis(2-ethylhexyl)sulfosuccinate (AOT), sodium dodecyl sulphate (SDS), cetyltrimethylammonium bromide (CTAB), and Triton-X. Some cosurfactants used are aliphatic alcohols with a chain length of C_6-C_8. Organic solvents used for reversed micelle formation are usually alkanes or cycloalkanes with six to eight carbons. Reversed micelles can solubilize relatively large amounts of water, which makes them suitable for the synthesis of nanoparticles, because the water pool is in the nanometer range and can be controlled.[36]

Metal nanoparticles can be prepared by reducing metal salts in the reversed micelles with very good control over particle size and shape. Strong reduction agents such as $NaBH_4$, N_2H_4, and sometimes hydrogen gas were used. Pt, Rh, Pd, Ir, Ag, Au, Cu, Co, Ni, FeNi, CuAu, CoNi, etc., have been synthesized using this method.[36] For example, Cu nanoparticles are produced using reverse micelles, where copper diethyl sulfosuccinate, $Cu(AOT)_2$, water, and isooctane were used . Reverse micelles are formed in two regions for the phase diagram: $0 < w < 5$ and $30 < w < 40$, where w is the ratio $[H_2O]/[AOT]$. Syntheses in these two regions for the phase diagram induce formation of Cu nanoparticles with average particle sizes larger (12 nm) than those at higher water content (7.5 nm) as shown in Figure 1.7. This was explained by the fact that the redox potential changes with the water structure inside the water pool. At low water content, the number of nuclei formed is rather small and large nanocrystals

are produced.[39] With the increase of the water content, the number of nuclei increases, inducing formation of smaller nanocrystals.

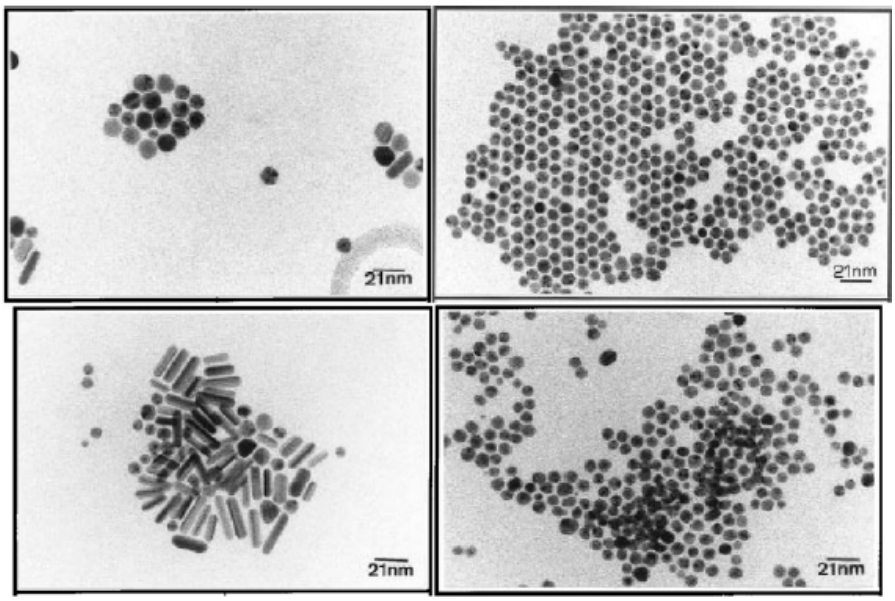

Figure 1.7 TEM images obtained after synthesis at of Cu NPs at different [H_2O]/[AOT] ratio

1.2.2 ELECTROCHEMICAL REDUCTION OF SALTS

M. T. Reetz at the Max Plank Institut has developed an electrochemical method for the preparation of transition metal nanoparticles.[40] This large-scale synthetic procedure allows one to obtain size-controlled particles. A sacrificial anode is used as a metal source. This anode is oxidized in the presence of quaternary ammonium salt, which is both the electrolyte and the stabilizing agent. The ions are then reduced at the cathode to yield the metallic nanoparticles. With this process, Reetz and co-workers were able to generate acetonitrile/THF dispersed Pd colloids with various sizes. The mechanism proposed by the authors consists of (i) dissolution of the anode to form metal ions (oxidation of Pd to Pd^{2+}); (ii) migration of the metal ions to the cathode; (iii) reduction of the metal ions at the surface of the cathode; (iv) aggregation of the particles stabilized by the ammonium ions around the metal cores; and then (v) precipitation of the Pd nanoparticles (Figure 1.8). This process presents several advantages: (i) particle size can be controlled by varying the current intensity[41] (higher current intensity gives smaller particles); (ii) isolation of the nanoparticles is simple as they precipitate out of the solvent when formed; and finally (iii) the synthesis occurs with good yields (>95%). This synthetic procedure can be applied to easily oxidized transition metals such as Ni or Cu. The solubility of the colloids obtained can be modulated from nonpolar solvents such as pentane to polar solvents as water by changing the polarity of the protecting agent (tetraalkylammonium halide for apolar solvents or sulfobetaine for polar solvents).[41] For less easily oxidized metals such as Pt, Rh, or Ru, the anode and cathode used are made of Pt and the metallic precursor is a transition metal salt. In this new process the anode is no more sacrificed and the metallic precursor is reduced by electrolysis

in the presence of a quaternary ammonium salt which is both the electrolyte and the stabilizing agent.

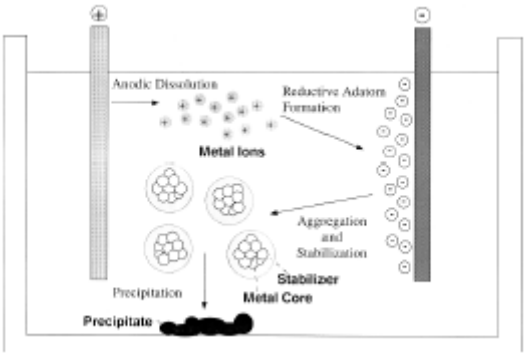

Figure 1.8 Reetz's electrochemical synthesis of TMNPs

1.2.3 THERMAL, PHOTOCHEMICAL, OR SONOCHEMICAL DECOMPOSITION

1.2.3.1 Thermolysis[21]

Many organometallic compounds are thermally decomposed to their respective zerovalent element. The syntheses of Pd and Pt organosols by thermolysis of precursors such as palladium acetate, palladium acetylacetonate, or platinum halides have been reported in the literature. The solvents used had high boiling points such as methyl-*iso*butylcetone. These syntheses were performed without stabilizing agents, and as a result broad size distributions and large particles were observed.

1.2.3.2 Photolysis or Radiolysis[21]

Photochemical synthesis of metallic nanoparticles can be obtained either by transition metal salt reduction by radiolytically produced reducing agents or degradation of an organometallic complex by radiolysis. The goal of these synthetic procedures is to obtain zerovalent metals under conditions, which prevent the formation of bulk metal. Ionization radiations are generated by X- or γ-ray generators. UV-visible irradiation is generated by Hg or Xe lamp. One advantage of radiolytic methods is that a large number of atoms is homogeneously and instantaneously produced during the irradiation thus providing favorable conditions for the formation of nearly monodispersed particles (<15% dispersion calculated by TEM imaging and NIH Image software counting of 300 particles). Over the past 20 years, a wide range of transition metal nanoparticles such as Ag, Au, Ir, Pt, Pd, or Cu colloids were prepared by this method. Several reducing agents can be generated during radiolytic procedure. Thus, the radiolysis of aqueous suspension of transition metal salts produced solvated electrons or H· and OH· originating from water radiolysis. These species can react with the molecules in solution to give new radicals able to reduce metal salts (Scheme 1.5).

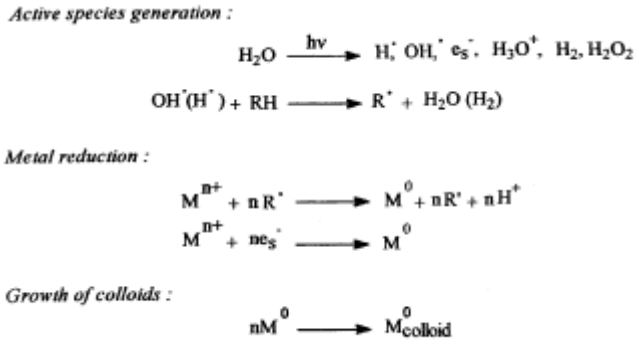

Scheme 1.5 photochemical synthesis of TMNPs

By irradiating a solution of $Cu(ClO_4)_2$ containing sodium formate Cu nanoparticles are formed through the reduction of Cu^{2+} by both solvated electrons and CO_2 generated during radiolysis. Similarly, the radiolysis of an aqueous solution of $Pd(NH_3)_4Cl_2$ and 2-propanol also results in the formation of Pd colloids by both solvated electrons and 1-hydroxy-1-ethylmethyl radicals ($(CH_3)_2COH\cdot$) generated by the reaction of H· and OH· with 2-propanol. In an original example of radiolytic Pt colloid synthesis, both the nanoparticles and the protecting polymer are produced simultaneously by radiolysis of a solution containing the monomer (acrylamide) and the metal salt (H_2PtCl_6). The radiolytic preparation of transition metal nanoparticles is also possible in organized environments such as micelles or micoemulsions. The photolysis of metal salts is also an efficient method to prepare transition metal colloids. Thus, the UV-visible irradiation of Au, Ag, or Pt salts in reverse microemulsions in the presence of surfactants or polymers yielded metallic nanoparticles. Toshima prepared Pt and Pd colloids in the presence of micelles of a wide range of surfactants by photolysis and hydrogen reduction. They reported that the UV-visible irradiation yields smaller and better dispersed nanoparticles. Another aspect was described by Fendler and coworkers who used UV-visible irradiation to encapsulate Pt nanoparticles into polymerized vesicles. The vesicle reticulation and the colloid formation occur simultaneously during irradiation. Mayer and Esumi reported the UV-visible photolytic synthesis of Au nanoparticles stabilized by block copolymers, polyelectrolytes, or dendrimers (polyamidoamine: PAMAM).

1.2.3.3 Ultrasonic Reduction[21]

Sonochemistry is due to acoustic cavitation phenomena causing the formation, the growth, and the explosion of bubbles in a liquid media. The very high temperature (>5000 K), the pressure (>20 MPa), and the cooling rate (>107 K s-1) reached during cavitation gave to sonicated solutions unique properties. These extreme conditions were used by Süslick to obtain Fe particles, or Co alloys by reduction of metal salts. In the same way, Gedanken reported the preparation of Ni, Cu, Pd, Fe, Fe oxide, or Fe nitride. The sonochemical reduction of transition metal salts occurs in three steps: the generation of the active species, the reduction of the metal, and the growth of the colloids. These three steps occur in different compartments (Scheme 1.6): (i) In gaseous phase into the cavitation bubbles where high temperature and pressure allow water pyrolysis to form H· and OH·, (ii) at the interface between the cavitation bubbles and the solution, and finally (iii) in the solution. This synthetic procedure

was applied to colloidal synthesis and a wide range of surfactant or polymer stabilized transition metal nanoparticles such as Au or Ag, Au, Pt, Pd were generated. Nagata demonstrated the influence of the stabilizing agent and of the addition of alcohol on the kinetic of nanoparticles formation. Finally, Gedanken and co-workers prepared quaternary ammonium stabilized Pd colloids solubilized in an organic solvent (THF). Due to the low vapor pressure of the metallic salts, the reduction cannot happen in the gaseous phase. The reduction occurs mainly at the bubble/solution interface and in solution. Nagata suggested that the protecting agents in solution form alkyl radicals under sonolysis. These radicals react on transition metal salts to yield zerovalent metals (Scheme1.6).

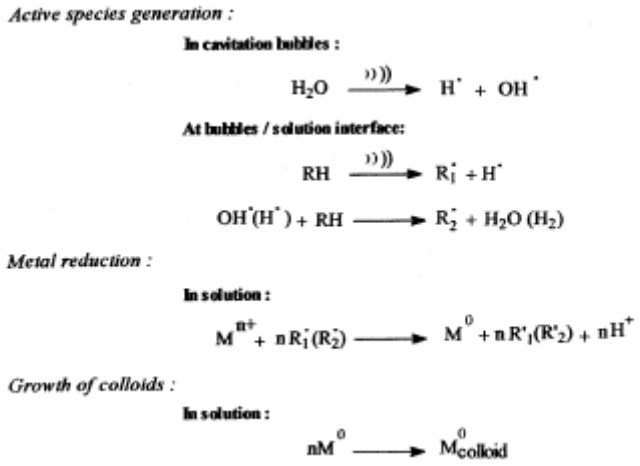

Scheme 1.6. Ultrasonic synthesis of TMNPs

1.2.4 DISPLACEMENT OF LIGANDS FROM ORGANOMETALLIC COMPOUNDS

Some zerovalent organometallic complexes can be converted into colloidal suspension of metals by reduction or ligands displacements. Using this procedure, Bradley and co-workers generated Pt and Pd (PVP) stabilized organosols.[42] $Pt(dba)_2$ and $Pt_2(dba)_3$ dimer can be reduced by hydrogen at atmospheric pressure to obtain 2.5 nm nanoparticles. With a pressure of 3 atm, the same reduction gave 4 nm particles. The use of carbon monoxide allows also obtaining smaller particles (2 nm). With this reducing agent $Pt(dba)_2$ and $Pd(dba)_2$ can be reduced to generate nanoparticles organosols in the presence of cellulose acetate or cellulose nitrate in THF.[43] The olefinic ligand reduction of zerovalent complexes can be applied to the preparation of colloidal suspensions. Thus, hydrogenation of Ru(COD)(COT) yields, in the presence of either PVP, cellulose nitrate or cellulose acetate, 1 nm Ru nanoparticles, while in presence of $P(Cy)_3$ the main product is a stoichiometric monometallic complex (Figure 1.9).[44] Spontaneous decomposition or 3 atm hydrogenation of $Ni(COD)_2$ has been used to prepare PVP stabilized nanoparticles soluble into CH_2Cl_2. Co, Cu, or Au PVP stabilized colloids were also generated from various organometallic complexes by this synthetic procedure.[21]

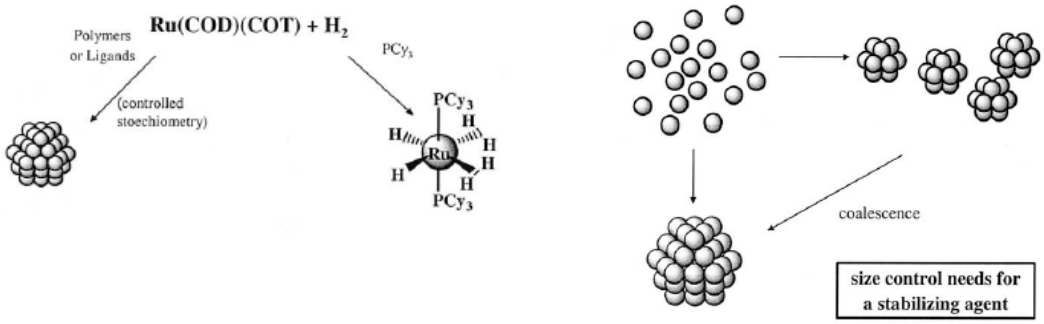

Figure 1.9. Illustration of the general synthetic method followed by Chaudret group for Ru NPs Synthesis

1.2.5 METAL VAPOUR SYNTHESIS

Conceptually, if not practically, the simplest method to of preparing colloidal metals is the condensation of atomic metal vapours into a dispersing medium.[45] Since the activation energy for agglomeration of metal atoms is very low, the possibility of competing molecular complex formation processes which have higher activation energies can be mitigated by operating at low temperatures. The use of metal vapours co-condensed with organic vapours to synthesized colloidal metals in nonaqueous media is known since the dawn of the last century. However, this procedure was only extensively studied in the 70s. This method, known as metal vapour synthesis (MVS), consists of the evaporation at reduced pressure of relatively volatile metals by means of resistive heating or electron beam and a subsequent co-condensation at low temperature of these metals with the vapours of organic solvents on the walls of a reactor cooled with liquid nitrogen. In the vapour phase, in excess of organic vapours, metal atoms are present, which are then trapped in the frozen matrix of the solvent. Below the Tammen temperature (defined as the half of the solvent melting point), no diffusion of the metal atoms may occurs. When the frozen metal/organic mixture is allowed to warm, nucleation and growth take place and a colloidal dispersion of the metal was then obtained after melting (Scheme 1.7). The resulting organosols, generally called SMAD (Solvated Metal Atoms Dispersions), can be considered as kinetically stable suspensions of very reactive "naked" clusters, because no strong coordinating ligands are present, which in some cases can be stored in inert atmosphere at room temperature for long times. Because of the great reactivity of metal vapours, they can react with the organic solvent during aggregation, decomposing it, and leading to incorporation of carbonaceous fragments in the forming metal clusters. Moreover, the interaction with the frozen matrix quench very quickly the energy, leading to unusual distorted geometries, thermodynamically not stable. As a result, the isolated metal colloids show generally very high catalytic activity and unusual properties.[3]

MVS find useful applications in preparation of supported TMNPs catalysts, obtained simply by mixing the SMAD with the solid support (generally a metal oxide, but also insoluble polymers, etc…). The metal quickly separate from the solvent, by interacting with the support surface, affording catalytic systems which are very active because of the absence of poisons (i.e., halide from metal salts precursors in

catalysts prepared by reduction methods) and the presence of several defect sites (kinks, terraces, adatoms, etc…) due to the already mentioned distorted geometries.

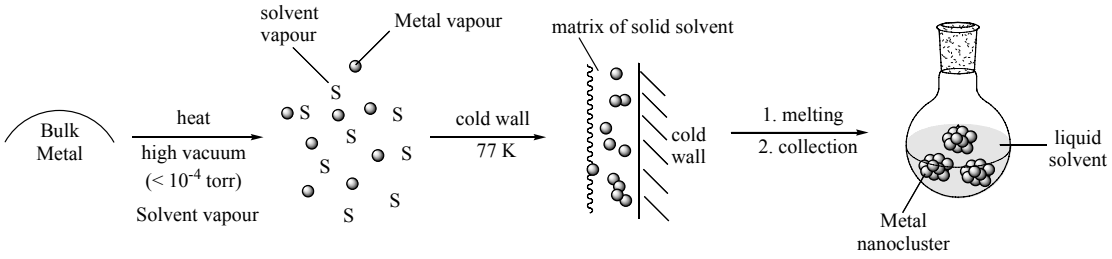

Scheme 1.7 Metal vapour synthesis of TMNPs

The development of metal vapour routes to TMNPs is often limited by the apparatus, because very high vacuum and relatively elevated temperatures are required in order to vaporize the metal. This synthetic procedure can be conducted either in a rotating[46] or in a static[47,48] reactor (Figure 1.10 a and b). Generally, the metal vapours are generated from a resistively heated hearth or an electron beam furnace and condensed on the walls of the reactor together with the organic solvent vapours. A recent reactor developed by Bradley[10] co-condenses metal vapour with aerosols of organic solvents (Figure 1.10c). This process resolves the problems of volatile solvents.

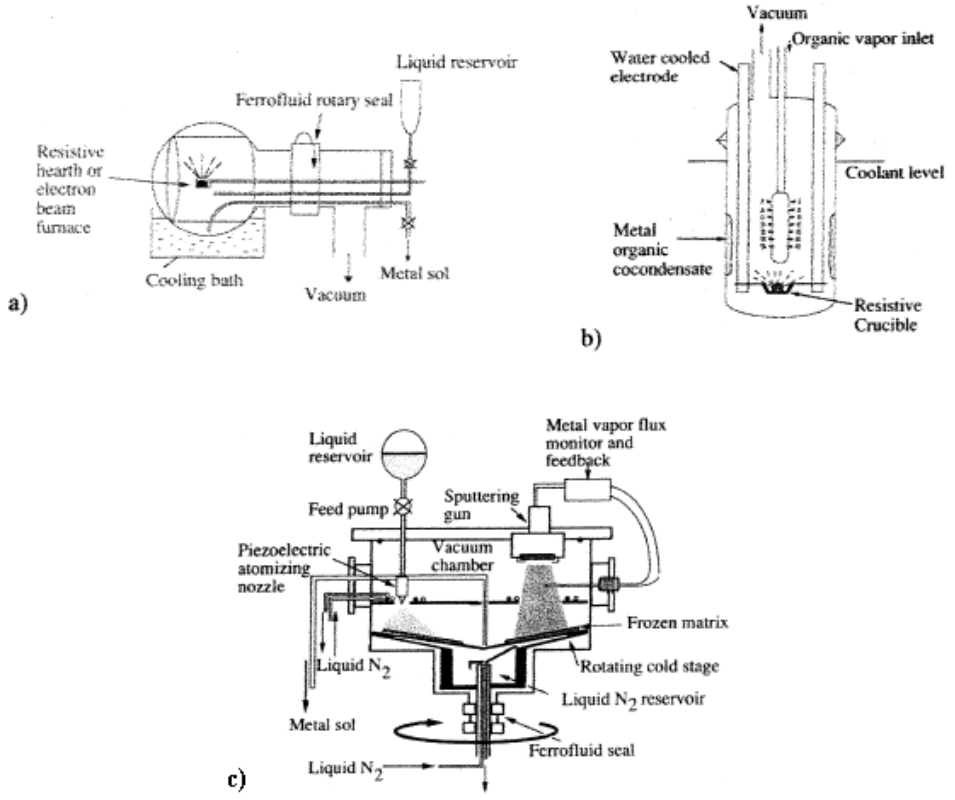

Figure 1.10 Apparatus for MVS: a) rotating reactor; b) static reactor; c) Bradley's reactor

All these systems allow the synthesis of organosols of TMNPs, potentially without limitations in the choice of metal if the appropriate organic solvent is used.[49] Klabunde and co-workers demonstrated the preparation of various suspensions of TMNPs, for example Au and Pd colloids were obtained by co-condensation of metal vapours in acetone at 77K, followed by warming.[50] The intensely coloured colloidal suspensions of the metals showed particle sizes were between 5 and 30 nm and are stable for several months. Simple removal of solvent results in aggregation and ultimately film formation. An analogous procedure was used to condense Au in solution of polystyrene,[51] poly(methyl methacrylate),[52] or polyacetylene[53] to obtain Au colloids of 2 to 15 nm. Colloidal metals could also be generated by metal vapour condensation in fluorinated solvents.[53] Five nanometer Co colloids[54] stabilized by surfactants were also generated in toluene by metal vapour condensation. Smaller particles of Pd, Cu, Ni, Pt, Pr, Yb, or Er with a size about to 2 nm were obtained by co-condensation of metal vapour into solvents for the stabilization such as methylcyclohexane and isobutylaluminoxane[55] or butan-2-one, methylethyl ketone (MEK), and acetone (MMK).[56] The main drawback in employ of MVS for TMNPs synthesis is the poor reproducibility, due to the scarce control in the evaporation of bulk metal. Furthermore, the particles obtained by standard MVS procedures are generally amorphous and show large size distributions. The dispersity can be greatly reduced with a digestive ripening process, in presence of strong ligands. Gold nanoparticles (5-9 nm in diameter) with narrow size distribution were obtained after digestive ripening of Au SMAD with organic thiols, amines, phosphines and silanes. Superlattices of small Ag and Au nanoparticles were obtained after digestive ripening of respective SMAD with alkylthiols in refluxing toluene (Figure 1.11).

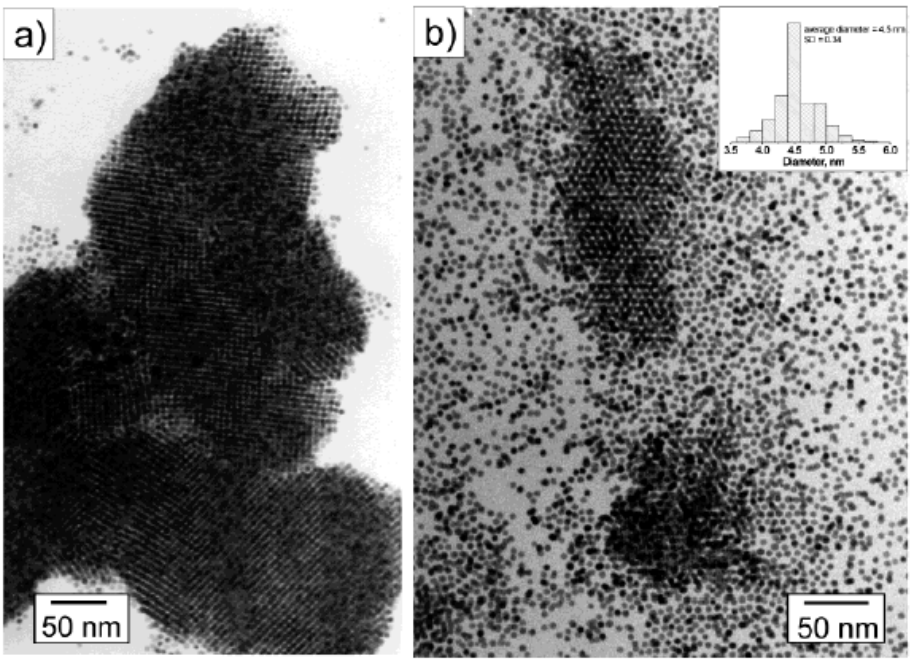

Figure 1.11. (a) TEM image of the gold colloid after digestive ripening with octanethiol showing the 3D superlattices. (b) TEM image of a hot and diluted Au-C8SH colloid depicting the separate particles. The inset in (b) shows the particle size distribution.

1.3 TRANSITION METAL NANOPARTICLES CHARACTERIZATION

The quick development of nanoscience in the last decades can surely be attributed to the parallel birth or improvement of numerous characterization and analysis techniques. It is now possible to see matter at nanometers resolution and, in some case, single atoms can be visualized, an improvement that was hard even to imagine only a few years ago. Scheme 1.8 resumes the various techniques, showing the kind of information which can be obtained from them.[16] Some of the most representative and innovative methods are described below.

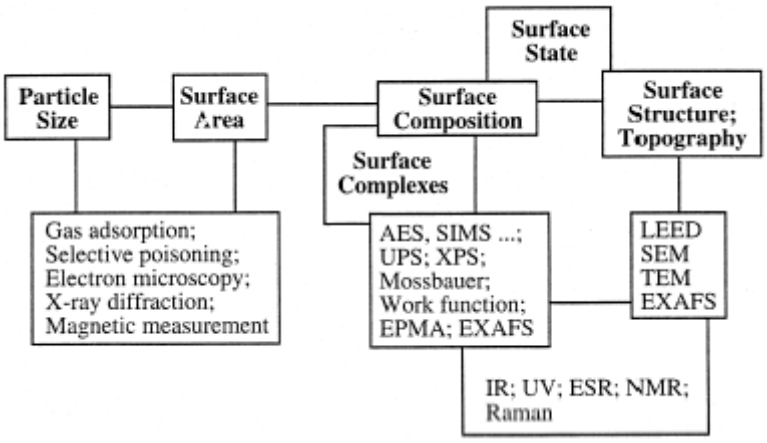

Scheme 1.8 main methods of characterization of TMNPs

1.3.1 HIGH RESOLUTION TRANSMISSION ELECTRON MICROSCOPY (HRTEM)[16]

The most widely used technique for characterizing nanoclusters is transmission electron microscopy (TEM) or high resolution TEM (HRTEM), techniques which provide direct visual information on the size, shape, dispersity, structure, and morphology of nanoclusters. HRTEM is capable of routine magnifications of ≥ 800.000 to, typically, ±2 Å resolution. Potential drawbacks of this technique include (i) the many reported examples of electron-beam-induced nanocluster structural rearrangement, aggregation, or decomposition; (ii) the inherent problems in interpreting two-dimensional images of three-dimensional samples; (iii) the small sample sizes, meaning that only a finite number of nanoclusters may be examined and counted, which may not be representative of the sample as a whole (and, in any event, are often only 10^{-22} or so of Avagadro's number!). Some author asserted that inferring ensemble average properties such as average diameter or shape based on the limited regions examined in typical TEMs is akin to determining the street layout of New York city by examining a square centimeter of side walk: it just is not statistically significant;[57] finally, (iv) the fact that samples must be dried and examined under high-vacuum condition, meaning that no direct information is gained on how the nanoclusters exist *in solution*. Additionally, HRTEM images shows only the metallic core, not giving any information about the surrounding shell, if present.

In some modern instrument, HRTEM is coupled with EDS (Energy Dispersive X-ray Spectroscopy), which allows a spatial qualitative analysis of the chemical elements present in the observed sample. In those case in which 2D or 3D nanoparticles superlattices are present, it is possible to estimate the shell thickness by measuring the distance between single particles. Despite the mentioned potential limitations, HRTEM has arisen as the technique of choice for the initial characterization of nanoclusters due to the atomic-level resolution possible, the speed of analysis, and the powerful visual images that are obtained.

1.3.2 UV–VISIBLE SPECTROSCOPY AND DYNAMIC LIGHT SCATTERING[16]

1.3.2.1 Uv-vis spectroscopy

TMNPs shows interesting optical properties. The more relevant is the presence of a surface plasmon resonance (SPR), which is responsible, for example, of the bright red colour of Au colloids. The origin of SPR is attributed to the collective oscillation of the free conduction electrons induced by an interacting electromagnetic field. Mie was the first to describe them quantitatively by solving Maxwell's equations with the appropriate boundary conditions for spherical particles. The total extinction cross section composed of absorption and scattering is given as a summation over all electric and magnetic multipole oscillations. The Mie theory has the advantage of being conceptually simple and has found wide applicability in explaining experimental results. For nanoparticles small compared to the wavelength λ of the exciting light ($\lambda << 2R$) only the dipole absorption of the Mie equation contributes to the extinction cross section σ_{ext} of the nanoparticles. The Mie theory then reduces to the following relationship (quasi-static or dipole approximation):

$$\sigma_{ext} = \frac{9V\epsilon_m^{3/2}}{c} \cdot \frac{\omega\epsilon_2(\omega)}{[\epsilon_1(\omega) + 2\epsilon_m]^2 + \epsilon_2(\omega 2)^2} \qquad 1.6$$

where V is the spherical particle volume, c the speed of light, ω the angular frequency of the exciting radiation, and ε_m is the dielectric constant of the surrounding medium (assumed to be frequency independent). $\varepsilon_1(\omega)$ $\varepsilon_2(\omega)$ denote the real and imaginary part of the dielectric function of the particle material, respectively. From eq 1.6 it follows that resonance occurs when $\varepsilon_1(\omega) \sim -2\varepsilon_2(\omega)$ if $\varepsilon_2(\omega)$ is small or only weakly dependent on ω. The bandwidth and peak height are roughly determined by $\varepsilon_2(\omega)$. However, within the dipole approximation there is no size dependence except for a varying intensity due to the fact that the volume V depends on the particle radius R. Experimentally, one however observes a strong size dependence of the plasmon bandwidth. The position of the absorption maximum is also affected although both a blue-shift and a red-shift have been observed with decreasing particle size. As a modification to the Mie theory for small particles, the dielectric function of the metal nanoparticles itself is assumed to become size dependent $\varepsilon = \varepsilon(\omega, R)$ and therefore rendering a size-dependent absorption cross section even within the dipole approximation (intrinsic size effects). For very small clusters (< 2 nm), quantum effects predominate and no SPR is observed.

Au, Ag and Cu nanoparticles shows very intense SPR in the visible region and UV-Vis spectra are routinely reported as characterization of these systems, while for other metals UV-Vis characterization is quite unusual. UV–Vis has been used to determine both particle size and the degree of cluster aggregation in the sample. For transition metal nanoclusters, some in-depth studies have been published which correlate UV–Vis spectra to particle size. Reetz's UV–Vis characterization of 1.4 nm, 2.3 nm, and 4.1 nm TOAB stabilized Pd nanoclusters is one such example. For colloidal particles which have an absorption band in the visible region, the λ_{max} is dependent on the size and the shape of the particles, as well as how close the particles are relative to each other. Hence, not only particle size can be determined by UV–Vis spectroscopy, but phenomena such as aggregation can also be studied. In cases where the surface plasmon resonance can be identified, changes in surface *composition* can also be followed. The ability to *tune* the optical properties of a system by changing particle size, degree of aggregation, or surface composition holds potential for many applications.
On the other hand, the multitude of factor which can affect absorption spectra of nanoparticles (size distribution, shape, surface charge, ligand shell composition, solvent polarity, distance between particles, etc…) make very difficult a quantitative evaluation of particle size by means of UV-Vis analysis and generally only comparison between very similar, well characterized and monodisperse systems can be done, in a qualitative way.

1.3.2.2 Dynamic Light Scattering[58]

Dynamic light scattering (DLS) is used to obtain information about particle sizes in solution, as well as interactions between macromolecules such as proteins. In chemistry, DLS is a common technique for measuring the sizes of polymer clusters, but is less common for the measurement of nanoclusters, the dominant technique being ex situ transmission electron microscopy. Particle size from fitting DLS data requires knowledge of the diffusion coefficient of the clusters and viscosity of the solvent. DLS is advantageous in that it is non-invasive and is performed on a solution sample, so that the cluster solution requires little manipulation and can be recovered after analysis. In the nanocluster literature, DLS measurements are often compared to measurements from other techniques, most commonly transmission electron microscopy; the agreement is generally close, at least in cases where no sample damage has occurred from electron microscopy.

1.3.3 INFRARED SPECTROSCOPY (IR) AND SURFACE ENHANCED RAMAN SPECTROSCOPY (SERS)[16]

1.3.3.1 Infrared spectroscopy

Infrared spectroscopy (IR) has been used as a surface probe in nanocluster systems, commonly done by adsorbing carbon monoxide onto the surface of the metal nanocluster. Carbon monoxide is an ideal ligand because it readily adsorbs to metal surfaces, and has characteristic vibrational frequencies around 1800–2100 cm^{-1} once adsorbed or coordinated to the metal surface. IR can easily distinguish between

various mode of absorption of CO, giving information about the surface structure of metal. IR is also suitable to detect metal-ligand interaction in nanoparticles capped with organic ligands (thiols, amines), by observing shifts in vibrational frequencies due to the coordination at the metal surface.

1.3.3.2 Surface Enhanced Raman Spectroscopy

To a lesser extent, Surface Enhanced Raman Spectroscopy SERS has been used to probe the surfaces of small metal particles, often by following the absorption of pyridine on gold and silver sols (Pyridine as an adsorbate is known to initiate nanocluster agglomeration). SERS has also been used to follow adsorbed molecules or ions formed during cluster synthesis (i.e., adsorbed citrate during aqueous Fe(II) reduction of Ag(I)). The drawback of SERS is that its use is limited to metals which have a well-defined plasmon band needed to provide the required signal enhancement (essentially Au and Ag).

1.3.4 SCANNING TUNNELING MICROSCOPY (STM) AND ATOMIC FORCE MICROSCOPY (AFM)[16]

1.3.4.1 Scanning Tunneling Microscopy

Scanning Tunneling Microscopy (STM) is a very useful technique because makes possible the determination of the *total diameter of a nanocluster, including the stabilizing ligand shell*. STM is also an effective probe of the electronic properties of such nanoparticles. Early STM investigations of ligand-stabilized nanoparticles were not conclusive, but in 1991 Schmid et al. published the first STM images of his phosphine-stabilized Au_{55} clusters where the ligand shell was clearly visible. Although the resolution of the metal core was not as good as anticipated, Schmid found that the overall diameter of the clusters *including the ligand shell* was 2.2 nm, in good agreement with the expected diameter of 2.0 - 2.4 nm. In 1994, Reetz et al. published a combined STM/TEM study of tetraalkylammonium stabilized Pd nanoclusters. He was able to determine the thickness of the stabilizing ligand shell by subtracting the STM-determined diameter from the TEM-determined diameter (Figure 1.11). Reetz et al. found that the thickness of the stabilizing R_4NBr layer was in good agreement with theoretical models. However, tip effects must be considered, and Schmid and Peschel have shown that this technique may overestimate a particle's diameter, particularly when individual particles are imaged. Despite the recent advances, STM remains an under-utilized nanocluster characterization technique. The drawbacks of STM include: (i) the nanoparticles tend not to stick well to the substrate surface, preventing good images from being obtained; (ii) the geometry of the tip shape may lead to inaccurate measurements or artifacts in the image; (iii) the tunneling mechanism is not well understood; (iv) the samples examined are often dried solids, and hence no rigorously logical conclusions can be made about what the nanoclusters look like *in solution*; and finally (v) the specific techniques applied to image nanoclusters are far from mature, so that standard literature protocols have not been established.

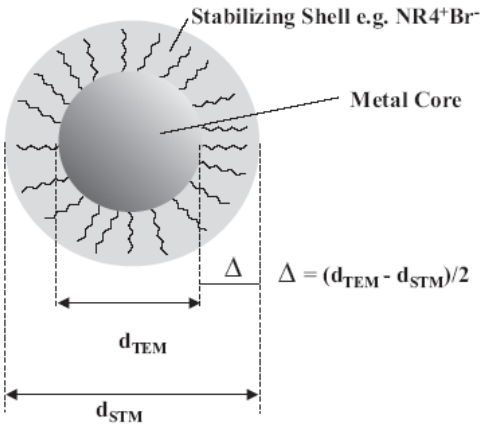

Figure 1.11. Visualization of TEM and STM diameters

1.3.4.2 Atomic Force Microscopy

Others have used atomic force microscopy (AFM) to image nanoclusters. This technique, contrary to STM, is purely mechanical: a cantilevered tip attached to a spring is dragged across a sample. The increase or decrease in the height of the tip is measured, yielding a surface height profile as a function of distance. The advantage of this technique, relative to STM, is that it can be carried out on *nonconducting* samples.

1.3.5 X-RAY BASED METHODS (XRD, XPS, EXAFS AND XANES)[59]

X-Ray methods are informative for non-destructive elemental and structural analyses. X-Ray diffraction gives structural information on nanoparticles, including qualitative elemental information. Characteristic X-ray absorption, electron emission by X-ray bombardment and X-ray emission by electron irradiation give clear information on the varieties and amounts of the elements contained in nanoparticles. Here, we would like to summarize some X-ray methods often used for the characterization of metallic nanoparticles.

1.3.5.1 X-Ray diffraction

X-Ray diffraction (XRD) is a strong method to investigate the solid structure of metal nanoparticles. For monometallic nanoparticles, the phase changes with increasing diameter of nanoparticles can be investigated with XRD.[60] The presence of bimetallic particles as opposed to a mixture of monometallic particles can also be demonstrated by XRD since the diffraction pattern of the physical mixtures consists of overlapping lines of the two individual monometallic nanoparticles and is clearly different from that of the bimetallic nanoparticles. However, when these metals are divided into small nanoparticles consisting of less than hundreds of atoms, the acquisition of structural information may be difficult.

1.3.5.2 X-ray Photoelectron Spectroscopy

X-ray Photoelectron Spectroscopy (XPS) is generally used to probe the electronic structure of TMNPs. Since electronic structure is affected by particle size, interactions with surrounding heteroatoms (ligands, supports) and oxidation state of metal, we can get information about these parameters with XPS measurements.

1.3.5.3 EXAFS and XANES[59]

Two potentially powerful methods for directly observing the nucleation process utilize X-ray spectroscopy: X-ray absorption near-edge spectroscopy (XANES) and extended X-ray absorption fine structure spectroscopy (EXAFS). These methods are valuable because they give information about the identity of atoms in the nanoclusters, as well as information about the nearest neighbors of the atoms, allowing atomic-level characterization. The recent, major advances in X-ray optics as well as the analysis of multiple-shell scattering currently make these techniques among the most attractive for studying nanoclusters. Frenkel and coworkers have pioneered the use of these X-ray spectroscopies to study the formation of transition-metal nanoclusters.

1.3.6 MASS SPECTROMETRY (LDI, MALDI-TOF, ESI-TOF)[61]

Mass spectrometry has been used successfully for the characterization of small clusters. Laser desorption/ionization mass spectrometry (LDI-MS) and matrix assisted laser desorption/ionization-mass spectrometry (MALDI-MS) are powerful tools for characterization of Au clusters. Significant recent results have also been obtained with electrospray ion sources. In LDI-MS, there is no efficient energy-dissipating matrix, and laser pulse volatilization of Au MPCs leads to the destruction of the ligand monolayers, leaving only $[Au_N]^-$ or $[Au_NS_x]^-$ (or their positive counterparts) for mass analysis and detection. Both positive and negative ion modes can be used. The isolation of Au clusters in the 14-15 kDa range protected with thiolate and with phosphine ligands has been established from mass spectral data. Also 2-methylaniline protected Au clusters has been analyzed with MALDI-MS technique, but only the organic shell, constituted by polymeric species of starting amine, was detected.[62] Very small Au_n clusters protected by glutathione monolayers (with n = 18, 21, 25, 28, 32, 39) has been recently isolated and characterized by ESI-MS.[63]

1.3.7 NMR AND NMR-DOSY

1.3.7.1 NMR[16]

There are two uses for nuclear magnetic resonance NMR spectroscopy of nanoclusters: studies probing the intra-core metallic atoms, and studies probing the ligands that surround the metal core. NMR studies of the metallic core (i.e., ^{105}Pd or ^{195}Pt NMR) are typically more difficult. This is because the nuclear-spin lattice relaxation time, and the nuclear resonance frequency itself, are sensitive to any metallic property the cluster may exhibit. This change in frequency is known as the

Knight shift, and is a consequence of the interaction of the metal nucleus with the conduction electrons. The largest Knight shift observed is -3.5% for Pt, which corresponds to 35,000 ppm. In very small particles and in favorable cases, the Knight shift allows resonances for surface and interior metal particles to be identified.
NMR spectroscopy is one of the few techniques which can provide some information about nanoparticles *in solution*, and in a very cheap and fast way. ^{1}H, ^{13}C, and ^{31}P NMR, can be used to characterize TMNPs stabilized in solution with organic ligands. An obvious potential limitation is that the nanoparticles have to be isolated from the preparation solvent and redissolved in a deuterated one, so they must be quite unaffected by these operations ("bottleable" nanoparticles). When NMR analysis is feasible, information about the interaction of metal surface with adsorbed ligands can be obtained, by comparing the spectra of free and bonded species (in analogy with routine organometallic chemistry NMR characterization), in order to establish the kind of ligand coordination at metal surface. Ligand exchange experiments can be easily followed with NMR. Unfortunately, little information can be obtained about particles size. In a work published by Murray et al.,[31] particle size in long chain alkylthiol-capped gold nanoparticles has been quantitatively related to signal broadening of methylene hydrogens, but this remains an isolated and very particular case.

1.3.7.2 Diffusion Ordered Spectroscopy[64,65]

DOSY has extensively used in this PhD work, and will be discussed more in detail.
Diffusion-ordered spectroscopy (DOSY) NMR is a two-dimensional NMR experiment, in which the signal decays exponentially according to the self-diffusion behaviour of individual molecules. This leads to two dimensions; one dimension accounts for conventional chemical shift and the other for diffusion behaviour. Because the diffusion behaviour is related to properties of an individual molecule, such as size, shape, mass and charge as well as its surrounding environment, such as solution, temperature and aggregation state, each component in a mixture can be pseudo-separated, based on its own diffusion coefficient on the diffusion dimension. The strength of DOSY is that it can be used as a non-invasive method to obtain both physical and chemical information, in a very easy and cheap way.
The basis for diffusion measurements is the fact that magnetic field gradients can be used indirectly to label the position of NMR-active nuclei through their Larmor frequency. Stejskal and Tanner[66] have shown that the signal intensity for a single free-diffusing component is described in the case of rectangular pulse gradients by Equation 1.7, and gives Equation 1.8, where γ is the gyromagnetic ratio, G is the pulsed gradient strength, Δ is the time separation between the pulsed-gradients, δ is the duration of the pulse, and D is the diffusion coefficient.

$$I_{(2\tau,G)} = I_{(0,0)} \exp\left(\frac{-2\tau}{T_2}\right) \exp(-\gamma^2 G^2 \delta^2 (\Delta - \delta/3) D) = I_{(2\tau,0)} \exp(-\gamma^2 G^2 \delta^2 (\Delta - \delta/3) D) \quad 1.7$$

$$\ln\left(\frac{I_{(2\tau,G)}}{I_{(2\tau,0)}}\right) = -\gamma^2 G^2 \delta^2 (\Delta - \delta/3) D = -b\,D \quad 1.8$$

The product $\gamma^2G^2\delta^2(\Delta-\delta/3)$ is termed the b value. Thus, a plot of $\ln(I_{(2\tau,G)}/I_{(2\tau,0)})$ versus the b values for an isotropic solution should give a straight line, the slope of which is equal to –D. So, the attenuation of signal intensity can be used to obtain the diffusion coefficient value of the corresponding species. Diffusion sequences (PFGSE, STE, Figure 1.12) were introduced long before the advent of 2D NMR spectroscopy, but an important technical development at the beginning of the 1990s was that of diffusion ordered spectroscopy (DOSY), which was introduced by Johnson, Jr. and co-workers.[67]

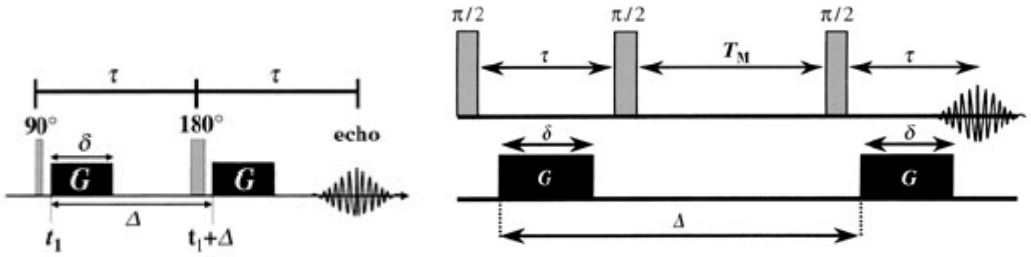

(a) PFGSE (b) STE

Figure 1.12 (a) PFGSE sequence; (b) STE sequence

The diffusion experiments presented above can be processed and displayed as a 2D matrix with chemical shifts plotted along one axis and diffusion coefficients plotted along the perpendicular axis (Figure 1.13). While the chemical shift information is obtained by fast Fourier transformation (FFT) of the time domain data, the diffusion information is obtained by an inverse Laplace transformation (ILT) of the signal decay data. The goal of the DOSY experiment is to separate species spectroscopically (not physically) present in a mixture of compounds. In this sense, the use of the DOSY experiment is reminiscent of the physical separation of compounds by chromatography. Thus, DOSY is also termed "NMR chromatography". Figure 1.13 illustrates this concept.

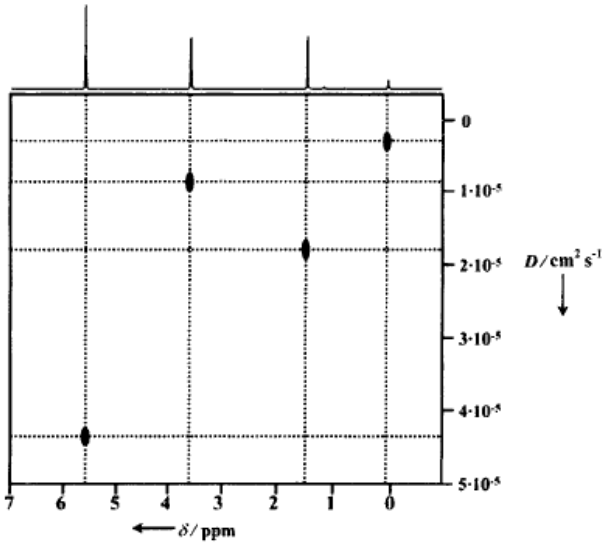

Figure 1.13. 2D DOSY spectrum showing four different species characterized by four different diffusion coefficients.

Each horizontal line represents a distinct diffusion coefficient and, hence, all the peaks on this horizontal line correlate with signals in the chemical shifts dimension, and should be attributed to a specific molecular species. At a certain frequency, where a continuum of diffusion coefficients should be considered, the data sets I(s), which describe the attenuation of this signal, should be described as Equation 1.9 ($\lambda = D(\Delta-\delta/3)$ and $s = \gamma^2G^2\delta^2$).

$$I(s) = \int_0^\infty a(\lambda)\exp(-\lambda s)\mathrm{d}\lambda \qquad 1.9$$

From Equation 1.9 it can be seen that I(s) is the Laplace transform of a(λ) and that a(λ) is the Laplace spectrum of the diffusion coefficients. Thus, the desired spectrum a(λ) is the inverse Laplace transform (ILT) of the decay function I(s). It should be noted that a perfect transform produces the Laplace transform of delta functions and the inverse transformation should therefore exist. The required situation is that a unique transformation will exist as in the case of the FT. However, there is no perfect transformation and the ILT may have more than one solution.
Hence, when running a DOSY experiment it is preferable that the diffusion coefficients differ as much as possible from one another and the standard errors in the diffusion coefficients be as marginal as possible. Analysis of complex samples with small differences in diffusion coefficients, or severely overlapping in the chemical shift dimension is still a big challenge for DOSY.[64,65]

It is well known that diffusion is closely related to molecular size, as seen from the Einstein–Smoluchowski equation (Eqn 1.10), where k_b is the Boltzmann constant, T is the absolute temperature, f is the so-called hydrodynamic frictional coefficient, N is Avogadro's number, and R is the gas constant.

$$D = \frac{k_b T}{f} = \frac{RT}{Nf} \qquad 1.10$$

For a sphere in a continuous medium of viscosity η, *f* is given by the Stokes Equation (Eq. 1.11). In this equation, r_s is the hydrodynamic radius, often called the Stokes' radius.

$$f = 6\pi\eta r_s \qquad 1.11$$

Combining Equations 1.10 and 1.11 leads to the familiar Stokes–Einstein equation (Eq. 1.12). It should be noted, however, that, different theories are needed to describe the hydrodynamic frictional coefficient *f* for molecular species of different geometries or with dimensions comparable with the Van Der Waals volume of the solvent and this will be discussed more in detail in the following chapters.

$$D = \frac{k_b T}{6\pi\eta r_s} \qquad .12$$

1.3.7.3 DOSY analysis of TMNPs in solution

A reference work[68] in characterization of ligand stabilized nanoparticles, in which DOSY analysis is proposed as method of measuring particle size, shows quite good prediction of the Stokes radius (or hydrodynamic radius) of thiol-capped gold particles in solution. The values are rather comparable to those obtained with other standard techniques. It should be noted that the radius obtained with DOSY is a core + shell radius, such as in STM measurements.
Despite this promising result, DOSY technique has been only little used in determining particle size in solution, essentially by the same authors. This method has been employed quite successfully for analysis of Au nanoparticles coated with linear alkylthiols[31], thiopronin[69] and ω-ferrocenyl-functionalized thiols[33b]. It should be underlined that the measured hydrodynamic cluster radius are less than the sum of the core radius and fully extended alkanethiolate chain length, suggesting that the ligand shell of dissolved clusters may be densely packed around the metal surface.[69]

1.4 TRANSITION METAL NANOPARTICLES IN CATALYSIS

The catalytic properties of transition metal catalyst, as colloids or supported nanoparticles have generated great interest over the past years.[21] In fact, these new catalysts often combine the precious characteristics of higher reactivity and selectivity. This can be explained by the structural specificities of the colloidal state of the catalyst: these materials have a very large specific surface, and consequently a large percentage of catalyst's metal atoms is available to the substrates. Thanks to their properties, it is obvious that these materials have been tested as catalyst for various kinds of reactions. Transition metal colloids are widely used as catalyst for hydrogenation of olefins. More recently, the range of reactions investigated has increased. Four classes of reactions will be considered: (i) hydrosilylation, (ii) oxidation, (iii) C-C coupling reactions, and (iv) selective hydrogenation.

1.4.1 HYDROSILYLATION REACTIONS

The hydrosilylation reaction (Scheme 1.9) is one of the most important ways to prepare silicone polymers and in general functionalized compounds containing C-Si bonds.

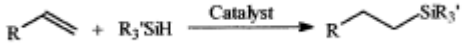

Scheme 1.9 hydrosilylation reaction of unsaturated substrates

Organometallic complexes with Co, Ni, Pd, or Pt and more recently Au were used in homogeneous phase to catalyze this reaction. However, these complexes are generally only precursors to the really active species: a colloidal suspension of metal

particles generated during an induction period.[21] With transmission electron microscopic observation, Lewis demonstrated the presence of Pt nanoparticles. These particles were generated by the reduction of organometallic complexes by silanes used as reagents. With these works in mind, Schmid[70] used Pt colloids and Pt/Au or Pt/Pd bimetallic colloids supported on alumina to catalyze the hydrosilylation of oct-1-ene with heptamethyltrisiloxane (HMTS). The final product was obtained with a good selectivity after 24 h. When the Pt/Pd colloids were used, the catalytic activity increased to raise 96% of conversion in 12 h. These colloids were recovered without major loss of activity by filtration of the support. Our group, recently showed that MVS derived AuNPs supported on Carbon shows lower activity but higher selectivity towards β-(E) product in terminal alkynes hydrosilylation than analogous Platinum based catalysts.[71]

1.4.2 OXIDATION REACTIONS

Most reactions catalyzed by metal colloids concern reduction reactions. Only a few, but increasing, examples of oxidation reactions were described in the literature. However, these reactions represent important industrial catalytic processes which may benefit of progresses in the field of nanoclusters catalysis.
For example, the synthesis of adipic acid, which is an essential intermediate for the preparation of Nylon 6 and Nylon 6,6, is industrially obtained by catalytic oxidation of cyclohexane with Cobalt (Scheme 1.10).[21]

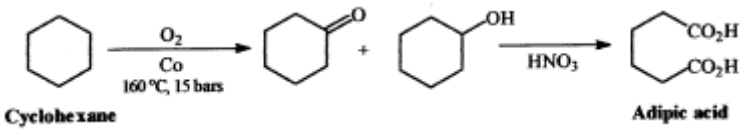

Scheme 1.10 Synthesis of adipic acid by catalytic oxidation of cyclohexane with Co NPs

The most interesting metal for oxidation reaction, at present, is without doubt gold, which only twenty years ago was still considered chemically inert.

1.4.2.1 CO oxidation

AuNPs catalyzed low temperature CO oxidation is the most relevant example of size dependent catalytic activity of nanoparticles and will be further examined in the next Chapter. Because of the importance of this reaction, which disclosed the way of all the gold catalyzed reactions, several reviews are dedicated to this topic.[72] To briefly resume all the studied carried out, the catalytic performances of gold catalysts markedly depend on the preparation methods and conditions because the following three factors define the genesis of unique catalysis by gold: strong contact between Au particles and the support, selection of the support, and the size of the Au particles.

1.4.2.2 Hydrocarbons oxidation

The oxidation of cycloalkane by tBHP catalyzed by transition metal colloids has been studied (Scheme 1.11).[73]

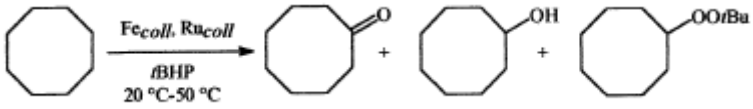

Scheme 1.11 TMNPs catalyzed oxidation of cycloalkanes

This reaction was performed under different conditions: with Fe nanoparticles in reverse microemulsions or with Ru colloids in biphasic water/organic media. The substrate cyclooctane was used as the organic phase, whereas the Ru nanoparticles were dispersed in the aqueous phase. This biphasic system allows the recycling of the aqueous phase containing the Ru particles without any loss of activity. After optimizing the reaction conditions, cyclooctanol and cyclooctanone were the main reaction products. Cyclohexane partial oxidation under oxygen catalyzed with MVS derived Cu catalysts deposited on various supports has been investigated very recently by our research group.[74] In this study is showed that for some Cu catalysts, depending of the nature of support, activity decrease with time because particles coagulate during reaction. This can be considered an evidence of particle size effect, simply ascribable to lowering of particle exposed surface.

Interest in partial oxidation of propene using Au-based catalysts was ignited by the discovery of selective epoxidation of propene by gold catalysts reported by Haruta et al. in 1998.[75] The selectivity for propene oxidation depends strongly on the nature of the metal oxide support and presence of H_2 and O_2 is necessary for high selectivity in propylene oxide. Only small, supported AuNPs (less than 5 nm in diameter) efficiently promote epoxidation of propene. The method used for supported catalyst preparation is also important.

1.4.2.3 Alcohol oxidation

Transition metals, both in homogeneous and in heterogeneous phase, are generally very active catalyst for selective alcohol oxidations. In particular, in the last years, interest in AuNPs and Au containing bimetallic systems for oxidation of alcohols to aldehydes is greatly increased.[76] These reactions often shows a size-dependent behaviour and will be discussed in the next Chapter.

1.4.3 C-C COUPLING REACTIONS

Cross coupling reaction for the formation of C-C bonds are generally performed with homogeneous Palladium complexes or salts as catalysts. However increasing attention has been paid to the use of heterogeneous systems, in order to improve the utilization of such reactions in fine chemistry. Moreover, it has been recently observed that in the usual experimental conditions of some coupling reactions (namely, Heck reaction), PdNPs are formed even if a mononuclear species of Pd is

used as precursor[77] and have a very important role in catalyst activity. Palladium is the metal of choice for this kind of reactions, even if very rare examples of other metal catalysts or alloys exists (see following sections).

1.4.3.1 Heck reaction

During the past decade, several groups have tried to use colloidal suspensions to catalyze Heck coupling reaction (Scheme 1.12).

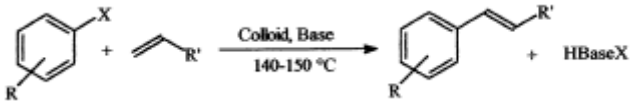

Scheme 1.12 Generic Heck reaction

Herrmann was the first to describe the use of Pd nanoparticles to catalyze this coupling reaction.[78] The Pd colloids were prepared by the Bonnemann's method and were stabilized by a quaternary ammonium salts: the tetraoctylammonium bromide. Reetz has also used Pd to prepare via their electrochemical process a colloidal suspension in propylene carbonate.[79] These nanoclusters were efficient to catalyze Heck coupling reactions at high temperature (160 °C). And finally, Antonietti,[80] Bradley,[81] Crooks[82] have respectively considered block copolymers (polystyrene-b-poly-4-vinylpyridine), poly(vinylpyrrolidone), or perfluorinated polyether-poly(propyleneimine) (PPPI) dendrimers to stabilize Pd nanoparticles used in Heck coupling reactions. In all cases, the catalytic activity observed during the Heck coupling depended on the substrate studied. Generally, a higher activity was observed when arenes are substituted with an electron-withdrawing group such as nitro or carbonyl. These observations are similar to those observed in the case of Pd molecular complexes. More investigations are required to determinate the true catalyst and to characterize it. Among these different suspensions, the colloids developed by Antonietti and Bradley seem to be the most interesting. In fact, these particles stabilized by a block copolymer have a higher thermal stability (at least 140 °C) and catalytic lifetime. MVS derived Palladium catalysts, supported on functional resins, such as Poly-(vinyl-4-pyridine),[83] or polyphospazene polymers (PDMP)[84] has been proved to be also useful for Heck reactions of aryl iodides with terminal alkenes or enines (Heck cascade cyclization). Such polymeric supports provide a high reusability of catalytic systems, strongly limiting metal leaching in solution and preserving particles from sintering.

1.4.3.2 Suzuki and Stille coupling

Reetz and co-workers have described the use of Pd or Pd/Ni nanoparticles as catalysts for the Suzuki coupling reaction (Scheme 1.13).[85]

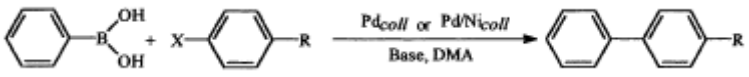

Scheme 1.13 Pd or Pd/Ni colloids catalyzed Suzuki coupling

The colloidal suspensions stabilized by tetrabutylammonium bromide, used as catalyst for the Suzuki reaction, were prepared by their electrochemical method and were redispersed in DMA. As for the classical Suzuki reaction, bromide derivatives showed a better activity than chloride derivatives. Moreover, the use of substrates with electron-withdrawing substituents increases the activity. Finally, bimetallic Pd/Ni colloids lead to a better conversion rate. Recently, El-Sayed describes the synthesis of palladium nanoparticles prepared in the presence of different stabilizers such as poly(amido-amine) dendrimers (PAMAM), block copolymer polystyrene-b-poly(sodium acrylate), poly(N-vinyl-2-pyrrolidone) and PVP. The effects of these stabilizers on the metallic nanoparticles stability and catalytic activity in the Suzuki reactions in aqueous solution have been investigated.[86] AuNPs catalyzed homocoupling of boronic acids has also been reported,[87] but this reaction is not very suitable for synthetic applications. As well, PdNPs catalyzed Stille and Sonogashira couplings has been performed.[88]

1.4.4 HYDROGENATION REACTIONS

The use of dispersed or immobilized transition metal nanoparticles as catalysts for hydrogenation reactions of terminal, internal, or cyclic olefins has been widely studied. In fact, transition metal colloids have recently shown good activities in chemo-, regio-, stereo-, or enantioselective hydrogenations of various substrates.

1.4.4.1 Selective hydrogenation of unsaturated aldehydes.

Selective hydrogenation of unsaturated aldehydes to form unsaturated alcohols is a crucial step for the preparation of several compounds used in fine chemistry and particularly for fragrances. Nevertheless, the reduction of carbonyl group in the presence of a double bound is not straightforward since most of the conventional catalysts reduce preferentially the double bond to give the saturated aldehyde. For example, Liu and co-workers achieved the reduction of cinnamaldehyde into cinnamic alcohol with Pt nanoparticles stabilized by PVP as catalyst (Scheme 1.14).[89]

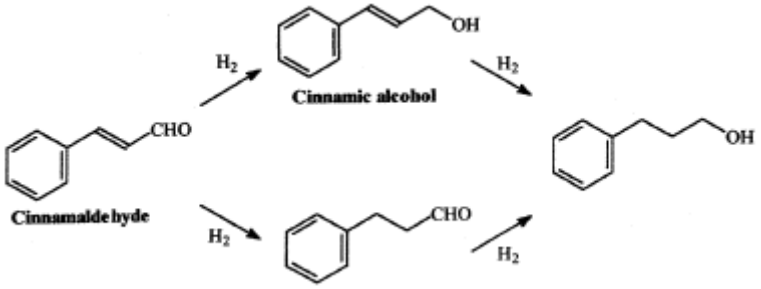

Scheme 1.14 Reaction pathway of Cinnamaldeyde hydrogenation

The reaction was performed under 40 atm of hydrogen and a selectivity of 12% in cinnamic alcohol was obtained after 38% conversion. Selectivity of 98.5% or 98.8% in cinnamic alcohol for 83% of conversion could be reached by addition of various

cations such as Fe^{3+} or Co^{2+}.[90] The authors proposed that an interaction between the cation and the oxygen of the carbonyl could facilitate the adsorption of the double bound on the metallic surface, thus justifying the activity and selectivity obtained with their Pt colloids (Figure 1.13).

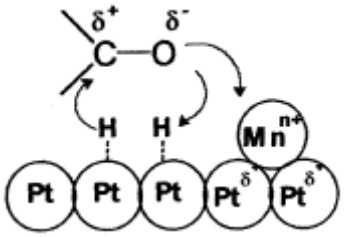

Figure 1.13 Schematic representation of cation effect in determining selectivity in unsaturated carbonyl compounds hydrogenation

Ru or Pt nanoparticles stabilized by PVP were employed as catalyst to achieve the hydrogenation of citronellal into citronellol (Scheme 1.15) with a selectivity of 95%.[91]

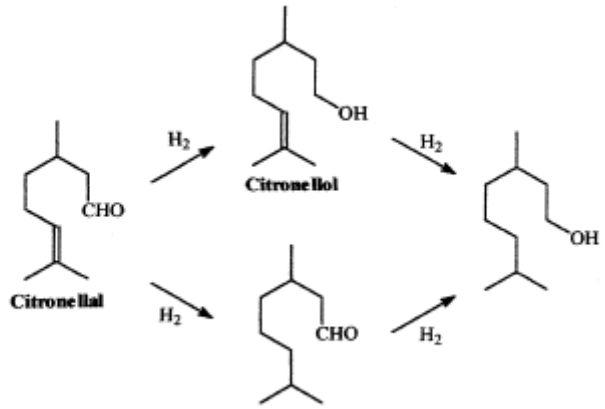

Scheme 1.15 Reaction pathway of Citronellal hydrogenation

The hydrogenation of citral (Scheme 1.16) was investigated with functionalized resin-supported MVS derived PtNPs catalysts (Figure 1.14).[92] Reaction proceed in mild conditions and selectivities towards the unsaturated alcohols geraniol and nerol are very good, and can be increased by addition of metal cations, even if in this last cases the reaction rate is lowered.

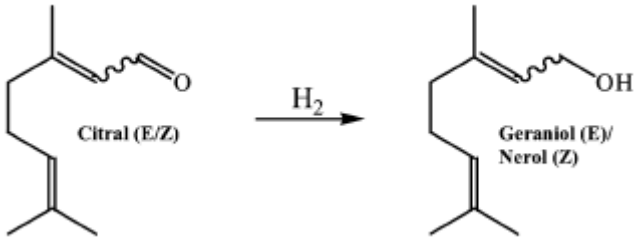

Scheme 1.15 citral hydrogenation to geraniol and nerol

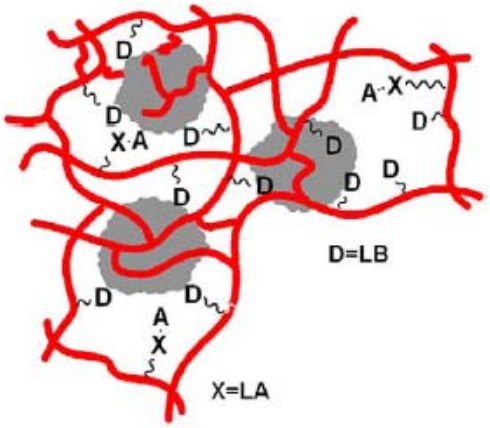

Figure 1.14: metal catalyst supported on functional resin. A: Lewis acid units (typically a metal ion); X: metal coordinating or ion-exchanging functions; D: Lewis base units.

1.4.4.2 Selective reduction of chloronitrobenzene.

Halogenated aromatic amines are important intermediates of the herbicide and pesticide chemistry. The classical approach to synthesize these compounds is based on the use of hydrochloric acid. An alternative reaction is to perform the selective hydrogenation of chloronitrobenzene with heterogeneous catalysts (Scheme 1.16). In such a process, it is necessary to reduce the nitro group without dehalogenation.

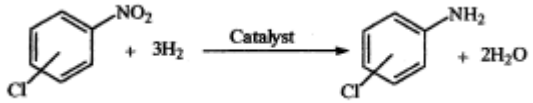

Scheme 1.16 catalytic reduction of Chloronitrobenzene

Several research groups tried to carry out this reaction with the help of transition metal colloids, especially bimetallic systems.[21] Generally, supported colloids were used. A size-dependent distribution of products has been found by our group in Platinum catalyzed Chloronitrobenzene hydrogenation and will be described in the next Chapter.

1.4.4.3 Enantioselective hydrogenations

The first example of asymmetric reaction made with colloidal particle was reported by Lemaire and coworkers. They described the hydrogenation of 2-methylanisoleor o-cresol trimethylsilyl ether. The asymmetric hydrogenation was induced by a chiral amine ((R)-dioctylcyclohexyl-1-ethylamine) which was also the protecting agent of the Rh particles (Scheme 1.17).[93] Nevertheless, ee values obtained were poor (~5%)

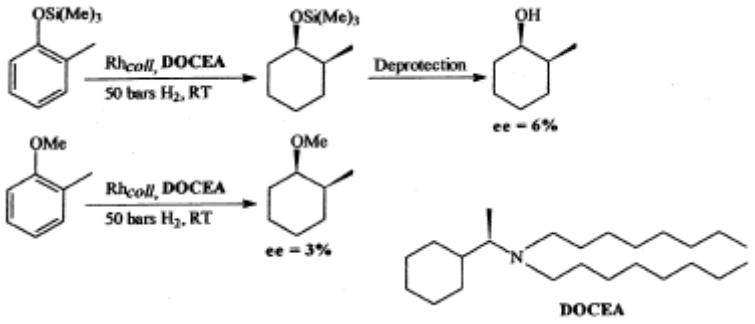

Scheme 1.17 First example of NPs catalyzed asymmetric hydrogenation

This concept of chiral stabilizing agent has been used by Bonnemann to hydrogenate ethyl pyruvate into ethyl lactate with Pt colloids. The nanoparticles were stabilized by a dihydrocinchonidine salt (DHCIN) and were used in liquid phase or immobilized on charcoal or silica. This system allows the hydrogenation of ethyl pyruvate into (R)-ethyl lactate with 75-80% ee (Scheme 1.18).[94]

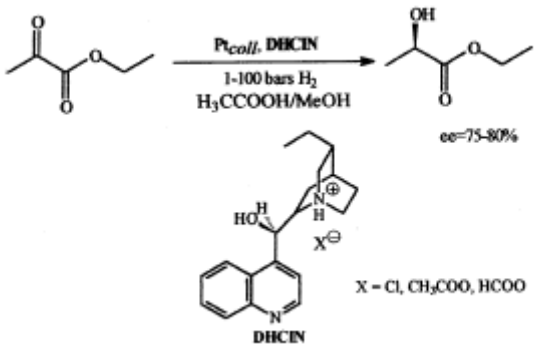

Scheme 1.18 PtNPs catalyzed asymmetric hydrogenation of ethyl piruvate

More recently, other reaction conditions appeared in the literature. Various ee values were stated for the hydrogenation of ethyl pyruvate catalyzed by Pt colloids stabilized by PVP and modified with cinchonidine (ee: 95-98%)[95] or catalyzed by solvent stabilized Pt and Pd nanoparticles prepared by metal vapor synthesis routes (ee: up to 30%).[96] In the last case, Whyman observed a reversed sense of the enantioselectivity (R)- vs (S)-enantiomer and an acceleration in reaction rate relative to the unmodified system.

1.5 REFERENCES

[1] Y. Wang, J. Zhang, X. Wang, J. Ren, B. Zuo, Y. Tang, *Topics in catal*. **2005**, 35, 35 - 41
[2] Ott, L. S.; Finke R. G. *Inorg Chem*. **2006**, *45*, 8382-8393
[3] K. J. Klabunde, *Free Atoms, Clusters and Nanoscale Particles*,. Academic Press, New York, 1994
[4] Ott, L. S.; Finke R. G. Coordination Chemistry Reviews **2007**, 251, 1075–1100
[5] A.S. Eppler, G. Rupprechter, L. Guczi, G.A. Somorjai *J. Phys. Chem. B*, **1997**, 101, 9973.
[6] Swihart, M. T. *Curr. Opin. Coll. Inf. Sci*. **2003**, *8*, 127-133
[7] Haruta, Cattech, **2002**, 6 (3), 102-115.
[8] Schmid, G. in *Nanoscale materials in chemistry* (see introduction, ref. 1c)
[9] See references in *Synthetic Approaches to Metallic Nanomaterials*, Richards, R; Bonnemann, H., Chapter 1 in *Nanofabrication Towards Biomedical Applications*. C. S. S. R. Kumar, J. Hormes, C. Leuschner (Eds.) Copyright **2005** WILEY-VCH Verlag Gmb H & Co. KGaA, Weinheim.
[10] J. S. Bradley, in: Clusters and Colloids (Ed.: G. Schmid), VCH, Weinheim, **1994**.
[11] Lewis, N. L.; Lewis, N. *J. Am. Chem. Soc.* **1986**, *108*, 7228-7231.
[12] Lewis, L. N.; Lewis, N. *Chem. Mater*. **1989**, *1*, 106-114.
[13] Larpent, C.; Brisse-Le Menn, F.; Patin, H. *New. J. Chem*. **1991**, *15*, 361-366.
[14] Larpent, C.; Brisse-Le Menn, F.; Patin, H. *J. Mol. Catal*. **1991**, *65,*35-40.
[15] (a) G. Schmid, R. Pfeil, R. Boese, et al., *Chem. Ber.* **1981**, *114*, 3634–3642; (b) H.-G. Boyen, G. Kastle, F. Weigl, B. Koslowski, C. Dietrich, P. Ziemann, J. P. Spatz,3 S. Riethmuller, C. Hartmann, M. Moller, G. Schmid, M. G. Garnier, P. Oelhafen, *Science*, **2002**, 297, 1533 - 36
[16] Aiken III, J. D.; Finke, R. G., *J. Mol. Cat. A: Chemical* **1999**, 145, 1 – 44
[17] (a) A. C. Curtis, D. G. Duff, P. P. Edwards, et al*., Angew. Chem. Int. Ed. Engl*. **1987**, 26, 676; (b) D. G. Duff, A. Baiker, P. P. Edwards, *Langmuir* **1993**, 9, 2301–2309.
[18] P. R. van Rheenen, M. J. McKelvey, W. S. Glaunsinger, *J. Solid State Chem*. **1987**, 67, 151–169.
[19] D. G. Duff, A. Baiker, in Preparation of Catalysts VI, ed. G. Poncelet, J. Martens, B. Delmon, P. A. Jacobs, P. Grange, Elsevier Science, Amsterdam, **1995**, 505–512.
[20] K.-L. Tsai, J. L. Dye, *Chem. Mater*. **1993**, 5, 540–546.
[21] A. Roucoux, J. Schulz, H. Patin, *Chem. Rev*. **2002**, 102, 3757-3778
[22] Hirai, H.; Wakabayashi, H.; Komiyama, M. *Chem. Lett*. **1983**, 1047.
[23] Mayer, A. B. R.; Antonietti, M. *Colloid Polym. Sci*. **1998**, 276, 769.
[24] (a) Balogh, L.; Tomalia, D. A. *J. Am. Chem. Soc*. **1998**, 120, 7355; (b) Esumi, K.; Nakamura, R.; Suzuki, A.; Torigoe, K. *Langmuir* **2000**, 16, 7842.
[25] Nakao, Y.; Kaeriyama, K. *J. Colloid Interface Sci.* **1986**, 110, 82.
[26] Bonnemann, H., Richards, R. M. *Eur. J. Inorg. Chem*. **2001**, 2455 - 2480.
[27] H. Modrow, S. Bucher, J. Hormes, et al., *J. Phys. Chem. B* **2003**, 107, 3684–3689.
[28] Viau, G.; Brayner, R.; Poul, L.; Chakroune, N.; Lacaze, E. Fiévet-Vincent, F., Fiévet, F. *Chem. Mater.* **2003,** *15,* 486-494
[29] Gittins, D. I.; Caruso, F. *Angew. Chem., Int. Ed*. **2001**, 40, 3001.
[30] M. Brust, M. Walker, D. Bethell, D. J. Schiffrin,, R.Whyman*, J. Chem. Soc. Chem. Comm*. **1994**, 7, 801
[31] M. J. Hostetler, J. E. Wingate, C.-J. Zhong, J. E. Harris, R. W. Vachet, M. R. Clark, J. D. Londono, S. J. Green, J. J. Stokes, G. D. Wignall, G. L. Glish, M. D. Porter, N. D. Evans, R. W. Murray, *Langmuir* **1998**, 14, 17-30
[32] Faraday, M. *Philos. Trans.* **1857**, 147, 145-181.
[33] (a) Chen, S.; Murray, R. W. *Langmuir* **1999**, 15, 682-689; (b) Hostetler, M. J.; Green, S. J.; Stokes, J. J.; Murray, R. W. *J. Am. Chem. Soc.* **1996**, 118, 4212-4213.
[34] Daniel, M. C.; Astruc, D. *Chem. Rev.* **2004**, 104, 293-346
[35] (a) Templeton, A. C.; Hostetler, M. J.; Kraft, C. T.; Murray, R. W. *J. Am. Chem. Soc.* **1998**, 120, 1906-1911. (b) Hostetler, M. J.; Templeton, A. C.; Murray, R. W. *Langmuir* **1999**, 15, 3782-3789.
[36] C. Burda, X. Chen, R. Narayanan, M. A. El-Sayed, *Chem. Rev.* **2005**, 105, 1025-1102
[37] Pileni, M. P. *J. Phys. Chem. C* **2007**, 111, 9019-9038
[38] (a) Boutonnet , M.; Kizling, J.; Stenius, P.; Maire, G. *Colloids Surf.* **1983**, 5, 209; (b) Eriksson, S.; Nylén, U.; Rojas1, S.; Boutonnet, M. *Appl. Catal. A.: General* **2004**, *265*, 207-219

[39] Tanori, J.; Pileni, M. P. *Langmuir* **1997**, 13, 639.
[40] Reetz, M. T.; Helbig, W. *J. Am. Chem. Soc.* **1994**, 116, 7401.
[41] Reetz, M. T.; Quaiser, S. A. *Angew. Chem., Int. Ed. Engl*. **1995**, 34, 2240.
[42] (a) Bradley, J. S.; Hill, E. W.; Behal, S.; Klein, C.; Chaudret, B.; Duteil, A. *Chem. Mater.* **1992**, 4, 1234.; (b) De Caro, D.; Bradley, J. S. *New J. Chem*. **1998**, 22, 1267.
[43] Duteil, A.; Queau, R.; Chaudret, B.; Mazel, R.; Roucau, C.; Bradley, J. S. *Chem. Mater*. **1993**, 5, 341.
[44] Chaudret, B.; Philippot, K. *C. R. Chimie* **2003**, 6, 1019–1034
[45] J.R. Blackborow and D. Young, Metal Vapour Synthesis in Organometallic Chemistry, Springer-Verlag, New York, 1979
[46] Benfield, F. W. S.; Green, M. L. H.; Ogden, J. S.; Young, D. *J. Chem. Soc., Chem. Commun.* **1973**, 866.
[47] Andrews, M.; Ozin, G. A.; Francis, C. G. *Inorg. Synth.* **1981**, *22*, 116.
[48] Klabunde, K. J.; Timms, P.; Skell, P. S.; Ittel, S. D. *Inorg. Synth.***1979**, *19*, 59.
[49] (a) Klabunde, K. J.; Ca´rdenas-Trevino, G. In Active Metals: Preparation, Characterization, Applications; Furstner, A., Ed.; VCH: New York, 1996; pp 237-278; (b) Klabunde, K. J. *Platinum Met. Rev*. **1992**, *36*, 80.
[50] (a)Lin, S. T.; Franklin, M. T.; Klabunde, K. J. *Langmuir* **1986**, *2*, 259; (b) Cardenas-Trivino, G.; Klabunde, K. J.; Brock Dale, E. *Langmuir* **1987**, *3*, 986.
[51] Klabunde, K. J.; Habdas, J.; Ca´rdenas-Trivino, G. *Chem. Mater.* **1989**, *1*, 481.
[52] Olsen, A. W.; Kafafi, Z. H. *J. Am. Chem. Soc.* **1991**, *113*, 7758.
[53] Zuckerman, E. B.; Klabunde, K. J.; Olivier, B. J.; Sorensen, C. M. *Chem. Mater.* **1989**, *1*, 12.
[54] (a) Klabunde, K. J.; Youngers, G.; Zuckerman, E. J.; Tan, B. J.;Antrim, S.; Sherwood, P. M. *Eur. J. Solid State Inorg. Chem.* **1992**, *29*, 227; (b) Kilner, M.; Mason, N.; Lambrick, D.; Hooker, P. D.; Timms, P. L. J. Chem. Soc., Chem. Commun. **1987**, 356.
[55] Bradley, J. S.; Hill, E.; Leonowicz, M. E.; Witzke, H. *J. Mol. Catal.* **1987**, *41*, 59.
[56] Cardenas, G. T.; Oliva, R. C. *Mater. Res. Bull.* **2000**, *35*, 2227.
[57] Wilcoxon, J. P.; Martin, J. E.; Provencio, P. *Langmuir* **2000,** *16,* 9912-9920.
[58] Finney, E. E.; Finke, R. G. *J. Coll. Int. Sci.* **2008**, *317*, 351-374.
[59] Toshima, N.; Yonezawa, T. *New. J. Chem*. **1998**, 1179-1201.
[60] J. P. Wilcoxon; B. L. Abrams Chem. Soc. Rev., 2006, 35, 1162–1194
[61] Balasubramanian, R.; Guo, R.; Mills, A. J.; Murray R. W. *J. Am. Chem. Soc*. **2005**, *127*, 8126-8132.
[62] C. Subramaniam, R. T. Tom, T. Pradeep J. Nanoparticle Res. **2005**, 7, 209–217
[63] Y. Negishi, Y. Takasugi, S. Sato, H. Yao, K. Kimura, T. Tsukuda *J. Am. Chem. Soc.* **2004**, 126, 6518-6519
[64] R. Huo, R. Wehrens, J. van Duynhoven, L.M.C. Buydens *Anal. Chim. Acta* **2003**, 490, 231-251.
[65] Cohen, Y.; Avram, L.; Frish, L. *Angew. Chem. Int. Ed*. **2005**, 44, 520 – 554.
[66] O. E. Stejskal, J. E. Tanner, *J. Chem. Phys*. **1965**, 42, 288 –292.
[67] Morris, K. F.; Johnson Jr., C. S. *J. Am. Chem. Soc.* **1993***,115,* 42914299
[68] R. H. Terrill; T. A. Postlethwaite, C.-H. Chen; C.-D. Poon, A. Terzis, A. Chen, J. E. Hutchison, M. R. Clark, G. Wignall, J. D. Londono, R. Superfine; M. Falvo; C. S. Johnson Jr., E. T. Samulski, R. W. Murray *J. Am. Chem. Soc.* **1995***,117,* 12537-12548.
[69] O. Kohlmann, W. E. Steinmetz, X.-A. Mao, W. P. Wuelfing, A. C. Templeton, R. W. Murray, C. S. Johnson, Jr. *J. Phys. Chem. B* **2001,** *105,* 8801-8809
[70] Schmid, G.; West, H.; Mehles, H.; Lehnert, A. *Inorg. Chem.* **1997**, *36*, 891.
[71] Caporusso A. M.; Aronica, L. A.; Schaivi, E.; Martra, G.; Vitulli, G.; Salvadori, P. *J. Organomet. Chem.* **2005**, *690*, 1063-1066.
[72] See, for example, Haruta, M. *Gold Bull*. 2004, 37, 27-35.
[73] Launay, F.; Roucoux, A.; Patin, H. *Tetrahedron Lett.* **1998**, *39*, 1353.
[74] C. Evangelisti, G. Vitulli, E. Schiavi, M. Vitulli, S. Bertozzi, P. Salvadori, L. Bertinetti, G. Martra *Catal. Lett*. **2007**, *116*, 57.
[75] Hayashi, T.; Tanaka, K.; Haruta, M. *J. Catal.* **1998**, *178* (2), 566-575.
[76] Hutchings, G. J. *Catal. Today* **2005**, *100*, 55–61.
[77] De Vries, J. G. *Dalton Trans.*, **2006**, 421–429.
[78] Beller, M.; Fischer, H.; Ku¨ hlein, K.; Reisinger, C.-P.; Herrmann, W. A. *J. Organomet. Chem*. **1996**, 520, 257.
[79] Reetz, M. T.; Lohmer, G. *Chem. Commun.* **1996**, 1921.

[80] Klingelho¨fer, S.; Heitz, W.; Greiner, A.; Oestreich, S.; Fo¨rster, S.; Antonietti, M. *J. Am. Chem. Soc.* **1997**, *119*, 10116.
[81] Le Bars, J.; Specht, U.; Bradley, J. S.; Blackmond, D. G. *Langmuir* **1999**, *15*, 7621.
[82] Yeung, L. K.; Crooks, R. M. *Nano Lett*. **2001**, *1*, 14.
[83] Caporusso, A. M.; Innocenti, P., Aronica, L. A.;Vitulli, G.; Gallina, R.; Biffis, A.;Zecca*, M.;* Corain, B. *J. Catal*., **2005**, 234, 1–13
[84]Panziera, N.; Pertici, P.; Barazzone, L.; Caporusso, A. M.; Vitelli, G.; Salvadori, P.; Borsacchi, S.; Geppi, M.; Veracini, C. A.; Martra, G.; Bertinetti, L. **J. Catal**., **2007**, *246*, 351-361.
[85] Reetz, M. T.; Breinbauer, R.; Wanninger, K. *Tetrahedron Lett.***1996**, *37*, 4499.
[86] Li, Y.; El-Sayed, M. A. *J. Phys. Chem. B* **2001**, *105*, 8938.
[87] H. Tsunoyama, H. Sakurai, N. Ichikuni, Y. Negishi, T. Tsukuda *Langmuir* **2004,** *20,* 11293-11296.
[88] M. Moreno-Manas, R. Pleixats Acc. Chem. Res. **2003,** 36, 638-643.
[89] Yu, W.; Liu, H.; An, X.; Ma, X.; Liu, Z.; Qiang, L. *J. Mol. Catal.* A: Chem. **1999**, 147, 73.
[90] Yu, W.; Liu, H.; Liu, M.; Tao, Q. *J. Mol. Catal. A: Chem.* **1999**, *138*, 273.
[91] Yu, W.; Liu, M.; Liu, H.; Ma, X.; Liu, Z. *J. Colloid Interface Sci.* **1998**, *208*, 439.
[92] Centomo, P.; Zecca, M.; Lora, S.; Vitulli, G.; Caporusso, A.M.; Tropeano, M.L.; Milone, C.; Galvagno, S.; Corain, B. *J. Catal*. **2005**, *229*, 283–297.
[93] Nasar, K.; Fache, F.; Lemaire, M.; Beziat, J. C.; Besson, M.; Gallezot, P. *J. Mol. Catal.* **1994**, *87*, 107.
[94] Bonnemann, H.; Braun, G. A. *Angew. Chem., Int. Ed. Engl.* **1996**, *35*, 1992.
[95] Kohler, J. U.; Bradley, J. S. *Langmuir* **1998**, *14*, 2730
[96] Collier, P. J.; Iggo, J. A.; Whyman, R. *J. Mol. Catal. A: Chem*. **1999**, *146*, 149.

CHAPTER 2

INVESTIGATIONS OF GROWTH MECHANISMS OF TRANSITION METAL NANOPARTICLES AND INFLUENCE OF PARTICLE SIZE IN CATALYTIC BEHAVIOUR

"It isn't that they can't see the solution. It is that they can't see the problem."

Gilbert K. Chesterton

2.1 INTRODUCTION

One of the most important and difficult challenges in modern nanoscience is the development of a reproducible synthesis of particles with desired size, shape and dispersity. In the main field of application of TMNPs, catalysis, the importance of these parameters in determining catalysts activity and selectivity has been recognized. In Chapter 1 we resumed the various synthetic approaches to TMNPs, which in some cases can be performed with a certain control over particle size. It is quite clear that a designed synthesis of nanoparticles characterized by pre-selected size, requires the complete knowledge of the processes which governs the formation of nanoscaled phases starting from given precursors. These processes are often very complexes and not completely understood, and an exhaustive theoretical study is generally unfeasible. Moreover, the great variety of preparation methods, make very difficult to find a general theory, because each case has to be treated separately. It is evident that synthesis in different medium (homogeneous solutions, two-phase systems, microemulsions, gas phase and so on) or starting from different materials (metallic salts, zerovalent organometallic complexes, metal vapours and so on), cannot be faced safely with the same approach.
In 1997, Finke[1] reviewed the works appeared in literature concerning the study of nucleation and growth of nanoparticles and he observed that "*The state of modern mechanistic investigations of nanoclusters formation is even more primitive*". This is particularly true for transition metal nanoparticles, where supersaturation classical theories doesn't seems to work[1] and typical phenomena such as Ostwald ripening are not clearly observed. However, various empirical methods to successfully control the cluster size during nanoparticles synthesis has been published, even if mechanism has not been satisfactorily elucidated. In the following sections, we will describe both theoretical and experimental approaches to the problem of size control in transition metal nanoparticles synthesis.

2.2 TRANSITION METAL NANOPARTICLES NUCLEATION AND GROWTH STUDIES

The greatest flaw of classical nucleation theory (CNT),[2] which basic principles are described in section 1.1, is that it treats nuclei as bulk material having macroscopic properties. The key assumptions involved here are that (i) the nucleus behaves as the bulk, and (ii) the surface free energy of the cluster is the same as that of an infinite planar surface.[3] Both of these assumptions become unreasonable when considering a nucleus of only several (or even several hundred) atoms or molecules; the center of the cluster is far from the thermodynamic limit, and the sharp curvature of the cluster significantly increases the free energy of its surface. Accurate definitions and values of surface energy γ are unavailable for small nuclei vs bulk material. An attempt to solve this problem has been made by Sugimoto et al., who formulated an expression for the solid–liquid interfacial energy,[4] and then used their formulation to calculate the value of γ for silver halide particles. Their result is shown in Eq. 2.1

$$\gamma = -N^{\sigma} \lambda k_{\mathrm{B}} T \ln x_{(\infty)} \qquad 2.1$$

where N^{σ} is the surface density of surface monomers (a "monomer" in the case of AgX clusters studied here is defined as a single AgX unit, where X = Cl, Br, I), λ is the ratio of open sites on a surface monomer to that of a free monomer, k_B is the usual Boltzmann constant, T is the temperature, and $x_{(\infty)}$ is the solubility of the bulk material given by the mole fraction of monomers in the liquid phase. The authors were able to use textbook values for the AgX crystals, such as the lattice parameter and molar volume, to calculate γ for the clusters. They also showed theoretically that γ is independent of the size of the cluster, and then verified this experimentally.[5]
Many experimental procedure has been developed starting from nucleation and growth theories, with quite good results in terms of control over particle size and distribution, even if these theories are still incomplete and generally not applicable to real systems, because of their actual complexity that requires very strong assumptions.

2.2.1 LAMER MECHANISM FOR SULPHUR SOLS

The first and most cited work on experimental application of theoretical studies on colloids formation mechanism, was performed in the 50s' by LaMer.[6] He developed a theory based on supersaturation and diffusion controlled growth of particles, starting from his experience on precipitation of sulphur sols. The LaMer mechanism predicts that as the colloid precursor is consumed, its concentration falls below supersaturation, and hence no more nucleation takes places thereby achieving the needed key separation of nucleation and growth in time that is required for the formation of a near-monodisperse size distribution (Figure 2.1). Regardless of whether or not the LaMer mechanism is correct in a given case, this separation of nucleation and growth in time is a key for all non-physically restricted (e.g., non-micellar) syntheses of near monodisperse nanoclusters.

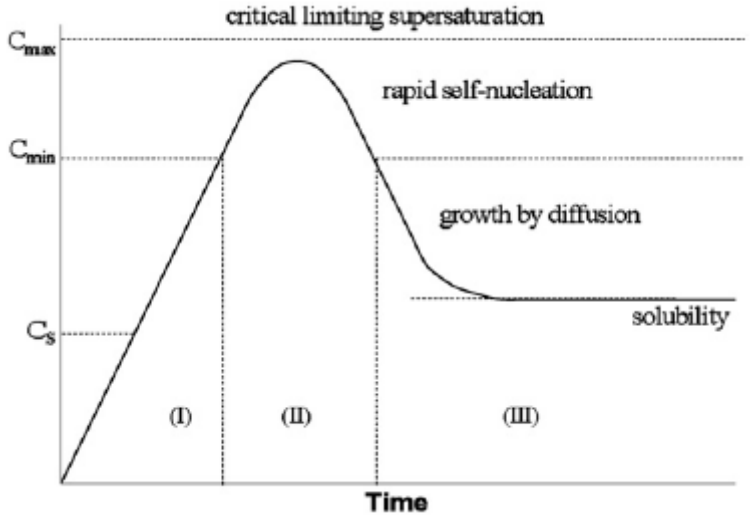

Figure 2.1 LaMer diagram of supersaturation.

The LaMer mechanism has been widely applied in various preparations of near-monodisperse particles in homogeneous solutions,[7] yet success is often achieved only following tedious, trial-and-error attempts tuning the main variables, such as the concentration of reactants. Generalizations between preparations are few, and the range of possible variations within each preparation is often small; hence, each new colloidal particle requires what is tantamount to a new synthetic strategy. It is also now believed that the LaMer mechanism is, as a mechanistic chemist would expect, rigorously appropriate only to the system it was developed for: sulphur sols, and other, closely analogous systems. This can explain why others have referred to the LaMer mechanism as "overcited"[7] (perhaps much fairer to LaMer's pioneering work would be the term "inappropriately cited"),[1] a phenomenon which really only points to the dearth of new, broadly applicable and kinetically verified alternative mechanisms in the intervening nearly 50 years.

2.2.2 TURKEVICH MECHANISM FOR GOLD SOLS

If the LaMer mechanism is of historical importance in nanoparticles nucleation and growth studies and seems to be, at least conceptually, suitable for several nanostructured systems, his validity for transition metal nanoparticles formation has been criticized.[1,8] Turkevich firstly proposed for citrate stabilized aqueous gold colloids obtained by salts reduction,[8] an "organizer" mechanism, to explain the marked temperature dependence of the rate of nucleation, hard to understand from the point of view of a supersaturation-based mechanism. In his "organizer theory," various species in the reaction solution bind to the gold ions to form "copolymers" of gold ion and the "organizer." The "organizer" in this case was proposed to be the citrate ion, which would become oxidized to acetonedicarboxylic acid upon reduction of the gold ions. Further evidence presented for this process was that when acetonedicarboxylic acid was added to chloroauric acid instead of citrate, the nucleation curve did not show an induction period. Therefore, the induction period was proposed to be the time that is necessary for the citrate ion to become oxidized to acetonedicarboxylic acid, which rapidly reduces the gold ions to Au^0. It is now

believed that induction period was actually due to the formation of critical nuclei.[1] Moreover, Turkevich observed that in the case of his gold colloids, growth rate was *directly* proportional to the particle size, in complete disagreement with a diffusion controlled growth and that the rate curve had an unusual sigmoidal form: an induction period, a very fast rise in the number of nuclei, a slowing down of nuclei formation and finally, a cessation of the nucleation process, although the starting reagents were still present (Figure 2.2).

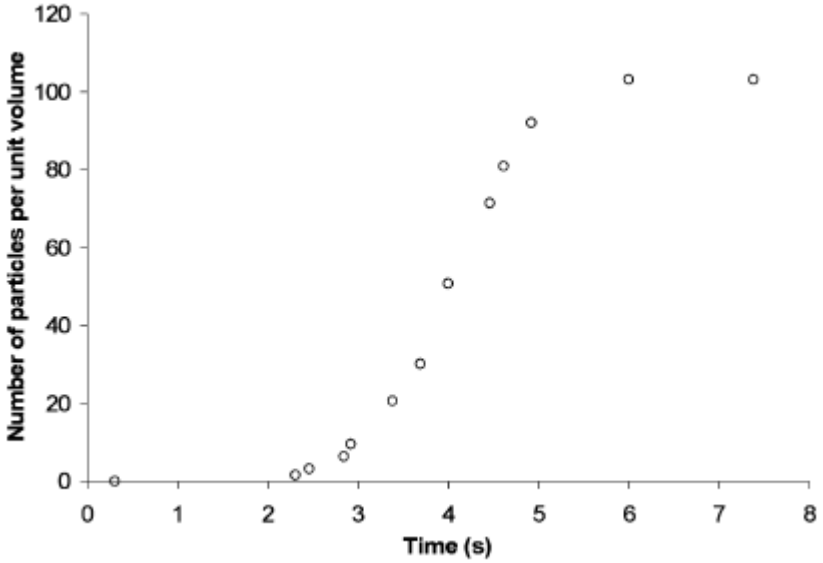

Figure 2.2 Nucleation curve for the reduction of $HAuCl_4$.

The "organizer" model, while obscure in its chemical details in comparison to LaMer's straightforward, 2-step mechanism, is experimentally well-supported and was a step toward a more relevant mechanism for the formation of transition-metal nanoclusters. However, Turkevich's mechanism uses only words to describe the nanocluster nucleation and growth process. Restated, the "organizer" model lacks precise chemical equations that sum to the observed stoichiometry and which define the rate constants of the nucleation and growth steps, keys to a more detailed mechanistic understanding of the nanocluster formation process.

2.2.3 FINKE MECHANISM FOR TRANSITION METALS

A very similar idea was successively (more than 40 years later!) developed by Finke, in his series of paper[1,9] on polyoxoanion stabilized Iridium and Platinum nanoclusters (see also section 1.2.1.1). In the initial studies, he proposed and widely discussed a mechanism characterized by a slow and continuous nucleation step, which occurs far from the supersaturation regime, followed by a fast autocatalytic surface growth, not controlled by diffusion. The kinetics of nanocluster nucleation and growth are measured using the reporter reaction of cyclohexene hydrogenation, what is actually measured is the loss of hydrogen during NPs formation and growth. In this way, in situ/operando kinetic measurement of the nanocluster nucleation and growth is achieved, yielding well-defined rate constants k_1 and k_2 for nucleation and growth,

respectively. The rate constants k_1 and k_2 are, necessarily, averages. The separation of nucleation and growth in time, necessary for narrow size distributions, is achieved in Finke's system as seen visually by the induction period followed by fast cyclohexene loss in the overall sigmoidal curve (Figure 2.3).

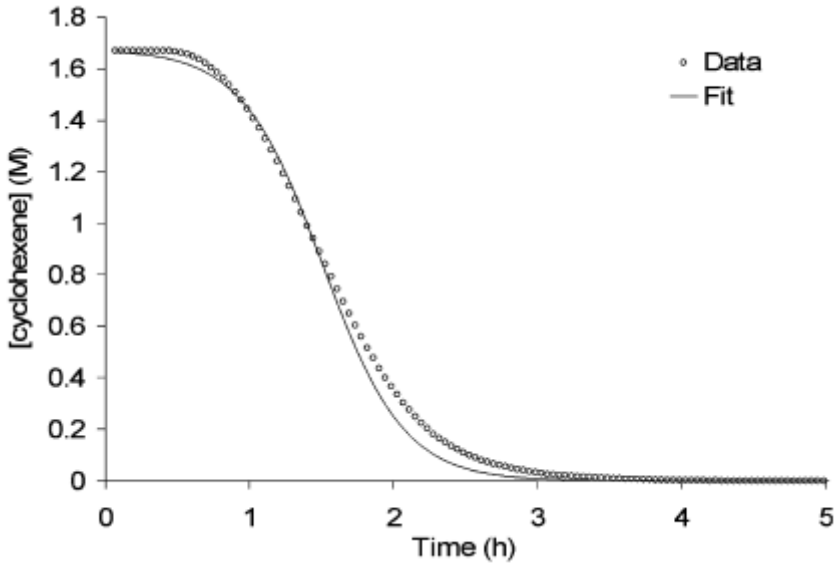

Figure 2.3 Typical cyclohexene loss vs time curve and curve-fit for the reduction of $[Bu_4N]_5Na_3[(1,5\text{-COD})Ir{\cdot}P_2W_{15}Nb_3O_{62}]$ under H_2. When some deviations vs the experimental data are seen, as in the above, deliberately chosen example of one of the poorer fits, these can often be quantitatively accounted for by a 3- or 4-step mechanism, vide infra.

The ratio of growth and nucleation rates, *R* (Eqn 2.2) can be used to determine the level of kinetic control over nanocluster formation.[1] Faster growth compared to nucleation, giving a higher value of *R*, ensures that growth of existing nuclei dominates over the formation of new nuclei, thereby achieving near-monodisperse (defined as ± ≤15% size distribution) nanoclusters. The $k_2[B]/k_1$ ratio is also a predictor of nanocluster size, smaller values correlating with smaller nanoclusters and larger values with larger nanoclusters.

$$R = \frac{\text{growth rate}}{\text{nucleation rate}} = \frac{k_2[\text{A}][\text{B}]}{k_1[\text{A}]} = \frac{k_2[\text{B}]}{k_1} \qquad 2.2$$

An important synthetic insight gained from the autocatalytic mechanism is the need to avoid heterogeneous nucleation when forming nanoclusters.[9c] Heterogeneous nucleation of metal on solid surfaces is often energetically more favorable (lower ΔG) than homogeneous nucleation.[2] In addition, since heterogeneous nucleation is often highly variable, reproducible nanocluster formation is not possible in the presence of heterogeneous nucleation. Since the initial reports of the 2-step, autocatalytic mechanism for nanocluster formation, a more general mechanism for transition-metal nanocluster formation has been described for Bu_3N stabilized Platinum nanoparticles, which includes nanocluster agglomeration, adding a third,

bimolecular agglomeration step[9d] and then, very recently, adding a fourth, autocatalytic agglomeration step.[9e,f] In these new steps, C represents larger, approaching-like metal particles, Scheme 2.1. The kinetic model proposed by this author seems to be quantitatively applicable to Turkevich's gold sols, as well as to others TMNP based systems.[10]

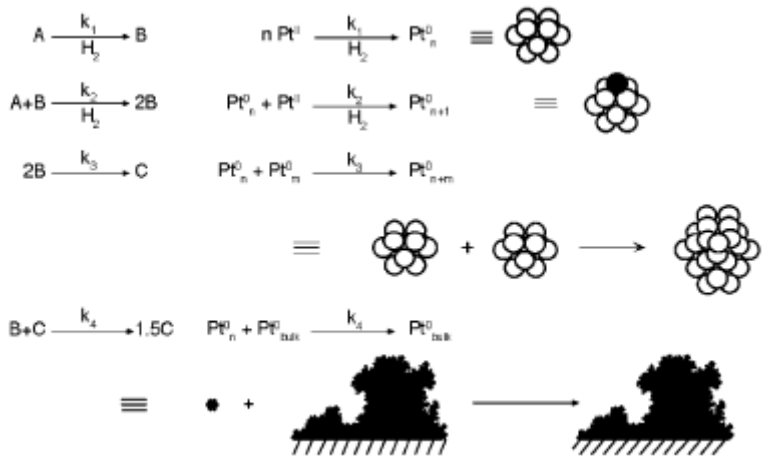

Scheme 2.1 Finke's mechanism of TMNPs growth

In the Finke–Watzky mechanism of slow nucleation and autocatalytic growth, the induction period is the time during which nucleation events are occurring, the formation of the critical nucleus, according to classical nucleation theory.[2] The rate constant k_1 is the nucleation rate constant, and the critical nucleus is the size of the cluster at the end of the induction period, when the clusters begin to grow and hence survive long enough to become catalytically active. Measurement of the size of the clusters at this point in the reaction should provide some idea about the number of atoms in the critical nucleus, which can then be compared to the number of atoms in the critical nucleus predicted by theory. Based on the GLC data for the hydrogenation of cyclooctadiene, for the $Ir^0{\sim}_{300}$ nanocluster system an upper limit of the critical nucleus was estimated as Ir^0_{15}.[1]

2.2.4 GROWTH STUDIES ON TMNPS PRODUCED BY MVS

Among the various vapour phase condensation processes to synthesize TMNPs, MVS is the less studied from the point of view of growth mechanisms, because it involves a very complex particles formation pathway, which starts in the gas phase, continues in a solid mixture, and finally ends in liquid solutions, in which the temperature is not kept constant (see description, section 1.2.5). Some very qualitative consideration has been made, however, about the single steps of particles formation.[11]

2.2.4.1 Gas phase

From energetic considerations, it is probable that MVS experiments concerning transition metal involve only atoms in the electronic ground state. In the MVS

standard conditions over 99% of the vapour is monoatomic and it is to be expected that *initial* condensation of metal vapours with substrates involves monoatomic species, because the mean free path of atoms is usually much larger than the dimensions of MVS apparatus. The existence of monoatomic metal species in inert gas matrices has been established. There is, however, considerably uncertainity as to the state of a matrix surface under conditions of continuous condensation and is therefore fallacious to assume that all the metal atoms maintain their integrity during co-condensation.

2.2.4.2 Co-condensation phase

The interaction of a metal with its surrounding matrix atoms represent the first "fixing" of the atom after traversing the quasi-fluid matrix surface zone where most of the kinetic energy is adsorbed. The reactive substrate is either the matrix material itself or material co-condensed within the matrix. Chemical interaction between some metal atoms and solvent may be immediate or commence only after a warm-up period, depending on the activation energy and bulk diffusion rates. To avoid metal aggregation, high substrate/metal ratio are ideally necessary.
Kinetic models have attempted to describe the processes of diffusion in the fluid surface zone of the matrix during deposition. Aggregation is diffusion controlled, so the Temperature can be effectively ignored. A further variable, that of a reactive substrate, may be introduced. The reactions which take place in the "reaction zone" may be then represented by the network depicted in Scheme 2.2.

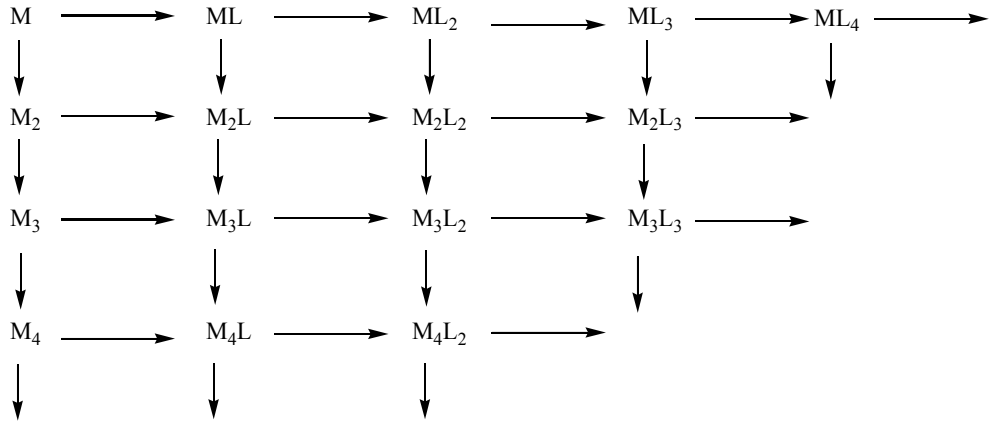

Scheme 2.2 Network of metal clusters formation in the "reaction zone"

It is assumed that only the metal atoms M and the solvent (or ligand) L can diffuse, so only two rate constant k_M and k_L are needed to describe the system. The system can thus be described mathematically by two models: a quenched reaction model, that assumes diffusion of M and L for a certain time after which the reaction is completely frozen out in the lower layers of the matrix; a steady state model, in which is assumed that concurrent deposition and freezing out of the matrix give rise to steady state conditions. Experimentally, the quenched reaction model gives a reasonable fit for various concentration of M; while the steady state model is increasingly inappropriate for increasing concentrations of M.[11]

2.2.4.3 Rigid matrix phase

Once any reaction product or unreacted species has lost all its excess energy it will be "frozen" into the underlying bulk co-condensate or rigid matrix zone. The convenient liquid nitrogen coolant bath used in most metal evaporation syntheses in order to quench the substrate vapour pressure, also cools the bulk co-condensate to a temperature sufficiently low to reduce species mobility within the matrix to a negligible amount. Individual species are unlikely to meet reaction partners, thus very little reaction can take place. For a given matrix, bulk diffusion effectively stops below the Tammen temperature (see section 1.2.5). To a good approximation, species trapped in a host matrix lose their mobility at the same temperature as the host material, though very small, light species such as atoms or dimers retain some mobility. Unreacted metal atoms may still be able to diffuse but because of the high solvent/metal ratio normally used, they have every chance to react with solvent, providing the activation energy does not exceed the available energy: otherwise the very low activation process of agglomeration to metal clusters will occur.

2.2.4.4 Fluid matrix phase

This stage can be short or long depending on the solvent mp and the bulk deposition temperature, usually 77 K (nitrogen b.p.). Initially the warming will have similar effect as that of annealing; i.e. diffusion of the mobile species. However, as the Tammen temperature is reached, less mobile species will begin to diffuse. Thus any species which owed their existence to effective isolation in the rigid deposit will be converted to new, more stable products or metal aggregates. At this stage metal particles nucleate and begin to grow. In addition, a whole series of new reactions with previously prohibitively high activation energy may occur with rising temperature. Such reactions may also occur in the solution phase.

2.2.4.5 Solution phase

Although much chemistry may have occurred on co-condensation or on warming the co-condensate further chemistry is likely when the cocondensate melts. All species are now mobile and as the temperature rises, new reactions and further agglomeration of metal cluster become possible. The technique of trapping by adding further ligand precursors has proven to be a useful method of isolating stoichiometric derivatives of compounds which may be themselves to be sensitive for isolation. It is likely that metal aggregates may grow with time in stored solutions. The trapping method could be in principle feasible to isolate stable clusters of different sizes, as their size increases gradually by coagulation, aggregation and agglomeration until powders precipitate from the solution.

2.3 OPEN QUESTIONS IN MECHANISTIC STUDY OF NANOPARTICLES NUCLEATION AND GROWTH

2.3.1 CONSIDERATIONS ABOUT REDUCTION STEP

One unanswered question is: what steps does the metal undergo in going from an ion in a salt to a zero-valent atom in a nanocluster? A number of hypotheses can be put forward, including: (i) Under H_2 reduction conditions, metal hydrides are a key to the nucleation process, $M_xH_y^{n\pm}$; (ii) The reduction of metal ions and removal of ligands is followed by nucleation of neutral, but highly energetic, M^0 atoms, presumably highly ligated ones so as to be meta-stable;[1,9b] (iii) The nucleation of metal ions, with some of their associated ligands, is followed by reduction of the overall cationic cluster, $M_xL_y^{n\pm}$; (iv) Some combination of the previous hypotheses. Experimentally supporting or disproving these hypotheses is a major challenge in understanding the nucleation of TMNPs. There is currently disagreement in the literature as to whether metal reduction to M^0, or critical nucleus formation to different species, occurs first.[9b,12] While the nucleation mechanism likely depends on reaction conditions, a more complete, more general picture of what happens during the nanocluster nucleation and growth processes does not exist at this time. The process of how nucleation occurs was considered in some detail in the work of Finke et al.[9] The high energy of free Ir^0 atoms is apparent when one considers that the ΔH_{vap} of Ir is 159 kcal/mol, which shows that free Ir^0 is very unstable thermodynamically in comparison to bulk Ir^0_n formation. As first noted there, this suggests one of two possibilities: first, that if single Ir^0 atoms are formed during the nucleation process to make Ir^0–Ir^0 bonds, then they must be stabilized by coordination by solvent, anionic ligands ($P_2W_{15}Nb_3O_{62}^{9-}$ in that system), or other ligands present, such as olefins. Alternatively, Ir–Ir bond formation may occur with at least one Ir atom still in a higher oxidation state (i.e., Ir^I–Ir^I or Ir^I–Ir^0), followed by reduction to all Ir^0_n. Restated, given that the formation of free (i.e., unsolvated or unligated) M^0 atoms in the nucleation process is thermodynamically disfavored, the remaining issues are: (i) when reduction takes place (as the final oxidation state of the metal in the nanocluster is M^0), and (ii) what are the roles of hydrides and other ligands in the nucleation process. Overall, it seems likely that nucleation has more of an "inner-sphere" nature than is represented, for example, in purely "outer-sphere," hard-sphere Monte Carlo simulation.[13] Henglein and coworkers have used thermodynamic arguments and absorption spectroscopy to propose the formation of Pt^I intermediates in the aqueous reduction of $[PtCl_4]^{2-}$ by hydrogen.[12] Pt^0, Pt–H, and Pt_2^0 hypotetic intermediates were dismissed on the grounds of high ΔG of reaction (70.3, 42.0, and 64.1 kcal/mol, respectively). These arguments appear to be flawed, however, as they assume completely bare Pt atoms or ions without ligation from any of the other species present. Henglein et al. reached a similar conclusion for the formation of Pd^0 colloids by radiolysis of Pd $(NH_3)_4Cl_2$.[14]

2.3.2 CONSIDERATIONS ABOUT PARTICLES STABILIZATION BY ORGANIC LIGANDS

A key factor in nucleation and growth studies on nanoparticles is given by stabilization. Since particles in solution are generally produced in presence of suitable stabilizing ligands, interaction between forming particles become very

complicated. Smoluchowski theory[2,15] makes the strong assumption that there's no energetic barrier in particles coagulation, so every collision between particles, governed by diffusion, results in coagulation. This has been proved to work well only for fast coagulating systems.[8b] To describe the kinetics of slow coagulation, Smoluchowski merely introduced a rate-reducing factor in his equations without going further to consider how this factor depended on the nature of the colloid and on the type and concentration of the electrolyte. When the Smoluchowski theory was applied to slow coagulation, however, it was found that the actual mechanism of this process was too complex to be accounted for by the theory. Such attempts have shown that in the course of coagulation the rate falls off much faster than the theory predicts.[8b] In some cases it has been observed that coagulation even stops completely at a certain stage.
DLVO theory (section 1.1) introduce an electrostatic interaction potential U(r) between the particles (assumed to be charged, obviously) for two spheres of radius *a* with constant surface charge *Z* separated by a center-to-center distance *r* in a fluid of dielectric constant ε:

$$U(r) = \frac{Z^2 e^2}{\epsilon} \left[\frac{\exp(\kappa a)}{1+\kappa a}\right]^2 \frac{\exp(-\kappa r)}{r} \qquad 2.3$$

where κ is the inverse of the Debye layer (1/κ), defined as: $\kappa^2 = 8\pi e^2 Z^2 C_\infty / \varepsilon kT$, in which C_∞ is the bulk concentration of the electrolyte. DLVO is often used to qualitatively explain the stability of nanoparticles in solution, but quantitative studies are neglected in nanoparticles literature.
In fact, growth studies concerning TMNPs synthesized in presence of strong ligand (as in the Brust-Schiffrin method, see section 1.2.1.4), are very rare and mostly empirical.[16]

2.3.3 FINAL REMARKS ON NUCLEATION THEORY

Although nucleation in general has been extensively studied, the high levels of accuracy and precision that are enjoyed by other fields of science remain elusive in the study of nucleation. A general shortcoming of nucleation theory is that much of the theory comes from fitting experimental data and adjusting theoretical parameters accordingly. As a result the theory in general has little predictive power.[17] Therefore, a main goal of nucleation theory is to improve the accuracy of the theory to better match, and then accurately predict, experimental observations. The large gap between a theoretical (mathematical) understanding of nucleation and an experimental (physical) understanding is a gap that is only recently being bridged by physicists and physical chemists. Closer agreement between theory and experiment is, therefore, a goal of nucleation science.
As a general conclusion we can say that to produce small and narrowly dispersed nanoparticles, the nucleation process must be relatively fast while the growth process remains relatively slow. The formation of particles with a narrow size distribution further requires that the nuclei of all species present form simultaneously and without subsequent nucleation of smaller particles. The major progresses in literature about

control over nanoparticles size during their synthesis, are still mostly empirical (see section 1.2).

2.4 PARTICLE SIZE EFFECTS IN TMNPS[18]

About two-thirds of the chemical elements are metals, which means that the electronic situation found in a metal is very common. Non-metals preferably form covalent bonds between each other, especially between atoms of the same elemtn, with the aim of achieving a noble gas electronic configuration. In some cases the combination of only two atoms is sufficient to achieve that state, as in H_2, N_2, O_2, F_2. etc. Other elements, such as carbon and phosphorous, build up infinite lattices to produce stable electronic configuration, as is known from graphite and diamond or red and black phosphorous. We understand these elementary structures and bonding situations as the most economical way to attain noble gas configurations. However, the fewer valence electrons an atom has the more difficult is to find a simple solution. Boron is an illustrative example of how complicated the relationship between identical atoms may become if the formation of simple covalent σ- and π-bonds does not result in noble gas-like situations. Two boron atoms will never be able to form a stable combination. Complicated electron deficiency bonds in B_{12} icosahedra are the result of a kind of "compromise" to generate a stable structure. The heavier homologues of these elements, for example, aluminium, tin, lead, bismuth, behave very differently form their lighter relatives. Why is this? Owing to their increased distance from the nucleus the other valence electrons can easily be removed from the atom. This increased electropositivity is characteristic for all heavier main group elements and especially for all transition elements: they form metals. The formation of a metallic state can best be illustrated by considering the interaction of, for instance, 2, 6, 10, etc. and finally of an infinite number of lithium atoms, having only a single electron in the *2s* orbital. Using the molecular orbital (MO) description, as is usual for covalently bonded atoms in molecules, the generation of a metal can be simply understood as the formation of an infinitely extended molecular orbital. Figure 2.4 illustrates this process in a simplified manner. Two lithium atoms combine via their $2s^1$ electrons to form a doubly occupied binding molecular orbital (Figure 2.xa). This situation is directly comparable with the formation of H_2 molecule by two $1s^1$ orbitals, but while H_2 is stable due to its He configuration, Li_2 has in addition 2 x 3 (not shown) unoccupied p-orbitals. Li_2 molecules indeed exist in the gas phase, but not under more usual conditions. Continuing this thought-experiment we will end up with, say, 1 mole of Li atoms combining, with 1 mole of bonding and 1 mole of antibonding molecular orbitals. 6×10^{23} MOs cannot further be strictly separated from each other; instead they form what we call an energy band, consisting of 6×10^{23} quasi-equivalent doubly occupied MOs, followed by the same number of unoccupied antibonding levels. This is the situation in a typical metal, responsible for its well known properties. The situation in lithium is relatively simple compared with that in heavier metals, especially of transition metals, where s, p, d and even f electrons may participate in the metallic bond. However the lithium situation describes the principles sufficiently.

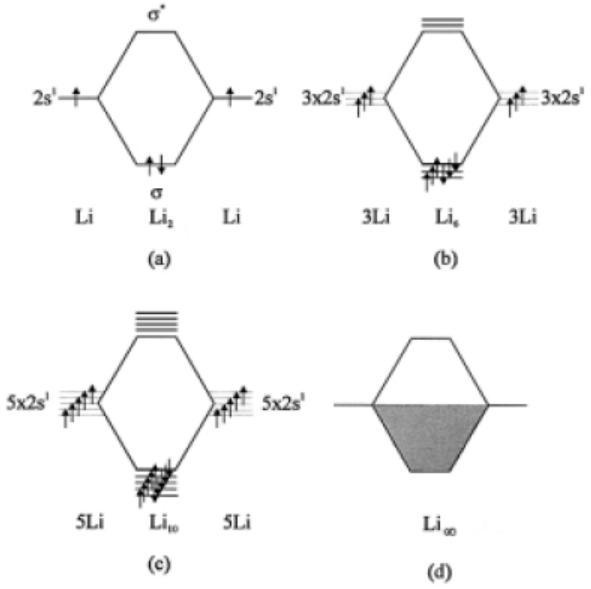

Figure 2.4 MO description of formation of bulk Li from Li atoms

To transform Figure 2.4d into a more descriptive image, a metal can also be described as consisting of a regular lattice of positively charged metal ions, embebbed in a gas of quasi-delocalized electrons. Most of these lattices consist of cubic or hexagonal close packings; others form cubic centered structures. Most of the properties of a metal can be deduced from this simple description. It should be noted, however, that much more knowledge is necessary for understanding of properties such as magnetism and conductivity in detail. Before discussion of some of the properties of bulk metals, a more quantitative insight into the electronic situation might be useful. The relation between the MO description of a finite molecular system and the "infinite" situation in a bulk metal is that the highest occupied molecular orbital (HOMO) is now called the Fermi energy E_F of the free electron model. E_F depends only on the density $\rho = N/V$ of the electrons (N = numbers of electrons, V = volume). Thus, E_F is independent of the particle size. Assuming that all levels up to E_F are occupied by a total of N electrons, it can be roughly estimated that the average level spacing $\delta \cong E_F / N$. Consequently, δ is inversely proportional to the volume $V = L^3$ (L = side length of the particle) or $\delta \alpha E_F(\lambda_F/L)^3$, with λ_F the wavelength of the electron of energy E_F. λ_F is of the order of interatomic distances. These considerations assume the wave character of the electron, including the fact that the allowed values for the wavelength λ are quantized; that is, for the model of an electron in a "box" of side L the ratio $2L/\lambda$ is an integer or, in other words, only discrete values for the energy are allowed. The separation values δ become larger the smaller the value of L. The development of the density of states (DOS) δ as a function of energy from a molecular system to a bulk d-metal is shown in Figure 2.5. This illustration corresponds in some respects to that in Figure 2.4, but now the understanding is based on the relation between the Fermi energy E_F and the density of the states. The typical band structure in Figure 2.5c originates from a non-differentiated infinite number of s and d electrons, whereas in (a) only well-separated energy levels are present. The highest occupied molecular orbital (HOMO) corresponds to E_F. The situation in (b) will later become most important, when the

electronic situation of nanosized particles will be discussed. At this point it suffices to mention that (b) is the most exciting situation with respect to materials properties.

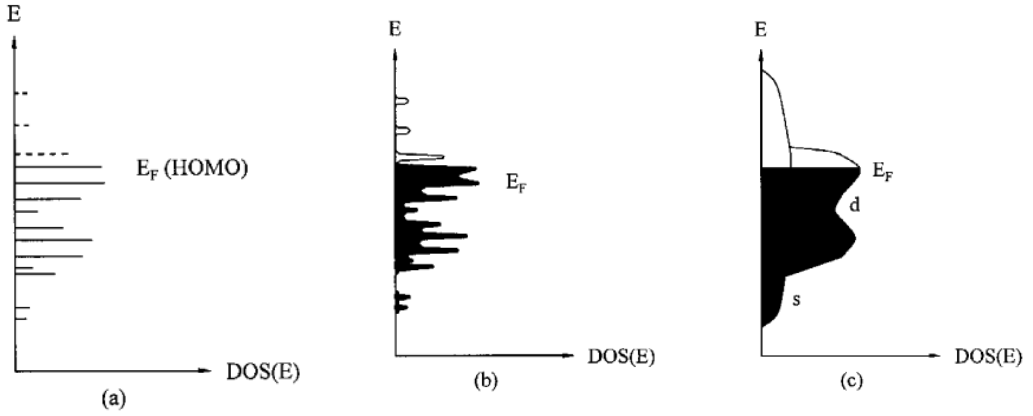

Figure 2.5 Density of states as a function of energy for a d-metal. a) single atom; b) nanoclusters; c) bulk metal

2.4.1 REDUCTION OF SIZE

The development of a metallic band structure requires a minimum number of electronic levels, which have to be very similar in energy so that electrons can move inside the particle by only thermal activation. All properties that we know for a bulk metal derive from the existence of such a band: the electrical conductivity as well as the specific heat, the metallic lustre, or the ductility, to cite just a few typical metallic characteristic. Let us make another thought-experiment. In the previous section we developed the metallic band structure using molecular orbitals with a few atoms up to a mole of lithium atoms. Conversely, we now ask how small a metal particle has to become to lose the band structure to such an extent that the effect can be observed. This situation corresponds to Figure 2.xb, where the unstructured s- and d-bands in (c) are beginning to be split but without forming truly discrete levels as in (a). It can be assumed that one mole of metal atoms, has a completely developed band structure. Assemblies of many fewer atoms also do, as we know from experience. Any metal particle that we can observe by naked eye or even under a light microscope can be considered to behave in a bulk-like way. This is not surprising, because even such a small particle as, say, 1 μm^3 cube of gold still consists of more that 10^{10} atoms. There is no doubt that 10^{10} atoms are able to form a band structure. But how far do have we to go in miniaturization to reach the borderline between bulk and molecule?

Before presenting practical examples, we can give a general answer to this question. Electrons in a three-dimensionally extended metal spread as waves of various wavelengths, usually called the "De Broglie wavelenght", referring to the French physicist Duc De Broglie. He first interpreted the relation between the wavelength and the mass of an electron through the formula $\lambda = h/(mv)$ (λ = electronic wavelength, h = Planck constant, m = mass of the electron, v = speed of the electron). Delocalization of electrons in the conductivity band of a metal is possible as long as the dimension of the metal particle is a multiple of the De Broglie wavelength λ. From this it follows that the smallest metal particle must have a

dimension of the order of λ or some multiple of it. Smaller particles have electrons localized between atomic nuclei; that is, they behave as typical molecules. It is to be assumed, however, that there is no sharp borderline between these two fundamental situations, but that this transition will be continuous and is, as will be discussed, also temperature-dependent. The description of bulk materials is made by means of the laws of classical physics. If we reach a size range where, in the case of metals, the band structure is beginning to disappear and discrete energy levels are becoming dominant, quantum mechanical rules have to replace those of classical physics. Quantum mechanics is a well established theory for describing the electronic situation in molecules and atoms. So far, there is nothing new; however, in relation to small particles, the use of quantum mechanics is somewhat special as we still talk about parts of a material, not about atoms or small molecules. The model of the "electron in a box", normally used for atoms, helps to describe simply the situation in small metal particles when size restrictions begin to influence electronic behaviour (Figure 2.6)

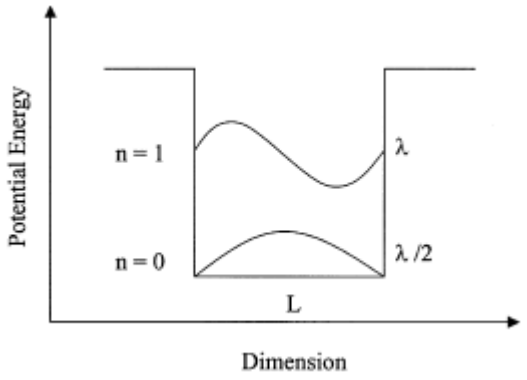

Figure 2.6 Electron in a box model

If L is the diameter of a metal particle, the situation at n = 0 corresponds to that of an s orbital in an atom. A metal particle of this "smallest size" therefore has an electronic ground state comparable with that of an atomic s orbital or, in other words, a metal cluster; such small particles can now also be considered as very large metal atoms. Exited states, such as n = 1, can then be compared with p orbitals, and so on. This is what makes a metal cluster different from the bulk where L is "infinitely" large, hosting an infinite number of electronic waves λ. In treating such mesoscopic systems quantitatively, formidable problems arise for particles consisting of only a few thousand atoms. They are too small to be considered as bulk, owing to strong size-effects; on the other hand, they are far too large to be handled as molecules. It would be considerably beyond the scope of this Chapter to describe these problems in more detail.[19]

With decreasing size of metal particles, the percentage of surface atoms increases (See general introduction). This is an important point to be considered when one discusses cluster properties. As a result of the reduction of the numbers of neighboring atoms, surface atoms have narrower d-bands, so that the density of states can vary considerably. Another surface effect is equally important: metal clusters in general are provided with a protective shell of ligand molecules (see sections 1.1 and 2.3.2). Otherwise we would not be able to prepare them by chemical methods and

especially to isolate and to investigate them as individual particles. Ligand-metal interactions dramatically influence the electronic nature of the metal atoms involved. Both the reduction of coordination number and, in the case of ligand-protected clusters, the metal-ligand bonds have to be considered when specific properties are discussed. As is known from numerous investigations, the ligation effects are short-ranged, so that inner-core atoms can be roughly separated from surface atoms for the purposes of discussion. Of course, the influence of surface atoms become more important the smaller the particle is. Physical measurements that give averaged information on the total particle are therefore always to be considered in this light, whereas methods distinguishing between differently bound atoms allow a more detailed description. Strictly speaking, only the inner-core atoms represent a minute piece of the bulk with strong quantum size effect. The restriction of the quasi-freely mobile electrons in a piece of bulk metal can be reached not only by reduction of the volume to the minute size of a "zero-dimensional" (0D) quantum dot but can also be gained by reducing the dimensionality from 3 to 2 or 1. If a piece of metal is reduced by making it thinner and thinner until the electrons can only move in two instead of three dimensions, we have performed a two-dimensional (2D) quantum confinement, called a "quantum well"- Further reduction in dimensionality finally ends in a "quantum" wire (1D), where the electrons can move in only one direction (Figure 2.7).

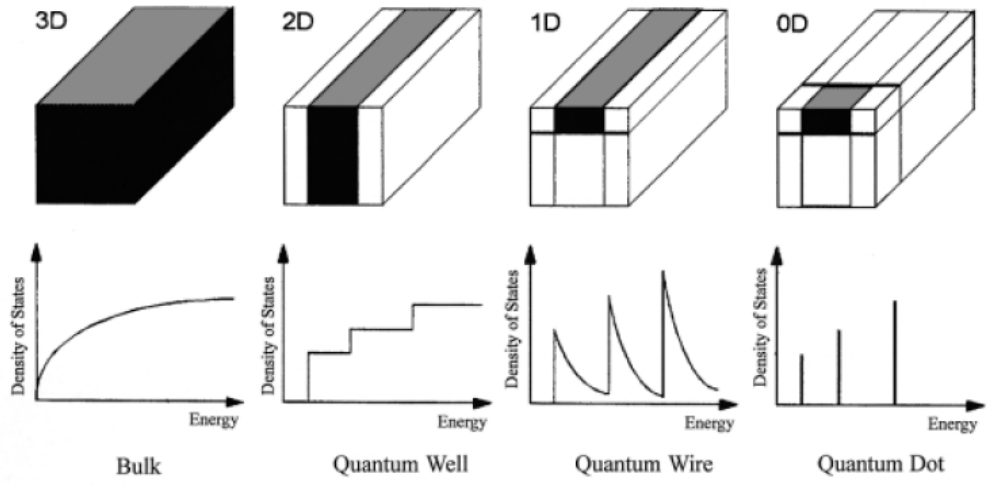

Figure 2.7 DOS as a function of energy for confined systems

2.4.2 SIZE DEPENDENT PROPERTIES

The above described remarked dependence of electronic structure of metal clusters with size, together with changes in surface area, are responsible of size dependent properties of metal nanoparticles. Some of these properties will be here resumed, with particular attention to size dependent catalytic behaviour of transition metal nanoparticles.

2.4.2.1 melting points

Let us first consider a property that is not directly dependent on the electronic situation in the particles, but is rather a consequence of the averaged coordination number of the participating atoms. By far the majority of metals form hexagonal or cubic close-packed structures with coordination numbers of 12, except for surface atoms when it is 9 or smaller, depending on whether faces, and which kind of faces, edges, corners are considered. However, it is typical for bulk materials that the surface atoms form a negligible part of the total number of atoms. The smaller a particle becomes, the more the proportion of surface atoms increases (see introduction of this thesis work). A spherical particle of 50 nm in diameter has only 6% of surface atoms, so that for micrometer-sized of even millimetre-sized particles these atoms can indeed be neglected with respect to their contribution to the average coordination number. The melting point of a solid is reached when the order of the lattices is beginning to be destroyed. For a distinct solid this a physical constant, but only so long as the surface is negligibly small in comparison with the total volume. For very small particles the number of surface atoms become equal to or even exceed the number of inner-core atoms. As the coordination number of surface atoms is 9 or smaller, these atoms are more easily rearranged than those in the center of the particle: the melting process starts earlier. In Figure 2.8 the relation beween particle size and melting point of gold particles is shown.[20]

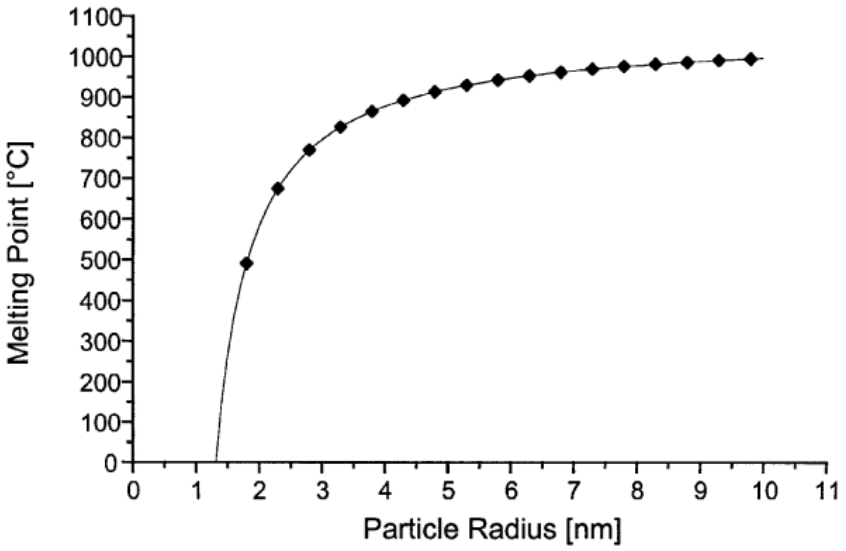

Figure 2.8 Melting point as a function of particle size for AuNPs

In conclusion, we can see that even thermodynamic properties of matter, which classically described are natural constant, change with the dimension of the material.

2.4.2.2 Magnetism

Diamagnetic materials have only spin-paired electrons. However, in practice it cannot be assumed that a macroscopic piece of a diamagnetic metal does have one or more unpaired electrons. This can in no way be measured because of the effectively

infinite number of atoms and electrons. However, if the particle size were smaller enough to make one umpaired electron measurable, the predicted so-called odd-even effect should become more visible. Among small diamagnetic metal particles there should be a 50 : 50 distribution of odd and even numbers of electrons. A series of palladium clusters of different sizes has been used to verify this prediction.[21] Figure 2.9 shows the experimental results.

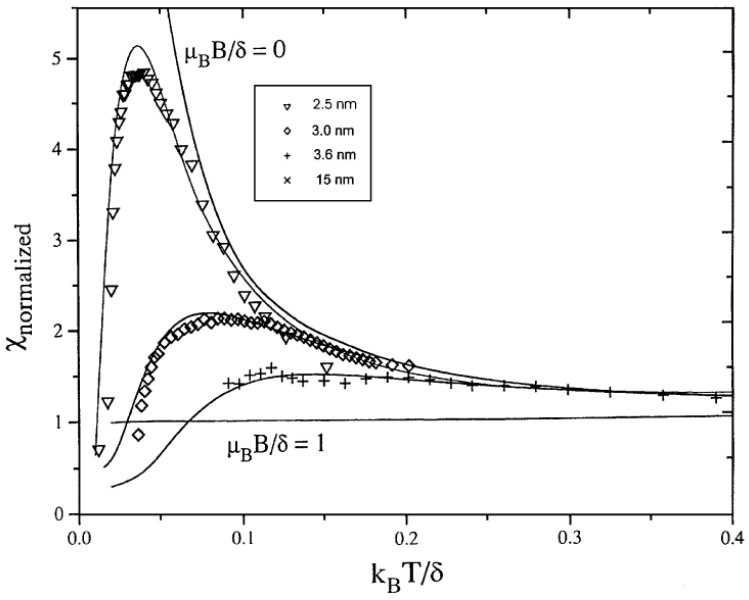

Figure 2.9 Electronic magnetic susceptibility of Pd clusters of different sizes

All samples show diamagnetic behaviour like that of bulk palladium down to temperatures of about 1 K. Below 1 K, however, there is a distinct difference. Whereas the 15 nm Pd clusters behave in bulklike manner, the smaller clusters show an increasing maximum of susceptibility with decreasing size.

2.4.2.3 interaction with electromagnetic radiation[22]

Metals can be polarized by electromagnetic irradiation exciting electrons. Considering the ideal case of an undamped oscillation of free electrons in a defect-free metal lattice, the solution of the wave equation results in an expression for the complex refractive index n:

$$n^2 = 1 - \frac{e^2 N_E}{\varepsilon_0 m_e \nu^2} \qquad 2.4$$

where N_E = density of electrons, m_e = electronic mass, ν = frequency of the electromagnetic radiation and ε_0 = dielectric constant of vacuum. The refractive index is related to the reflectivity R_v of a metal by the Beer equation

$$R_v = \frac{(n'-1)^2 + k^2}{(n'+1)^2 + k^2} \qquad 2.5$$

where k = absorption coefficient and n' = real part of the complex refractive index. If v is small enough, n^2 becomes smaller than 0 and n then consist of only the imaginary part n''. With n' = 0, the reflectivity R is 1, which means that metals reflect electromagnetic irradiation totally. Higher frequencies cause a real part of the complex refractive index n' > 1 with k = 0 and in the case of non-adsorbing metals n approximates to 1 and R to 0 (metal completely transparent). The frequency for the transition R = 0 to R = 1 for free electrons, called plasma frequency v_p is

$$v_{\mathrm{P}} = \sqrt{\frac{e^2 N_E}{\varepsilon_0 m_{\mathrm{e}}}} \qquad 2.6$$

In real metals, collision processes at defects induce damping of the oscillation. In addition to this source of damping in real lattices, the migration of electrons is also not free because, owing to the oscillation of the electrons, a damped dipole is caused in the field of the atomic nucleus. This leads to a dispersion of the refractive index and to a maximum in the spectral adsorption. Metals also deviate from the ideal model if their particle size is so reduced that the mean free path of the electrons exceeds the particles radius. In this case electrons can be excited by visible light to perform fluid-like plasmon oscillations (Mie theory, see section 1.xxx). The dipole and higher multipole moments are caused by surface charging, which is especially effective for spherical shapes (Figure 2.10). Size dependence of UV-vis absorption spectra is discussed in section 1.3.2.1 and chapter 4.

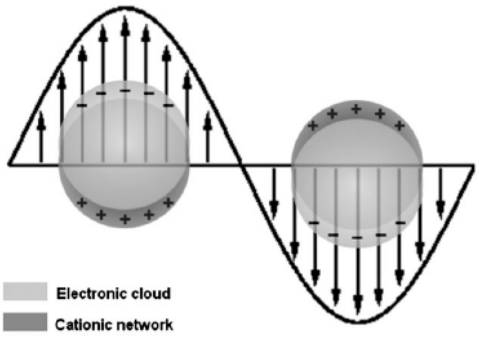

Figure 2.10 Schematic description of electronic cloud displacements in nanoparticles under the effect of a electromagnetic wave.

2.4.2.4 Conductivity

Electrical conductivity of metals is based on their band structure. If the so-called conduction band is only partially occupied by electrons, they can move in all

directions without resistance, provided there is a perfect metallic crystal lattice. There are not scattered by the regular building blocks, owing to the wave character of the electrons. A collective motion of electrons (current I) in a bulk metal is induced by applying a voltage U. Ohm's law describes the linear relation between U and I (U = RI, R = resistance of the material). The relation described above (and others not discussed) depend on the existence of a band structure, that is, the presence of freely mobile electrons in the lattice. As already discussed, the band structure begins to change if the dimension of a metal particle become small enough. Discrete energy levels finally dominate and, as a consequence, Ohm's law is no longer valid.
Conductivity of single nanoparticles has been measured and a typical U / I plot (for a ligand stabilized Au_{55} cluster) is depicted in Figure 2.11

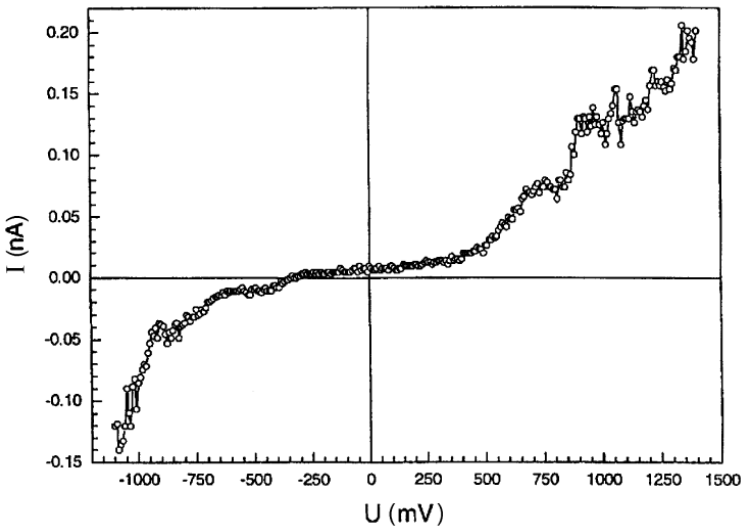

Figure 2.11

Is it shown that below a certain value of U (called Coulomb blockade), there is a negligible current. If this value is reached, electrons can be transferred by a tunneling current. It thus become possible to charge and to discharge a quantum dot in a quantized manner, which is condition for use of such particles in future generation of computers.

2.5 IMPORTANCE OF TMNPS PARTICLE SIZE IN CATALYSIS

We already discussed the importance of TMNPs in catalysis (see section 1.4). Now we will point our attention in those reactions in which particle size is a crucial parameter in determining activity and/or selectivity in catalytic transformation of the substrates. Because heterogeneous catalysis happens on metal surface, the first obvious influence of particle size in a transition metal catalyst performance, is the increment of surface area in decreasing particle size, which leads to a greater number of active sites per mole of metal. Indeed, a real comparison between heterogeneous catalysts would be done in terms of effective turnover numbers, defined as (moles of product) / (moles of active metal atoms x time). Apart this surface availability effect, particle size seems to be determinant for activity and selectivity of various reactions,

depending on the number of kinks, steps, terraces and other surface defects, which are of course strongly dependent from the dimensions of particles. A very interesting study has been conducted about structure-sensitivity of Heck coupling reaction (see section 1.4.3.1) by Bradley and Blackmond,[23] in which they evidenced that the Pd-metal catalyzed Heck coupling of aryl halides with olefins is a structure-sensitive reaction and that the Pd sites responsible for high activity are those with low metal-metal coordination number. Finally, the above discussed size-dependent electronic structure of metal nanoparticles, can also be important in determining reactivity and selectivity of catalytic reactions. The key point lies in the interaction between the incomplete d-band of the surface sites with the molecular orbitals of reactants and products. Historically, the premises of this concept were suggested by Sabatier.[24] The heat of adsorption of reactants and products, governed by the electronic factors, should be neither too strong nor too weak to give the optimum coverage for species competing at the surface, or for the products to desorb.
The concept of structure sensitivity, based on the observation that some reactions demand either low coordination number metal atoms or a specific arrangement of metal sites, is one of the fundamental phenomena in heterogeneous catalysis. Reactions have been grouped as structure-insensitive, such as simple hydrogenation reactions, or structure-sensitive, including carbon-carbon bond-breaking reactions. The observation of structure sensitivity in a heterogeneously catalyzed reaction classically requires the preparation of a series of catalysts which differ only in particle size. This is notoriously difficult to accomplish since heterogeneous catalysts of differing particle size are typically prepared by using different precursors, supports, or preparation conditions, producing catalysts which are intrinsically different from one another in ways other than simply their particle size. Colloid preparation techniques, however, can provide catalysts in which the size or structure of the metal particles may be varied in the absence of other perturbations and thus are excellent materials for investigations of catalytic site requirements.[23]
At present, the most studied size effect in transition metal catalyzed reaction concerns oxidations and hydrogenations. Let's discuss some examples.

2.5.1 SIZE DEPENDENT TRANSITION METAL CATALYZED OXIDATION REACTIONS

2.5.1.1 AuNPs catalyzed CO oxidation

Au has long been considered catalytically less active than other transition metals. However, highly dispersed Au has received considerable recent attention because of its extraordinary catalytic properties[25] first demonstrated by Haruta.[26] Au particles of less than 5 nm diameter have been found to be active for low temperature CO oxidation, propylene epoxidation, water gas shift reaction, NO reduction/dissociation, hydrogenation, SO_2 dissociation and selective oxidation.[25] Of the important reactions known to be catalyzed by supported Au particles, the low temperature CO oxidation has been received the most attention experimentally and theoretically.[25] However, the data in the literature vary widely, and the nature of the active Au species/structure/site remains obscure. It is generally accepted that the catalytic activity of Au depends to a large extent on the size of the Au particles, however other effects, such as the nature of the support material, the Au-support interface, the particle shape, and metal–support charge transfer, are purported to be

of fundamental importance. The low-temperature oxidation of CO on supported Au particles shows a marked increase in the turnover frequency (TOF, reaction rate per surface Au site per second) as the diameter of the Au particles is reduced below ~3.5 nm[27] (Fig. 2.12). A further reduction in the particle diameter below ~3 nm leads to a decrease in the catalytic activity. Despite the extensive recent efforts to address this unusual catalytic behaviour of ultra-small Au particles, no atomic-level understanding currently exists.

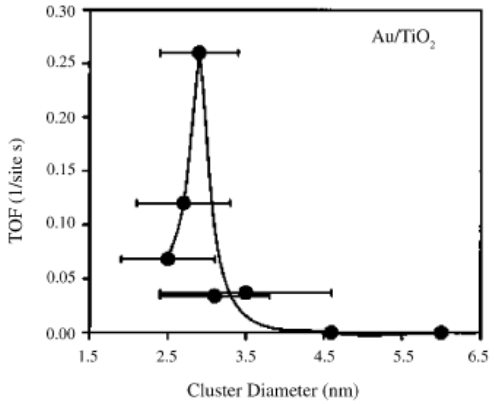

Figure 2.12 CO oxidation turnover frequencies (TOF's) at 300 K as a function of the average size of the Au particles supported on a high surface area TiO_2 support

To investigate the origin of the exceptional high activity for Au particles in the 3 nm size range, the tunneling current as a function of the bias voltage (I–V) for several Au particles of varying sizes supported on TiO_2 (110)-(1 x 1) for various Au coverages from 0.2 to 4.0 monolayers was measured and is plotted in Figure 2.13 as the band gap of the Au particle versus the particle size.[28] A metal-to-insulator transition occurs as the particle size falls below 3.5 nm in diameter and 1.0 nm in height (~300 atoms per particle).

Infrared reflection absorption spectroscopy (IRAS)[29] was used to study CO adsorption on Au particles ranging in size from 1.8 to 3.1 nm, supported on TiO_2. The CO vibrational frequency on the Au particles blue-shifts slightly (approximately 4 cm^{-1}) compared to CO on bulk Au, whereas the heats of adsorption increase sharply with decreasing particle size, from 12.5 to 18.3 kcal/mol (Figure 2.13). The maximum heat of adsorption occurred at approximately the same particle size where the catalytic activity maximizes and where a metal-to-insulator transition was observed by Valden et al.[28]

These studies helps to understand the size-dependent behaviour of gold nanoparticles in catalytic oxidation of CO, even if they doesn't take into account other parameters such as nature of support, defects on the metal surface and so on, which seems to be important as well in determining activity of Au catalysts in this reaction.

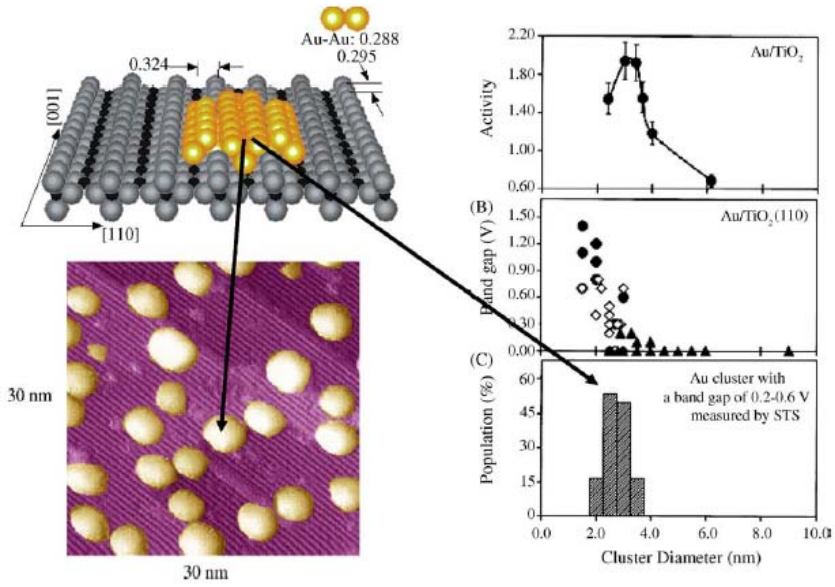

Figure 2.13 A model structure of bilayer Au island on TiO_2 (110) surface, and a STM image of Au/TiO_2 (110)-(1x1) with Au coverage of 0.25 ML (left). The activity for CO oxidation at 350 K (A), the measured band gap (B) and the relative population of Au particles that exhibit a band gap of 0.2-0.6 V (C) as a function of the Au particle size supported on TiO_2 (110) assuming total dispersion of the Au (right).

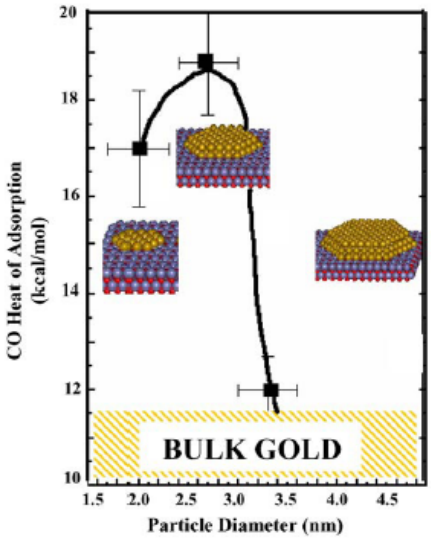

Figure 2.13 Zero coverage isosteric heats of adsorption as a function of mean particle diameter

2.5.1.2 AuNPs catalyzed alcohols oxidation

Prati and Rossi have found that Au supported on activated carbon is more active and selective than other noble metal catalysts for the oxidation in a Methanol-H_2O (6:4)

solvent of glycols to α-hydroxy acids, which are used in the cosmetics and food industries (Scheme 2.3).[30] Other authors confirmed the structure-sensitivity of this useful reaction.[31]

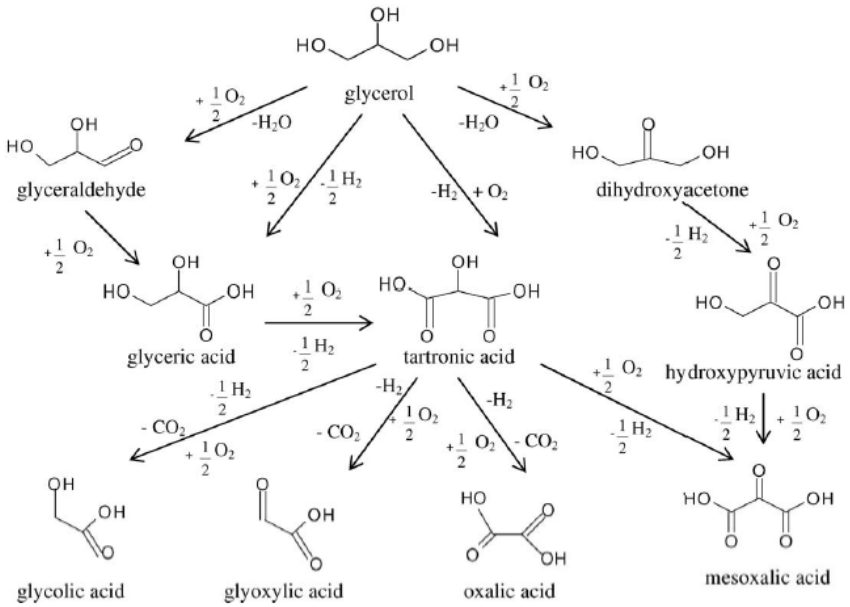

Scheme 2.3 Possible products of glycerol oxidation

Not only activated carbon, but also γ-Al_2O_3 and TiO_2 make Au active and selective.[32] An interesting feature in Figure 2.14 is that over activated carbon support, a maximum activity is observed when the mean diameter of Au particles is 7-8 nm, whereas the smaller Au particles give higher activity over γ-Al_2O_3 and TiO_2 support. This can be explained as follows: smaller Au particles can be easily fixed on the internal surfaces of carbon, and are consequently less accessible to reagents in the liquid phase than larger Au particles located on the external surfaces.

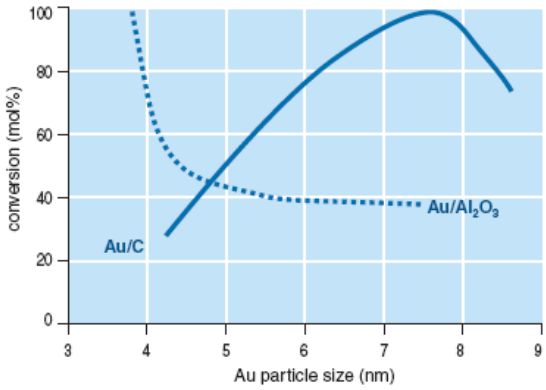

Figure 2.14 conversion vs particles size in glycols oxidation with gold deposited on different supports

A size effect has also been observed in selective benzylic alcohol oxidation to benzaldehyde with AuNPs supported on poly(N-vinyl-2-pyrrolydone) catalysts in

very mild experimental conditions (Scheme 2.4), with 1.3 nm particles being considerably more active than 9.5 nm ones.[33] Here, the difference in catalytic activity between two different Au systems cannot be explained only on the basis of surface area. A size effect has been also claimed in gold catalyzed selective oxidation of glucose.[34]

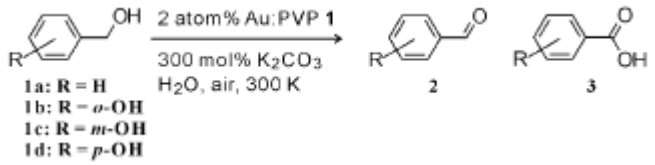

Scheme 2.4 Au/PVP catalyzed benzyl alcohols selective oxidation

2.5.2 SIZE DEPENDENT TRANSITION METAL CATALYZED HYDROGENATION REACTIONS

Transition metal catalyzed hydrogenation reactions have a long history (see section 1.4.4). Generally, hydrogenation of simple unsaturated substrates over metal surface is known to be structure insensitive, thus independent from particles size.[35] However, several studies demonstrates that in some selective reactions this parameter can play a major role in determining product distributions.

Early studies demonstrated the importance of particle size effects on mechanism and product distribution of hydrogenolysis reactions over Pt catalysts[36]: in methylcyclopentane hydrogenolysis under hydrogen pressure, selectivities for cleavage of three different bonds (*a*, *b*, *c* Figure 2.15) were affected by platinum crystallite size. The support had no effect in products distribution. The authors attributed their results to the presence of different types of surface defects. In hindsight it is tempting to say that bond a is susceptible on small crystallites simply because it is accessible to the "protruding" edges or corners on a small polyhedral shape, whereas on larger crystals far fewer such sites would be avalaible: indeed more flat planes would be present that might not be able to accept the *a*-bond site due simply to steric effects.

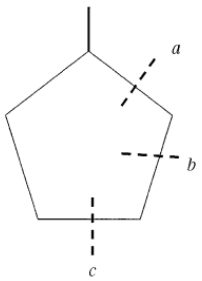

Figure 2.15 different kinds of cleavage of methylcyclopentane bonds

In a work of Klabunde,[37] MVS derived Ni catalysts prepared in different solvents (pentane and toluene), shows remarkable differences in particles size and morphology and exhibit quite different catalytic behaviour in a simple probe reaction, that of 1,3-butadiene hydrogenation (Figure 2.16)

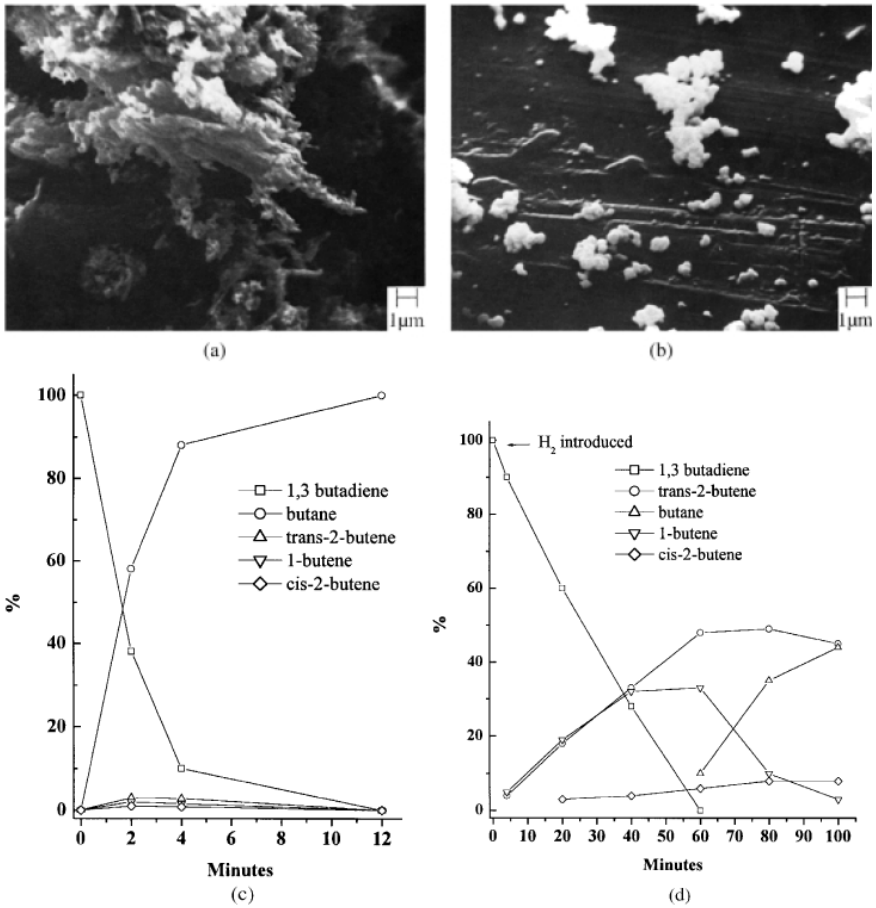

Figure 2.16 SEM of NiNPs formed from Nickel atoms (a) in cold pentane and (b) cold toluene; hydrogenation of 1,3-butadiene over (c) Ni-pentane and (d) Ni-toluene NPs.

In a related work, our group[38] has shown that SMAD synthesis of noble metal catalysts yields metal particles of very unusual properties, assumed to be due to their very small size. For example, Pt-SMAD catalysts were quite effective for hydrogenation of p-chloronitrobenzene to dicyclohexylamine (see section 1.4.4.2), a reaction that was found to be strongly correlated with particle size (Scheme 2.5).

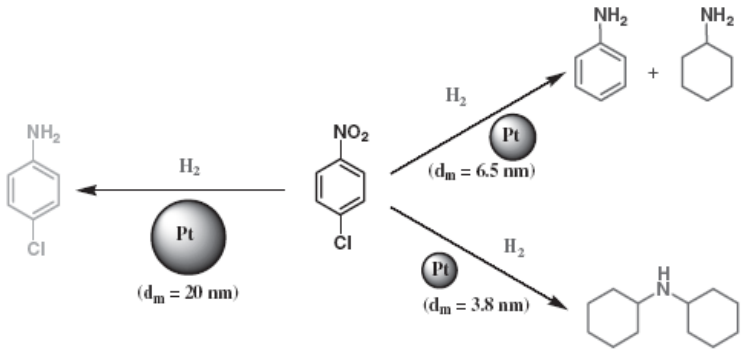

Scheme 2.5 Effect of particle size in PtNPs catalyzed chloronitrobenzene hydrogenation

2.5.2.1 Selective hydrogenation of α,β unsatured carbonyl compound

Another interesting reaction, from this point of view, is the hydrogenation of α,β unsaturated carbonyls (see section 1.4.4.1), as acrolein (propenal) or 3-phenylpropenal (cinnamaldehyde). In these cases the desired products are the unsaturated alcohols and not the saturated aldehydes or the saturated alcohols. It is well established that over Group VIII the C=C bond is hydrogenated faster than the C=O bond, and much effort has gone into finding catalysts that will achieve the desired goals.[24] From the literature review it is evident that the selectivity to unsaturated alcohol is better: (i) over Ir than Ru, Pt, Rh or Pd; (ii) on large metal particles; (iii) when graphite or TiO2 are used as supports in place of carbon or silica; (iv) on metals supported on zeolites containing alkali cations; (v) on bimetallic catalysts like PtFe/C. Moreover, the selectivity depends on the substitution on the C=C and C=O bonds. On a series of model Ru/Al_2O_3 catalysts ($1.3 < d < 13$ nm), Coq and Figueras have studied the structure-sensitivity of (i) the gas-phase hydrogenation of acrolein[39] and (ii) the liquid-phase hydrogenation of cinnamaldehyde.[40] In the two reactions the TOF decreased when the Ru particle size decreased. The cinnamyl alcohol selectivity increased from 22% for an Ru particle size of ca. 1.2 nm to 80% on large crystallites of bulk Ru, in full agreement with the previous report from Galvagno et al.[41] This effect was particularly pronounced when the Ru particles are larger than 3 nm. Interestingly, this behavior was not observed for acrolein hydrogenation and the selectivity to allyl alcohol changed much less with Ru particle size. It is generally considered that particles larger than 4 nm suffer little change of morphology and are mainly populated with low index planes. The behaviour of large particles can thus be well explained on the basis of the geometric orientation of CAL on the metal surface, as proposed by Gallezot et al.[42] On the flat metal surface of large particles, CAL will be tilted far from the surface owing to repulsive interaction between the phenyl ring and Ru surface, thus protecting the C=C bond. By contrast, the unhindered acrolein molecule can adsorb as a flat species independent of the morphology of the Ru particles and thus showed only small changes in allyl alcohol selectivity. Of course, as already noted on section 1.4.4.1, other parameters such as solvent, temperature, hydrogen pressure, presence of additives and also stirring speed, may affect product distribution of these kind of reactions, regardless the nature of metal used.[43]

2.5.2.2 Asymmetric hydrogenations

Several concepts have been advanced and tested for the synthesis of solid materials suitable for enantiospecific of view, the most promising solid enantioselective catalysts are metals modified by the addition of a soluble chiral compound (see section 1.4.4.3). The concept of chiral modification has been applied primarily to the Pt group metals and Ni, and there are only a few catalyst systems that afford high enantioselectivity (>90% ee).[44] Commonly used modifiers are the naturally occurring cinchona alkaloids and tartaric acid (TA). The Raney Ni-TA-NaBr system has been established as the choice for the hydrogenation of unfunctionalized and β-functionalized ketones (Scheme 2.6a).[45] Platinum modified by cinchona alkaloids is the best catalyst for the hydrogenation of activated ketones. Better than 90% ee has

been reported for α-dicarbonyl compounds (in particular α-ketoesters, Scheme 2.6b).[46] Chirally modified Pd has the broadest application range, including the highly selective hydrogenation of α,β-unsaturated carboxylic acids (Scheme 2.6c)[47] and 2-pyrones.[48] All these reactions, with focus on catalytic system morphology, has been recently reviewed.[44]

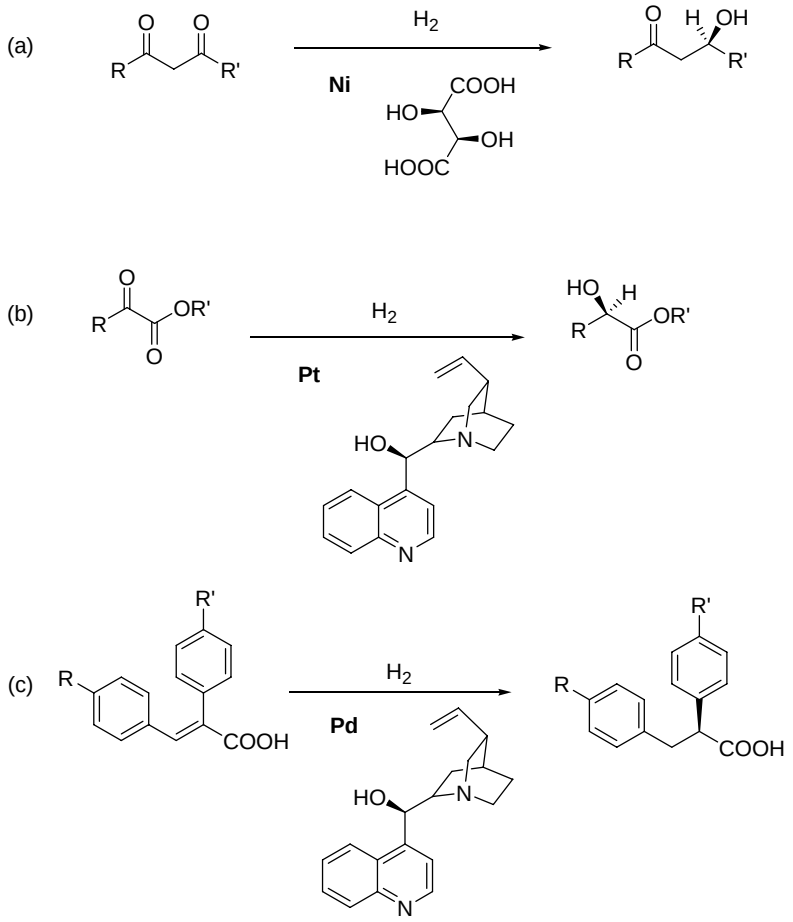

Scheme 2.6 (a) Ni-TA-NaBr catalyzed asymmetric hydrogenation of β-diketones; (b) Pt-CD catalyzed hydrogenation of activated ketones; (c) Pd-CD catalyzed hydrogenation of unsaturated carboxylic acids

There are analogies between a soluble transition metal complex possessing ligands as the source of chiral information and a metal surface where the adsorbed modifier controls the stereochemical outcome of the surface reaction. The latter catalyst system is, however, far more complex and structurally less defined. The chiral modifier interacts with not one single transition metal atom but an ensemble of surface metal atoms (Figure 2.17),[49] and the metal surface imposes substantial geometrical constraint for the modifier-substrate interaction.

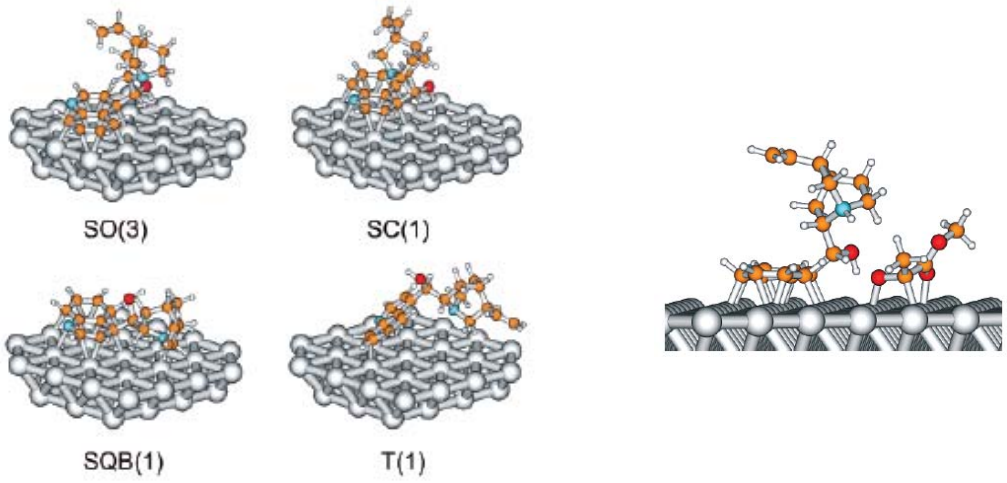

Figure 2.17 Computational models of interaction of chinconidine (left) and cinchonidine-ethyl pyruvate (right) on Pt flat surface.

In addition, the surface geometry of heterogeneous metal catalysts contains various types of surface sites with different coordination (terrace, step, edge, kink, vacancy, and adatom) and thus different adsorption properties. From these considerations, structure-sensitivity of heterogeneous enantioselective reactions is quite evident.
Obviously, the surface structure should have a strong influence on the adsorption of substrate and modifier and on their interaction resulting in enantioselection, but studies in this direction are in an early stage. An illustration to the complex and poorly understood role of metal surface is the sometimes dramatic influence of catalyst pretreatments (such as pre-reduction, corrosion in acidic medium, sonication). Contradictory observations on the effect of metal particles size on enantioselectivity in various reactions are observed, partly due to different surface impurities originating from catalyst preparation and to side reactions that are also structure sensitive.[44] Selectivity enhancement induced by restructuring of the metal particles during transformation of the substrate is an intriguing phenomenon that further demonstrates the structure sensitivity of enantioselective reactions. Nitta clearly evidenced a particle size effect in Pd-cinchona alkaloids catalyzed hydrogenation of α,β-unsaturated acids (Figure 2.18).[50]

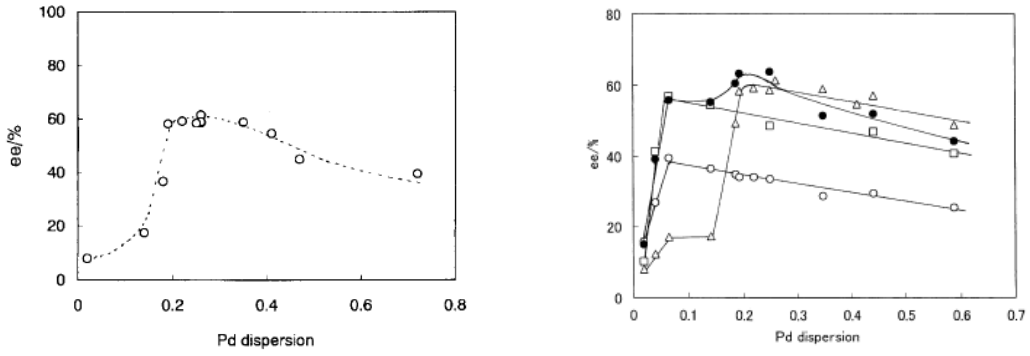

Figure 2.18 size effect in hydrogenation of unsaturated acids over modified Pd

In this case exists an optimum value of particle dispersion (i.e. particle size) to achieve high enantioselectivities, which is dependent of the solvent used (Figure 2.18b). It has been proposed that enantioselectivity depends on the adsorption mode of an adduct between substrate and chiral modifier on the metal surface (Figure 2.19). It means that if particles are too small, there is not sufficient surface for adsorption, while if they are too big, adsorption fails due to steric hindrance. Both cases results in a decrease of enantioselectivity.

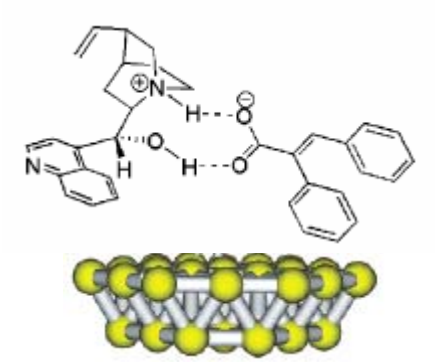

Figure 2.19 Model of interaction of chinconidine-acid complex on metal surface

2.6 REFERENCES

[1] Watzky, M.; Finke, R. G. *J. Am. Chem. Soc.* **1997,** *119,* 10382-10400
[2] for an extensive description of CNT see, for example, (a) Sugimoto, T. *Monodispersed Particles*, Elsevier, 2001; (b) Ruckenstein, E.; Djikaev, Y. S. *Adv. Coll. Int. Sci*. **2005**, 118, 51-72.
[3] Everett, D. H. *Basic Principles of Colloid Science*, Royal Society of Chemistry, London, 1988.
[4] (a) Sugimoto, T. *J. Colloid Interface Sci.* **1996**, *181*, 259; (b) Sugimoto, T. *J. Colloid Interface Sci*. , **1996**, *183*, 299.
[5] Sugimoto, T.; Shiba, F. *J. Phys. Chem. B* **1999,** *103*, 3607.
[6] LaMer, V.K.;Dinegar, R. H. *J. Am. Chem. Soc*. **1950**, *72*, 4847.
[7] Matijevic, E. *Chem. Mater.* **1993**, *5*, 412.
[8] (a) Turkevich, J.; Stevenson, P. C.; Hillier, J. *Faraday Discuss.* Chem. Soc. **1951**, 11, 55; (b) Enusun, B. V.; Turkevich, J. *J. Am. Chem. Soc*. **1963**, *85*, 3317; (c) Turkevich, J. *Gold Bull*. **1985**, *18*, 86.
[9] (a) Aiken, J. D., III; Finke, R. G. *J. Am. Chem. Soc.* **1998**, *120*, 9545. (b) Widegren, J. A.; Aiken, J. D., III; Ozkar, S.; Finke, R. G. *Chem. Mater.* **2001**, *13*, 312; (c) Widegren, J.A.; Bennett, M.A.; Finke, R.G. *J. Am. Chem. Soc.* **2003**, *125*, 10301; (d) Hornstein, B. J.; Finke, R. G. *Chem. Mater.* **2004**, *16* (1), 139; (e) Besson, C.; Finney, E. E.; Finke, R. G. *Chem. Mater.* **2005,** *17,* 4925-4938 (f) Besson, C.; Finney, E. E.; Finke, R. G. *J. Am. Chem. Soc*. **2005**, *127*, 8179-8184.
[10] Finney, E. E.; Finke, R. G. *J. Coll. Int. Sci.* **2008**, *317*, 351-374.
[11] Blackborow, J. R.; Young, D. Metal Vapour Synthesis in organometallic chemistry. Springer-Verlag: Berlin - Heidelberg, New York, 1979
[12] Henglein, A.; Giersig, M. *J. Phys. Chem. B* **2000**, *104*, 6767.
[13] Cacciuto, A.; Auer, S.; Frenkel, D. *Nature* **2004**, *428*, 404.
[14] Michaelis, M.; Henglein, A. *J. Phys. Chem.* **1992**, *96*, 4719.
[15] (a) Smoluchowski, M. *Phys. Z.* **1916**, *17*, 585.; (b) Smoluchowski, M. *Z. Phys. Chem*. **1917**, *92*, 129.
[16] (a) Leff, D. V.; Ohara, P. C.; Heath, J. R.; Gelbart, W. M. *J. Phys. Chem.* **1995**, *99,* 7036-7041; (b) Liu, X. ; Worden, J. G.; Huo, Q.; Brennan J. P. *J. Nanosci. Nanotechnol*. **2006**, *6*, 1054-1059.
[17] Lubetkin, S.D. *Langmuir* **2003**,*19*, 2575.
[18] see Schmid, G. in Nanoscale Materials in Chemistry, Ed. Klabunde, K. J., John Wiley and sons, 2001.
[19] For more detailed overwievs of the electronic energy structure of clusters see, for example, J. De Jongh, Physics and Chemistry of Metal Cluster Compounds, Kluwer Academic Publishers, Dordrecht, 1994.
[20] Castro, T.; Reifenberger, R.; Choi, E.; Andres, R. P. Phys. Rev. B, 1990, 13, 8548
[21] Volokitin, Y.; Sinzig, J.; de Jongh, L. J.; Schmid, G.; Moiseev, I. I. *Nature* **1996**, *384*, 621.
[22] For a description of the theory see, for example, Moores, A.; Goettmann, F. New J. Chem., 2006, 30, 1121–1132.
[23] Le Bars, J.; Specht, U.; Bradley, J. S.; Blackmond, D. G. *Langmuir* **1999,** *15,* 7621-7625
[24] Coq, B.; Figueras F. *Coord. Chem. Rev.* **1998**, *178–180*, 1753–1783.
[25] Chen, M. S.; Goodam, D. W. *Catal. Today* **2006**, *111*, 22-33.
[26] Haruta, M.; Yamada, N.; Kobayashi, T.; Iijima, S. *J. Catal*. **1989**, *115*, 301–309.
[27] (a) Haruta, M.; Tsubota, S.; Kobayashi, T.; Kageyama, H.; Genet, M.J. ; Delmon, B. *J. Catal*. **1993**, *144*, 175–192; (b) Bamwenda, G.R.; Tsubota, S.; Nakamura, T.; Haruta, M. *Catal. Lett*. **1997**, *44*, 83–87.
[28] Valden, M.; Lai, X.; Goodman, D.W. *Science* **1998**, *281*, 1647-1650.
[29] Meier, D.C.; Goodman, D.W. *J. Am. Chem. Soc*. **2004**, *126*, 1892–1899.
[30] Bianchi, C.; Porta, F.; Prati, L.; Rossi, M. *Topics in Catal*. **2000**, *13*, 231.
[31] Demirel-Gulen, S.; Lucas, M.; Claus, P. *Catal. Today* **2005**, *102–103*, 166–172.
[32] Porta, F.; Prati, L.; Rossi, M.; Coluccia, S.; Martra, G. *Catal. Today* **2000***, 61*, 165.
[33] Tsunoyama, H.; Sakurai, H.; Negishi, Y.; Tsukuda, T. *J. Am. Chem. Soc.* **2005**, *127*, 9374-9375
[34] Y. Onal, S. Schimpf, P. Claus, J. Catal. 223 (2004) 122.
[35] Boudart, M. *Chem. Rev*. **1995**, *95*, 661-666.
[36] (a) Gault, F. G. *Adv. Catal*. **1981**, *30*, 1; (b) Corrolleur, C.; Gault, F. G. ; Juttard, D. ; Maire, G. ; Muller, J. M. *J. Catal*. **1972**, *27*, 466.

[37] (a) Klabunde, K. J.; Efner, H. F.; Murdock, T. O.; Ropple, R. J. Am. Chem. Soc. 1976, 98, 1021; (b) Klabunde, K. J. ; Davis, S. C. ; Hattori, H.; Tanaka, Y. J. Catal. 1978, 54, 254.
[38] (a) Vitulli, G. Pitzalis, E.; Terrazzani, A.; Alessandra, P.; Pertici, P. Salvadori, P.; Martra, G. *Mater. Sci. Forum* **1997**, part 2 "Synthesis and Properties of Mechanically Alloyed and Naniocrystalline Materials", p. 235; (b) G. Vitulli, C. Evangelisti, A.M. Caporusso, P. Pertici, N. Panziera, S. Bertozzi, P. Salvadori, in *Metal nanoclusters in catalysis and materials science: the issue of size-control*, Edited by B. Corain, G. Schmid, N. Toshima, Elsevier, (2007), *in press*.
[39] Coq, B. ; Figueras, F. ; Geneste, P. ; Moreau, C. ; Moreau, P. ; Warawdekar, M.G. *J. Mol. Catal*. **1993**, *78*, 211.
[40] Coq, B.; Khumbar, P.S.; Moreau, C.; Moreau, P.; Warawdekar, M.G. *J. Mol. Catal.* **1993**, *85*, 215.
[41] Galvagno, S.; Capanelli, G.; Neri, G.; Donato, A.; Pietropaolo, R. *J. Mol. Catal*. **1991**, 64, 237.
[42] Gallezot, P.; Giroir-Fendler, A.; Richard, D. in: W. Pascoe (Ed.), Catalysis of Organic Reactions, Marcel Dekker, New York, 1991, p. 1.
[43] (a) U. K. Singh, M. A. Vannice Applied Catalysis A: General 213 (2001) 1–24; (b) P. Maki-Arvela, J. Hajek, T. Salmi, D.Yu. Murzin Applied Catalysis A: General 292 (2005) 1–49
[44] Mallat, T.; Orglmeister, E.; Baiker, A. *Chem. Rev*. **2007**, *107*, 4863-4890.
[45] Osawa, T.; Harada, T.; Takayasu, O. *Curr. Org. Chem.* **2006**, *10*, 1513.
[46] (a) Studer, M.; Okafor, V.; Blaser, H. U. *Chem. Commun.* **1998**, 1053; (b) Huck, W. R.; Mallat, T.; Baiker, A. *Ad*V. *Synth. Catal.* **2003**, *345*, 255.
[47] Nitta, Y.; Watanabe, J.; Okuyama, T.; Sugimura, T. *J. Catal.* **2005**, *236*, 164.
[48] Huck, W. R.; Mallat, T.; Baiker, A. *New J. Chem.* **2002**, *26*, 6.
[49] Vargas, A.; Baiker, A. *J. Catal.* **2006**, *239*, 220.
[50] Nitta, Y.; Kubota, T.; Okamoto, Y. *J. Mol. Catal. A: Chem.* **2004**, *212*, 155.

CHAPTER 3

METAL VAPOUR SYNTHESIS OF STABILIZED PLATINUM NANOPARTICLES. STUDIES ON GROWTH AND CATALYTIC PROPERTIES

"In cases of major discrepancy it's always reality that's got it wrong… reality is frequently inaccurate."

Douglas Adams

3.1 INTRODUCTION

Platinum is one of the most used metals for catalysis. Its catalytic activity in combustion reactions is known since the first years of XIX century, when catalysis was still emerging as science. For example, oxidation of ethanol by a Platinum wire was used in Davy's mine lamps, in 1825, and this is the first known practical application of catalysis.[1] At present, platinum catalysts has very important applications, being employed in catalytic converters and in fuel cell,[1] as well as in many industrial processes, such as production of nitric acid, gasoline reforming, silicones curing, production of fine chemicals (in particular by enantioselective hydrogenation).[2,3] Platinum is generally active in several catalytic reactions as zerovalent metal and as Pt(II) or Pt(IV) in salts and complexes, both in homogeneous and in heterogeneous phase. We were interested in platinum nanoparticles and in chapter 1 and 2 we already gave some examples of their employment in catalytic transformation. For example, in the relevant case of asymmetric hydrogenation of α-functionalized carbonyl compounds catalyzed by heterogeneous platinum nanoparticles (see section 2.4.3.2), there are many studies concerning the structure-sensitivity of this reaction. One of the most important parameters which have to be taken into account in order to have high e.e.s is the platinum particles size of the catalyst. In that regard, this chapter deals with the preparation of size controlled Pt nanoparticles and illustrate some preliminary application in catalysis.

3.2 GROWTH STUDIES OF METAL VAPOUR SYNTHESIS DERIVED PtNPs

The combination of platinum with mesitylene in MVS preparation of Pt nanoparticles, has been found to be very useful for studies on the clustering of Pt atoms in solution. The co-deposition of Pt vapour with mesitylene vapour affords solvated Pt atoms containing very small Pt_n aggregates (which in this work is indicated as **Pt/mes**). In standard conditions (see experimental section) the metal content in the recovered solution is around 0.25 – 0.35 mg/mL (1.3 – 1.8 mM). In the

presence of supports or on standing at room temperature, a clustering to supported or unsupported Pt solid particles of about 2.3 nm and 3.8 nm respectively takes place in few hours (Scheme 3.1).[4]

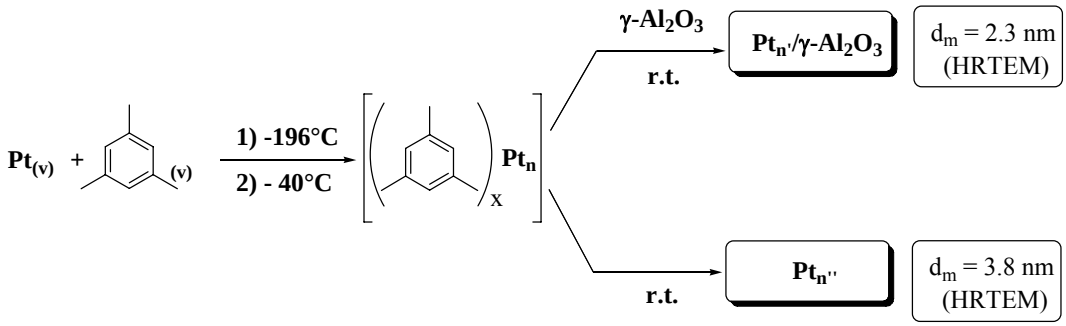

Scheme 3.1

Since not much is known about the clustering process occurring in these systems, we performed a study about the factors which could affect the final particle size in **Pt/mes** solution.

3.3 USE OF 1,1,3,3 DIVINYLTETRAMETHYLSILOXANE AS STABILIZING LIGAND

The clustering process of solvated Pt atoms, resulting in the formation of insoluble Pt nanopowders, can be prevented by adding 1,1,3,3-divinyltetramethyldisiloxane (DVS), to the mesitylene solution (Scheme 3.2). The usefulness of silane ligands - in particular vinylsiloxanes - in stabilization of Pt nanoparticles, was already reported (see Chapter 1).

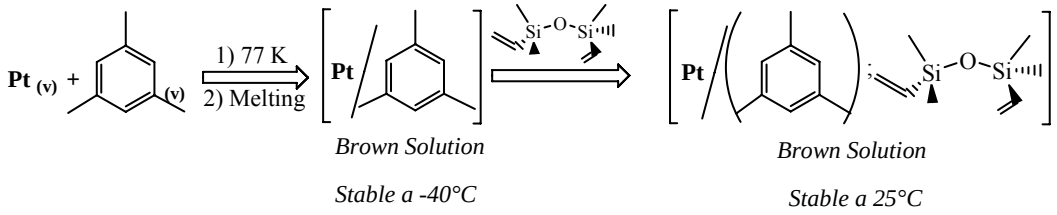

Scheme 3.2

The solvated Pt atoms become thermally stable and can be handled and characterized. In a typical experiment Pt/mes solution (5 ml, 6.0 μmol Pt) was added, at 25°C in a schlenk tube (50 ml), to a large excess of DVS (2 ml, 8.7 mmoles, molar ratio DVS/Pt = 1300:1). The DVS ligand is able to restrain the clustering processes of the Pt nanoparticles, forming a protective shell around the metal (Scheme 3.3). The thermally stable obtained solution, was stirred at 25°C for 15 minutes. After that, the solvent has been removed under vacuum, keeping the solution at $5 \cdot 10^{-5}$ mBar for 30 minutes at 25°C. The brown solid product, which is indicated as **Pt(mes)/DVS**, can be completely redissolved in apolar solvents for characterization in solution. ^{1}H-NMR related techniques were extensively utilized for this scope. In particular, DOSY analysis provide the measurement of diffusion coefficient of the species

present in solution (see section 1.3.7), which could allow to obtain, by careful handling of the data, a good estimation of particle size. Before illustrating the characterization of platinum nanoparticles synthesized in this work, we will describe some studies on applicability of DOSY analysis, based on observations made for model compounds.

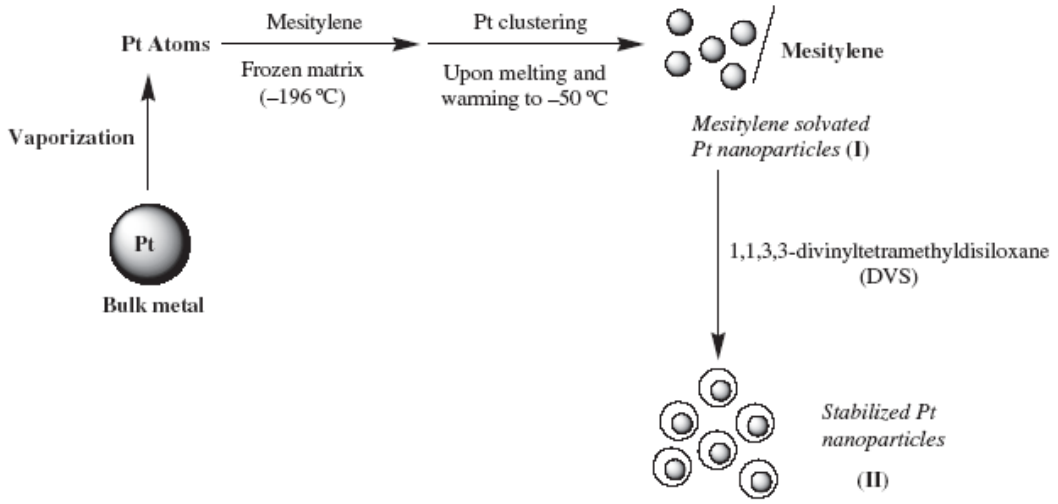

Scheme 3.3

3.3.1 REFINEMENT OF DOSY ANALYSIS FOR PARTICLE SIZE DETERMINATION IN SOLUTION

A fundamental point in the analysis of nanoparticles is the determination of their size distributions. The spherical hydrodynamic radius (r_H) of the diffusing species can be estimated from the experimentally determined self-diffusion translational coefficient (D_t) by taking advantage of the Stokes-Einstein equation:

$$D_t = \frac{kT}{c\pi\eta r_H} \qquad 3.1$$

where k is the Boltzmann constant, T is the temperature, c is a numerical factor, and η is the solution viscosity.

Because the error on D_t is usually lower than 5%, accurate values of r_H can be derived once the three other parameters of eq 1, T, c, and η, are correctly evaluated. While T and η can be measured, the selection of the proper c factor is critical. This is particularly true for big-size molecules, for which c can be approximated to 6. To avoid the measurement of T and η, an internal standard of known van der Waals radius (r_{VdW}) can be used to determine the proportional constant between D_t and r_H of eq 3.1.[5] In our case, TMS was used as internal standard to correct possible fluctuations in the viscosity of the solution owing to the presence of the solute.
Two assumptions are implicit in this procedure: (a) r_{VdW} is a good representation of r_H for the internal standard and (b) the proportional constant for the standard and that for the sample are the same and, since they are in the same solution and experience

the same T and η, this means that they have the same c factor. Assumption (a) is usually considered correct. Since the c factor substantially depends on the size of the diffusing species, assumption (b) is only respected if the standard and the sample have the same or, at least, comparable dimensions. Otherwise, c has to be evaluated. An acceptable semiempirical estimation of c can be obtained through eq 3.2[6] derived from the microfriction theory proposed by Wirtz and co-workers, in which c is expressed as a function of the solute-to-solvent ratio of radii.[7]

$$c = \frac{6}{\left[1 + 0.695\left(\frac{r_{\mathrm{solv}}}{r_{\mathrm{H}}}\right)^{2.234}\right]} \qquad 3.2$$

Combining eqs 3.1 and 3.2, the Stokes-Einstein equation, eq 3.3, is obtained in which D_t depends on both r_H and the spherical hydrodynamic radius of solvent (r_{solv}).

$$D_{\mathrm{t}} = \frac{kT\left[1 + 0.695\left(\frac{r_{\mathrm{solv}}}{r_{\mathrm{H}}}\right)^{2.234}\right]}{6\pi\eta r_{\mathrm{H}}} \qquad 3.3$$

To study the range of applicability of equation 3.2 respect to equation 3.3 species with different diffusion coefficient have been analyzed by DOSY experiments, including a range from $6.5 \cdot 10^{-10}$ m^2/sec to $21.6 \cdot 10^{-10}$ m^2/sec. For this scope simple organic molecules have been studied, such as benzene, mesitylene, DVS, 1,3,5,7-tetravinyl-1,3,5,7-tetramethylciclotetrasiloxane (TVCTS) and also mono and dinuclear organometallic complexes. In particular two complexes of zerovalent platinum have been synthesized: $Pt(nbn)_3$ and $Pt_2(DVS)_3$ (Scheme 3.4, see experimental section).[8] In all samples TMS was used as internal standard to correct possible fluctuations in the viscosity of the solution owing to the presence of the solute. ^{1}H-NMR and DOSY spectra of $Pt_2(DVS)_3$ in C_6D_6 are reported in Figure 3.1.

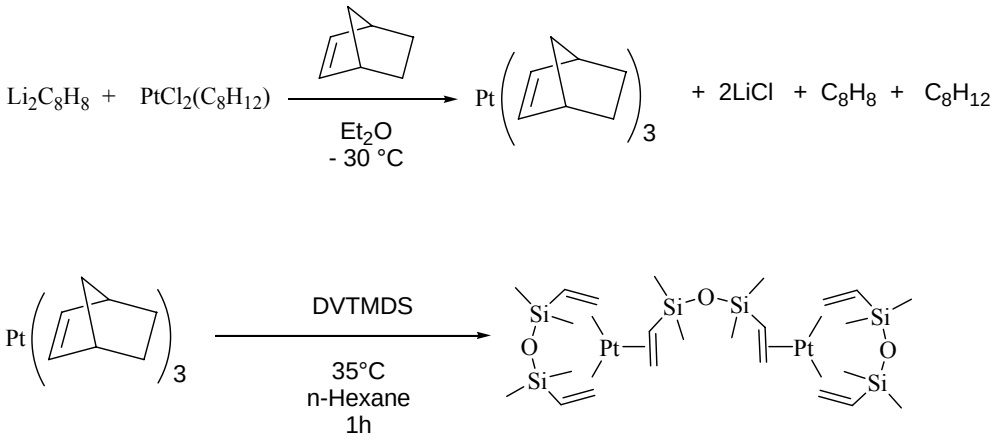

Scheme 3.4 Synthesis of $Pt_2(DVS)_3$ complex

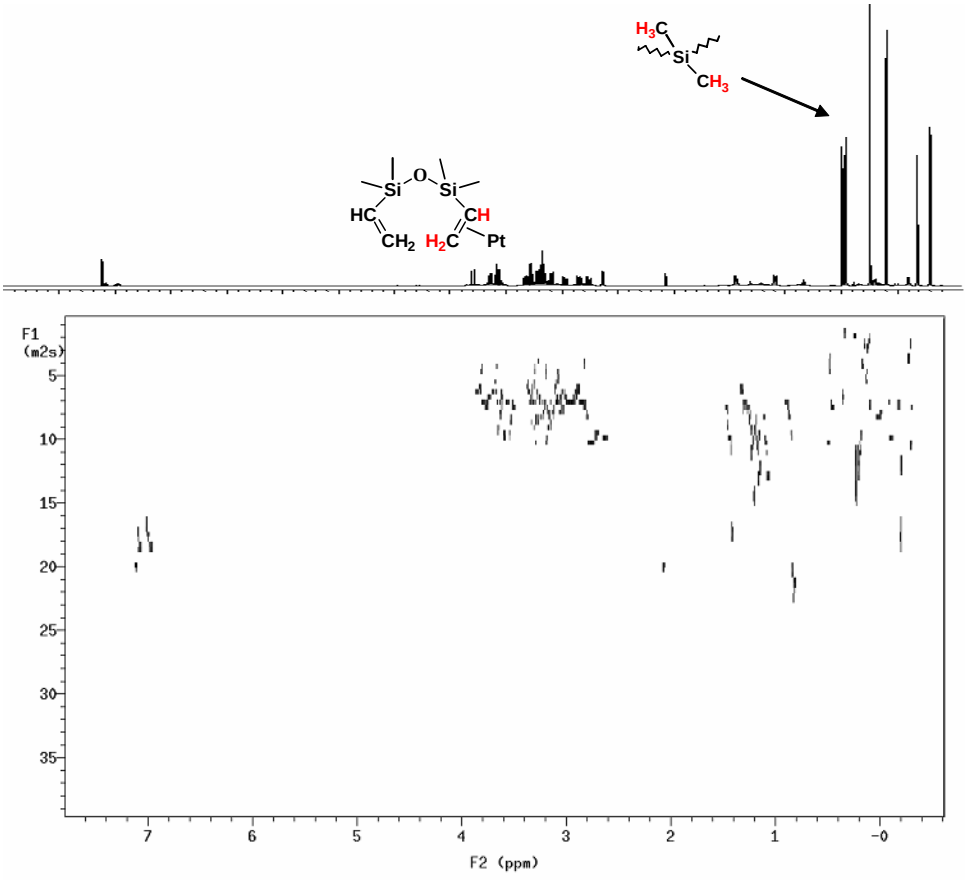

Figure 3.1 ^{1}H-NMR and DOSY spectra of $Pt_2(DVS)_3$ complex

The values of the diffusion coefficients of the analysed samples are reported in Table 3.1. By using equations (1) (with c = 6) and equation (3) the spherical hydrodynamic radius (r_H and $r_{H(Corr.)}$ respectively) can be calculated and compared with simulated values (Table 3.1).

Table 3.1. Values of the diffusion coefficients of the analysed samples with their hydrodynamic radii obtained by using Skokes-Einstein equation (1) and Gierer -Wirtz equation (3) respectively.

Compound	Diffusion Coefficient (m^2/sec)	r_H (Å) (a)	$r_{H(corr)}$ (Å) (b)	r_{MM} (Å) (c)
Benzene	$21.6 \cdot 10^{-10}$	1.65	2.7	2.87
Mesitylene	$17.7 \cdot 10^{-10}$	2.0	3.0	3.32
DVS	$13.0 \cdot 10^{-10}$	2.7	3.6	3.78
TVCTS	$11.0 \cdot 10^{-10}$	3.2	4.0	4.43
$Pt(nbn)_3$	$9.6 \cdot 10^{-10}$	3.7	4.4	4.33
$Pt_2(DVS)_3$	$6.5 \cdot 10^{-10}$	5.4	5.8	5.45

(a) spherical hydrodynamic radius from eq.(1); (b) spherical hydrodynamic radius from eq.(3); (c) spherical radius obtained from Van der Waals volume of structure optimized with MMFF and/or PM3 semiempirical model (Spartan 04 software);

As evidenced from the data reported in the above table and confirmed by results present in the literature,[9] for small molecules (with diffusion coefficient bigger than 6.5 10^{-10} m^2/sec) the equation of Gierer –Wirtz is more accurate than the Stokes – Einstein equation. For compounds with small diffusion coefficient (and then big size) the values of spherical hydrodynamic radius obtained by Stokes – Einstein equation agree with those obtained by Gierer –Wirtz equation.

By using the two equation above reported (equation (1) and (3)) a sphere-like shape of examined compounds in solution has been supposed. To fit with the real shape of the molecule in solution the molecules can be considered as ellipsoidal. Relative to the spherical model, the ellipsoidal model imposes a shape factor to extract the molecular dimensions from the measurement of D obtained by using NMR spectroscopy, as given in Equation 3.4.[10]

$$f = f^{\circ}\left(\frac{P^{-1/3}(P^2-1)^{1/2}}{\ln\left[P+(P^2-1)\right]^{1/2}}\right) \qquad 3.4$$

where P is the ratio of the semimajor to the semiminor axis of the ellipsoids, with P being always greater than one, f^0 is the friction coefficient (eq. 3.5) and f is the correct friction coefficient (eq.3.6):

$$f^0 = 6\pi\eta r_H \qquad 3.5$$

$$f = \frac{6\pi\eta r_H}{\frac{3\, r_{solvent}}{2\, r_H} + \frac{1}{1+\frac{r_{solvent}}{r_H}}} \qquad 3.6$$

The ratio between f and f^0 could be obtained by equation 3.7.

$$\frac{f}{f^0} = \frac{r_{eq.}}{r_H} \qquad 3.7$$

The spherical equivalent radius (r_{eq}) may be calculated from the partial specific volume (v) of the species (obtained by x-ray crystallographic analysis) and its molecular weight (M) by using Equation 3.8, in which N_A is the Avogadro constant.[11]

$$r_{eq} = \sqrt[3]{\frac{3Mv}{4\pi N_A}} \qquad 3.8$$

Combining the equations 3.4, 3.7 and 3.8 it is possible to obtain the value of P (ratio of the semimajor to the semiminor axis of the ellipsoids).

The spherical equivalent radius (r_{eq}) which is determined by x-ray crystallographic analyses can be now compared with the hydrodynamic radius (r_H) obtained from DOSY experiments. In particular, in Table 3.2, r_{eq}, r_H, f/f^0 and P for the Pt synthesized complexes are reported.

Table 3.2. Equivalent radius (r_{eq}) determined by x-ray crystallographic analyses, hydrodynamic radius (r_H) obtained from DOSY experiments f/f^0 and P of the $Pt(nbn)_3$ and $Pt_2(DVS)_3$ complexes.

Compound	**Diffusion Coefficient (m^2/sec)**	**r_{eq} (Å)**	**$r_{H(corr)}$ (Å)**	**f / f^0**	**P**
$Pt(nbn)_3$	$9.6 \cdot 10^{-10}$	4.7	4.4	1.078	2.51
$Pt_2(DVS)_3$	$6.5 \cdot 10^{-10}$	6.0	5.8	1.022	1.64

The above data show that the values of radius of a near spherical compound obtained with DOSY experiments agree with those obtained by x-ray crystallographic analyses. These results confirm that (i) DOSY is a powerful technique to evaluate the size of metal-organic systems in solution and (ii) Stokes-Einstein equation (1) can be reasonably used for the estimation of core-shell diameters.

3.3.2 CHARACTERIZATION OF Pt(mes)/DVS SYSTEM.

3.3.2.1 ^{1}H-NMR, gHSQC and TOCSY analysis

A sample of **Pt(mes)/DVS**, obtained as above, was dissolved using C_6D_6 as solvent (0.7 ml) containing 0.1 % of TMS and the solution was transferred in a NMR tube under argon atmosphere. TMS was used as internal standard both for ^{1}H-NMR analyses and for NMR-DOSY analyses. In particular for the DOSY experiments the diffusion coefficients of the species in solution could be corrected on the basis of diffusion coefficient of TMS, to prevent possible fluctuations in the viscosity of the solution owing to the presence of the solute. The platinum concentration in the NMR tube was 1.86 mg/ml.
To minimize the errors on the preparation procedure of the samples, all the samples were prepared exactly following the above procedure, maintaining constant the metal-ligand ratio and the stabilization and the evaporation time. In Figure 3.2 is reported the ^{1}H-NMR spectrum of **Pt(mes)/DVS** in C_6D_6.

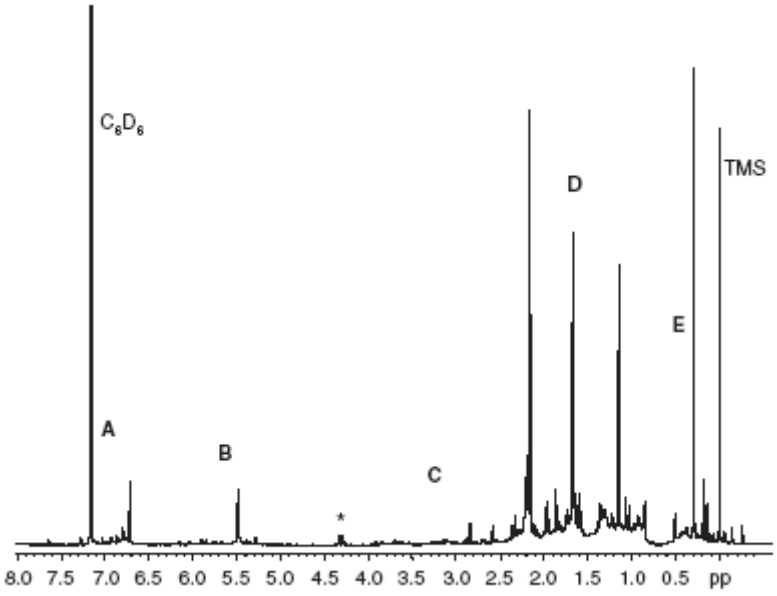

Figure 3.2 ^{1}H-NMR spectrum of Pt(mes)/DVS at 25°C, in C_6D_6

The ^{1}H-NMR spectrum of **Pt(mes)/DVS** at 25°C, in C_6D_6, is constituted by five distinct regions:

- 6.5 ppm – 7.8 ppm, region A
- 4.8 ppm – 6.4 ppm, region B
- 2.4 ppm – 4.0 ppm, region C
- 0.6 ppm – 2.4 ppm, region D
- 0.7 ppm – 0.1 ppm, region E

To have additional information concerning the attribution of ^{1}H-NMR signals and on the species present in solution, gHSQC (gradient Heteronuclear Single Quantum Coerence) and TOCSY (Total Correlated Spectroscopy) maps were performed. gHSQC analysis map gave the scalar heteronuclear ^{1}H - ^{13}C correlation between proton and carbon nuclei directly bound each other and allowed us to distinguish between CH, CH_2 and CH_3 groups on the basis of their different phases (CH and CH_3 positive and CH_2 negative shown by a single counter level). Its analysis show that in the A and B regions are presents exclusively CH protons. TOCSY analysis allowed us to detect ^{1}H-^{1}H scalar correlation inside isolated fragments and led to establish that aromatic CH protons of region A were connected by chemical bonds exclusively with CH_3 protons of the region D (2.0 ppm – 2.2 ppm). Any methylene group is not detected inside A and B regions, pointing out the absence of free double bonds of DVS. Methylene and methine groups of double bonds are detected in the region C, which is characteristic of metal π-bonded[8,12] double bonds. Integrated area of region D, including methyl resonances, exceeds that one expected for mesitylene and DVS moieties, revealing contributions from different species. As a matter of fact also remarkably low frequencies shifted methylene groups were detected inside regions D and E, which are according to metal-alkyl, as reported in the literature for organometallic compounds of this type[13] and for Pt nanoparticles formed during Pt catalyzed hydrosilylation reactions.[14] Metal-alkyl species probably arise from the

insertion of DVS double bonds into Pt-H bonds. The formation of hydride species by activation carbon–hydrogen bonds in organic solvents, such as toluene or mesitylene, by solvated metal atoms is well known[15] and also, can be confirmed by the determination, by GC-MS analysis, of homo-coupling products of mesitylene such as 1,2-di-(2,4-dimethylphenyl)-ethane (Scheme 3.5).

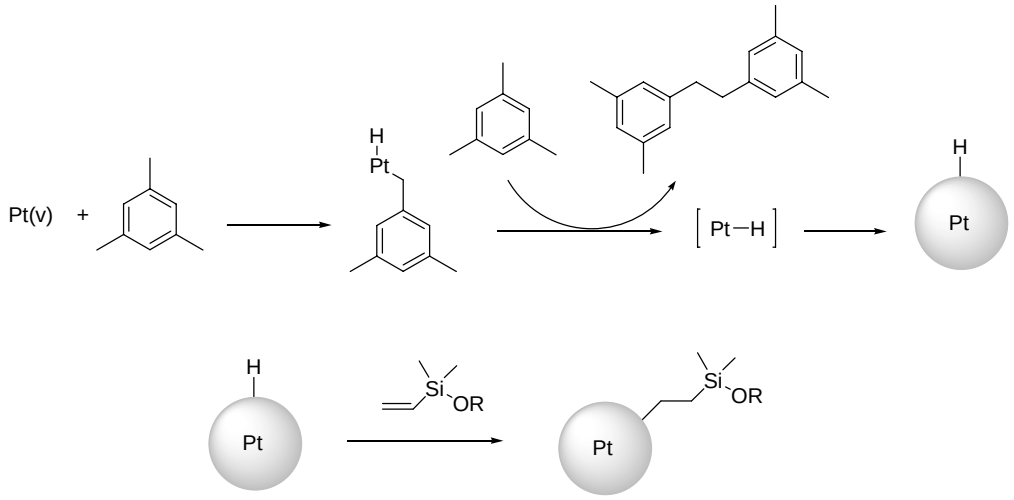

Scheme 3.5 Hypotetic mechanism of formation of Pt-Alkyl species

It is noteworthy that ^{1}H-NMR spectrum includes a signal at 4.3 ppm which is due to a CH_2 moiety which can be attributed to above said mesitylene dimer. Above said assignments were confirmed by the detection of through space dipolar interactions in the ROESY map. In fact, dipolar correlations between aromatic protons in the A and B regions and methyl resonances included in the D part of the spectrum were detected. Interestingly, ROE interactions were also observed between aromatic protons of the regions B and A and DVS protons in the 0.54–1.93 ppm spectral region. These correlations strongly indicate the simultaneous presence both of mesitylene and DVS ligands in the same nanoaggregates. Protons of the regions D and E do not give correlation with other region of the spectrum. These extensive study on **Pt(mes)/DVS** composition, suggest that the growth of **Pt/mes** nanoparticles obtained by MVS procedure is actually quenched through formation of σ- and π-bonded DVS species on the metal surface, preventing further aggregation to bulk metal powders (Scheme 3.6).

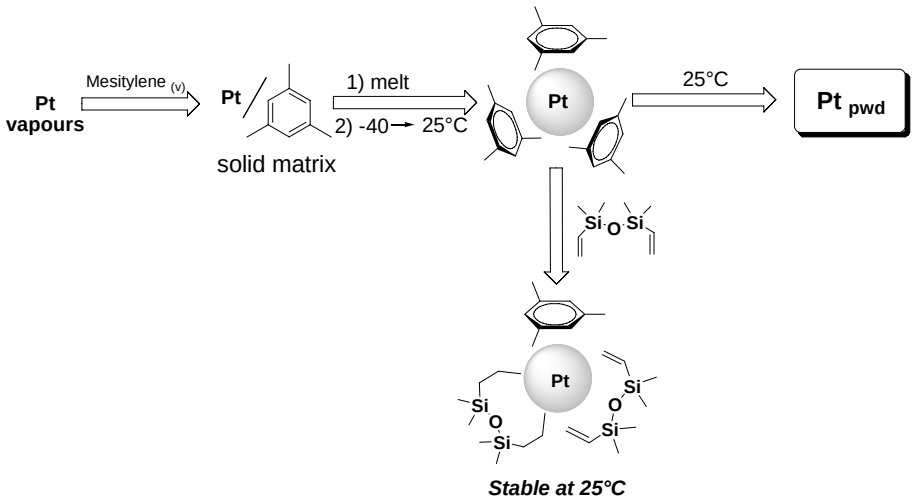

Scheme 3.6 Scheme of stabilization of Pt/mes solutions with DVS

3.3.2.2 Quantitative analysis of integrated signals of species in solution

For a semi-quantitative evaluation of the molar ratios of the different species in solution, evidenced by NMR analyses above described, the following protocol of analysis of integrated areas was used.

Non-coordinated mesitylene = (regA – C_6D_5H)/3 = 1.88 34%

Coordinated mesitylene = regB/3 = 1.07 19.5%

DVS-π = regC/6 = 0.39 7%

Pt-Alkyl = (D+E-3(A-C_6D_5H)-3B-2C)/20 [a] = 2.18 39.5%

It can be observed that in the experimental condition used for preparation of these **Pt(mes)/DVS** solutions, Pt-alkyl species are formed preferentially and the % of Pt-vinyl is very low.

3.3.2.3 ^{1}H-NMR DOSY analysis and theoretical evaluation of shell thickness

The basic 2D DOSY spectrum displays conventional chemical shifts in one dimension and diffusion coefficient in the other dimension. Because of the relationship between diffusion rates and molecular radii, the diffusion dimension reveals the distribution of molecular sizes of different molecular species. The spectrum indicates the presence of very small solvated Pt clusters ranging from 0.8 to 2.0 nm in core-shell diameter (Figure 3.3).

[a] Pt-monoalkyl are neglected because of the low % of DVS-π

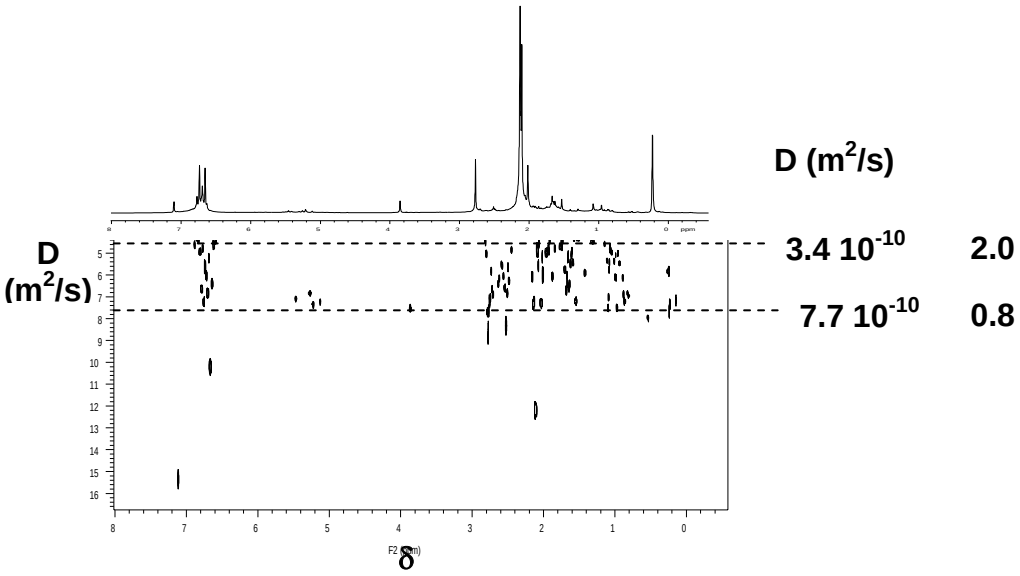

Figure 3.3 DOSY spectrum of Pt(mes)/DVS

In order to evaluate the metallic core diameter, the knowledge of the thickness of the organic surrounding shell is required. Since this value is not reported in literature data and the exact composition of our DVS-mesitylene stabilized Pt nanoparticles is unknown, we performed a theoretical calculation of optimized geometry on model cluster compounds with MMFF.
For our study we made a simplified model of Platinum clusters Pt_n (with $4 < n < 14$): (i) we used the σ-bonded DVS as sole ligand, since this is the most abundant species in the shell and (ii) we consider two limit situations in which each Platinum atom brings respectively one or two metal-alkyl bond (a bare Pt_{12} nucleus and clusters $Pt_{12}(DVS)_6$ and $Pt_{12}(DVS)_{12}$ are represented in Figure 3.4 as example). The results are summarized in Table 3.3 and Figure 3.5.

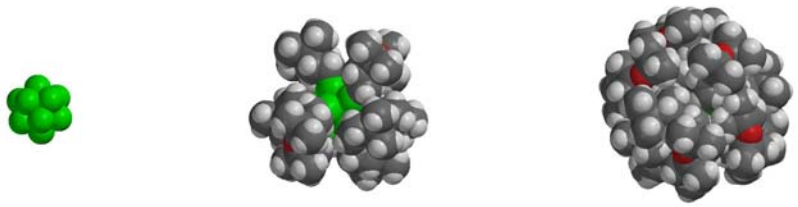

Figure 3.4 models of Pt_{12}, $Pt_{12}(DVS)_6$ and $Pt_{12}(DVS)_{12}$ optimized with MMFF (Spartan 04)

Table 3.3 Calculated Pt_nDVS_n clusters radii

Cluster	Van Der Waals volume (Å^3)	core-shell radius (Å)	core radius (Å)	shell radius (Å)
$Pt_4(DVS)_2$	530.32	5.0	2.7	2.3
$Pt_6(DVS)_3$	791.5	5.7	3.1	2.6
$Pt_8(DVS)_4$	1060.85	6.3	3.4	2.9
$Pt_{10}(DVS)_5$	1318.14	6.8	3.7	3.1
$Pt_{12}(DVS)_6$	1580.09	7.2	3.9	3.3
$Pt_{14}(DVS)_7$	1841.74	7.6	4.1	3.5
$Pt_4(DVS)_4$	921.34	6.0	2.7	3.3
$Pt_6(DVS)_6$	1456.51	7.0	3.1	3.9
$Pt_8(DVS)_8$	1936.37	7.7	3.4	3.3
$Pt_{10}(DVS)_{10}$	2409.02	8.3	3.7	4.6
$Pt_{12}(DVS)_{12}$	2872.07	8.8	3.9	4.9
$Pt_{14}(DVS)_{14}$	3334.69	9.2	4.1	5.1

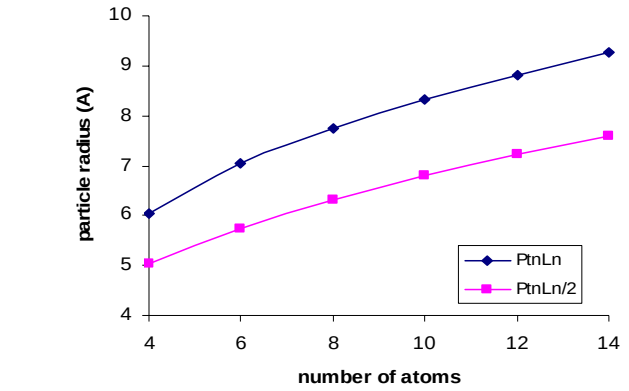

(a)

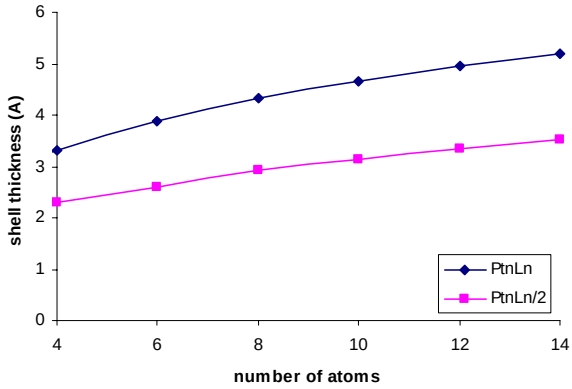

(b)

Figure 3.5 Plot of particles radius (a) and shell thickness (b) versus n

In the simulated system, particle radius increases with number of atoms, as well as shell thickness. In this last case, however, we observe that differences between adjacent clusters became smaller as the size increase. Additionally, for $n \geq 14$, it is unlikely that all atoms could be on the cluster surface so, above this value of n, a

cluster with a composition $Pt_n(DVS)_n$ is improbable. For these reason we did not perform calculations for bigger systems and suppose that a maximum value of shell thickness is reached. Thus, within these approximations, for bigger Pt clusters (n > 14, d > 1.6 nm) we will assume a shell thickness included in the range 3.5 – 5.1 Å (mean value = 4.3 Å), whereas for smaller systems we will refer directly to the above calculated values.

For **Pt(mes)/DVS**, DOSY analysis gives core-shell diameters ranging from 0.8 to 2.0 nm, corresponding to Platinum aggregates with core diameters of presumably less than 1.3 nm (2.0 – 2 x 0.35 nm). To estimate the number of Pt atoms in a cluster of given size, we can use this very simple geometric relationship:

$$n = \frac{V_{cluster}}{V_{Pt}} = \left(\frac{r_{cluster}}{r_{Pt}^{VdW}} \right)^3 \qquad 3.9$$

where r_{Pt}^{VdW} is the Van der Waals radius of Pt atom (1.75 Å). In the case of **Pt(mes)/DVS** we obtain $n \leq \sim 50$. The inferior limit, which correspond to an hydrodynamic diameter of 0.8 nm, is compatible with the presence of oligonuclear species (n = 4 or less), being also very close to the value obtained for the stoichiometric complex $Pt_2(DVS)_3$ (d_H = 1.08 nm, see previous section).

3.3.2.4 HRTEM analysis and comparison with Pt/mesitylene

Pt/(mes)DVS nanoparticles can be easily deposited on γ-Al_2O_3, simply by introducing a toluene solution of stabilized nanoparticles into a slurry of the support in the same solvent under vigorous stirring, exactly like the corresponding **Pt/mes** precursor (see section 3.1).
The supported system obtained in this case is characterized by a mean diameter of 1.7 nm, which is sensibly lower than the value measured for supported **Pt/mes** particles, as expected (Figure 3.6). Values obtained in the previous section by means of DOSY analysis are quite in agreement with those obtained by HRTEM.

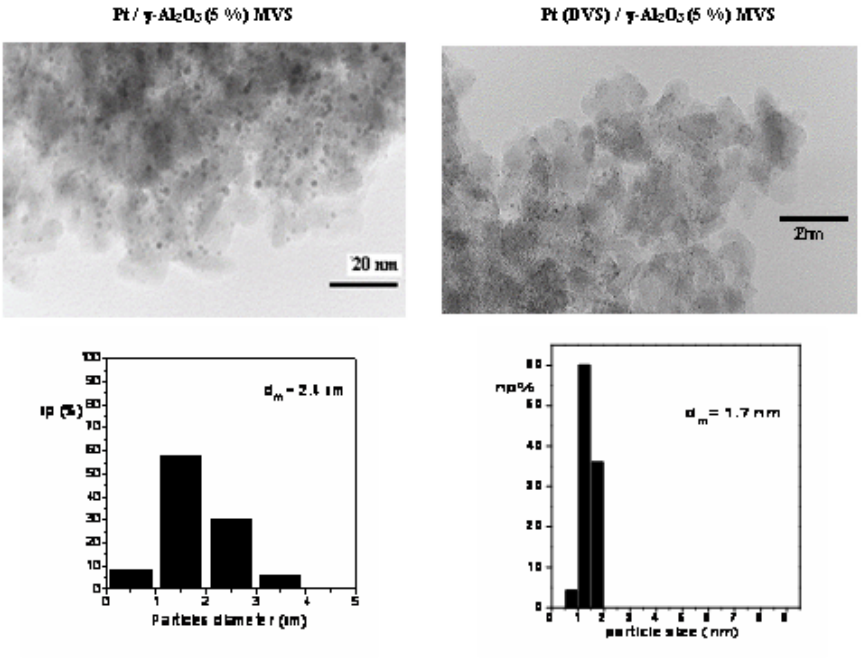

Figure 3.6 HRTEM pictures of Pt/Al_2O_3 derived from Pt/mesytilene (left) and Pt(mes)/DVS (right)

3.4 DVS CO-VAPORIZED WITH METAL

DVS, which has demonstrated to be a good stabilizing ligand for Pt nanoparticles, is also a very volatile compound. Thus, it can be used as co-solvent in MVS procedure. This could allow, in principle, to quench the particles growth at early stages, affording smaller nanoparticles than in previous cases (see section 2.2.4). The co-condensation of Pt vapour with DVS and mesitylene in great excess, at liquid nitrogen temperature, forms a frozen matrix which gives, on melting, a Pt-containing solution (which we indicate as **Pt/(DVS-mes)**) which is stable at room temperature (Scheme 3.7).

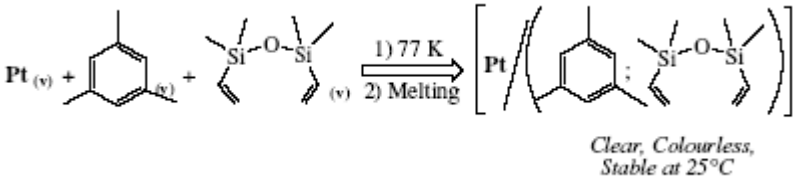

scheme 3.7

Pt/(DVS-mes) sample is in the form of a clear and colourless solution which can be stored at room temperature for several months, without changes in colour and without the formation of Pt metal. Moreover, the solid obtained by removing the volatiles from the **Pt/(DVS-mes)** solution under vacuum can easily be re-dissolved in aromatic and aliphatic solvents. The role of both DVS and mesitylene in providing soluble colourless Pt species was further demonstrated by vaporization experiments

of Pt and DVS without mesitylene: in these cases the formation of platinum powders was detected.

3.4.1 CHARACTERIZATION OF Pt/(DVS-mes) AND COMPARISON WITH ANALOGOUS SYSTEMS

The ^{1}H-NMR spectra of the analysed samples was obtained keeping under vacuum a portion of the Pt solutions and dissolving the solid obtained in C_6D_6 (0.7 ml) containing 0.1 % of TMS. The ^{1}H-NMR spectrum of **Pt/(DVS-mes)** was compared with those of **Pt/(mes)DVS** and a commercial Pt-Karstedt catalyst (Figure 3.7). The spectrum of **Pt/(DVS-mes)** was quite similar to those produced by the others samples. Combined use of 1D and 2D NMR techniques gHSQC (gradient Heteronuclear Single Quantum Coherence); TOCSY (TOtal Correlated SpectroscopY); ROESY (Rotating-frame Overhauser Enhancement SpectroscopY) and DOSY (Diffusion-Ordered SpectroscopY) involving the detection of scalar and dipolar couplings, as well as translational diffusion, provided information on the nature of the species, whose resonances contribute to the main spectral regions A – E (see Figure 3.7), and on their average sizes.

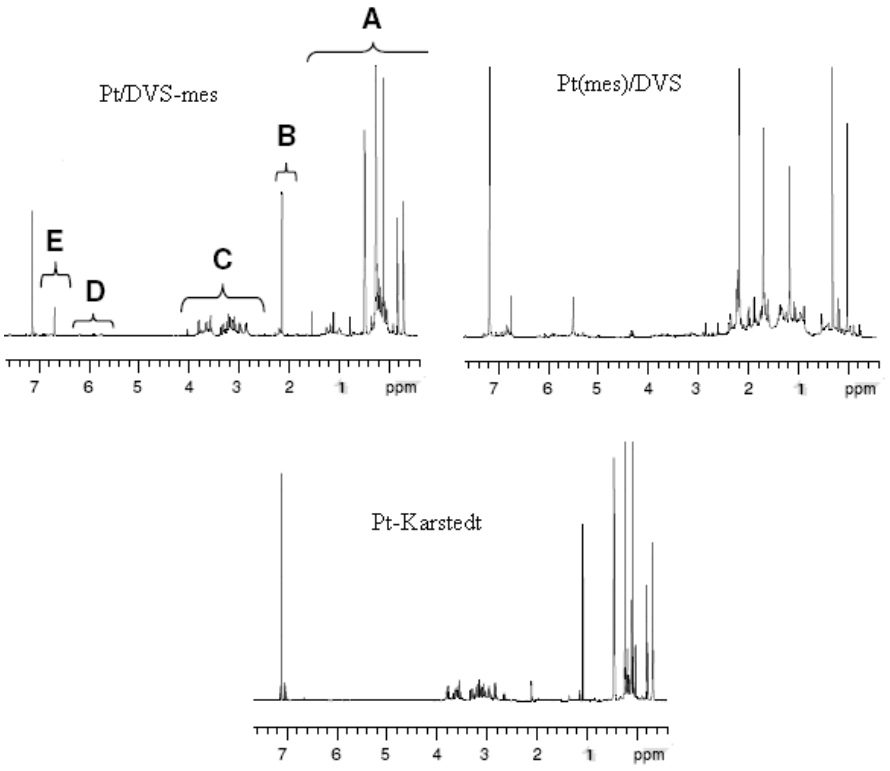

Figure 3.7 Comparison of ^{1}H-NMR of Pt/(DVS-mes), Pt(mes)DVS and Pt Karstedt

HSQC analysis demonstrated that region E was constituted by methine protons which gave rise to, in the TOCSY map, long-range scalar correlations with methyl groups inside B region. Therefore region E can be unequivocally assigned to aromatic protons of mesitylene moieties. Spectral region D corresponded to methine and methylene vinyl moieties (HSQC) of DVS at chemical shifts very close (Figure

3.8) to those of free DVS ligands. Thus, these signals were assigned to free double bonds not directly bonded to the metal, but included in its coordination sphere. As matter of fact, protons of region D gave ROE interactions with protons of C spectral region through space.

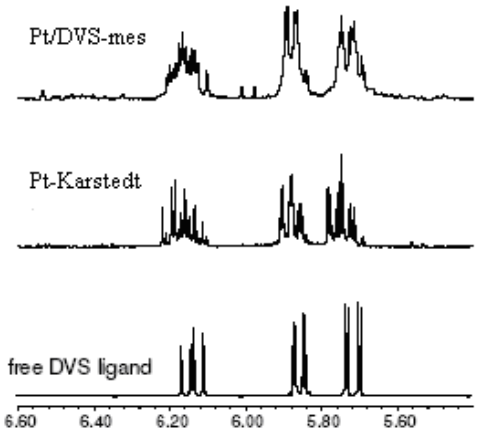

Figure 3.8 Comparison of olefinic protons of Pt/DVS-mes, Pt-Karstedt and free DVS ligand

Region C (Figure 3.7) contained protons giving direct ^{13}C scalar correlations inside methine and methylene moieties (Figure 3.9a), which were attributed, as for D region, to signals of double bonds. Their remarkable low frequencies shift was attributed to coordination with the metal, in accordance with the literature data.[16] Thus region C included π-bonded double bonds of DVS, part of which was assigned to DVS moieties with both double bonds complexed to the metal and with only one double bond complexed to the metal and the other one uncomplexed (region D, Figure 3.7), as revealed by abovementioned dipolar correlation occurring between protons of regions D and C. Moreover, some dipolar interactions were detected between DVS and mesitylene protons in regions E, C and E, A (Figure 3.9) to indicate species in which DVS and mesitylene belong to the same coordination sphere of platinum. Finally region A included methyl groups of DVS species, but, surprisingly also showed the presence of highly shielded methylene moieties (HSQC) (Figure 3.9b), which are unexpected in this region and can be reasonably assigned only to metal-alkyl species arising from the insertion of DVS into Pt-H bonds.[17] As in the previous case, the sources of hydride species might be mesitylene solvent, since in the mixture dimeric 1,2-bis(3,5-dimethylphenyl)ethane was clearly identified by GC-MS analyses.

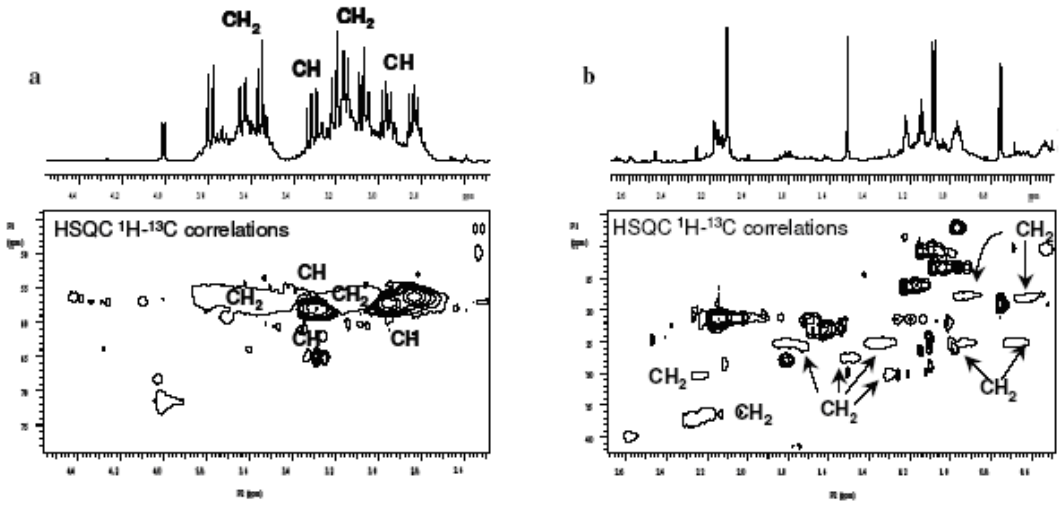

Figure 3.9 Heteronuclear correlation in Pt/DVS-mes: (a) olefinic region; (b) aliphatic region

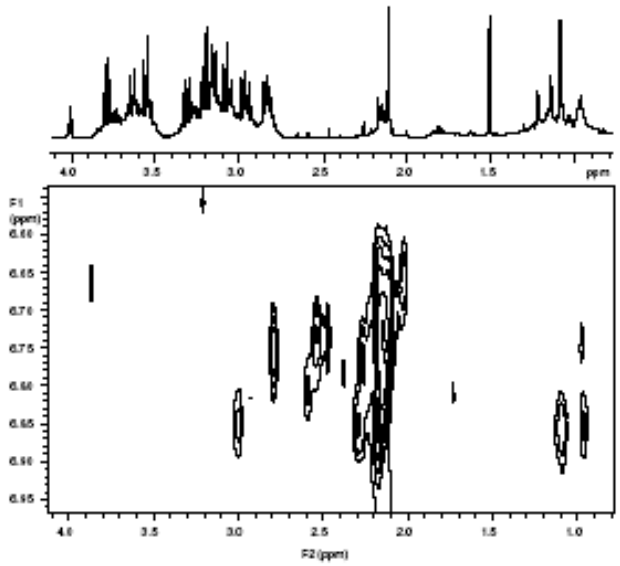

Figure 3.10 Homonuclear dipolar interactions in Pt/DVS-mes

Thus **Pt/(DVS-mes)** prepared by co-vaporization of platinum both with DVS and mesitylene contained species very similar to those detected for **Pt(mes)/DVS** prepared by adding DVS to solutions obtained by co-vaporization of Pt and mesitylene only. However, as can be seen in Figure 3.7, quite different integrated areas of the A and E spectral regions were observed. Previously discussed spectral assignments allowed us to establish that protons of double bonds of DVS contributed only to C and D regions and protons of mesitylene contributed only to E and B regions. A+B region has contributions only from the methyl resonances of mesitylene and from the methyl groups of DVS. Due to the fact that the integrated area of the region A+B exceeded the expect one on the basis of contributions from DVS and mesitylene, the excess of integrated area must be correspond to alkyl-metal species protons. Quantitative analyses of integrated areas of regions A – E led to the conclusion that **Pt/(DVS-mes)** contained essentially DVS chelated (41%) and alkyls

species (49%) bonded to platinum atoms and low amounts of mesitylene and DVS mono-coordinated Pt-species, whereas **Pt(mes)/DVS** had mesitylene and alkyls species.

Finally, DOSY analysis allows us to determine the diffusion coefficients of the species present in solution. Diffusion coefficients are correlated to molecular sizes on the basis of Equation 3.1, strictly holding for medium to high molecular weight and spherical molecules. The value measured for **Pt/(DVS-mes)** revealed the presence of Pt species having an average diffusion coefficient between 5.8 and 7.4 x 10^{-10} m^2/s which, on the basis of Equation 3.1, corresponds to hydrodynamic diameter ranging from 0.9 to 1.2 nm (Figure 3.11). On the basis of our theoretical considerations (see previous section), this would correspond to $Pt_{2\text{-}8}$ clusters. DOSY analysis carried out on Karstedt catalyst revealed a similar diffusion coefficient of Pt species in solution (6.0 x 10^{-10} m2/s) corresponding to hydrodynamic diameter of 1.1 nm. As above reported, the same analysis for **Pt/(mes)DVS** showed diffusion coefficients ranging from 7.7 to 3.4 x 10^{-10} m^2/s corresponding to a wider platinum size distribution (0.8 – 2.0 nm in diameter) than the previous discussed samples. The results of the NMR structural investigation of the different Pt samples can be schematically represented as in Figure 3.12.

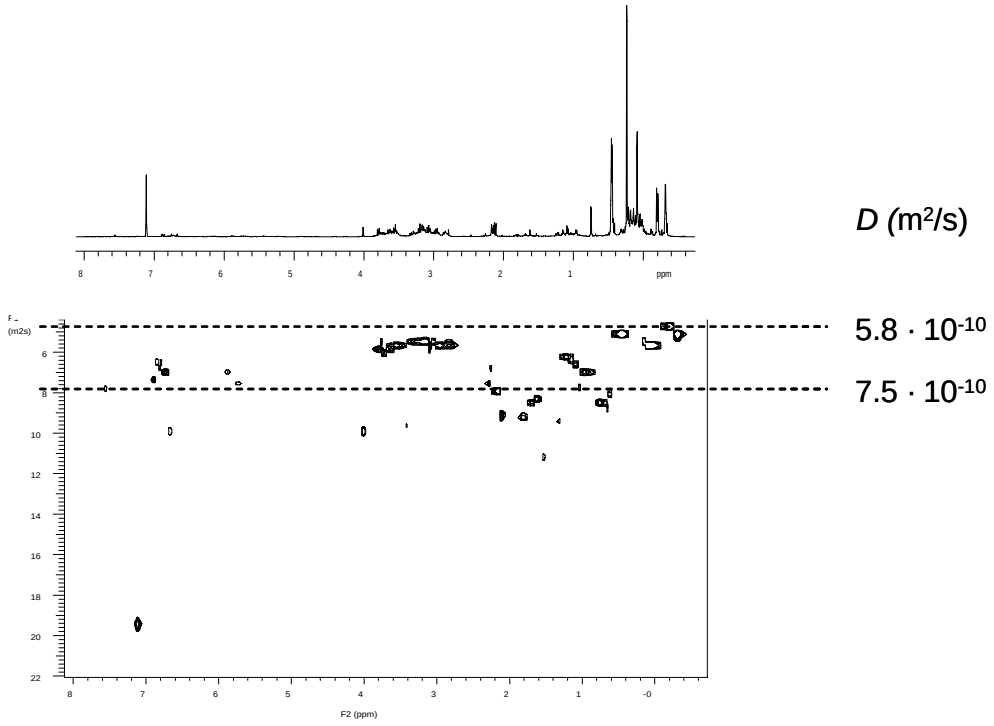

Figure 3.11 DOSY spectrum of Pt/DVS-mes

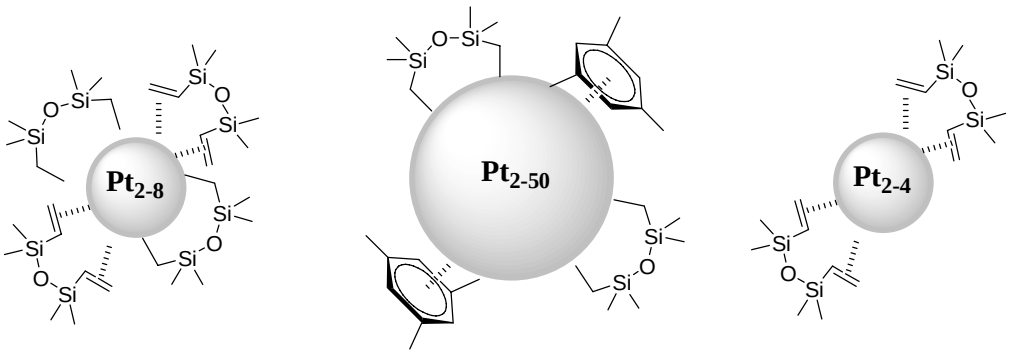

Figure 3.12 Schematic representation of the Pt clusters analyzed in this section

As can be seen from the data shown in Figure 3.12, there is a significant difference between **Pt/(DVS-mes)** and **Pt(mes)/DVS** in the order of magnitude of the platinum atoms aggregation (number of Pt atoms 2 - 8 versus 2 - 50). Like Pt-Karstedt, **Pt/(DVS-mes)** is colourless, while **Pt/(mes)DVS** is brown: the difference in the Pt size can satisfactory account of this variation in colour, in agreement with literature.[18] It is demonstrated that when DVS is co-vaporized with metal, growth process of platinum nanoparticles is effectively quenched at early stages, affording very small aggregates whereas, the addition of DVS after isolation of **Pt/mes** solutions, allow the formation of larger and polydisperse stabilized clusters (Scheme 3.8).

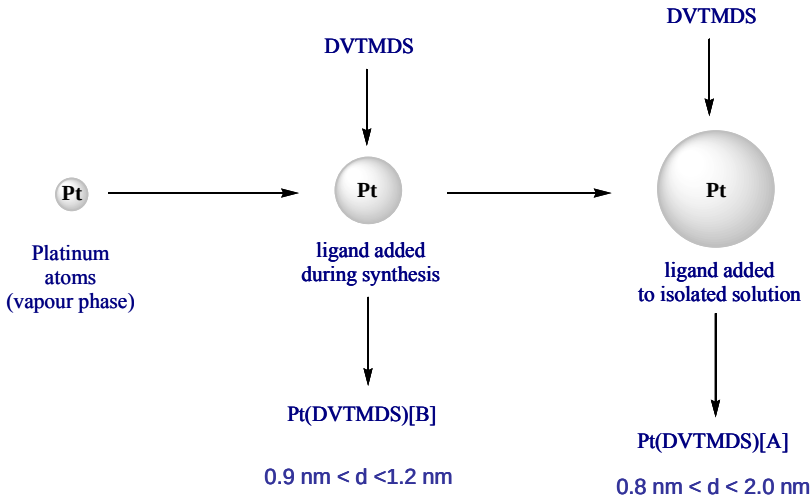

Scheme 3.8

3.5 EFFECT OF CONCENTRATION

In order to have a better insight into the factors affecting the nucleation and growth of the Pt nanoparticles, which are crucial points in the preparation of size-tailored nanoparticles, Pt/mes samples, prepared at various Pt-concentrations, have been stabilized by quenching the growth of Pt particles with 1,1,3,3-

divinyltetramethyldisiloxane (DVS) as further stabilizing ligand and NMR studies have been undertaken. The nature of nanoaggregates formed in solution has been investigated, as usual, by ^{1}H-NMR techniques. The ^{1}H-NMR (600 MHz, 25 °C) spectrum of Pt/Mesitylene-DVS stabilized sample dissolved in C_6D_6 containing 0.1% of TMS was first recorded to obtain information about the kind of Pt species that are present in solution. Detected signals do not change their chemical shifts, shape and relative intensity at different concentrations, being all very similar to those showed in the previous sections for **Pt(mes)/DVS**.
DOSY analysis was used, as usual, for the estimation of particle size in solution. Core diameters were estimated following the already discussed method (see section 3.2). Results are summarized in Table 3.4.

Table 3.4 Estimated particles size in Pt(mes)/DVS solutions prepared at different concentrations

[Pt] (mg/mL)	Diffusion coefficients (10^{-10} m^2/s)	Core-shell diameter (nm)	Core diameter (nm)
0.13	6.1 - 3.2	1.1 – 2.1	0.6 - 1.4
0.25	7.7 – 3.5	0.8 – 2.0	0.5 - 1.3
0.35	5.5 - 3.9	1.3 - 1.8	0.7 - 1.1
1.0	5.3 – 3.9	1.3 – 1.7	0.7 - 1.0
2.1	3.5 - 2.5	1.9 – 2.7	0.9 - 2.0
3.1	5.6 - 2.5	1.2 – 2.7	0.6 - 1.7

Diluted systems ([Pt] < 1.0 mg/mL) shows comparable values of particle diameters, while for concentrated solutions ([Pt] > 2.1 mg/mL) the particle size increases sensibly, as well as the size distribution. This concentration effect can be easily explained, in a qualitative way, considering that for more concentrated **Pt/mes** solutions, before addition of DVS ligand, the collision between particles is most probable than in diluted ones, leading to an extensive growth of particles and to a broadening in the size distribution.

3.6 GROWTH STUDIES IN ISOLATED SOLUTIONS

In order to gain a better understanding of the growth process of platinum particles in solution before precipitation and, hence, to improve knowledge of the experimental parameters controlling growth processes, we investigated the influence of temperature on particle sizes. To this aim Pt/mesitylene solutions were prepared, kept at two different temperatures 25 °C and -40 °C, respectively, and the growth of nanoparticles was quenched by addition of DVS at different times. The size of the DVS-stabilized platinum nanoparticles was evaluated by ^{1}H NMR-DOSY experiments.
Pt vapour, generated by resistive heating of a tungsten wire surface coated with electrodeposited Pt (40 mg), was co-condensed with mesitylene (80 ml) in a glass reactor described elsewhere (see section 1.2.5 and experimental section) The reactor chamber was warmed at the melting point of the solid matrix (- 40°C), and the resulting yellow-brown solution was siphoned and handled by Schlenk techniques. The content of the metal, evaluated by atomic absorption analysis (AAS), was 0.35

mg/mL. In a typical experiment, the **Pt/mes** solution was kept at 25°C and -40°C , respectively, by a thermostat bath. When the temperature reached the temperature, a 5 ml portion of the solution (1.75 mg of Pt, $9 \cdot 10^{-3}$ mmoles), was added to a large excess of 1,3-divinyltetramethyldisiloxane (DVS) (molar ratio DVS/Pt = 1000/1; 2.0 ml, 9 mmoles) in a Schlenk tube (50 ml), at different times (0, 30', 60', 90', 120', 240', 360' for the sample kept at 25°C and 0, 30', 60', 90', 120', 6 h, 24 h for the sample at -40°C). The resulting thermally stable solutions were stirred at 25°C for 15 minutes. The solvent was removed under vacuum by keeping the solution at $5 \cdot 10^{-5}$ mBar for 30 minutes at 25°C.

As previously demonstrated, addition of DVS to the solution of mesitylene-solvated platinum atoms, gives stable aggregates (see previous sections) which can be handled by conventional techniques and characterized by NMR analysis, after removal of the solvent and dissolution of the resulting brown solid in C_6D_6.

^{1}H-NMR analyses of the platinum samples (Figure 3.13) were very similar to those previously reported, and did not undergo significant changes in the samples prepared at 25 °C and -40 °C. The identity of species present in solution was quenched by combined use of 2D homo and heteronuclear scalar and dipolar correlation techniques (see previous sections). The presence of mesitylene, π-bonded DVS and alkyls derived from insertion of DVS vinyl groups into Pt-H species bound to the Pt surface was confirmed (see previous discussions). Even though the nature of the species involved at the different stage of growth process of platinum nanoparticles did not change over the time, a variation of the metal particle dimensions of the different samples occurred. The variation in the metal particle dimensions was effectively detected by the NMR DOSY technique, which enabled measurement of the diffusion coefficients of the platinum aggregates. They can be correlated with molecular sizes on the basis of equation 3.1, which strictly holds for medium to high spherical molecules.

Solutions were kept at 25 °C or – 40 °C and stabilized by adding DVS at different times. The stabilized solutions at different times were investigated by ^{1}H-NMR DOSY spectroscopy. Sizes of Pt aggregates were calculated from the measured diffusion coefficients by use of Equation 3.1 and the theoretical treatment described in section 3.3.1.

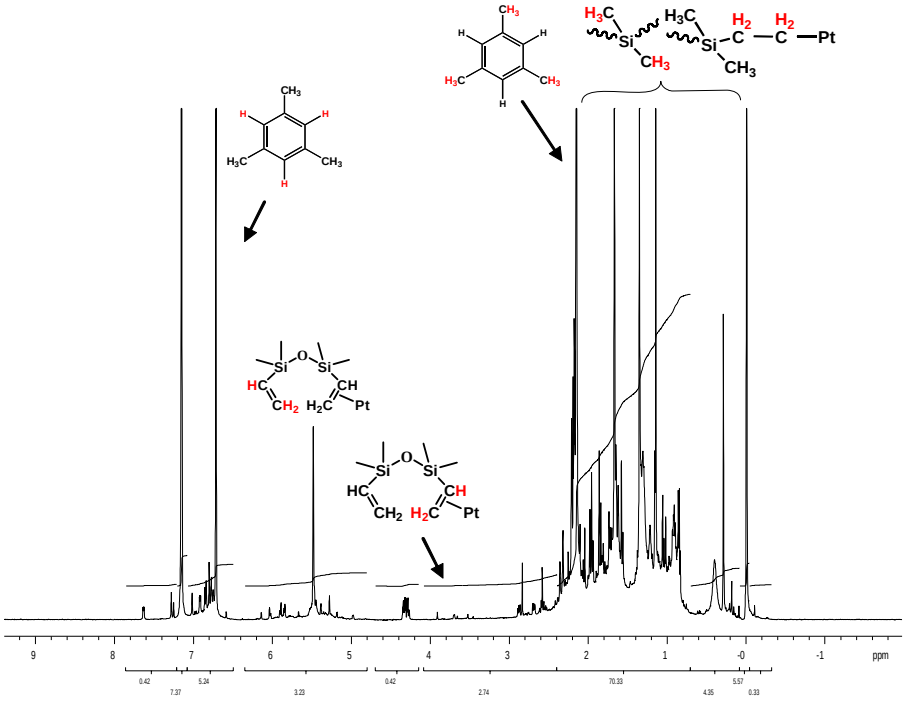

Figure 3.13 ^{1}H-NMR spectra of Pt(mes)/DVS at t = 30' (spectra of samples at different times are very similar)

DOSY analysis of samples clearly revealed that signals detected in the spectral regions C and B in the ^{1}H-NMR spectrum (Figure 3.13, see previous sections), attributed to platinum species containing π-bonded or chelated DVS, show diffusion coefficients centred at the average value of 7.0 x 10^{-10} m^2/s. This value did not change in all the samples stabilized at different times and, on the basis of Equation (1), corresponds to very small platinum particles with hydrodynamic diameter of 1.0 nm. In the low frequencies region (spectral regions D and E) the resonance of which were attributed mainly to Pt-alkyl species, the average value of the diffusion coefficient changed over time, indicative of a size-evolution of the platinum particles (Table 3.5, Figure 3.14).

Table 3.5. Time evolution of hydrodynamic diameter of Pt-alkyl aggregates at 25°C calculated by the Stokes-Einstein equation from diffusion coefficients measured by NMR DOSY analyses.

Sample	Time of addition of DVS (min.)	D (10^{10} m^2/s)	Hydrodynamic diameters (d_H) (nm)	Core diameters (nm)
Pt / mes (C_{Pt} = 0.35 mg/mL)	0	3.9 – 5.5	1.3 – 1.8	0.7 – 1.1
	30	3.8 – 5.0	1.4 – 1.9	0.7 – 1.2
	60	3.5 – 4.6	1.5 – 2.0	0.8 – 1.3
	90	3.2 – 4.2	1.7 – 2.2	0.9 – 1.4
	120	2.5 – 4.2	1.7 – 2.8	0.9 – 1.7

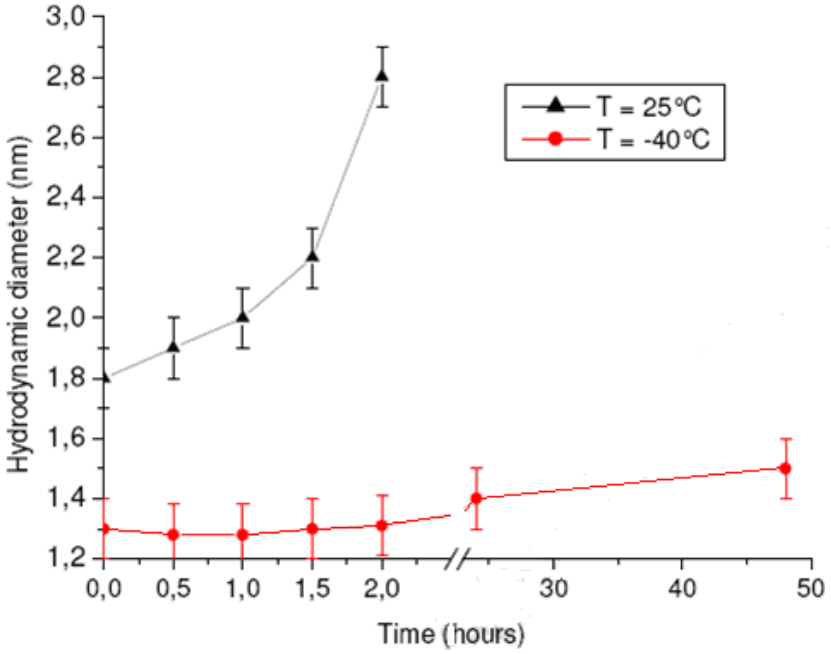

Figure 314. Time evolution of the maximum hydrodynamic diameter of Pt-alkyl aggregates at 25°C and at -40 °C calculated by the Stokes-Einstein equation from diffusion coefficients measured by NMR-DOSY analyses.

As is evident from Table 3.5, the quenching of metal aggregation at T = 25°C and t = 0 caused by addition of DVS to a **Pt/mes** solution with a Pt concentration of 0.35 mg/mL produced very small Pt-alkyl species with a distribution of diffusion coefficients ranging from 3.9 10^{-10} m^2/s to 5.3 10^{-10} m^2/s, corresponding to very small aggregates of platinum alkyls in solution with a very narrow distribution of hydrodynamic diameters in the range 1.3 – 1.8 nm.
DOSY data showed that the platinum particles formed from samples at longer times have smaller diffusion coefficients (Table 3.5), indicative of a growth of particle size over time (see spectra in experimental section).

A plot of the hydrodynamic diameter versus time derived from the minimum diffusion coefficient of the Pt-aggregates for each sample (Figure 3.14) showed that the Pt particles grow to a maximum hydrodynamic diameter of 2.8 nm in 2 hours. After 2 hours partial precipitation began and diffusion coefficients could no longer be measured because of the presence of insoluble particles, which obviously are not detected by solution NMR. HRTEM analyses on the insoluble platinum powder showed the presence of spongy aggregates with a diameter less than 1 μm formed by closely packed Pt particles of 3.8 nm in diameter (see section 3.1). This proves that after about 2 hours the nucleation stage is completed, and a fast autocatalytic stage then follows, as is customarily assumed for such systems.[19,20]
The stabilization of a Pt/mesitylene solution by addition of DVS at different times was repeated at -40°C. The ^{1}H-NMR spectra of these samples were very similar to those obtained at 25°C (Figure 1); in contrast, NMR DOSY analyses showed the

hydrodynamic diameters to be significantly smaller. In fact, platinum aggregates in the initial solution showed a maximum hydrodynamic diameter of 1.3 nm. In this case, however, the samples obtained by addition of DVS at different times over a period of 24 hours did not show a significant difference in diffusion coefficient values (Figure 3.15b), thus demonstrating the stability of mesitylene-solvated Pt nanoparticles at this temperature.

3.7 CATALYTIC TESTS

Some preliminary tests of catalytic activity of the Platinum nanoparticles synthesized in this work has been performed.
The platinum-catalyzed addition reaction of hydrosilanes to unsaturated bonds (hydrosilylation reaction) is a versatile reaction for the synthesis of organofunctional silanes and polysiloxanes, for the crosslinking of polymers and for the manufacture of silicone-organic polymers.[21] Several decades ago Speier showed the activity of hexachloroplatinic acid (H_2PtCl_6) in hydrosilylation of unsaturated substrates,[22] which led to the development of several Pt-based salts and complexes to add silanes to olefinic and acetylenic carbon-carbon bonds. An important class of transition metal compounds used as hydrosilylation catalysts are Pt(0) complexes containing vinylsiloxane ligands,[23] among which the most commonly used industrially is Karstedt's catalyst obtained by reaction of 1,3-divinyltetramethyldisiloxane (DVS) with hexachloroplatinic acid (H_2PtCl_6).[24] A disadvantage of the resulting catalysts is the corrosive nature of the system, due to the formation of HCl, which can be removed through a base treatment,[7] but under these conditions a reduction of catalytic activity and storage stability occurs.[25]

The **Pt/(DVS-mes)** system had already proved more active than commercially available Pt catalyst in the cross-linking of silicon materials.[26] In order to extend the comparison to low molecular weight systems, the addition of diethoxymethylsilane to allylamines was studied in this work, in the presence of the platinum solution prepared by MVS, **Pt/(DVS-mes)** and with the commercially available Pt-Karstedt catalyst. In this respect it is interesting to note that the hydrosilylation of this class of functional unsaturated compounds with common Pt catalysts (Speier's, Karstedt's catalysts) has been reported to be problematic in the case of allylamines, because of poor reproducibility or low activity; to solve this problem the use of Pt/C or PtO_2 at 85°C in a sealed tube under Ar was suggested.[27] In order to simplify the comparison with those results, the MVS derived systems were tested under Ar in the hydrosilylation of N,N-dimethylallylamine or N-ethyl-2-methylallylamine, in homogeneous conditions (Table 3.6). Both Pt catalysts proved active even when the reactions were carried out at 0°C or 25°C, respectivelyand with a substrate/metal molar ratio = 10000. With respect to this, it can be noted that for allyl hydrosilylations a problem may be the isomerization of the allyl group to an internal double bond, at a rate that is competitive with the hydrosilylation process. However, in the present case the reactions were remarkably clean, as confirmed by GLC analyses, where substrate 1, 2, 3a, 3b and mesitylene could account for > 95% of the total area. Moreover, ^{1}H and ^{13}C NMR spectra of the crude products showed the resonances expected for the regioisomeric mixture 3a / 3b, with no signal of any double bond isomerization compound (e.g. N,N-dimethylprop-2-enylamine, N-

isopropylideneethylamine or N-ethyl-2-methylprop-2-enylamine).[28] By contrast, less than 5 % conversion after 5 and 24 hours respectively was obtained using of PtO_2 under the same conditions, demonstrating that for secondary and tertiary allylamines the soluble catalysts, are definitively more effective than the previously reported heterogeneous system.

Table 3.6 Hydrosilylation of Allylamines with various Pt catalysts

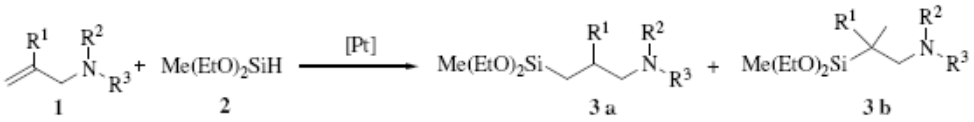

1 2 3 a 3 b

Entry	Substrate	Catalyst	T (°C)	t (h)	Conversion[a] (%)	Ratio[a] 3a / 3b
1	R^1 = H R^2 = Me R^3 = Me	Pt/(DVS-mes)	0	0.4	90	85 / 15
2		Pt-Karstedt	0	0.4	67	85 / 15
3		PtO_2	0	5	< 5	-
4	R^1 = Me R^2 = Et R^3 = H	Pt/(DVS-mes)	25	8	95	> 99 / 1
5		Pt-Karstedt	25	8	65	> 99 / 1
6		PtO_2	25	24	< 5	-

However, by comparing the **Pt/(DVS-mes)** system with the Karstedt catalyst, some differences could also be observed. In fact, although very similar regioselectivity values were obtained (regioisomer ratio 3a/3b = 85/15 and >99/1 for N,Ndimethylallylamine and N-ethyl-2-methylallylamine, respectively), significantly larger conversions were obtained using the former catalytic system (Table 3.6, entries 1 vs. 2 and 4 vs. 5, respectively). As observed in the curing of vinyl silane resins,[24] the Pt system obtained by MVS appears therefore more active than the Karstedt catalyst also in the hydrosilylation of low-molecular weight unsaturated compounds, containing amino groups. Interestingly, because both sample I and sample III solutions were evaporated under vacuum before the hydrosilylation runs, the variations in the catalytic activity cannot simply be ascribed to the "poisoning" due to the excess of free DVS in the commercial catalyst.

The **Pt/(DVS-mes)** system prepared by co-condensation of Pt vapour and a mixture of mesitylene and DVS ligand is very promising as a hydrosilylation catalyst, because of its catalytic activity, its stability at room temperature and its clear colourless appearance compared to the already reported MVS-derived sample II. As previously observed in the curing of vinyl silane resins,[24] and, here demonstrated in the hydrosilylation of low-molecular weight unsaturated compounds such as allylamines, **Pt/(DVS-mes)** showed higher catalytic activity than the Karstedt catalyst. The characterization of such system by combined NMR approaches allowed us to relate its enhanced activity to the presence of Pt-alkyl species and Pt-mesitylene

interactions (absent in the Karstedt catalyst), which could easily be replaced by the incoming unsaturated substrate.[29]
The synthetic procedure proposed here, also makes it possible to obtain a greater control of the metal particle diameter leading to a narrower size distribution. With regards to this, the considerable value of NMR DOSY spectroscopy for the effective and reliable evaluation of particle sizes in solution must be stressed.

3.8 CONCLUSIONS

Among the various preparative routes metal vaporization chemistry provides a valuable synthetic way to weakly stabilized nanostructured metal particles. DVTMDS is a suitable ligand to quench the particles growth at different stages. In particular:

(i) metal vapour synthesis of Pt NPs in presence of vapours of mesitylene, affords a Pt/mes SMAD, stable at low temperature. By storing the obtained solution at r.t. for some hours, a finely divided Pt powder (d_m = 3.8 nm) spontaneously precipitates;

(ii) if the ligand is added to a just prepared SMAD of **Pt/mes**, a stable solution of stabilized Pt NPs is collected, in which the ligand is coordinated mainly by σ bonds to the metal surface, togheter with mesitylene. Particles size reach a maximum of 1.3 nm, which correspond to clusters of some tens of Pt atoms;

(iii) if the ligand is co-vaporized with Pt and mesitylene, smaller particles are obtained, which are capped with essentially the vinylsiloxane ligand both as σ and π species. The particle size is smaller than in the previous case, reaching 0.5 nm which is compatible with the presence of oligonuclear Pt species (2 to 8 atoms for cluster). Points (i), (ii) and (iii) are summarized in Figure 3.15.

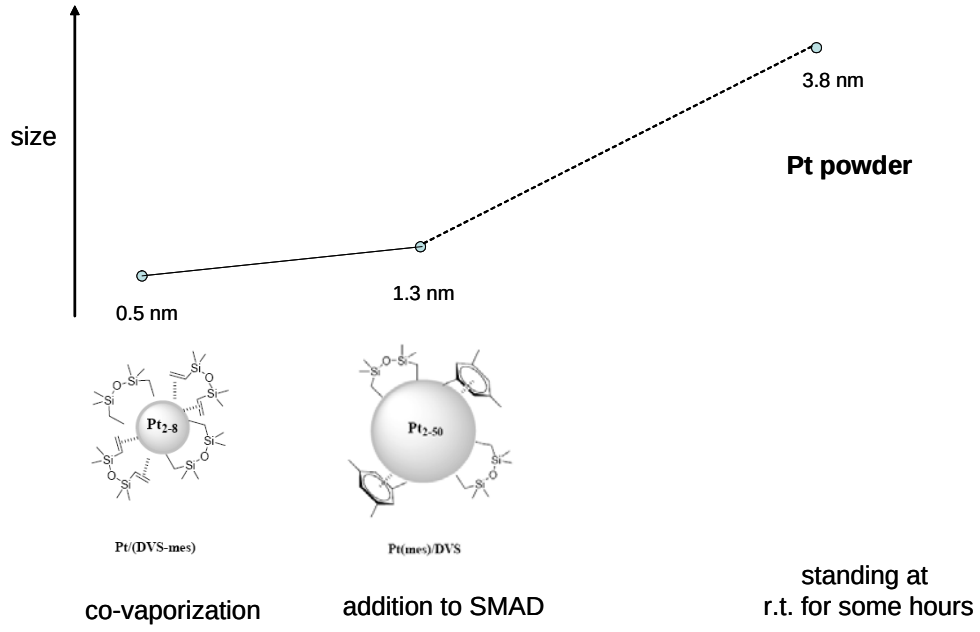

Figure 3.15 MVS derived Pt NPs prepared in different conditions.

(iv) the possibility to control the dimension of soluble platinum nanoparticles changing the concentration of metal in solution was also evidenced. In particular, systems obtained at lower concentration of platinum leaded to nanoparticles with smaller dimensions which have proved to be a very interesting starting material for the study of the growth of platinum nanoparticles in solution. Then, starting from these solutions was evidenced that the temperature plays a crucial role in the clustering process; at 25°C, the particle sizes increase over a period of two hours from a maximum hydrodynamic diameter of 1.8 nm (t = 0) to a maximum hydrodynamic diameter of 2.4 nm (see above, Figure 3.14). After that critical value, precipitation occurs. On the other hand, at -40°C, the particle sizes do not significantly change over the same time (maximum hydrodynamic diameter = 1.4 nm after 24h).

Additionally, was evidenced that NMR DOSY analyses provide a powerful tool for assessing the growth of metal nanoparticles in solution and a simple theoretical model to establish the shell thickness of such systems was presented.

Some preliminary results of allylamines hydrosilylation are also showed, to prove the efficiency of such systems as soluble Pt NPs containing catalysts.

3.9 REFERENCES

[1] Concepts of Modern Catalysis and Kinetics. I. Chorkendorff, J. W. Niemantsverdriet Copyright 2003 WILEY-VCH Verlag GmbH & Co. KGaA, Weinheim ISBN: 3-527-30574-2
[2] Blaser, H. U.; Spindler, F. Studer M. Applied Catalysis A: General 221 (2001) 119–143
[3] Blaser, H. U.; Pugin, B.; Spindler F., J. Mol. Cat. A **2005**, *231*, 1–20
[4] Salvadori, P.; Vitulli, G.; Evangelisti, C. unpublished results
[5] Mo, H.; Pochapsky, T. C. *J. Phys. Chem. B* **1997**, *101*, 4485.
[6] Chen, H.-C.; Chen, S.-H. *J. Phys. Chem.* **1984**, *88*, 5118.
[7] A. Gierer, K.Z. Wirtz, *Naturfosch. A,* 8 **1953** 522.
[8] Hitchcock, B.; Lappert, M.; Warhust**,** N. J. W. *Angew. Chem. Int. Ed. Engl.* **1991**, *30*, 438-440.
[9] Zuccaccia, D.; Macchioni, A. *Organomet.* **2005**, *24*, 3476-3486.
[10] Candau S. J. in "*Surfactant Solution: New Methods of Investigation*" (Ed.: R. Zana), Marcel Dekker, New York, **1987**, Chapter 3.
[11] Waldeck, A. R.; Kuchel, P. W.; Lennon, A. J.; Chapman, B. E. *Prog. Nucl. Magn. Reson. Spectrosc*. **1997**, *30*, 39.
[12] Green, M.; Howard, J.A.K.; Spencer, J.L. Stone, F.G.A. *J. C. S. Chem. Comm*. **1975**, 449.
[13] Romeo R.; D'Amico, G. *Organomet.* **2006**, *25*, 3435.
[14] Huang, J.; Liu, Z.; Liu, X.; He, C.; Chow, S. Y.; Pan, J. *Langmuir* **2005**, *21*, 699-704.
[15] Vitulli, G.; Uccello-Barretta, G.; Pannocchia, P.; Raffaelli, A. *J. Organomet. Chem.* **1986**, *302*, C21.
[16] See as example: Gund, A.; Keppler, B.K.; Nuber, B. *Inorg. Chem*. **1995**, *34*, 2788.
[17] See as example: Hackett, M.; Iber, J.A.; Jernakoff, P.; Whitesides, G.M. *J. Am. Chem. Soc.* **1986**, *108*, 8094.
[18] Lewis, L.N.; Wengrovius, J.H.; Burnell, T.B.; Rich, J.D. *Chem. Mat*. **1997**, 9, 761.
[19] Besson, C.; Finney, E.E.; Finke, R.G. *Chem. Mater.* **2005**, *17*, 4925-4938.
[20] Watzky, M.A.; Finke, R.G. *Chem. Mater*. **1997**, *9*, 3083-3095.
[21] (a) B. Marciniec, *Comprehensive Handbook on Hydrosilylation*, Pergamon Press: Oxford, England, 1992 and references therein; (b) Patai, S., Rappoport, Z. *The Chemistry of Organic Silicon Compounds*, Wiley: New York, 1989, 1482, and references therein.
[22] Speier, J.L.; Webster, J.A.; Barnes, G.H. *J. Am. Chem. Soc.* **1957**, *79*, 974.
[23] (a) Marciniec, B.; Gulinski, J.; Urbaniak, W.; Nowicka, T.; Mirecki, *J. Appl. Organomet. Chem*. **1990,** *4*, 27; (b) Willing, D.N. U. S. Patent 3,419,593; (1968).
[24] (a) Karstedt, D.B. U. S. Patent 3,775,452 (1973); (b) Stein, J.; Lewis, L.N.; Gao, Y.; Scott, R.A. *J. Am. Chem. Soc.* **1999**, *121*, 3693; (c) Lewis, L.N.; Colborn, R.E.; Grade, H.; Bryant, G.L.; Sumpter, C.A.; Scott, R.A. *Organomet.* **1995**, *14*, 2202; (d) Riding, K.D.; Crivello, J.V.; Lee, U. S. Patent 3,814,730; (1992).
[25] Lewis, L.N. U. S. Patent 6,030,919; (2000).
[26] Vitulli, G. ; Evangelisti, C.; Ciardelli, F.; Salvadori, P.; Rocchi, F. European Patent Application, EP 1 797 949, (2007).
[27] Sabourault, N.; Mignani, G.; Wagner, A.; Mioskowski, C.; Org. Lett. **2002**, *4*, 2117.
[28] (a) Tatsumi, T.; Hashimoto, K.; Tominage, H. *J. Organomet. Chem*. **1983**, *252*, 105; (b) Findeisen, K.; Heitzer, H. *Synthesis* **1981**, 702; (c) de Jeso, B.; Pommier, J.-C.; *J. Chem. Soc., Chem. Commun.* **1977**, 565.
[29] Maitlis, P.M. *Chem. Soc. Rev.* **1981**, *10*, 1.

CHAPTER 4

METAL VAPOUR SYNTHESIS OF STABILIZED GOLD NANOPARTICLES. STUDIES ON GROWTH AND CATALYTIC PROPERTIES

"By and large, the only skill the alchemists of Ankh-Morpork had discovered so far was the ability to turn gold into less gold."

Terry Pratchett

4.1 INTRODUCTION

Gold nanoparticles are the first and still most studied TMNPs. Several reviews appeared in the last years to emphasize the unique properties showed by this metal, when particle size falls in nanometers range.[1] The most exciting and growing field of application of AuNPs is undoubtedly catalysis. Historically, gold was regarded to be catalytically inert, but since the discovery in the late 1980s of surprisingly high catalytic activity for low-temperature CO oxidation, it has been shown that gold becomes active for many reactions of synthetic interest when stabilized in the form of nanoparticles attached to several inorganic or polymeric supports. It was clearly evidenced that particle size is a crucial factor in determining catalytic activity of supported gold particles in CO oxidation, as well as in others oxidation reactions (see section 2.4.2). On the other hand, it has been also pointed out that particles morphology, nature of the support and superficial oxidation state of the metal are very important factor which may affect catalytic performance of AuNPs in CO oxidation. All these findings have increased the efforts made by scientist to achieve size-selective synthesis of AuNPs and, consequently, to investigate the factors which affects particles formation and growth, as indicated by the recent literature.[2] It has to be noted that in usual synthetic approaches to size-controlled AuNPs, strong stabilizing ligands are often required, which can dramatically decrease the catalytic activity because of poisoning effects. This problem has been recently posed and some efforts has been made to obtain monodisperse, ligand free and size-selected supported AuNPs.[3]

Metal vapour synthesis of AuNPs is a well established route to supported gold catalysts (see section 1.2.5). Unfortunately, studies on factors affecting particle size obtained by this method are generally not much considered and very little is known about mechanisms which are involved in particles nucleation and growth. With this study we wants to throw a light into the potentialities of this technique in size-selective synthesis of AuNPs, trying to understand the processes of particles formation and evolution in time, during or after their synthesis.

4.2 GROWTH STUDIES OF METAL VAPOUR SYNTHESIS DERIVED AuNPs

MVS technique is described in detail in section 1.2.5. The solvent of choice for preparation of Au NPs is acetone. Briefly, co-condensation of gold vapours with a large excess of acetone vapours in high vacuum at liquid nitrogen temperature affords a brown-purple coloured frozen Au/acetone matrix. After melting, a deep-purple coloured solvated gold atoms solution stable at low temperature (-50°C) under inert atmosphere is obtained (**Au/ac**). In presence of support or on standing at room temperature, supported or unsupported AuNPs are isolated from the starting solution, respectively. For standard procedures, **Au/ac** SMAD with metal content of about 0.3 - 0.5 mg/mL (1.5 - 2.0 mM in Au) are obtained, affording particles with 3.0 - 4.0 nm of mean diameter for supported systems (depending on the nature of the support) or 4.2 - 4.5 nm for unsupported metallic powders, as revealed by HRTEM analysis of representative samples (Scheme 4.1).

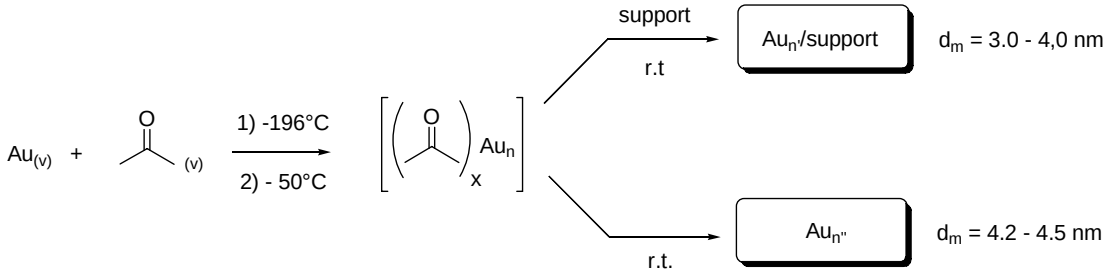

Scheme 4.1 Metal vapour synthesis of supported and unsupported AuNPs

In our description of MVS, in the previous sections we observed that in the vapour phase the metal is present mostly as monoatomic species, and in this form is trapped in the solid matrix. Above the Tammen temperature, atoms can diffuse in the solid and particles nucleation and growth can take place, and this is visible by changes in the colour of the matrix (see section 2.2.4). During the warm-up process the Au atoms are very mobile, and reactions with the solvent can compete with the clustering process. As Au-Au bond are formed, each resultant cluster may have different reactivity with the solvent. In other words, atoms have different reactivities than small cluster, and small clusters have different reactivities than larger clusters.[4] Usually reactivity decrease in increasing size, so as the cluster grow and continue to move through the solvent, reacting or being solvated, eventually a stage must be reached where it is energetically costly to move two clusters together and desolvate them to allow further Au-Au bond formation. Therefore, the colloidal particles remain solvated and suspended in solution by Brownian motion.[4] For this reason, Au SMAD can be considered a kinetically stable dispersion of metal clusters. As the solution is allowed to warm to room temperature, particles can coagulate, affording larger clusters, eventually in presence of supports, which can stops the growth process at early stages (n'' > n' > n, Scheme 4.1). Since clustering process in MVS of AuNPs shows to happens gradually, it seemed to us possible to quench the particles growth during the various stages, by adding a strong stabilizing ligand at the appropriate time, in order to obtain DLVO stabilized systems (see sections 1.1 and 2.3.2) characterized by different particle size (Scheme 4.2). This could represent a new way to achieve a size-selective synthesis of TMNPs, giving at the same time

information about the growth processes during MVS which are, at present, scarcely investigated.

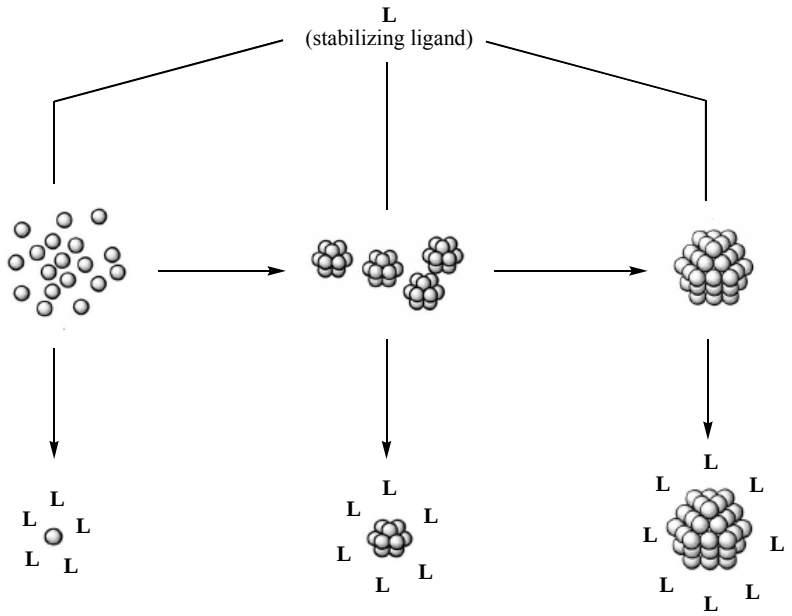

Scheme 4.2 General strategy for size-controlled metal vapour synthesis of TMNPs

4.3 THIOLS AS QUENCHING AGENT FOR AUNPS

Stabilizing ligand of choice for AuNPs are alkylthiols. Even if the exact nature of Au-thiol bond in stabilized gold nanoclusters is still unclear,[5] they represent the strongest class of ligand for this metal. So, we firstly investigate this compounds as quenching agents for AuNPs growth in MVS procedure. The ligands of choice were dodecanethiol (DT), a largely used stabilizers for AuNPs and *tert*-butanethiol (tBT), which could in principle afford more reactive AuNPs, because of its short and ramified structure, which could leave the particle surface less hindered and covered (Figure 4.1).

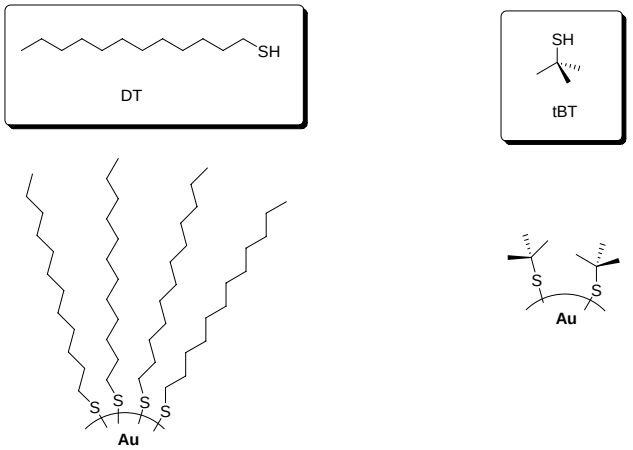

Figure 4.1 Schematic representation of Au surface for DT or tBT capped AuNPs

We tried to synthesize AuNPs, quenching their growth by addition of these ligands at three different stages: (i) after melting of the matrix and isolation of the cold solution; (ii) before melting of the solid matrix; (iii) during metal vaporization. We will describe the procedures followed, the characterization of products obtained and some properties of the systems.

4.3.1 LIGAND ADDED TO JUST PREPARED SMAD

4.3.1.1 Preparation

In a first study, we added a large molar excess of dodecanethiol (DT) to an **Au/ac** solution, immediately before their isolation (at -50°C). No visible change occurs in the solution, even at room temperature, until the excess acetone in removed under vacuum and the resulting solution is gently warmed above acetone boiling point (60°C). At this stage the colour of the solution turns from purple to reddish-purple, indicating that refraction index of the species present in solution is changed, because of the interaction between NPs and the new ligand. The produced NPs will be indicated as **Au(ac)/DT**. It is interesting to observe that to allow interaction of AuNPs with DT molecules, acetone must be removed by evaporation and heating, indicating that Au-acetone interaction is quite strong, according to literature (Scheme 4.3).[6] During these operations, no precipitation of bulk metal is observed in presence of thiol, while in its absence, bulk Au completely precipitate from the solution as black powder or as a thin film deposited on the glassware.

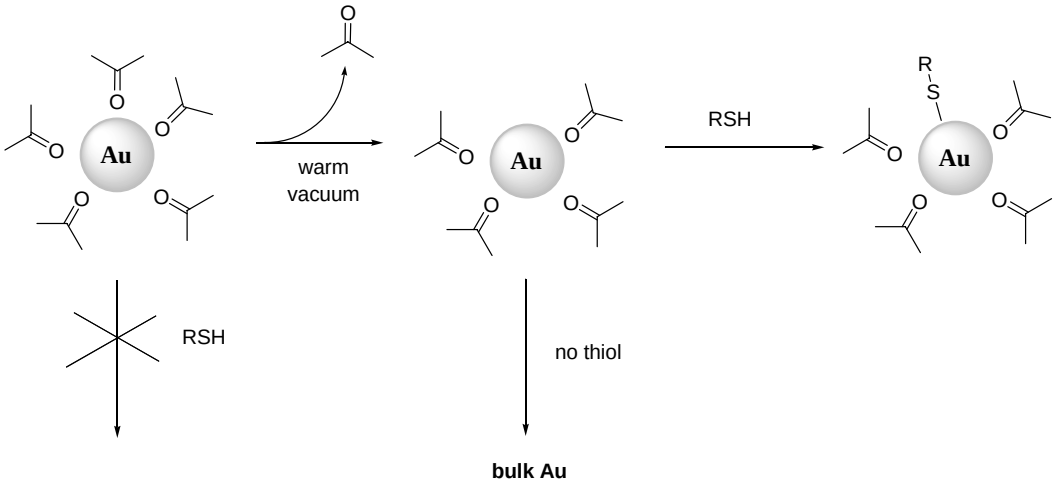

Scheme 4.3 Plausible mechanism of acetone - DT exchange on Au surface

Every attempt to stabilize the Au-acetone solutions with tBT failed. If tBT is added instead of DT, a black powder precipitate during warming at 60°C, which cannot be redissolved in any solvent, demonstrating that no stabilization occurs and that the particles aggregate to bulk metal, as in the case of warming without addition of stabilizing ligands.

4.3.1.2 Characterization

The **Au(ac)/DT** NPs can be easily isolated from the excess thiol by precipitation with ethanol of the thiol-capped AuNPs and filtration (Scheme 4.4). The dark solid can be redissolved in apolar solvents (toluene, n-hexane, chloroform, dichloromethane), without precipitation of metal. The system was characterized with UV-Vis (Figure 4.2), ^{1}H-NMR (Figure 4.3), and DOSY (Figure 4.4) analysis, described respectively in sections 1.3.2, 1.3.7.1 and 1.3.7.2

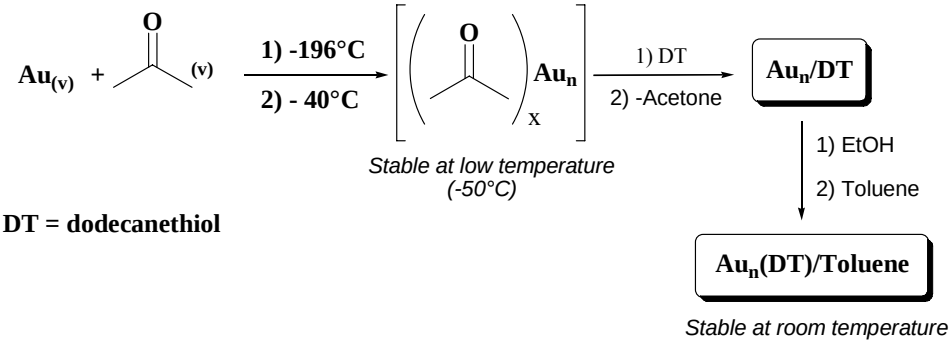

Scheme 4.4 Synthesis of Au(ac)/DT

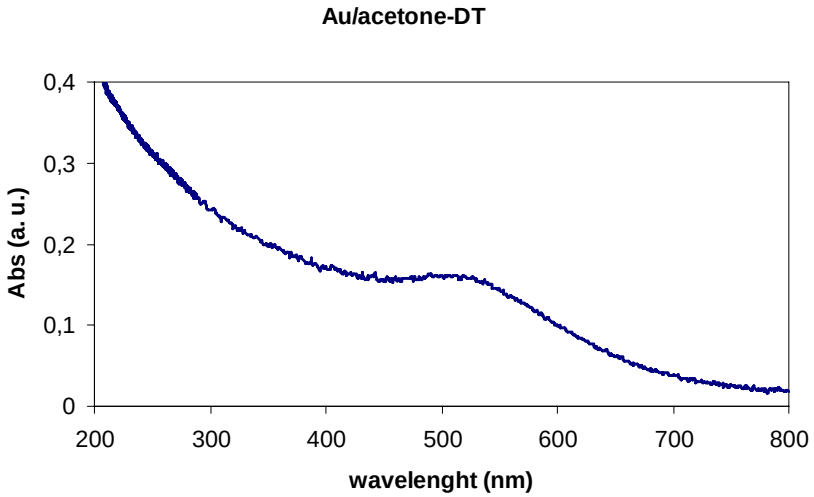

Figure 4.2 UV-Vis spectra of Au(ac)/DT NPs in toluene

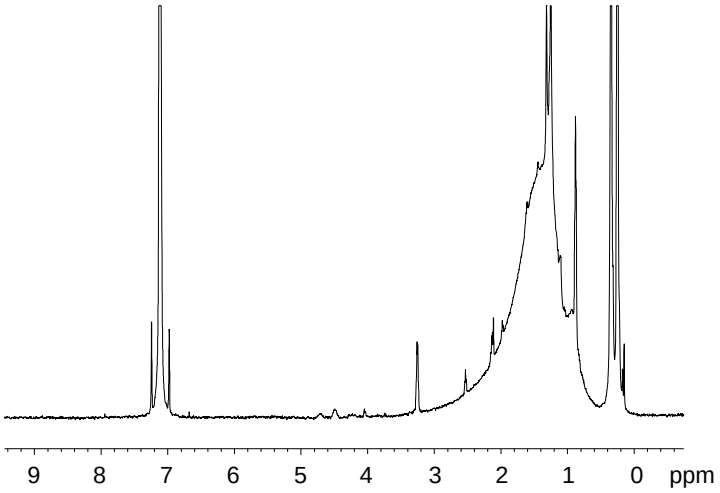

Figure 4.3 ^{1}H-NMR spectra in C_6D_6 of Au(ac)/DT

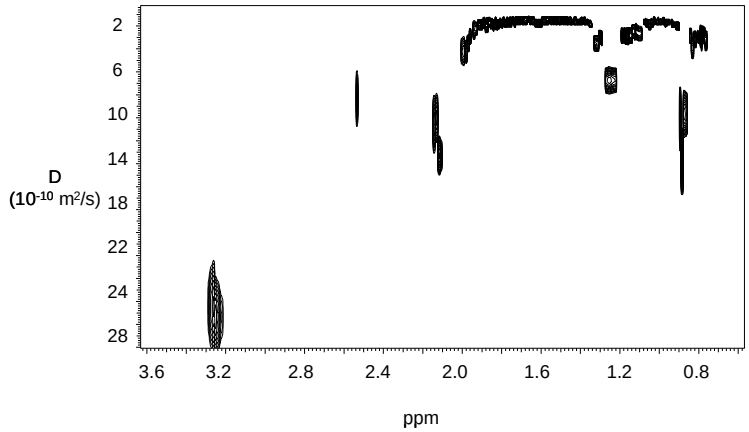

Figure 4.4 DOSY spectrum of Au(ac)/DT in C_6D_6

We can obtain various information from this analysis. The plasmon peak in the UV-Vis spectrum present a broad and weak absorption band with a maximum at a wavelength of about 510 nm. This is compatible with presence of Au nanoparticles with diameters in the range 2 - 10 nm.[7] ^{1}H-NMR in C_6D_6 shows a typical broadening of the aliphatic protons signals of dodecanethiol, due to coordination on the nanoparticles surface and the reduced mobility of methylenic protons. The narrow peak at about 1.4 ppm can be ascribed to the presence of residual coordinated acetone. From DOSY analysis we can attempt to have an estimation of particle size. We found a very narrow distribution of diffusion coefficients (D) of the species present in diluted solution of C_6D_6 (viscosity $\eta = 0.642$ cP), at $1.5 \cdot 10^{-10}$ m^2/s (Figure 4.5), which is probably a mean value for the species present in solution (see discussion about DOSY, section 1.3.7.2). Using the Stokes-Einstein relationship for "stick" boundary conditions, high dilution and solvent volume negligible with respect of particle size (see discussion in chapter 3), we can estimate a medium hydrodynamic particles diameters of about 4.5 nm. It has to be kept in mind that these values are obtained from the diffusion coefficient of the aliphatic protons of

dodecanethiol molecules coordinated to the metal surface, so they are referred to the whole particle, metallic core plus surrounding organic shell (Figure 4.5). In the following sections we will attempt to evaluate the core diameter, in order to make comparisons between particles prepared in different conditions. Regardless the exact value of core diameter, we can just observe that particle size seems to be not very different from those obtained for supported or unsupported powder (Scheme 4.1), leading to the conclusion that AuNPs growth, at the solution isolation step, is already in an advanced stage. It has to be noted, however, that in order to achieve stabilization of AuNPs with alkylthiol, the solution has to be warmed to 60°C, operation which may cause some aggregation between particles. This problem can be avoided by using other kind of ligands, as we will see in the following section.

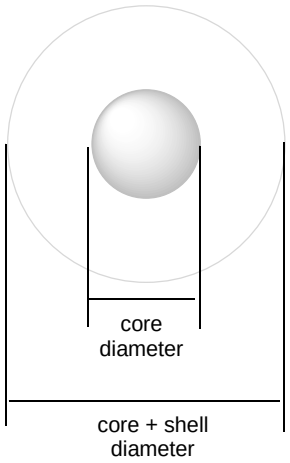

Figure 4.5 Schematic representation of a core-shell NP

4.3.2 LIGAND ADDED TO SOLID MATRIX

4.3.2.1 Preparation

The previous experiments lead to the conclusion that in the product obtained by MVS procedure, after melting of the solid matrix and isolation of the resulting solution at low temperature, AuNPs growth is in an advances stage and particles size have already reached values very close to those measured for supported or unsupported powder obtained without addition of stabilizers.
In order to investigate what happens before isolation, we conducted some experiments of particles trapping in the solid matrix. Because reaction between acetone solvated particles and alkylthiol has proven to be difficult below 60°C, we switched to cyclohexane as co-vaporization solvent, which is completely inert as stabilizers and would not interfere in interaction between Au particles and thiol, even at the low exercise temperature. We don't expect that the nature of solvent could influence the particle size during the vaporization phase, because metal mobility in the cold solid matrix is very limited, regardless the solvent used (see section 2.2.4). After co-condensation of Au vapours with cyclohexane vapours, before melting of the matrix, we siphoned under vacuum a solution of an excess of DT in cyclohexane directly on the solid (Scheme 4.5). After melting, we isolated a brown-red solution, stable at room temperature, which we indicate as **Au/DT**.

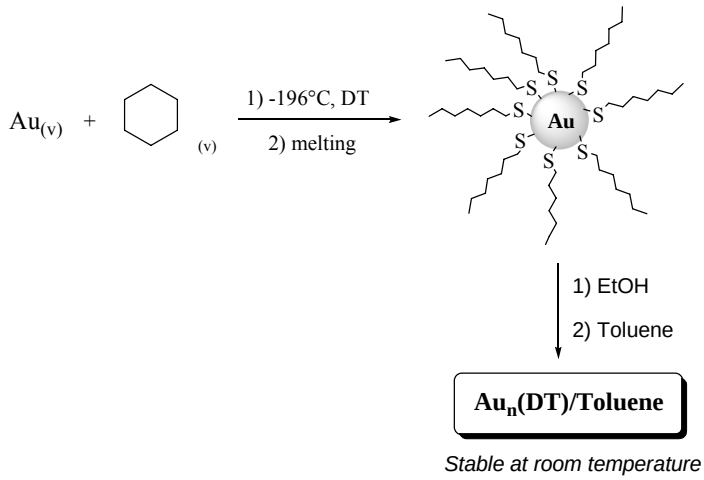

Scheme 4.5 Synthesis of Au/DT

4.3.2.2 Characterization

Excess thiol can be removed as usual by precipitation and washing with ethanol, after evaporation of cyclohexane under vacuum, and the particles characterized as above. The recorded spectra are reported in Figure 4.6, 4.7 and 4.8.

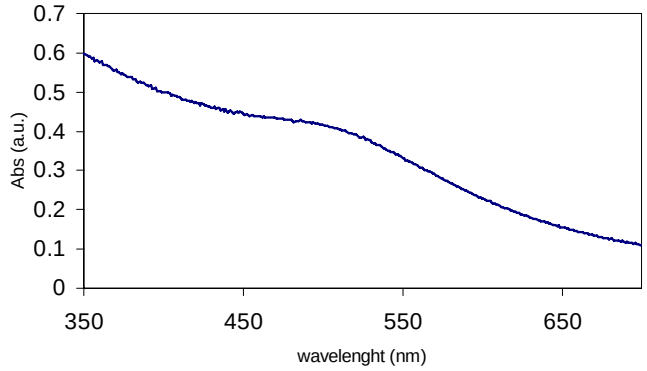

Figure 4.6 Uv-vis spectrum of Au/DT in toluene

The plasmon peak in UV-Vis spectrum is very weak, suggesting that particles are very small, as confirmed by DOSY, in which diffusion coefficients are sensibly higher than for **Au(ac)/DT** system ($D = 2.2 \cdot 10^{-10}$ m^2/s) and corresponds to an hydrodynamic diameter of 3.0 nm. So, particles obtained by direct interaction of stabilizing thiol with the solid matrix are smaller than those of previous experiments, as expected.

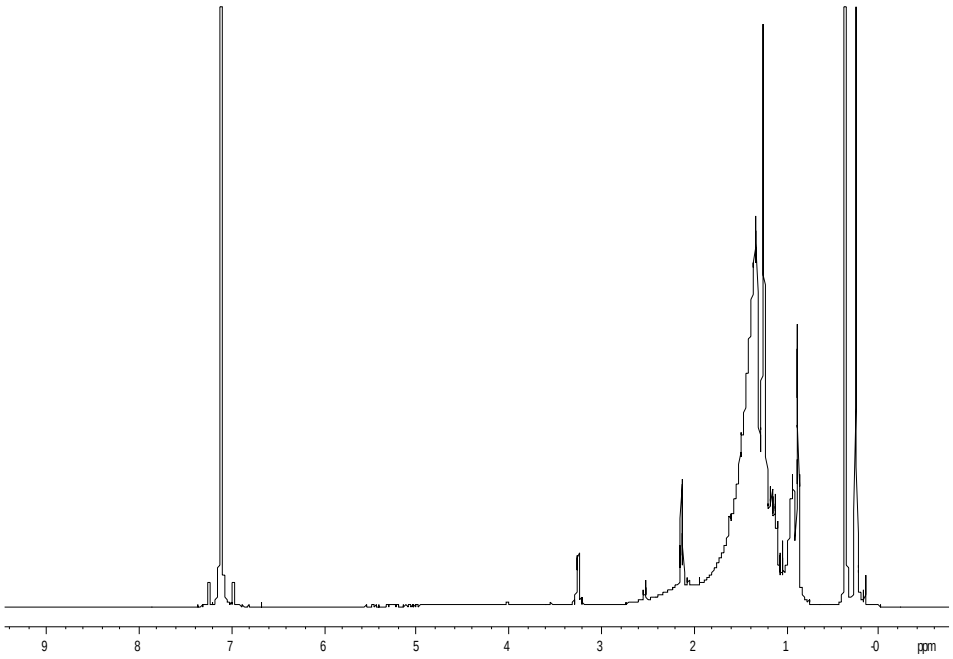

Figure 4.7 ^{1}H-NMR spectrum of Au/DT in C_6D_6

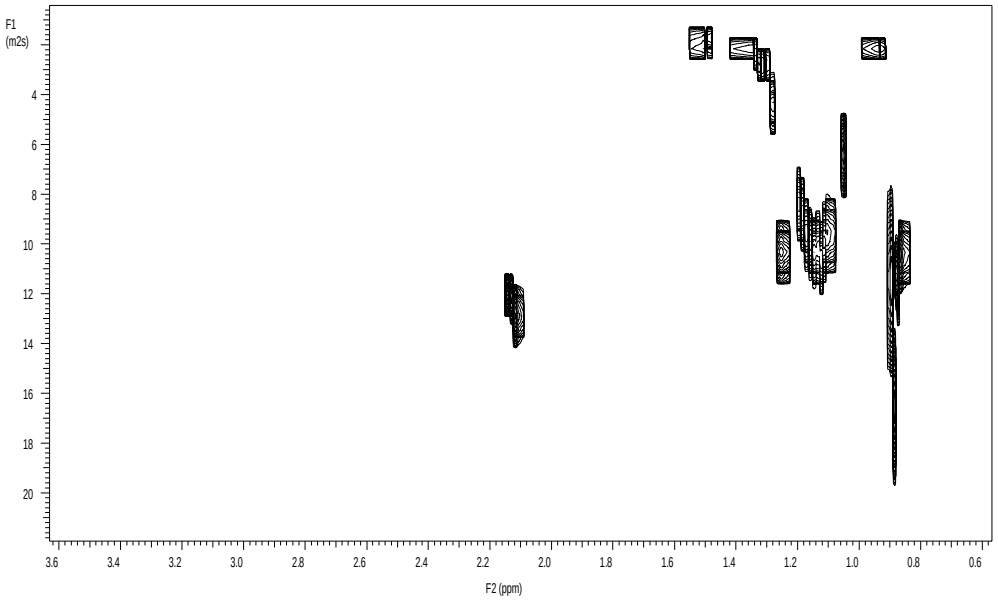

Figure 4.8 DOSY spectrum of Au/DT in C_6D_6

4.3.3 LIGAND CO-VAPORIZED WITH METAL

The last step in investigation of nucleation and growth of AuNPs during MVS different stages with thiol as quenching agents, was the simultaneous vaporization of Au with a suitable thiol. DT is not appropriate, because of its very low vapour pressure even at high temperatures. We chose for this experiment *tert*-butanethiol (tBT) for two reasons: (i) its high volatility; (ii) as already mentioned, its ramified structure, which could afford more reactive AuNPs than DT protected ones.

4.3.3.1 Preparation

A solution of tBT in cyclohexane, 1:9 v/v was used as co-condensation solvent. The colour of the solid matrix was green-brown, indicating that at this stage particle size are sub-nanometric. After melting a brown solution is recovered, which is stable at room temperature for several months. The excess thiol can be very easily removed by evaporation under vacuum, affording **Au/tBT** nanoparticles as a brown solid. Unexpectedly, when the solid is washed with ethanol, it partially dissolves, affording a pale brown solution.

4.3.3.2 Characterization

The soluble and insoluble systems, which we called respectively **Au/tBT$_S$** and **Au/tBT$_{NS}$**, have been characterized as usual (Figure 4.9, 4.10 and 4.11). Both systems contains AuNPs with particle size of less than 2 nm, as evidenced by absence of plasmon resonance in UV-Vis spectrum. The complexity of ^{1}H-NMR spectrum of **Au/tBT$_S$** sample, is presumably due to the presence of low molecular weight products, formed by uncontrolled reactions between the ligands utilized for the synthesis. Diffusion coefficient value obtained by DOSY analysis, leads to the conclusion that soluble particles are smaller than insoluble ones ($3.5 \cdot 10^{-10}$ m^2/s for **Au/tBT$_S$** versus $3.0 \cdot 10^{-10}$ m^2/s for **Au/tBT$_{NS}$** corresponding, respectively, to 2.0 and 2.2 nm of hydrodynamic diameters) and this agree with literature solubility data.[8]

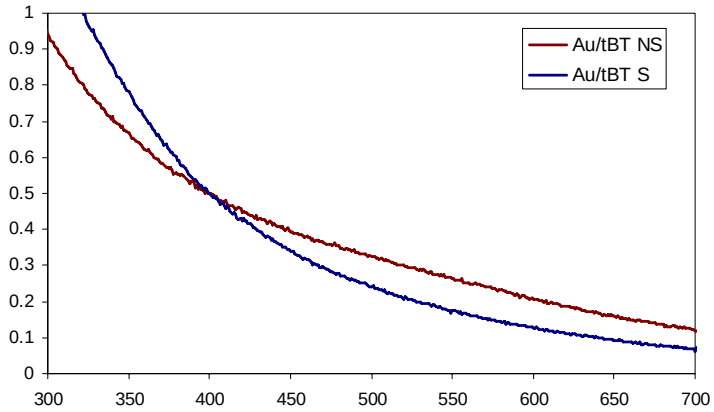

Figure 4.9 Uv-vis spectra of Au/tBT in toluene

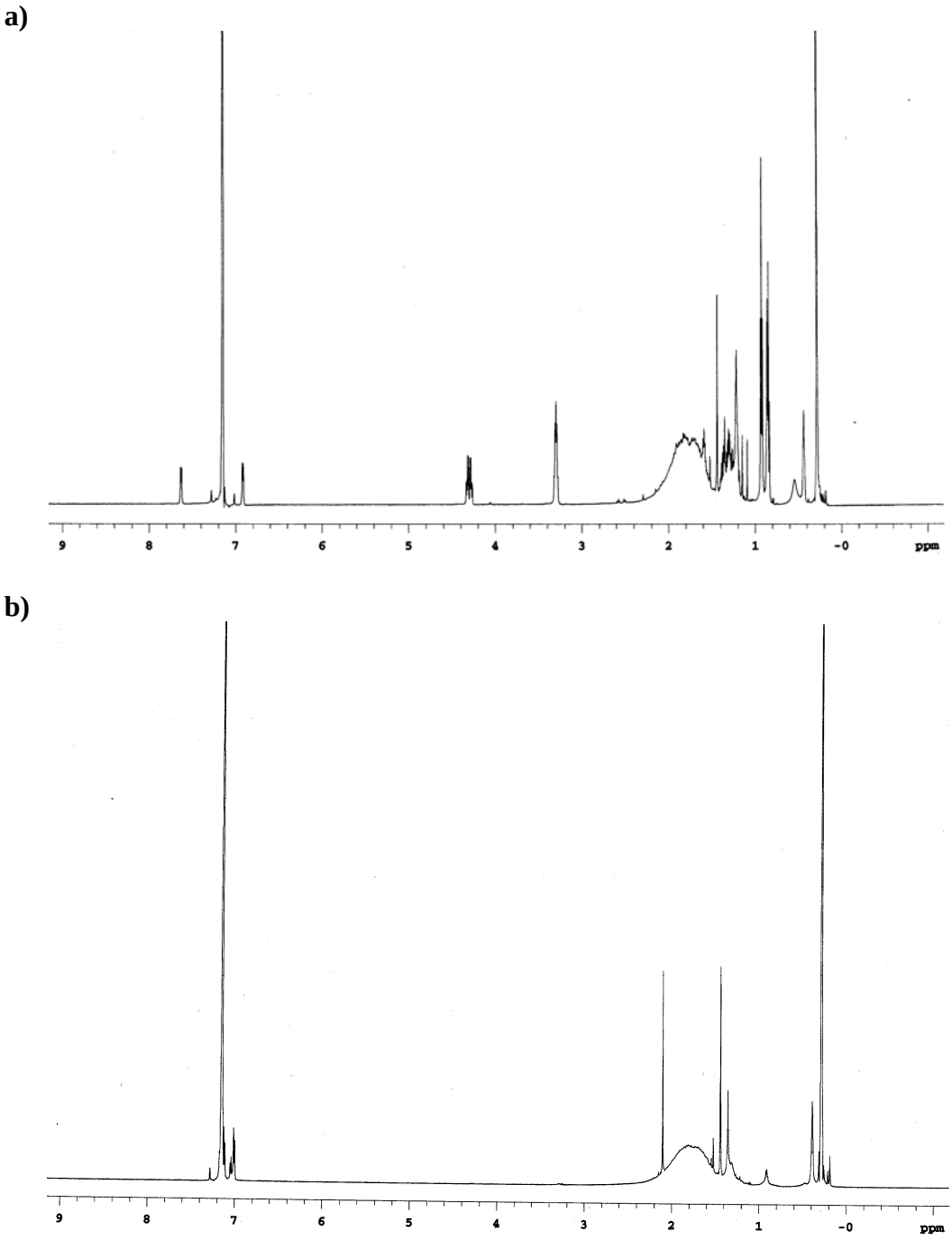

Figure 4.11 ^{1}H-NMR spectra of a) Au/tBT$_S$ and b) Au/tBT$_{NS}$ in C_6D_6

a)

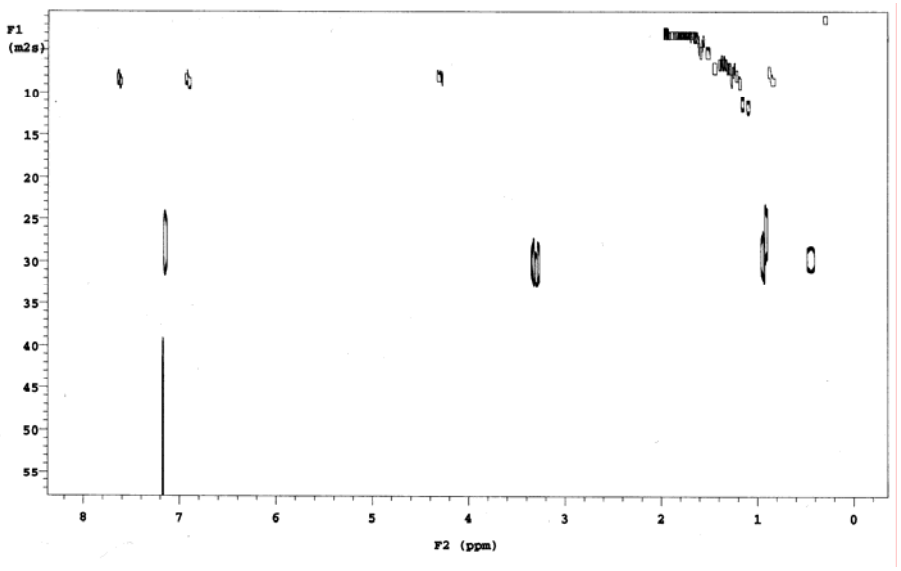

b)

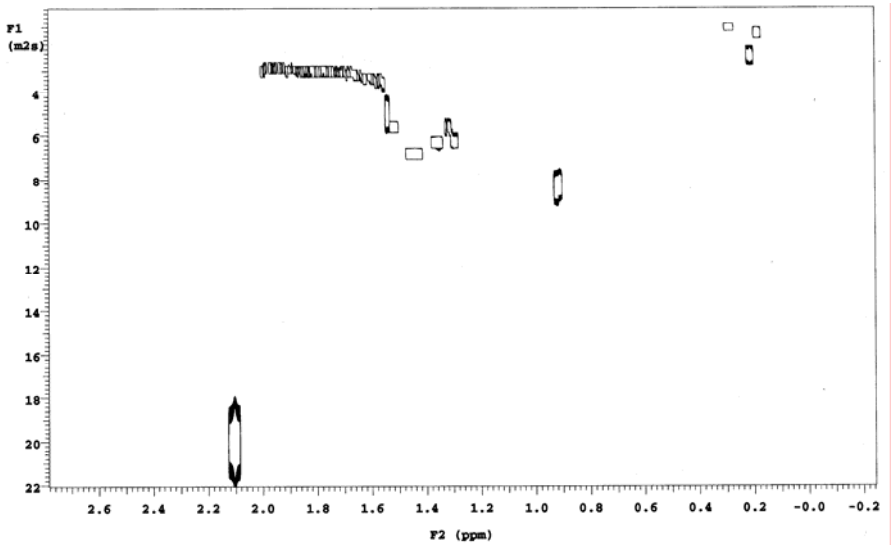

Figure 4.12 DOSY spectra of a) Au/tBT$_S$ and b) Au/tBT$_{NS}$ in C_6D_6

4.3.4 PROPERTIES OF Au/THIOL SYSTEMS

4.3.4.1 Thermal stability of Au/DT

Au/DT solutions are very stable. Prolonged heating in refluxing toluene don't cause any aggregation, as evidenced by no change in DOSY and UV-Vis spectra recorded after heating a representative sample at 110°C for 4 hours under inert atmosphere (Scheme 4.6).

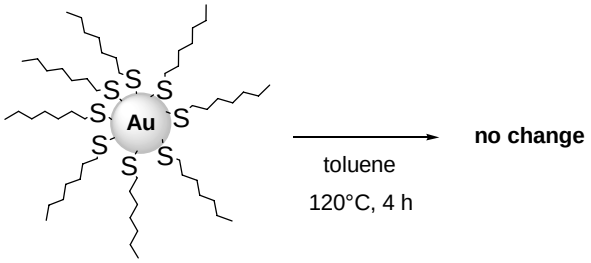

Scheme 4.6 Thermal treatment of Au/DT

According to Maye et al.,[2d] growth of particles may be observed by warming a solution of AuNPs in presence of an ammonium salt. To a toluenic solution of **Au/DT** we added methyl-trioctylammonium Bromide (MTOAB) and we observed the heating evolution of the system after 1 hour with UV-vis and DOSY (Figure 4.13 (a) and (b)). From both UV and DOSY spectra is evidenced that in presence of MTOAB particles increase their size by warming during the period of 1 hour. The plasmon peak maximum is red-shifted to 525 nm and the intensity is increased. Diffusion coefficient changes from the initial $2.2 \cdot 10^{-10}$ to $1.0 \cdot 10^{-10}$ m^2/s, which means in terms of hydrodynamic diameter a growth from 3.0 nm to 6.6 nm. After the time of 1 hour, precipitation of bulk gold begins to be observed, which is complete in 4 hours.

4.2.4.2 Chemical stability of Au/DT

Stability of these systems is evidenced also by lack of interaction with inorganic oxides. Deposition of such AuNPs on γ-Al_2O_3, starting from the toluene solution, doesn't occurs spontaneously, contrarily to the not protected systems, presumably because the thiol ligand prevent the direct interaction of metal with the oxide surface. A mechanical dispersion of Au/DT on γ-Al_2O_3 can be prepared by addition of a large excess of a non-solvent (EtOH) or by evaporation of toluene under vacuum from a mixture of AuNPs and the metal oxide.
The presence of reducing agents (Et_3SiH, $NaBH_4$), which could eventually break the Au-S bonds on the metal surface, with subsequent loss of stabilizing ligand, doesn't cause any change, as well.

a)

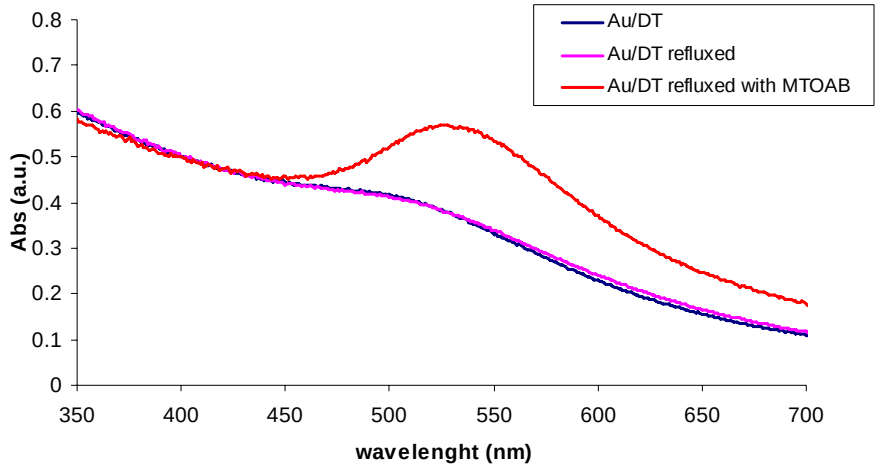

b)

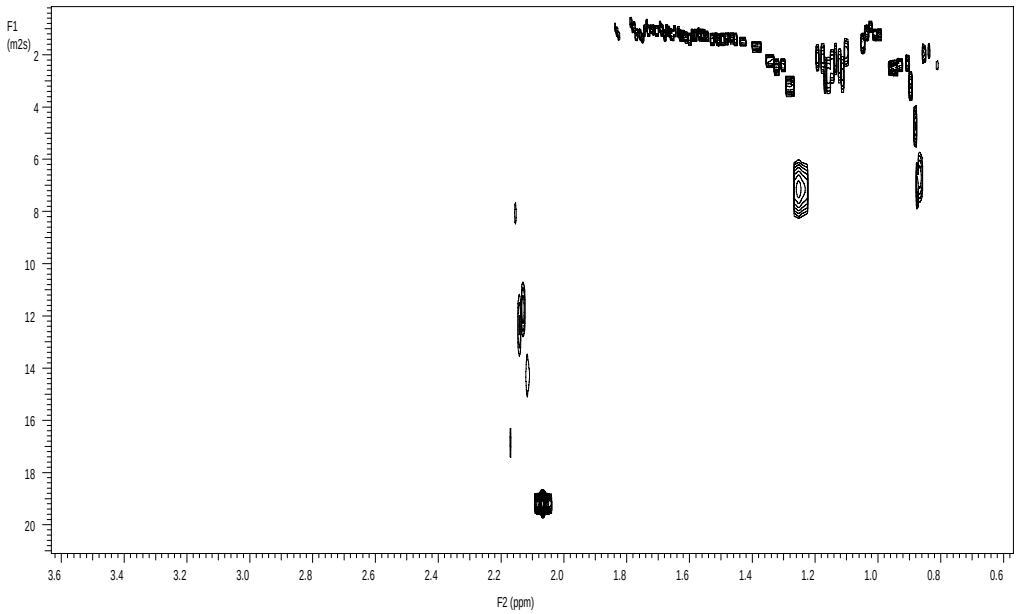

Figure 4.13 (a) Uv-vis spectra evolution of Au/DT: as prepared (blue line), refluxed in toluene without MTOAB (purple line) and refluxed in toluene with MTOAB (red line); (b) DOSY spectrum of Au/DT refluxed in toluene with MTOAB.

4.2.4.3 Thermal stability of Au/tBT

On the contrary, both **Au/tBT** nanoparticles dissolved in toluene decompose after 1 h at 110°C, affording a black powder, while they seems to be stable at lower temperatures (up to 100°C). UV-Vis spectrum of a partially decomposed solution of **Au/tBT$_{NS}$**, very similar to those in Figure 4.10, shows no plasmon resonance, suggesting that the agglomeration of particles to bulk powder is not the result of a gradual growth in solution, but more probably a very quick aggregation and precipitation (Scheme 4.7).

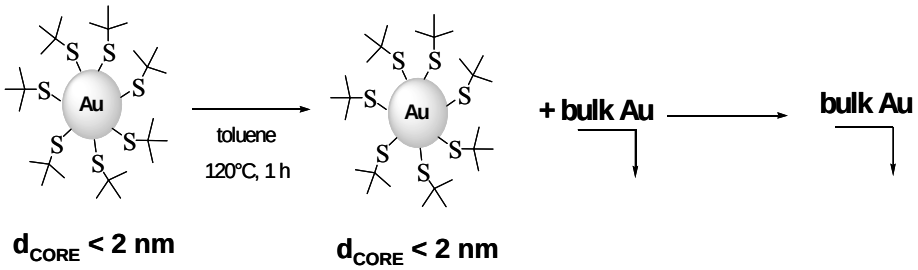

Scheme 4.7 Thermal treatment of Au/tBT$_{NS}$

Also in this case, the presence of MTOAB allows the particles of **Au/tBT$_{NS}$** to grow. If the salt is added, the solution colour turns from brown to purple when the Temperature of 90°C is reached. UV-vis spectra shows the presence of a plasmon resonance (Figure 4.14) in the heated samples. In this case, however, partial precipitation of bulk metal is observed even at this time. In 4 hours the precipitation is complete. UV spectra of sample after 2 hours and 3 hours of warming are very similar, suggesting that particles still present in solution have reached a sort of equilibrium. Because of the extensive precipitation of metal, DOSY analysis failed to detect species in solution.

4.3.4.4 Chemical stability of Au/tBT

In the case of **Au/tBT** systems, the deposition on γ-Al_2O_3 or Carbon from toluene solution is straightforward, indicating that interaction from metal and oxide surface occurs more easily than in previous case, as expected from a less covered metal surface.
The presence of reducing agents (Et_3SiH, $NaBH_4$), decrease the stability of such systems. Strongest reductant, such as sodium borohydride, cause quick precipitation of bulk metal even at room temperature, while in presence of ethanol or tryalkylsilane aggregation occurs at 90°C.
This "destabilizing effect" of reducing agents confirm the presence of Au-S bonds on the metal surface, which chemical reduction may cause the loss of stabilizing ligand.

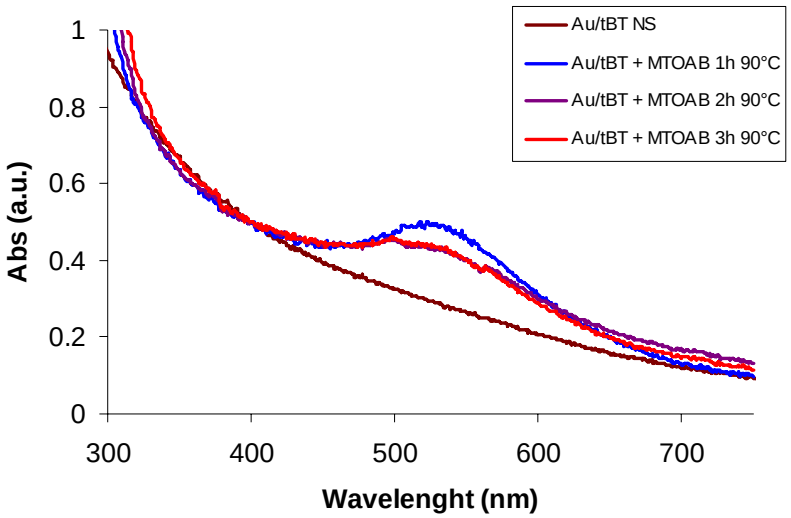

Figure 4.14 Uv-vis spectra evolution of Au/tBT

During the investigation of chemical stability of these systems, a very important observation was made: by adding Et_3SiH to an ethanolic solution of Au/tBT, bulk metal readily precipitate from the solution and evolution of bubbles was evidenced. Analyzing by GC-MS the remaining solution low amounts of $EtOSiEt_3$ were detected, deriving from the reaction of EtOH and Et_3SiH (Scheme 4.8). So, the gas formed in the solution is almost certainly molecular hydrogen. This observation led us to discover an unprecedent gold-catalyzed silane alcoholysis,[9] which will be discussed in more details in the last section of this chapter.

$$EtOH + Et_3SiH \xrightarrow{Au/tBT} EtOSiEt_3 + H_2$$

Scheme 4.8 reaction between ethanol and triethylsilane in presence of Au/tBT

4.3.5 PARTICLE SIZE DETERMINATION OF Au/THIOL SYSTEMS

Alkylthiols have demonstrated to be suitable stabilizers for MVS derived AuNPs. They actually work as quenching agents during the various stage of the synthesis, giving information about the mechanism of particle formation and growth. UV-vis, ^{1}H-NMR and NMR-DOSY analysis can be used as characterization protocol for this systems in solution. In particular, DOSY spectra provides the mean diffusion coefficient of thiol-capped AuNPs in diluted solution, allowing to make some comparison between the various systems, as resumed in Table 4.1.

Table 4.1 resume of particle size, as estimated with DOSY, of AuNPs prepared in different conditions

AuNPs sample	Diffusion coefficient in C_6D_6 (10^{-10} m^2/s)	core + shell diameter from DOSY Eqn. 1.12 (nm)
Au(ac)/DT	1.5	4.5
Au/DT	2.2	3.0 (3.5)[a]
Au/tBT_{NS}	3.0	2.2
Au/tBT_S	3.3	2.0

a) in parenthesis the value of core diameter obtained by HRTEM (see below)

It has to be noted that in order to compare systems in which AuNPs have different ligands (or no ligand at all) we need to know core diameter, so the thickness of the ligand layer around the metallic particle. Shell thickness is dependent from a series of factors and his determination is not a trivial task. His value is essentially determined by the conformation of thiol molecules at the interface from particle surface and solvent, which are in principle very numerous because of the high flexibility of linear C_{12} alkyl chains. From literature data about thiol protected gold clusters we often find values close to 1.2 nm for dodecanethiol layers,[7b,10] calculated by difference between diameter obtained from diffusion or STM measurement (core + shell) and those obtained by HRTEM pictures (metallic core). This value suggest that in these conditions alkyl chain of thiol molecules is quite completely extended in an all trans conformation. On the other hand, some authors[11] retain that the ligand shell of dissolved clusters can be regarded as having a densely packed, solid-like region near the Au surface and a free-draining region near the chain termini, with relatively mobile chain ends. This picture is consistent with the observation that hydrodynamic radii observed by diffusion-ordered spectroscopy (DOSY) for alkanethiolate-stabilized Au clusters are substantially smaller than the sum of the Au core radius and a fully extended, all trans alkyl chain length. Diffusion coefficient of free DT in deuterated benzene is $12.2 \cdot 10^{-10}$ m^2/s, which corresponds to an hydrodynamic diameter of 0.55 nm. It has to be noted that in this case we cannot consider the molecule as spherical, so this value cannot be used as an absolute measure of molecular size, but we can suppose that it could represent an average of the size of all the possible conformations of DT molecules in solution (Figure 4.15).

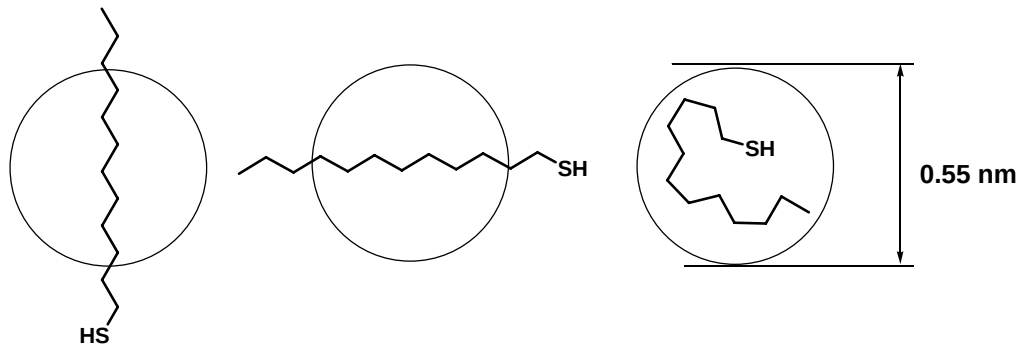

Figure 4.15 Examples of different DT conformations in solution

So, we performed a HRTEM of a sample of **Au/DT**, mechanically dispersed on γ-Al_2O_3 as previously indicated, to estimate particle size and shell thickness of our AuNPs. A representative picture and the related histogram of particle size distribution are reported in figure 4.16.

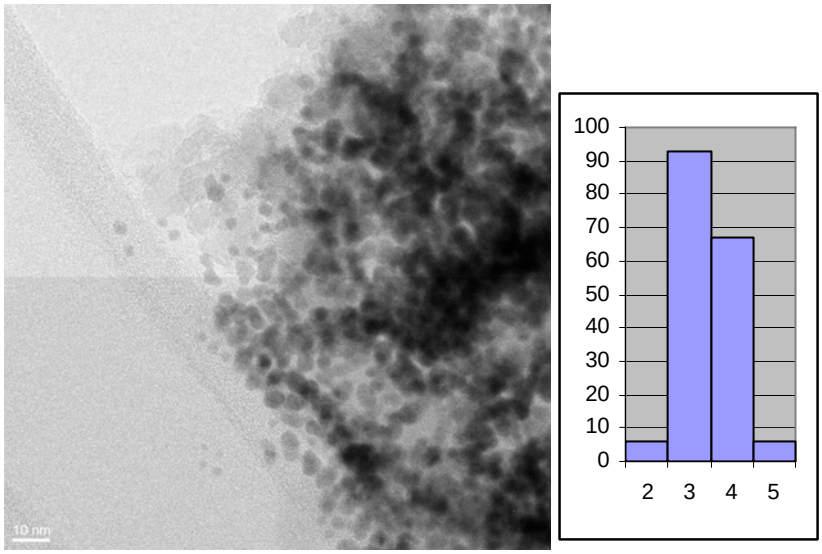

Figure 4.16 HRTEM of Au/DT

HRTEM pictures shows that AuNPs are deposited preferentially on amorphous region of the inorganic oxide and tend to form islands in which they stick together. In this regions the interparticle distance has a mean value of 0.6 nm and this can be considered as an approximate value of shell thickness, very similar to the value estimated from diffusion coefficient of DT. From the analysis of histogram, the resulting mean core diameter of **Au/DT** is 3.4 ± 0.9 nm, which is clearly not compatible with an hydrodynamic core + shell diameter of 3.0 nm. We can use HRTEM pictures to estimate a more accurate overall particle diameter as the sum of the core diameter and twice the estimated shell thickness, obtaining about 4.6 nm. Our observations may lead to two conclusions: (i) the diffusion coefficients obtained from DOSY analysis are overestimated or (ii) the hydrodynamic diameters obtained from Stokes-Einstein equation (Eqn 1.12) are underestimated. In both cases the diameters calculated by DOSY data in Table 4.1 for **Au/DT** systems are lower than real values, according to the already mentioned reports in ref 9. DOSY analysis, anyway, is suitable for qualitative comparison between different systems.

4.3.6 EFFECT OF SOLVENT

We also investigated the use of different solvents in preparation of thiol-capped AuNPs, starting from solvated Au atom dispersions. We repeated the same procedure as in previous experiment, using EtOH and a mixture EtOH-H_2O, 1:1 v/v, respectively. The choice of these solvents had three main purposes: (i) to investigate the effect of different polarity of the dispersing media; (ii) to have a solvent in which thiol-capped AuNPs are insoluble, making easy the isolation operation; (iii) to use a weakly coordinating solvent, in order to facilitate the interaction between particles and thiol molecules.

4.3.6.1 Au/EtOH-DT

Co-condensation of Au vapours with EtOH in usual conditions affords, after isolation at -50°C, a dark purple solution containing EtOH solvated gold dispersion, which not decompose after warming to room temperature. Uv-vis spectra of the obtained solution can be registered under air (Figure 4.17a), showing the presence of AuNPs. When excess DT is added, the metal completely precipitate as a grey-purple powder, which can be separated by filtration, washed with EtOH, and completely redissolved in apolar solvents, affording a bright purple solution. Uv-vis spectra in toluene has been registered (Figure 4.17b, purple line) and compared with that obtained by Au/acetone-DT (Figure 4.17b, blue line). The **Au(EtOH)/DT** system show a more intense plasmon resonance then Au/acetone-DT and the maximum is red-shifted at about 530 nm. This clearly indicates that AuNPs obtained by switching solvent from acetone to ethanol are sensibly bigger. From literature studies we can suppose that mean particles diameter are sensibly greater than 10 nm.[7]

a)

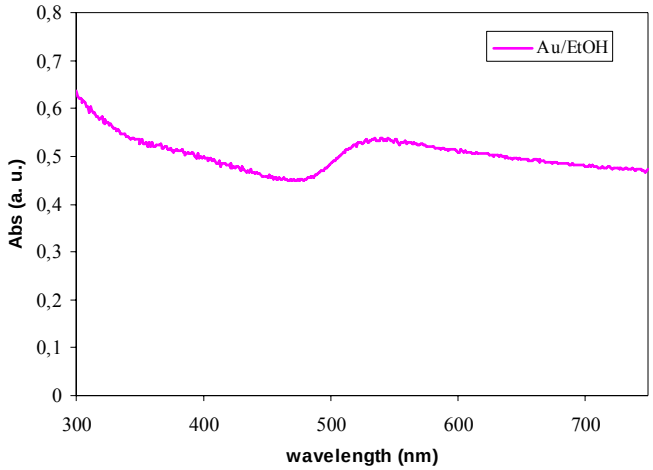

b)

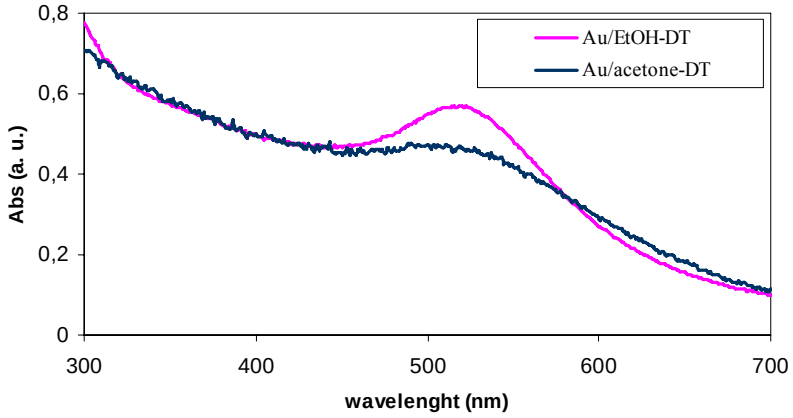

Figure 4.17 Uv-vis spectra of a) Au/EtOH b) Au(EtOH)/DT and Au(ac)DT

^{1}H-NMR and NMR-DOSY analysis of **Au(EtOH)/DT** samples dissolved in C_6D_6 has been also performed and are reported in Figure 4.18 and 4.19 respectively.

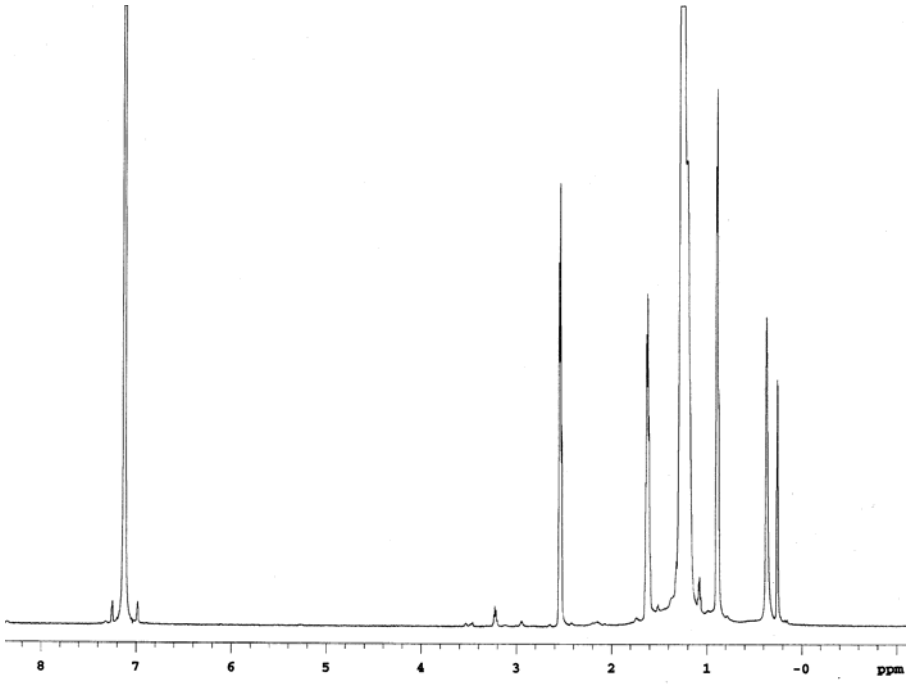

Figure 4.18 ^{1}H-NMR spectrum of Au(EtOH)/DT in C_6D_6

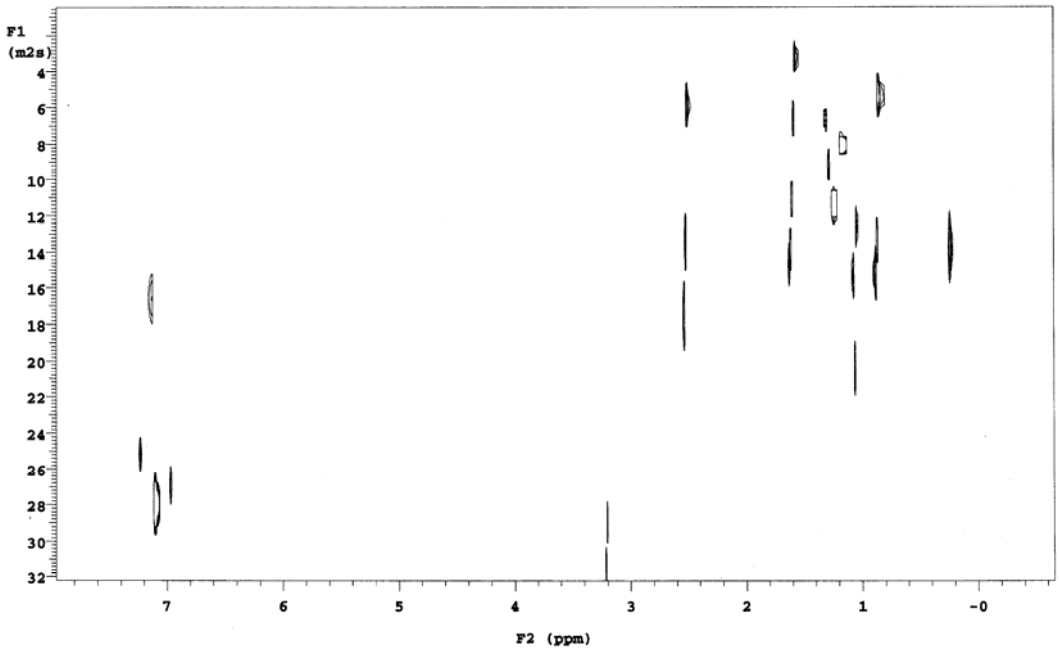

Figure 4.19 DOSYspectrum of Au(EtOH)/DT in C_6D_6

NMR spectra are very complexes. Several low molecular weight species are present, as evidenced by the broad range of diffusion coefficients in DOSY map, and assignations of chemical shift in ^{1}H-NMR spectrum is not trivial. The broad band in the 1 - 1.4 ppm region can be ascribed to coordinated DT, by analogy with the

previous system. Signals ascribable to EtOH cannot be undoubtedly detected. Diffusion coefficient values are mainly included in a region of low molecular weight species. All these observations make us suppose that in this procedure, during precipitation of AuNPs, several simple molecules, formed from EtOH and/or DT by uncontrolled reactions during MVS procedure, are incorporated within the particles, making difficult their isolation and interpretation of NMR data. The failure of DOSY in detecting thiol molecules coordinated to AuNPs, which in this case are very big (>10 nm), could suggest the presence of an upper detection limit for this technique.

4.3.6.2 Au(EtOH-H_2O)/DT

Vaporization of bulk Au in the MVS reactor in presence of a mixture 1:1 v/v of ethanol and water, affords a solution which is unstable even at low temperature (-50°C). In few minutes a black-purple Au powder completely precipitate from the solution. Surprisingly, the obtained particles, after separation from the liquid phase, can be redissolved in apolar solvent such as toluene by addition of an excess of DT and warming at 60°C, affording a purple-red solution. The usual purification with ethanol and characterization in solution have been performed and the registered spectra are reported in Figures 4.20, 4.21 and 4.22.

The UV-Vis absorption spectrum have the maximum of the plasmon peak at 520 nm. ^{1}H-NMR is very similar to that obtained for **Au(EtOH)/DT**, while the DOSY analysis shows remarked differences. In this case, there is a great concentration of aligned signals in the region of diffusion coefficients ranging from $1 \cdot 10^{-10}$ to $8 \cdot 10^{-10}$ m^2/s, which can be attributed, by means of chemical shift values, to thiol-capped AuNPs. As in **Au(EtOH)/DT** DOSY spectra, diffusion coefficient compatible with low molecular weight species are still present.

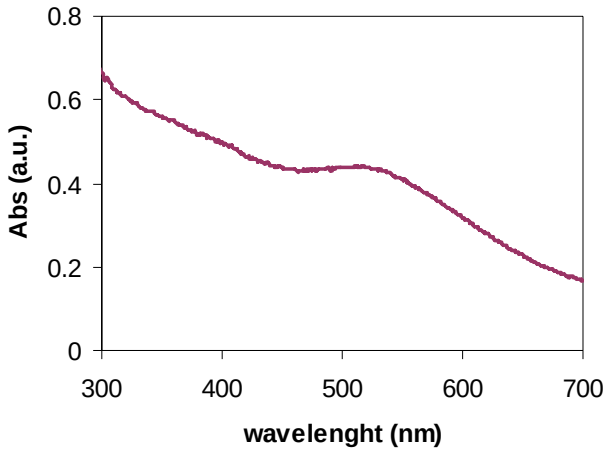

Figure 4.20 Uv-vis spectra of Au(EtOH-H_2O)/DT in toluene

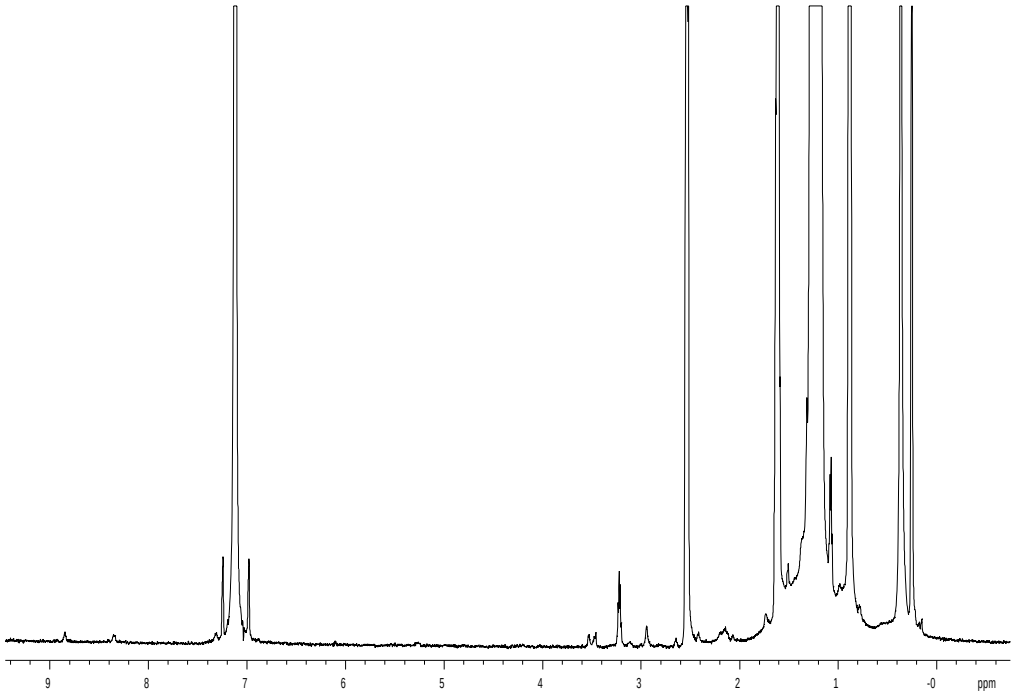

Figure 4.21 ^{1}H-NMR spectrum of Au(EtOH-H_2O)/DT in C_6D_6

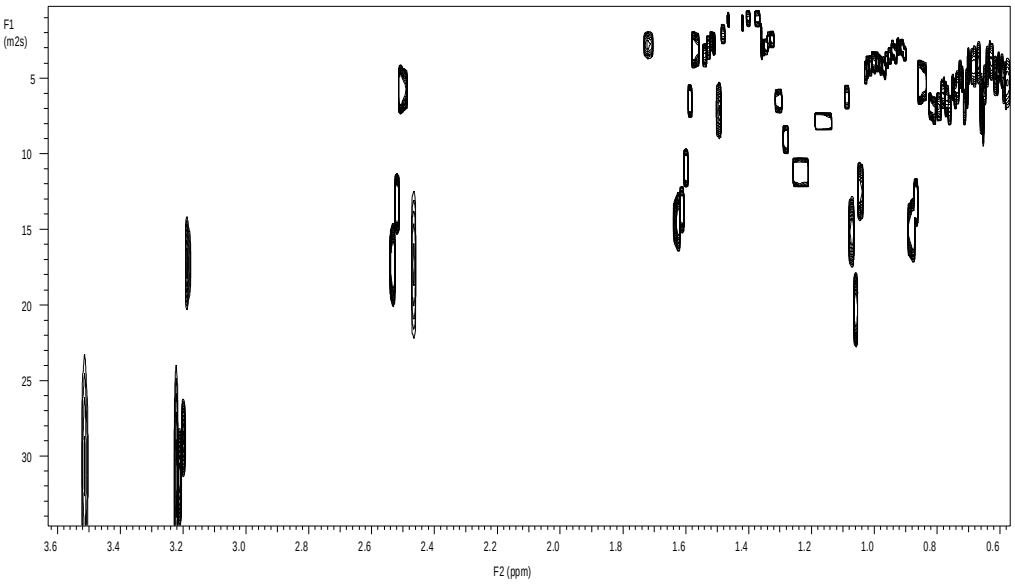

Figure 4.22 DOSY spectrum of Au(EtOH-H_2O)/DT in C_6D_6

4.4 DECYLAMINE AS STABILIZING LIGAND

Organic amines has proven to be suitable stabilizing ligand for AuNPs.[12] In some preparations they has been used both as reductant and capping agent.[13] With respect to thiols, amines are known to form less stable adducts with gold. If this behaviour generally represents a drawback in synthesis of stabilized systems (for example, particle size of gold nanoparticles prepared in presence of amines as stabilizing ligand are generally bigger than those prepared with thiols), the lack of stability can turn out to be useful for catalytic application of gold nanoparticles, because the capping agent can be in principle more easily removed after immobilization of particles, to make the metal surface accessible for catalysis, which is very difficult for thiol-capped systems.[14]
So, we explored the possibility to obtain size-controlled amine-capped AuNPs with our MVS procedure. We used decylamine as standard stabilizing ligand.

4.4.1 PREPARATION AND CHARACTERIZATION

The addition of decylamine (DA) in large molar excess to the **Au/ac** solution at room temperature or lower (-50°C) allows to obtain amine-capped gold nanoparticles (Scheme 4.9) which are insoluble in acetone and, after precipitation, can be easily dissolved in a wide range of organic solvent such as toluene, n-pentane, chloroform, affording stable purple solutions of **Au(ac)/DA** nanoparticles. These experimental conditions do not require any handling (heating or solvent evaporation) as in the previously discussed procedure. This is important because it can be supposed that in these conditions (room temperature or lower) no aggregation of particles occurs. For these reasons, we used DA to study growth of particles during the time after isolation of the Au/acetone solution. We also investigated the effect of metal concentration in the isolated solutions.

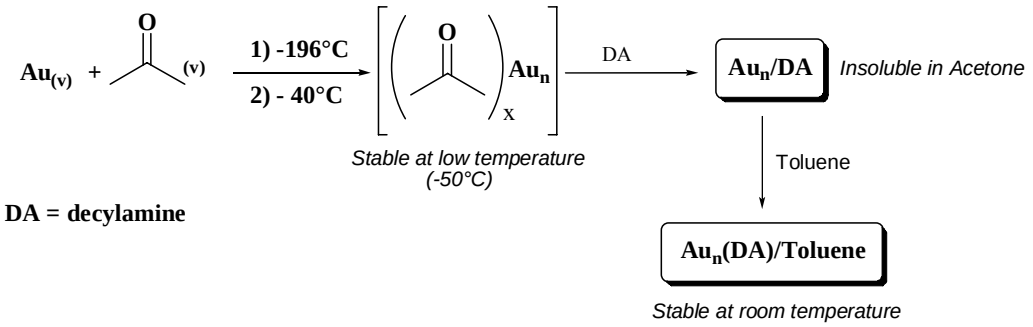

Scheme 4.9 Synthesis of Au(ac)/DA

We firstly prepared standard Au/acetone SMAD with a metal content of 0.1 mg/mL. The DA was added to portions of the starting solution during the time of 24 hours. During this time, no precipitation of bulk metal was observed. In several experiments, we noted that addition of DA in the early stages after isolation from the reactor (from t = 0 to t = 1 hour), results occasionally in a quick precipitation of bulk metal as an insoluble black powder, instead of the slow precipitation of amine-

capped NPs, completely soluble in apolar solvents. This unexplainable phenomenon is never observed when the amine is added after longer times.
In a typical procedure, an excess of DA was added to portions of an isolated Au/acetone solution at different time intervals from t = 0 to t = 24 hours. In all cases the metal completely precipitated from the solution as a dark solid at room temperature. The solid was then washed with dry EtOH, affording a grey-purple powder of Au(ac)/DA, soluble in apolar solvents. The systems were characterized with ^{1}H-NMR, DOSY, UV-vis and HRTEM.
^{1}H-NMR and DOSY spectra of the sample **Au(ac)/DA** at t = 0 dissolved in C_6D_6 are reported in Figure 4.23. The results of mean diffusion coefficient versus time are reported in Table 4.2

a)

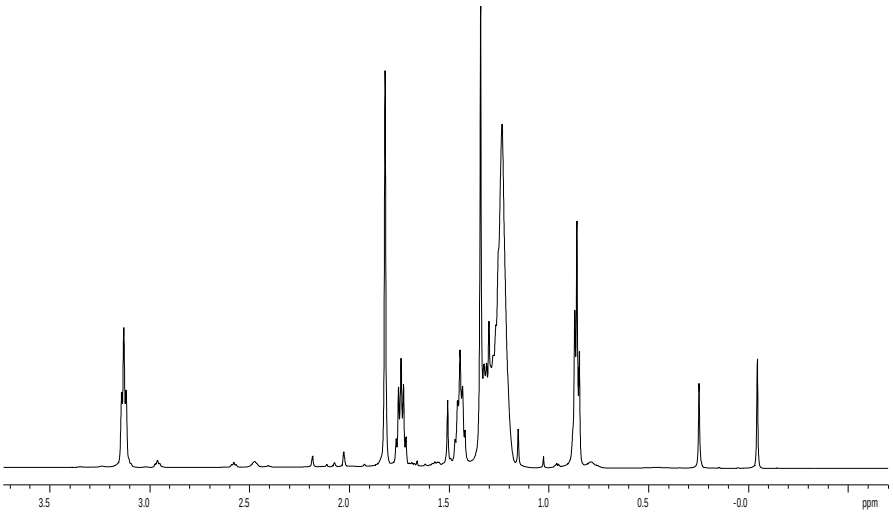

b)

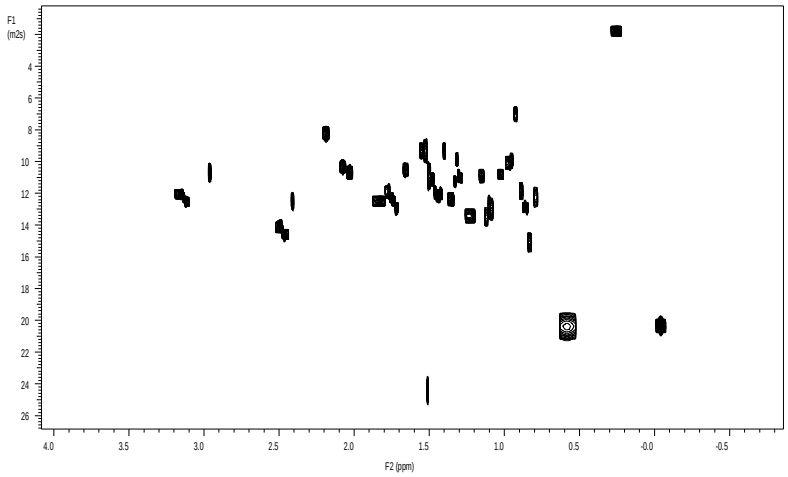

Figure 4.23 (a) ^{1}H-NMR and (b) DOSY spectrum of Au(ac)/DA in C_6D_6

Table 4.2 Hydrodynamic diameters of Au(ac)/DA as a function of ligand addition time

Time (h)	0	1	2	3	6	20	24
D (10^{-10} m^2/s)	9 - 13	3 - 10	6 -14	7 - 13	6 - 14	6 - 14	7 - 13
Hydrodynamic diameter (nm)	0.5 - 0.8	0.7 - 2.3	0.5 - 1.1	0.5 - 1.0	0.5 - 1.1	0.5 - 1.1	0.5 - 1.0

The ^{1}H-NMR and DOSY spectra of the analyzed **Au(ac)/DA** samples are all very similar to those reported in Figure 4.23. It is again evidenced the presence of several low molecular weight products, but in these cases diffusion coefficient values seems to be too high to be ascribable to amines bonded to metal nanoparticles (see table 4.2), with the exception of the sample at t = 1. We can try to explain this observation by considering the low strength of amine-Au interaction: we can suppose an equilibrium between free (D = $14 \cdot 10^{-10}$ m^2/s) and bonded decylamine in solution, and the diffusion coefficient measured by DOSY analysis - with a mean value of 10 x 10^{-10} m^2/s - could be an artifact, as results of a mean situation between adsorbed and desorbed amine (Scheme 4.10, see also section 1.3.7.2).

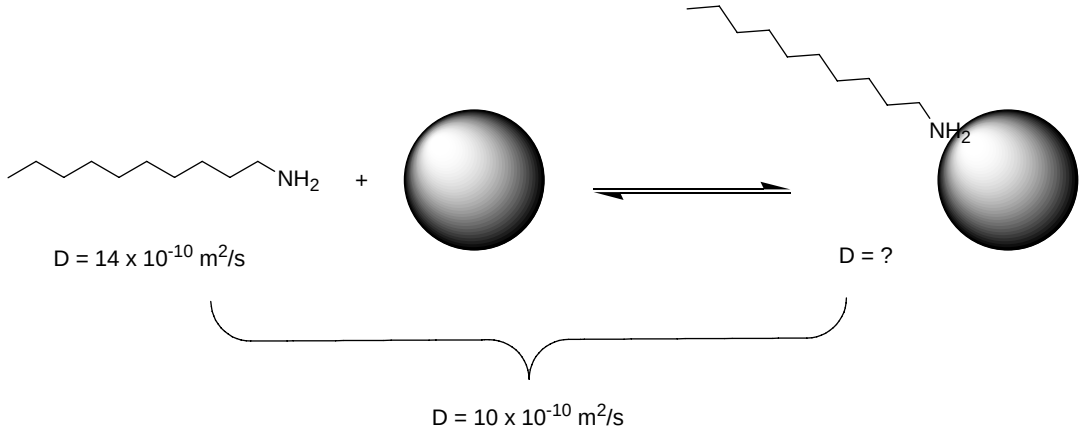

Scheme 4.10 Possible explanation for high values of measured diffusion coefficients for Au(ac)/DA

UV-vis spectra of some **Au(ac)/DA** samples dissolved in toluene are reported in Figure 4.24. They looks very similar, suggesting that during 24 hours no evident changes occurs in particles size.

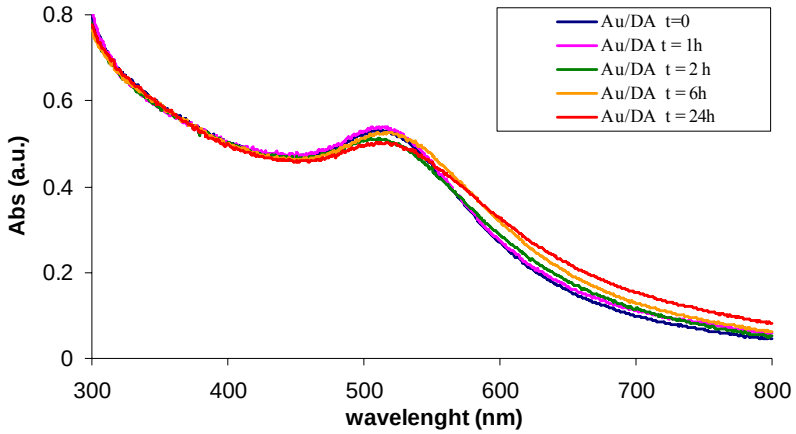

Figure 4.24 Uv-vis spectra of Au(ac)/DA samples in toluene

To definitely obtain the particle size value of **Au(ac)/DA** systems we performed HRTEM analysis of a representative sample (Figure 4.25). The mean diameter value is of 3.3 ± 1.0 nm.

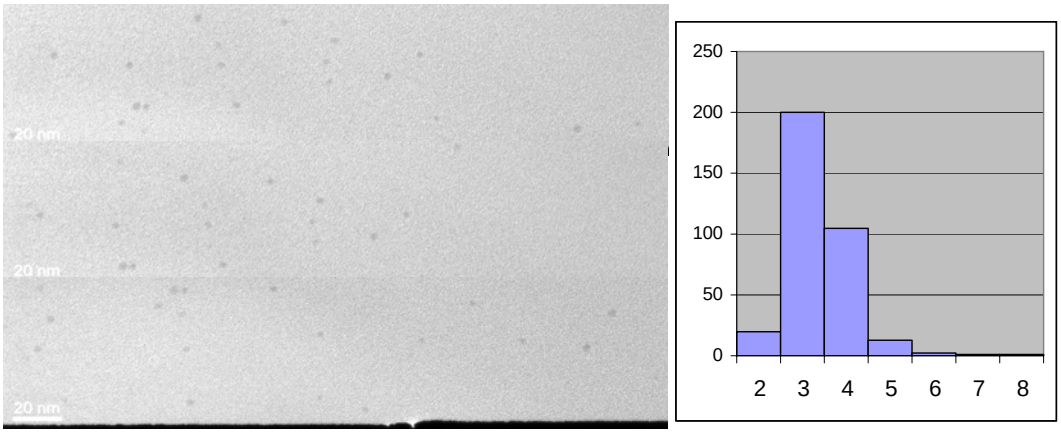

Figure 4.25 HRTEM of Au(ac)/DA

4.3.1.1 Thermal and chemical stability of Au/DA

Au/DA solutions present an intermediate situation between **Au(ac)/DT** and Au/tBT. Slow decomposition o bulk metal is observed upon warming to toluene reflux temperature. Presence of Et_3SiH accelerate the reaction. Supported systems are obtained by introduction of γ-Al_2O_3 into the solutions, but in some cases further addition of EtOH is required to achieve complete deposition.

4.4.2 EFFECT OF CONCENTRATION

4.4.2.1 Diluted solutions

Following the standard MVS procedure it is possible to obtain **Au/ac** SMAD characterized by different metal concentration, by changing the experimental conditions. In order to study the effect of concentration of the starting solution on particle size, we prepared SMAD with 0.1 mg/mL, 0.3 mg/mL and 1.0 mg/mL of Au and stabilize it a t = 0 by addition of an excess of DA. As characterization of the obtained systems we used HRTEM analysis on samples isolated in the usual conditions. **Au/ac** SMAD with 0.3 mg/mL of Au content is the system we used for the previous studies with dodecanethiol. In that case we obtained from DOSY analysis a core + shell diameter of 4.5 nm (section 4.1) that we presume to be underestimated. For the present **Au(ac)/DA** system, HRTEM reveal a mean core diameter of 4.0 ± 1.0 nm (Figure 4.26), which would correspond to a core + shell diameter of 5.1 nm if we assume a similar thickness for DT and DA shells (0.55 nm, see previous discussion in section 4.3.5). Considering that **Au(ac)/DT** particles are formed by warming **Au/ac** in presence of DT, it is plausible that they are bigger than **Au(ac)/DA** particles, which are formed without any additional handling, because aggregation phenomena may occur. Regardless the nature of stabilizing ligand, a value of about 4.0 nm can be considered plausible for a just isolated **Au/ac** solution with a metal concentration of 0.3 mg/mL. Because we know that supported systems and powder obtained at longer times after isolation preserve a similar particle size (see section 3.1), we can conclude that once the **Au/ac** SMAD is isolated, particles have already reached their final size, which don't change anymore with time. The particle mean diameters seems determined only from the metal concentration (3.3 nm for 0.1 mg/mL and 4.0 for 0.3 mg/mL). Now we will see that the situation is different for more concentrated solutions.

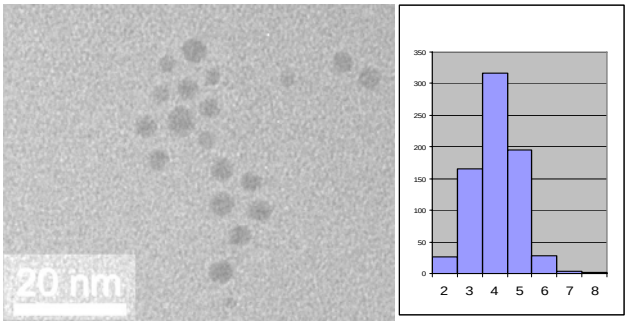

Figure 4.26 HRTEM of Au(ac)/DA

4.4.2.2 Concentrated solutions

To evaluate the Au aggregation process in high concentrated Au/acetone solutions (1.1 mg/mL), HRTEM analysis on decylamine-capped gold nanoparticles prepared by adding decylamine at different times, following the standard procedure, were performed. In Figure 4.27 we reported the HRTEM analysis of samples obtained by adding, at different times: t = 0, t = 3h, t = 5h, decylamine to a high concentrated Au/acetone solution (1.1 mg/mL) kept at room temperature. As clearly evidenced

from the HRTEM analysis, gold clusters present in the high concentrated **Au/ac** solution increase sensibly their particle size and broaden their distribution during time at room temperature (mean particle diameters are respectively 5.3 ± 1.0 nm, 6.4 ± 1.5 nm and 7.8 ± 2.0 nm). Decylamine appears a very useful ligand to quench the growth of gold nanoparticles in solution allowing to study growth processes of high concentrated solvated acetone gold clusters.

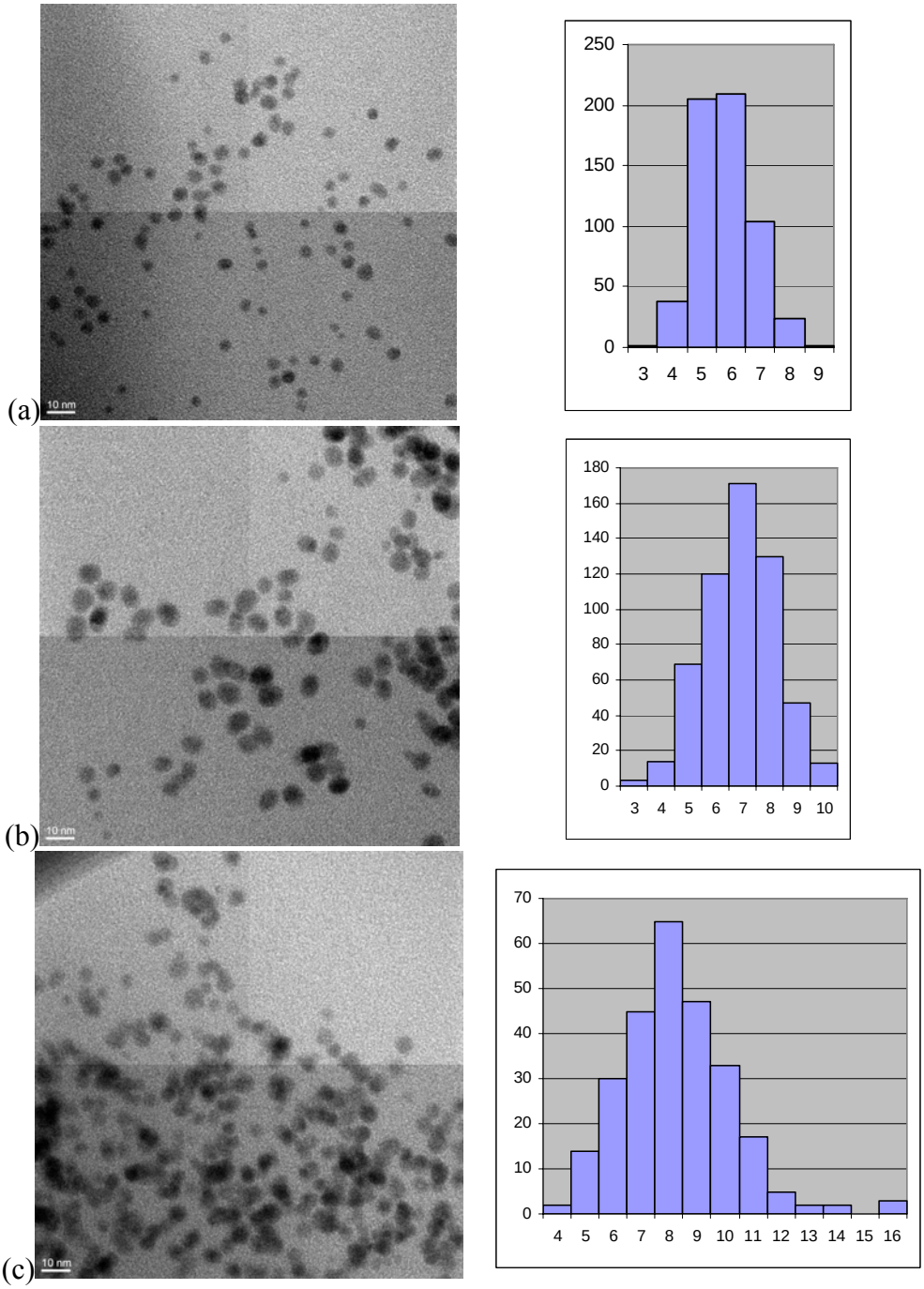

Figure 4.27. TEM analysis of samples obtained by adding, at different times: t = 0 (A), t = 3h (B), t = 5h (C), decylamine to a high concentrated Au/acetone solution (C_{Au} = 1.1 mg/ml) kept at room temperature.

Uv-vis spectra of the aforementioned **Au(ac)/DA** nanoparticles showed remarkable differences in the intensity of absorption peak, as expected (Figure 4.28).

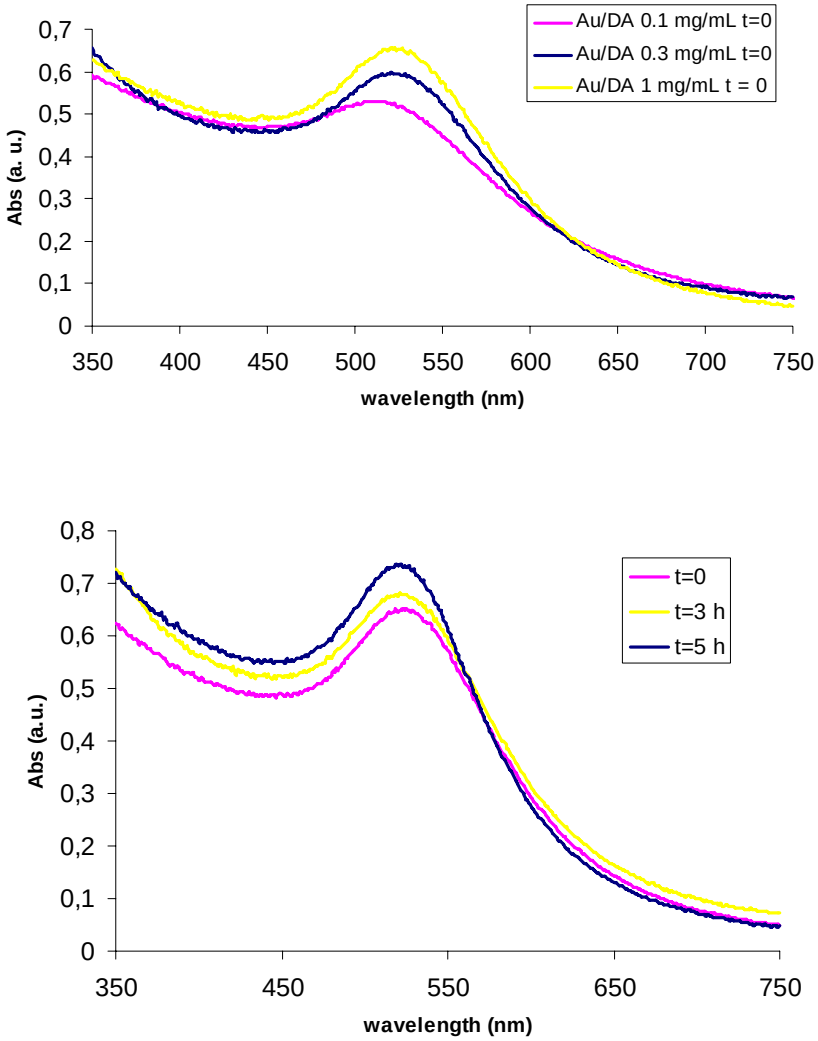

Figure 4.28 Uv-vis spectra in toluene of Au(ac)/DT prepared starting from **Au/ac** SMAD (a) different initial metal concentration; (b) concentrated solution, DA added at different times

4.5 CATALYTIC TESTS

Our group recently showed that supported AuNPs obtained by metal vaporization are very active catalysts for terminal alkynes hydrosilylation in heterogeneous phase.[15] Starting from the discovery of this new application of supported gold catalysts in organic synthesis, we explored the possibility to perform other kinds of reactions involving hydrosilanes. As anticipated in section 4.3.4.4, during the study of AuNPs stability in solution we found a new catalytic application of supported gold catalysts

in silane alcoholysis. So, we investigated the catalytic performances of our stabilized AuNPs in the above mentioned two kind of reactions (Scheme 4.11).

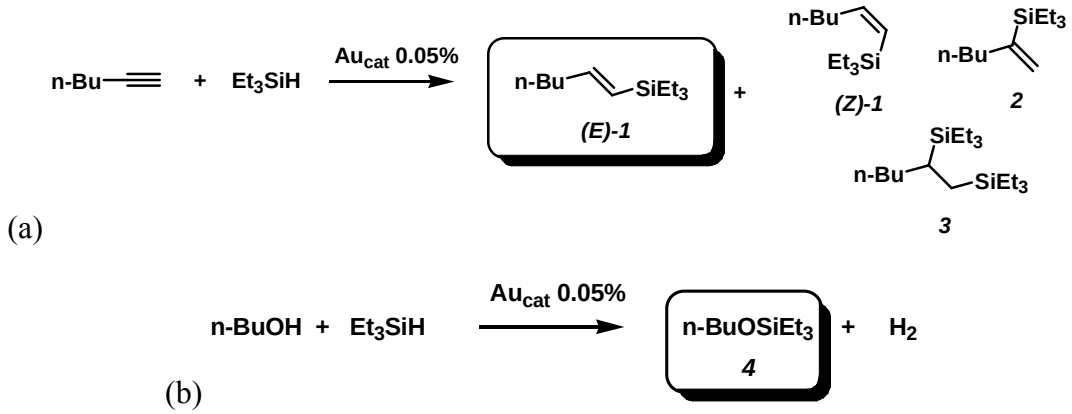

(a)

(b)

Scheme 4.11 (a) gold catalyzed hydrosilylation of 1-hexyne with triethylsilane; (b) gold catalyzed silane alcoholysis with butanol and triethylsilane

We firstly tried the reactions in homogeneous conditions, using the catalysts directly as toluenic solutions. The reactions were carried out in the same conditions as in ref 14 and 15, under inert atmosphere, at 90-100°C, with 0.05% mol of catalyst. All the systems capped with DT or DA resulted completely inefficient after 24 h, while with Au/tBT systems, precipitation of bulk gold is observed within 1 h in the reaction conditions (cfr. Section 4.3.4) and the mixtures showed low conversion (~5 %).

Thus, we switched to supported systems. All the AuNPs were deposited on γ-Al_2O_3 at 1 % of metal loading, by adding dropwise the NPs solutions to a slurry of support in toluene. After addition and stirring overnight, the catalyst was filtered, washed several time with EtOH to remove the excess ligand and dried under vacuum for several hours at r.t. It is important to note that all the nanoparticles spontaneously interact with the support and complete deposition is accomplished in some hours, with the notable exception of DT-capped systems, which require the addition of an excess of EtOH in the toluenic suspension. The results of 1-hexyne hydrosililation (Scheme 4.11a) and silane alcoholysis (Scheme 4.11b) are resumed in Tables 4.3 and 4.4.

Table 4.3 1-hexine hydrosilylation with triethylsilane catalyzed by supported and capped AuNPs

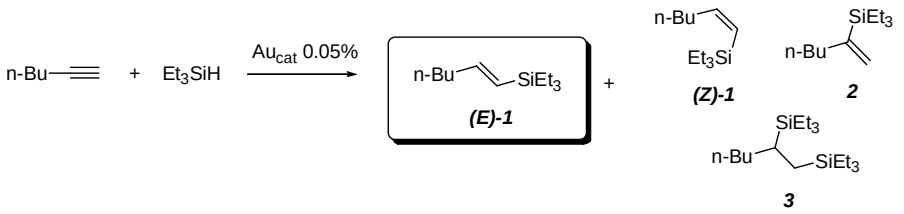

Entry	Au_{cat}	d_m (nm)	time (h)	conv (%)	selectivity *(E)-1* (%)	TOF (mol/ mol h)
1	Au/γ-Al_2O_3 1%[a]	4.0	0.25	80.5	92	6440
2	Au(tBT)/γ-Al_2O_3 1%	< 2	0.5	99	85	3960
3	Au(DA)/γ-Al_2O_3 1%	3.0	1.5	83	84.5	1106
4	Au(DA)/γ-Al_2O_3 1%	4.0	3	36	56	240
5	Au(DA)/γ-Al_2O_3 1%	5.0	12	59	67.5	98
6	Au(DA)/γ-Al_2O_3 1%	5.8	3	79	78	526
7	Au(DA)/γ-Al_2O_3 1%	8.0	1	99	81	1980
8	Au(DT)/γ-Al_2O_3 1%	3.5	12	-	-	-

a) from ref 14

Reactions performed in pyrex Carius tubes with 2 mmol silane, 8 mmol alkyne, 10^{-3} mg-atoms Au at 100°C and with no solvents for the given time. Conversion determined by GC analysis of the crude product.

Table 4.4 silane alcoholysis with butanol and triethylsilane catalyzed by supported and capped AuNPs

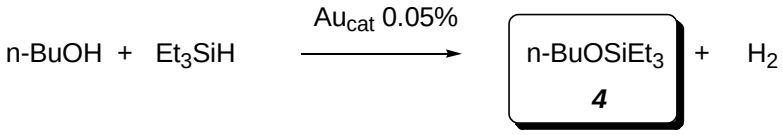

Entry	Au_{cat}	d_m (nm)	time (h)	conv (%)	TOF (mol / mol h)
1	Au/γ-Al_2O_3 1%	4.0	10	91	182
2	Au(tBT)/γ-Al_2O_3 1%	< 2	8	82	205
3	Au(DA)/γ-Al_2O_3 1%	3.0	18	99	110
4	Au(DA)/γ-Al_2O_3 1%	4.0	18	63.5	70.5
5	Au(DA)/γ-Al_2O_3 1%	5.0	38	91	48
6	Au(DA)/γ-Al_2O_3 1%	5.8	38	80	42
7	Au(DA)/γ-Al_2O_3 1%	8.0	38	73	38.5
8	Au(DT)/ γ-Al_2O_3 1%	3.5	38	-	-

Reactions performed in pyrex Carius tubes with 2 mmol silane, 2 mmol alcohol, 10^{-3} mg-atoms Au at 100°C and with no solvents for the given time. Conversion determined by GC analysis of the crude product.

Concerning the hydrosilylation of 1-hexyne we can see that the activity of the different catalysts can't be directly referred to the particle size. Probably the influence of residual amounts of ligand, especially DA, have the main influence on catalyst

behaviour. The presence of residual ligand seems to affect also the selectivity of the reaction towards the (E)-1 isomer. As confirmation of the important poisoning effect of DA we can compare entries 1 and 4: both catalysts contains 4.0 nm gold particles but the non-stabilized system is more active (more then one order of magnitude) then the DA-capped ones. Also the selectivity decrease from 92 % to 56 % for the stabilized catalyst. The DT stabilized particles are completely inactive. This poisoning effect is less remarked in silane alcoholysis, in which the activity seems to follow an expected decrease by increasing of the particle size, regardless the ligand used for stabilization.

4.6 CONCLUSIONS

Metal vapour synthesis provide an useful way to obtain AuNPs stabilized in solution. The solvent of choice is acetone, which provide small particles (about 4 nm), kinetically stable in diluited solutions for indefinite time. Au/acetone SMAD are not redissolvable once the solvent is completely evaporated, but interaction with suitable ligand such as dodecanethiol (DT), tert-butanethiol (tBT) and decylamine (DA), allows to isolate capped nanoparticles in which stability is greatly improved. These molecules has also proven to be useful to control growth processes of AuNPs during synthesis from metal vapours. In particular we found that some parameters governs the final size of synthesized particles:

(i) addition of stabilizing ligand at different stage of preparation: tBT can be directly co-vaporized with gold, affording stable solutions containing AuNPs characterized by a mean diameter of less than 2 nm. If a ligand (DT in this case) is added after formation of the cold matrix but before melting, 3 nm AuNPs are obtained. After matrix melting and recovery of the solution, 4 nm AuNPs are isolated if DA ligand is used. If tBT is added at this stage, it is not able to stabilize particles, while DT require heating to interact with metal, which operation can cause some particles aggregation. After isolation of the solution there's are evidences that particles growth stops and diluted solution can be stored at room temperature without any detectable change. This results are summarized in Figure 4.28.

(ii) co-condensation solvent: the choice of co-condensation solvent is crucial in determining particle size and stability in solution. Acetone seems to be the best choice, while EtOH and EtOH-H_2O affords not stable solutions containing large particles.

(iii) metal concentration: HRTEM analysis performed on samples at different starting metal concentration reveals the dependence of particle size by this parameter. More concentrated solutions contains bigger particles (Figure 4.29). Additionally, in highly concentrated solutions ([Au] = 1.1 mg/mL) particle size increases with time (Figure 4.30), contrarily to what happens in diluted systems, in which particle size remains unchanged after long times.

All the synthesized particles, except the DT capped ones, shows good activity in some reaction of interest in fine chemistry, such as hydrosilylation of 1-hexyne and silane alcoholysis, but only after deposition on an inert support.

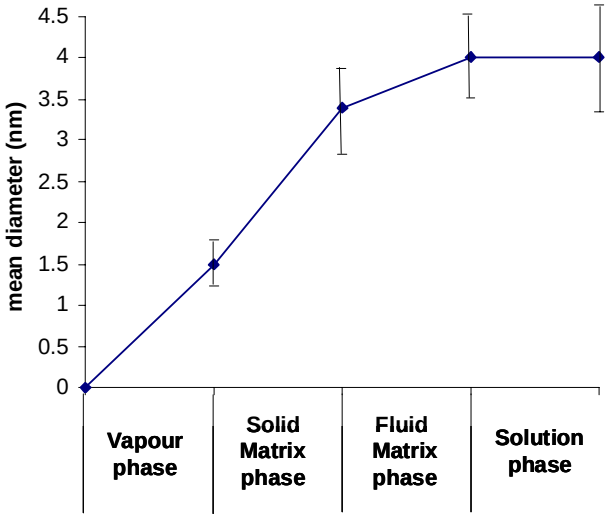

Figure 4.28 Au particle size during the various phases of metal vapour synthesis

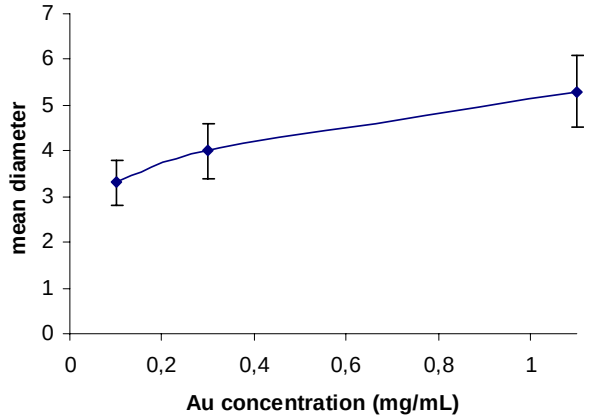

Figure 4.29 Au particle size as a function of concentration

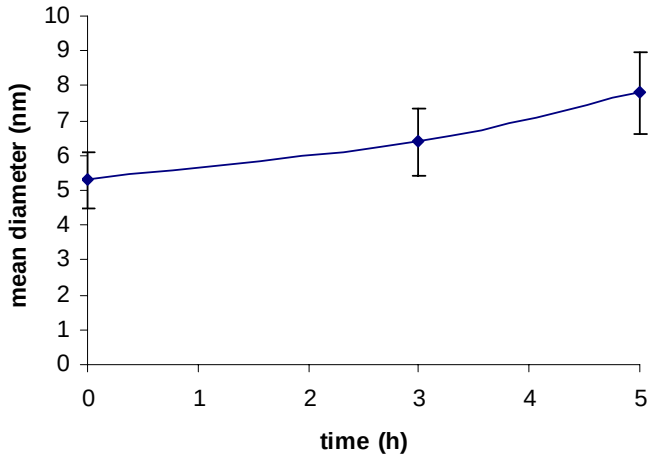

Figure 4.30 Au particle size as a function on time for concentrated solutions

4.7 REFERENCES

[1] (a) Templeton, A. C.; Wuelfing, W. P.; Murray, R. W. Acc. Chem. Res. **2000,** *33*, 27-36; (b) Haruta, M. Cattech 2002, *6*, 102; (c) Schmid, G.; Corain, B. *Eur. J. Inorg. Chem.* **2003**, 3081-3098; (d) Daniel, M.-C.; Astruc, D. *Chem. Rev.* **2004,** *104,* 293-346; (e) Hutchings, G. J. *Gold Bull*. **2004**, *37*, 1; (f) Haruta, M. *Gold Bull*. **2004**, *37*, 27; (g) Perez-Juste; J.; Pastoriza-Santos, I.;Liz-Marzan, L. M.; Mulvaney, P. Coord. Chem. Rev. 2005, *249*, 1870–1901; (h) Hutchings, G. J.; *Catal. Today* **2005**, *100*, 55–61; (i) Eustis, S.; El-Sayed, M. *Chem. Soc. Rev.* **2006**, *35*, 209–217; (j) Edwards, P. P.; Thomas, J. M. *Angew. Chem. Int. Ed*. **2007**, *46*, 5480 – 5486; (k) Min, B. K.; Friend, C. M. *Chem. Rev.* **2007,** *107*, 2709-2724.

[2] See Chapter 1. See also, for recent examples in size-controlled AuNPs synthesis or post-synthetic manipulations: (a) Koh, H.-D.; Kang, N.-G.; Lee, J.-S. *Langmuir* **2007,** *23,* 11425-11429; (b) Jørgensen, J. M.; Erlacher, K. Pedersen, J. S.; Gothelf, K. V. *Langmuir* **2005,** *21,* 10320-10323; (c) Teranishi, T.; Hasegawa, S.; Shimizu, T.; Miyake, M. *Adv. Mater.* **2001**, *13*, 1699; (d) Maye, M. M.; Zheng, W.; Leibowitz, F. L.; Ly, N. K.; Zhong, C.-J. *Langmuir* **2000,** *16,* 490-497.

[3] Zheng, N.; Stucky, G. D. *J. Am. Chem. Soc.* **2006**, *128*, 14278-14280.

[4] Lin, S.-T.; Franklin, M. T.; Klabunde, K. J. *Langmuir* **1986,** *2,* 259-260.

[5] Hasan, M.; Bethell, B.; Brust, M. *J. Am. Chem. Soc*. **2002**, *124*, 1132.

[6] Li, G.; Lauer, M.; Schulz, A.; Boettcher, C.; Li, F.; Furhop, J.-H. *Langmuir* **2003,** *19,* 6483-6491.

[7] (a) Link, S.; El-Sayed, M. A. *J. Phys. Chem. B* **1999,** *103,* 4212-4217; (b) Wilcoxon, J. P.; Martin, J. E.; Provencio, P. J. Chem. Phys. **2001**, *115*, 998; (c) Moores, A.; Goettmann F. *New J. Chem*. **2006**, 30, 1121–1132; (d) Scaffardi, L. B.; Pellegri, N.; De Sanctis, O.; Tocho, J. O. *Nanotechnology* **2005**, *16,* 158–163.

[8] Hicks, J.; Miles, D. T.; Murray, R. W. J. Am. Chem. Soc. 2002, 124, 13322-13328.

[9] Raffa, P.; Evangelisti, C.; Vitulli, G.; Salvadori, P. *Tetr. Lett.* **2008**, *49*, 3221-3224.

[10] Terrill, R. H.; Postlethwaite, T. A.; Chen, C.-H.; Poon, C.-D.; Terzis, A.; Chen, A.; Hutchison, J. E.; Clark, M. R.; Wignall, G.; Londono, J. D.; Superfine, R.; Falvo, M.; Johnson Jr., C. S.; Samulski, E. T.; Murray R. W. *J. Am. Chem. Soc.* **1995**, *117*, 12537-12548.

[11] Hoestetler, M. J.; Wingate, J. E.; Zhong, C.-J.; Harris, J. E.; Vachet, R. W.; Clark, M. R.; Londono, J. D.; Green, S. J.; Stokes, J. J.; Wignall, G. D.; Glish, G. L.; Porter, M. D.; Evans, N. D.; Murray, R. W. *Langmuir* **1998**, *14*, 17-30.

[12] Leff, D. V.; Brandt, L.; Heath, J. R. *Langmuir* **1996,** *12,* 4723-4730.

[13] Aslam, M.; Fu, L.; Su, M.; Vijayamohanan, K.; Dravid, V. P. *J. Mater. Chem*. **2004**, *14*, 1795-1797.

[14] Zeng, N.; Stuchy, G. D. *J. Am. Chem. Soc.* **2006**, *128*, 14278-14280.

[15] Caporusso, A. M.; Aronica, L. A.; Schiavi, E.; Martra, G.; Vitulli, G.; Salvadori, P. *J. Organomet. Chem*. **2005**, *690*, 1063–1066.

EXPERIMENTAL SECTION

A theory is something nobody believes, except the person who made it. An experiment is something everybody believes, except the person who made it.

Albert Einstein

GENERAL

Unless otherwise specified, all operations were performed under inert atmosphere of dry Argon. All reactants and reagents were purchased from Aldrich.

INSTRUMENTATION USED

- Atomic adsorption spectra were recorded at ICAS (Istituto di Chimica Analitica Strumentale) of C.N.R. in Pisa. The analysis were conducted by means of a Perkin-Elmer Spectrometer 4100 ZL equipped with an electrochemically heated graphite furnace.
- Gas-chromatographic analyses were performed with a DB1 capillary column (30 m x 0.52 mm, 5 μm) using He as the carrier gas and a flame ionization detector (FID).
- Electron micrographs were obtained by a Jeol 2000EX microscope. Before the introduction in the instrument, the samples, in the form of powders, were ultrasonically dispersed in isopropyl alcohol and a drop of the suspension was deposited on a copper grid covered with a lacey carbon film. Histograms of the particle size distribution were obtained by counting onto the micrographs at least 300 particles; the mean particle diameter (d_m) was calculated by using the formula $d_m = \Sigma d_i n_i / \Sigma n_i$ where n_i was the number of particles of diameter d_i .
- NMR measurements were performed on a Varian INOVA- 600 spectrometer operating at 600 MHz and 150 MHz for 1H and 13C, respectively. The temperature was controlled to ±0.1 °C. ^{1}H and ^{13}C NMR chemical shifts are referenced to TMS as internal standard. The 2D NMR spectra were obtained by use of standard sequences.
  - The ROESY (Rotating-frame Overhauser Enhancement SpectroscopY) spectra were recorded in the phase-sensitive mode, with mixing time from 100 ms to 600 ms.The pulse delay was maintained at 5 s; 256 increments of 4 scans and 2 K data points each were collected.The data matrix was zero-filled to 2 K×1 K and sinebell and sinebell shifted functions were applied for processing in both dimensions. 2D TOCSY spectra were recorded acquiring 4 scans with a 2 s relaxation delay, 128 increments, 2 K data points and a mixing time of 120 ms.
  - The gradient 1H, 13C-gHSQC spectrum was obtained in 32 transients per increment into a 2048 × 128 point data matrix.

- The gradient HMBC (Heteronuclear Multiple Bond Correlation) experiment was optimized for a long range ^{1}H-^{13}C coupling constant of 8 Hz.The spectra were acquired with 256 time increments, 32 scans per t_1 increment and a 3.5 ms delay period for suppression of one bond correlation signals. No decoupling during acquisition was used.
- DOSY experiments were carried out by using a stimulated echo sequence with self-compensating gradient schemes, a spectral width of 8000 Hz and 64 K data points. Typically, a value ranging from 50 to 190 ms was used for Δ, 1.0 ms for δ, and g was varied in 30 steps (16 transients each) to obtain an approximately 90-95% decrease in the resonance intensity at the largest gradient amplitudes. The baselines of all arrayed spectra were corrected before the data were processed. After data acquisition, each FID was apodized with 1.0 Hz line broadening and Fourier transformed. The data were processed with the DOSY macro (involving the determination of the resonance heights of all the signals above a pre-established threshold and the fitting of the decay curve for each resonance to a Gaussian function) to obtain pseudo two-dimensional spectra with NMR chemical shifts along one axis and calculated diffusion coefficients along the other.

APPARATUS FOR METAL VAPOUR SYNTHESIS

The apparatus for Metal Vapour Synthesis is constituted by a Pyrex glass reactor with a thickness of 7 mm and a capacity of 15 L and is represented schematically in Figure 1. The essential parts of the reactor, indicated by numbers in the figure, are listed here below:

1. glass-metal joint, which connect the reactor to the pump;
2. vapours trap, filled with liquid nitrogen;
3. glass reactor;
4. copper electrodes;
5. crucible in alumina for resistive heating of metal;
6. glass cylinder to avoid direct contact between metal and solvent;
7. tap for introduction of Argon;
8. reactor support in aluminium, equipped with O-ring;
9. glass tube for introduction of solvent vapours;
10. glass tube for SMAD siphoning;
11. support for electrodes.

The instrument is equipped with a dual stage rotary vane rebuilt mechanical vacuum pump Alcatel 2008A and a turbomolecular pump Alcatel 5100. The current for heating is produced by a Rial AEJ2 generator with a maximum power of 2 kW, equipped with an ammeter. The instrument is equipped with a 10 L dewar in stainless steel, used to cool the apparatus with liquid nitrogen.

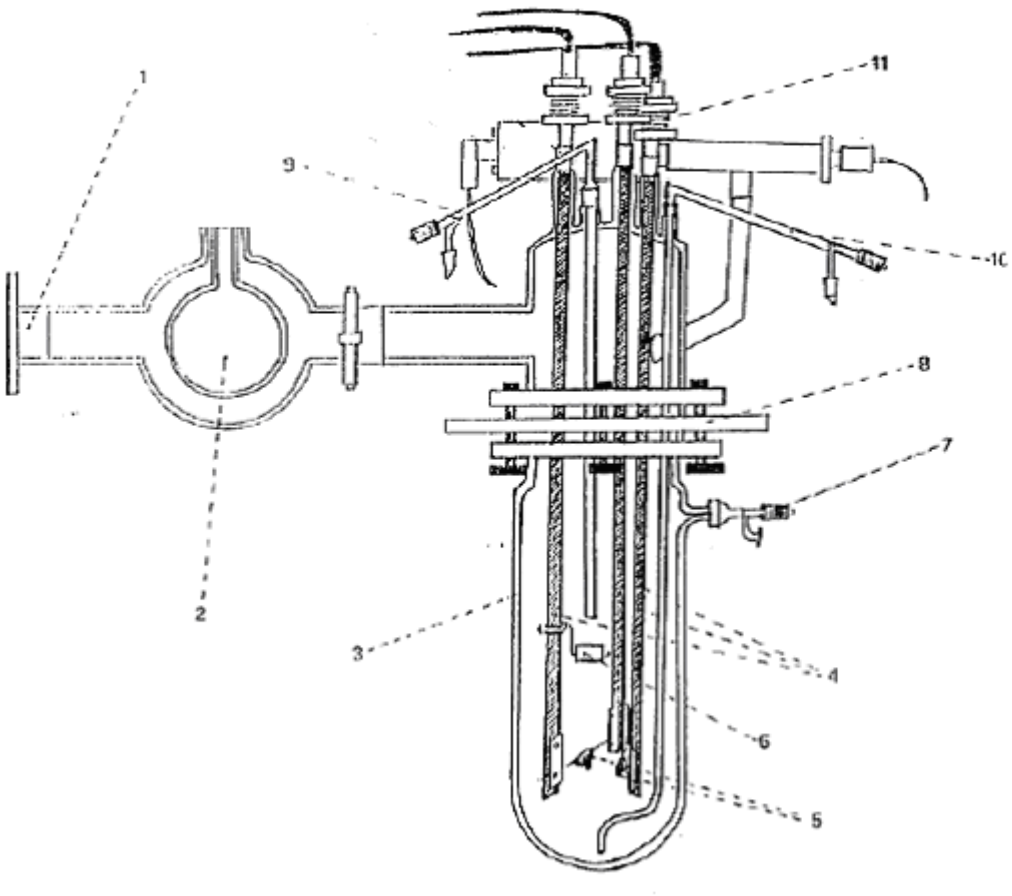

Figure 1. Apparatus for metal vapour synthesis

EXPERIMENTAL SECTION OF CHAPTER 3

GENERAL

All operations involving the metal vapour synthesis (MVS) were performed under a dry argon atmosphere. The co-condensation of platinum and mesitylene was carried out in the static reactor described above. The mesitylene-solvated Pt atom solutions were worked up under argon with use of standard Schlenk techniques. The amount of platinum in these solutions was determined by atomic absorption spectrometry in an electrochemically heated graphite furnace with a Perkin-Elmer 4100ZL instrument. All reactant and reagents were purchased from Aldrich.

- Mesitylene, diethyl ether and n-hexane were distilled over sodium and stored under argon.
- Toluene was degassed and stored under argon before use.
- 1,1,3,3-divinyltetramethyldisiloxane (DVS) was degassed and stored under argon before use.
- All other reactant and reagents were used as purchased.

PREPARATION OF MESITYLENE-SOLVATED Pt ATOMS: Pt/mes

(sections 3.2 and 3.5)

Standard solution

Pt vapour, generated by resistive heating of a tungsten wire surface coated with electrodeposited Pt (30 - 40 mg), was co-condensed with mesitylene (80 ml) in the reactor described above. The reactor chamber was warmed at the melting point of the solid matrix (- 40°C), and the resulting yellow-brown solution was siphoned and handled by Schlenk techniques. The content of the metal, evaluated by atomic absorption analysis (AAS), was 0.25 – 0.35 mg/mL (1.3 – 1.8 mM). To obtain solution at different concentrations, various amounts of metal and solvent were used, as described below.

Deposition on γ-Al_2O_3

150 mL of a Pt/mes solution with a metal content of 0.35 mg/mL, obtained by the previous procedure, were added dropwise and under inert atmosphere to a well stirred suspension of 1.00 g of γ-Al_2O_3 in degassed toluene. The metal was allowed to deposit overnight, until the surnatant become completely colorless. The so obtained 5 % Pt/ γ-Al_2O_3 powder was separated from the solution by decantation and washed several times with toluene and dried under vacuum for some hours, affording a brown powder, which was characterized by HRTEM analysis. The mean diameter of the Pt particles is 2.4 nm, as shown in Figure 2.

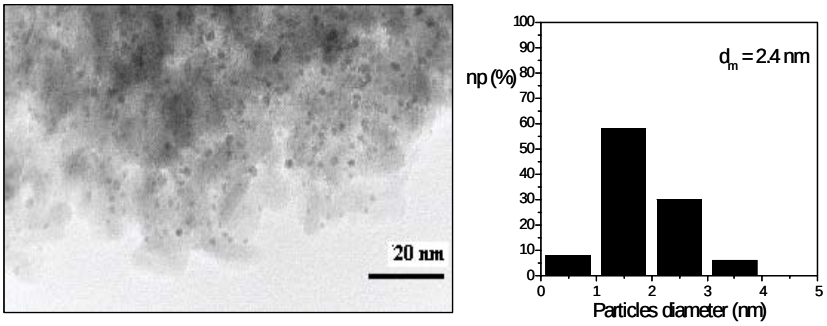

Figure 2. HRTEM of Pt/ γ-Al_2O_3 (5%) obtained from Pt/mes

Diluted solution

Pt vapour, generated by resistive heating of a tungsten wire surface coated with electrodeposited Pt (30 mg), was co-condensed with mesitylene (100 ml) in the glass reactor. The reactor chamber was warmed at the melting point of the solid matrix (−40 °C), and the resulting yellow-brown solution was siphoned and handled by Schlenk techniques. The content of the metal, evaluated by AAS, was 0.13 mg/mL.

Concentrated solutions

Pt vapour, generated by resistive heating of a tungsten wire surface coated with electrodeposited Pt (180 mg), was co-condensed with mesitylene (80 ml) in the glass reactor. The reactor chamber was warmed at the melting point of the solid matrix (−40 °C), and the resulting yellow-brown solution was siphoned and handled by Schlenk techniques. The content of the metal, evaluated by AAS, was 1.0 mg/mL.

Pt vapour, generated by resistive heating of a tungsten wire surface coated with electrodeposited Pt (180 mg), was co-condensed with mesitylene (60 ml) in the glass reactor. The reactor chamber was warmed at the melting point of the solid matrix (−40 °C), and the resulting yellow-brown solution was siphoned and handled by Schlenk techniques. The content of the metal, evaluated by atomic absorption analysis (AAS), was 2.1 mg/mL.

Pt vapour, generated by resistive heating of a tungsten wire surface coated with electrodeposited Pt (180 mg), was co-condensed with mesitylene (40 ml) in the glass reactor. The reactor chamber was warmed at the melting point of the solid matrix (−40 °C), and the resulting yellow-brown solution was siphoned and handled by Schlenk techniques. The content of the metal, evaluated by AAS, was 3.2 mg/mL.

STABILIZATION OF MESITYLENE-SOLVATED Pt ATOMS SOLUTIONS BY DVS: Pt(mes)/DVS

(section 3.3)

In a typical experiment, **Pt/mes** solution (1 - 3.5 mL, 0.25 - 0.35 mg/mL, 6.0 μmol of Pt) was added, at 25°C in a Schlenk tube (50 mL), to a large excess of DVS (2 mL,

8.7 mmoles, molar ratio DVS/Pt = 1300:1). The obtained solutions are stable at room temperature for indefinite time. After stirring at 25°C for 15 minutes, the solvent has been removed under vacuum, keeping the solution at $5 \cdot 10^{-5}$ mBar for 30 minutes at 25°C. A brown solid was obtained, completely soluble in aromatic solvents.

Preparation of NMR samples

Samples of the solid, obtained by evaporation under vacuum of 5 mL of stabilized solution, were dissolved in C_6D_6 (0.7 ml) containing 0.1 % of TMS and solutions transferred into a NMR tube under argon atmosphere. TMS was used as internal standard both for ^{1}H-NMR analyses and for NMR-DOSY analyses. The spectra of **Pt(mes)/DVS** are reported below (Figure 3).

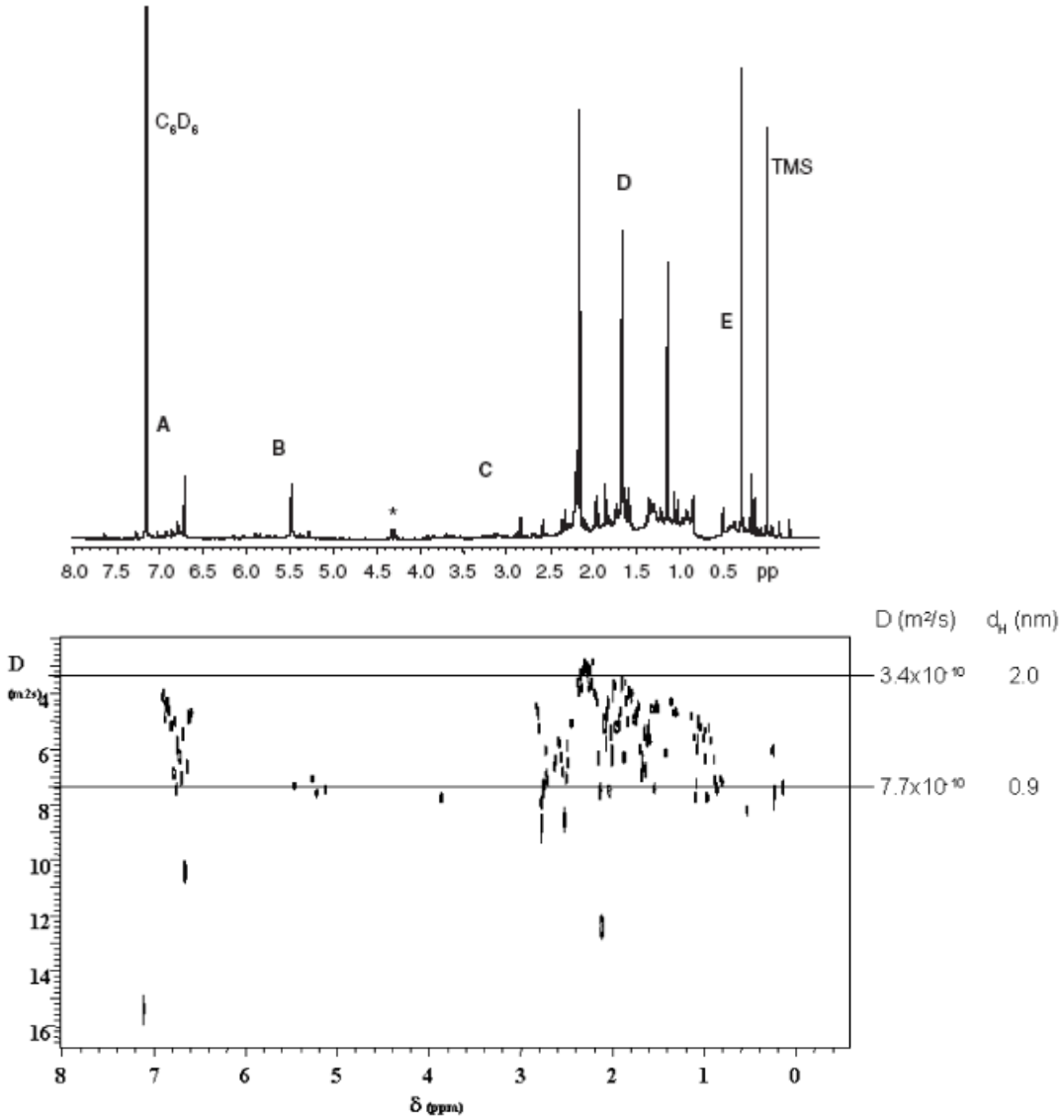

Figure 3. ^{1}H-NMR and DOSY spectra of Pt(mes)/DVS

Deposition on γ-Al_2O_3

30 mL of a Pt(mes)/DVS solution with a metal content of 0.35 mg/mL, obtained by the previous procedure, were added dropwise and under inert atmosphere to a well stirred suspension of 0.20 g of γ-Al_2O_3 in degassed toluene. The metal was allowed to deposit overnight, until the surnatant become completely colorless. The so obtained 5 % Pt/ γ-Al_2O_3 powder was separated from the solution by decantation and washed several times with toluene and dried under vacuum for some hours, affording a pale brown powder, which was characterized by HRTEM analysis. The mean diameter of the Pt particles is 1.7 nm, as shown in Figure 4.

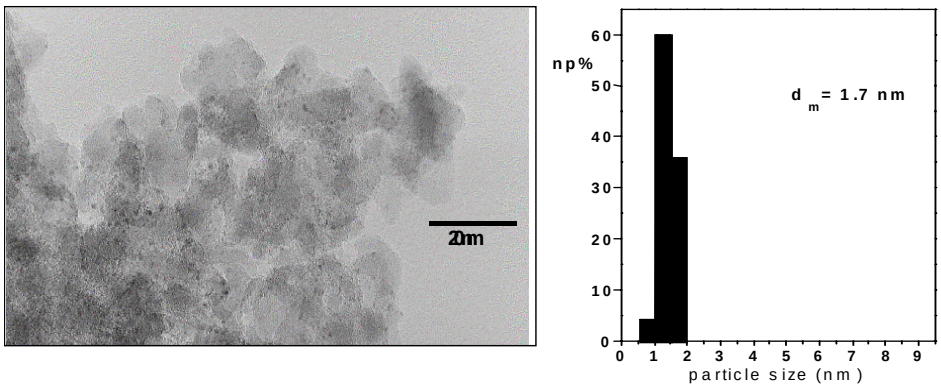

Figure 4. HRTEM of Pt/ γ-Al_2O_3 (5%) obtained from Pt(mes)/DVS

SYNTHESIS OF MODEL Pt COMPLEXES

(section 3.3.1)

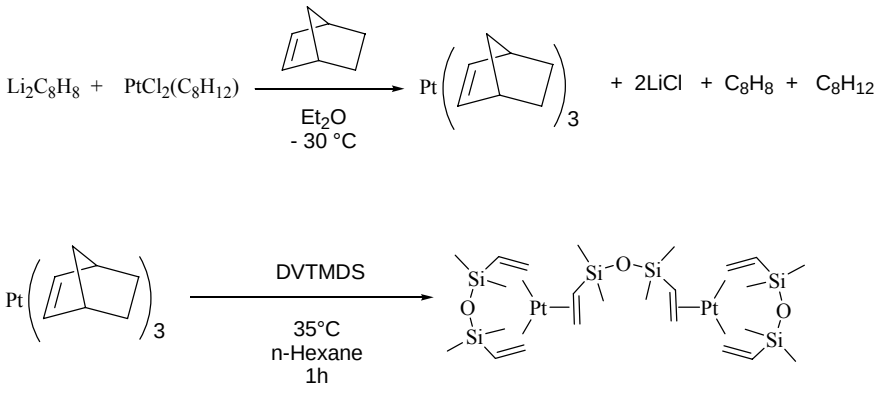

(1,3,5,7-cyclooctatetraene)dilithium

Lithium foils (600 mg, 86 mmol) ware suspended under nitrogen in dry diethyl ether (100 mL) in magnetically stirred 250 mL, two-necked, round-bttomed flask at 0°C. A 3.0 g sample (28 mmol) of 1,3,5,7-cyclooctatetraene was added and the mixture was stirred for 16 h. The small quantity of white precipitate was allowed to settle, an

aliquot of the orange solution was removed with a sirynge, and the molarity was checked by hydrolysis and titration against standard acid. A saturated solution of (1,3,5,7-cyclooctatetraene)dilithium is approximately 0.24 M.

Tris(bicyclo[2.2.1]hept-2-ene)platinum(0)

A 250 mL three-necked round-bottomed flask, fitted with a pressure-equalized dropping funnel, a nitrogen inlet and a magnetic stirring bar was placed in a cold bath at -30°C. Finely powdered [$PtCl_2(C_8H_{12})$] (0.5 g, 1.4 mmol) and bicyclo[2.2.1]hep-2-tene (0.95 g, 10 mmol) were added through the third neck. These were slurried with diethyl ether (5 mL) at -30°C. The freshly prepared (1,3,5,7-cyclooctatetraene)dilithium solution (5.0 mL, 1.2 mmol) was transferred with a syringe to the dropping funnel and then added over a 1 h period to the stirred slurry while the temperature was manteined at approximately -30°C. The reaction mixture was then allowed to warm at room temperature and the volatile material removed in vacuo. The residue was dried and extracted 3 times with distilled hexane (30 + 10 + 10 mL) under nitrogen. The extract was filtered through an alumina pad (5 mL) under nitrogen atmosphere and the solvent removed in vacuo, affording the product as a white solid (0.45 g, 0.93 mmol, 66 % yield). The compound was characterized by ^{1}H-NMR and DOSY analysis.

Tris(1,3-divinyl-1,1,3,3,-tetramethyldisyloxane)diplatinum(0)

The as synthesized tris(bicyclo[2.2.1]hept-2-ene)platinum(0) was dissolved in n-hexane (30 mL) in a two-necked round bottomed flask (100 mL) equipped with magnetic stirring bar, under nitrogen. To this solution, an excess of 1,3-divinyl-1,1,3,3,-tetramethyldisyloxane (1 mL, 4.35 mmol) was added and the solution was warmed to 35°C for 2h. After that, the volatile materials were removed in vacuo, affording the crude product as a yellow oil. After filtration on a pad of silica (eluent: n-hexane) and crystallization from cold n-hexane, white crystals of $Pt_2(DVS)_3$ (0.5 mmol, 53 % yield) were obtained and characterized with ^{1}H-NMR and DOSY, reported below (Figure 5).

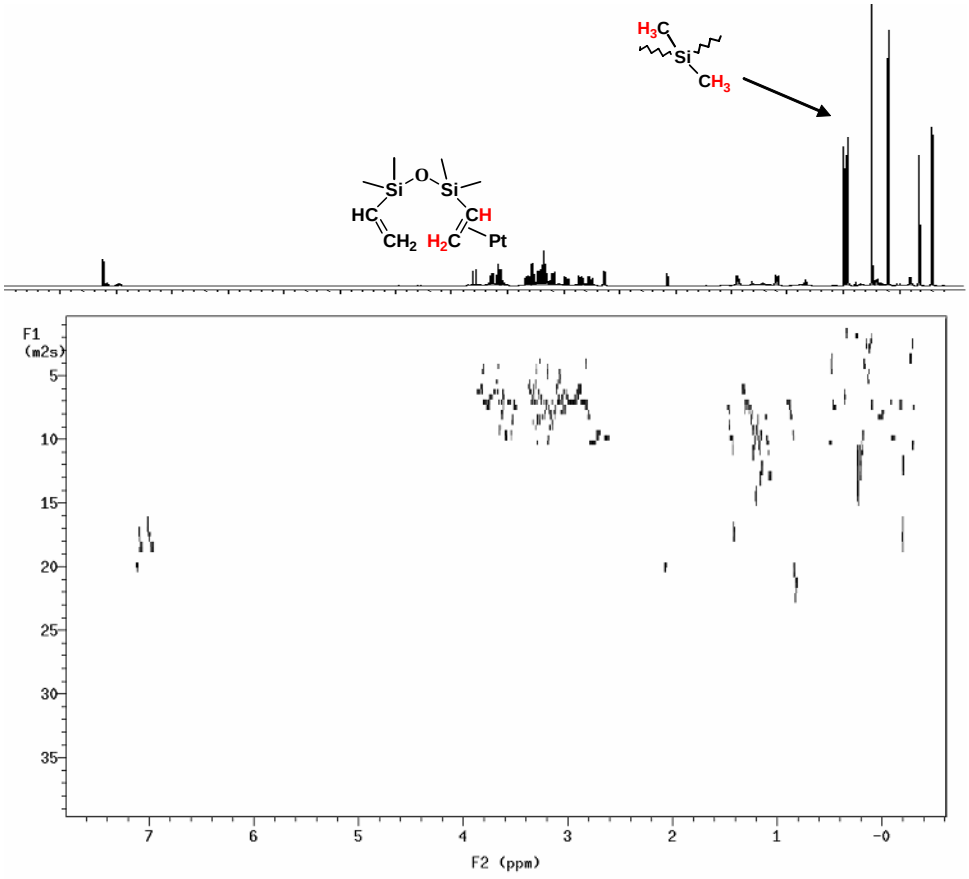

Figure 5. ^{1}H-NMR and DOSY spectra of $Pt_2(DVS)_3$

PREPARATION OF CO-VAPORIZED SOLUTIONS: Pt/(DVS-mes)

(section 3.4)

In a typical experiment, Pt vapour, generated by resistive heating of a tungsten wire surface coated with electrodeposited Pt (80 mg), was co-condensed with a mixture of mesitylene (40 ml) and DVS (15 ml) in a glass reactor. The reactor chamber was warmed at the melting point of the solid matrix (- 40°C), and the resulting pale yellow solution was siphoned and keep at room temperature (25°C). The content of the metal, evaluated by atomic absorption analysis (AAS), was 1.2 mg/mL. The obtained Pt/(DVS-mes) was characterized by ^{1}H-NMR, DOSY (Figure 6), gHSQC (Figure 7) and ROESY (Figure 8) analysis, previous evaporation of the solvent under vacuum and dissolution in deuterated benzene, as previously described for the other systems.

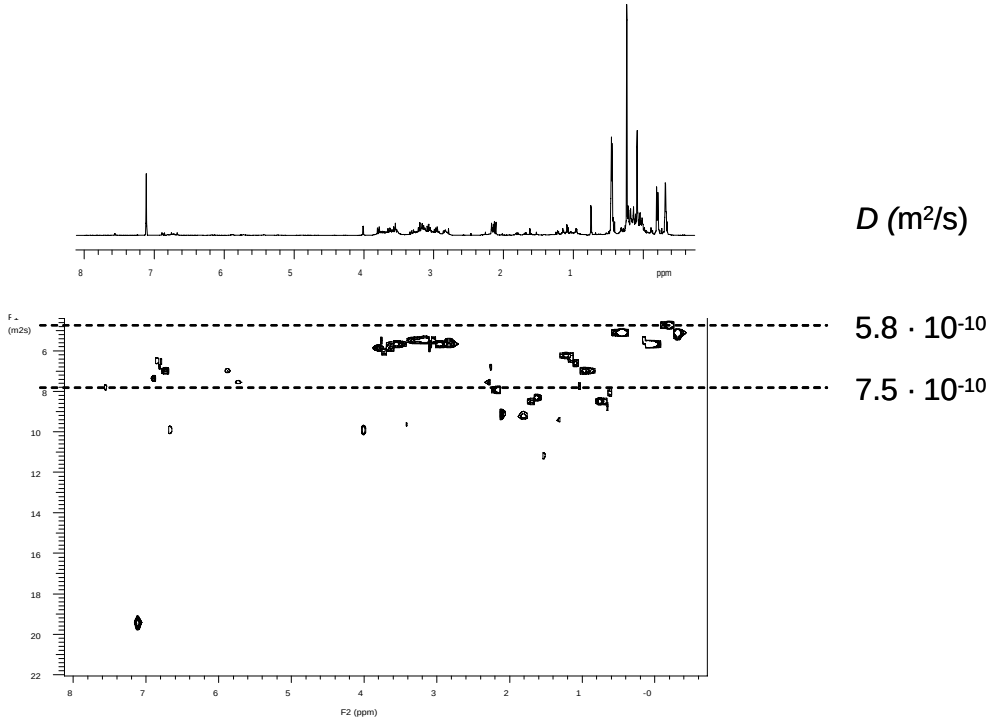

Figure 6. ^{1}H-NMR and DOSY spectrum of Pt/DVS-mes

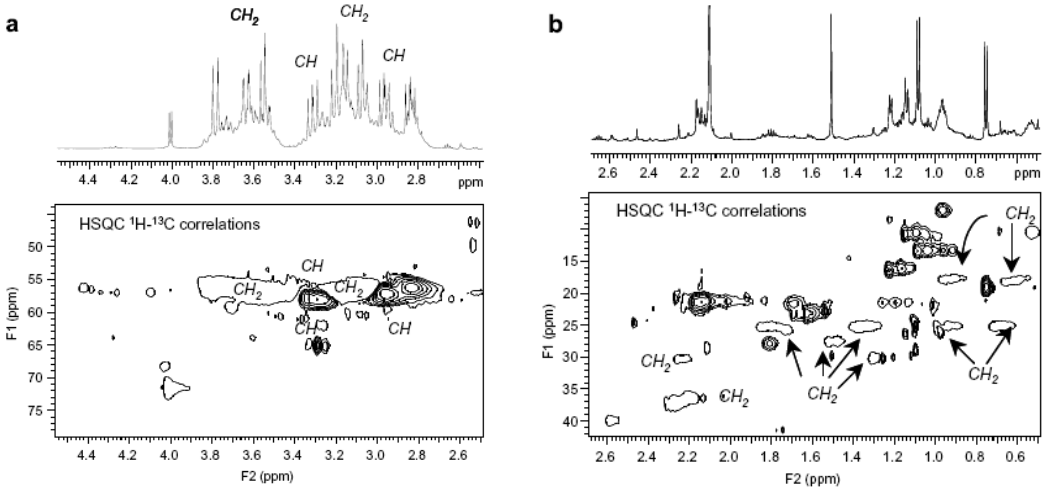

Figure 7. Heteronuclear correlation in Pt/DVS-mes: (a) olefinic region; (b) aliphatic region

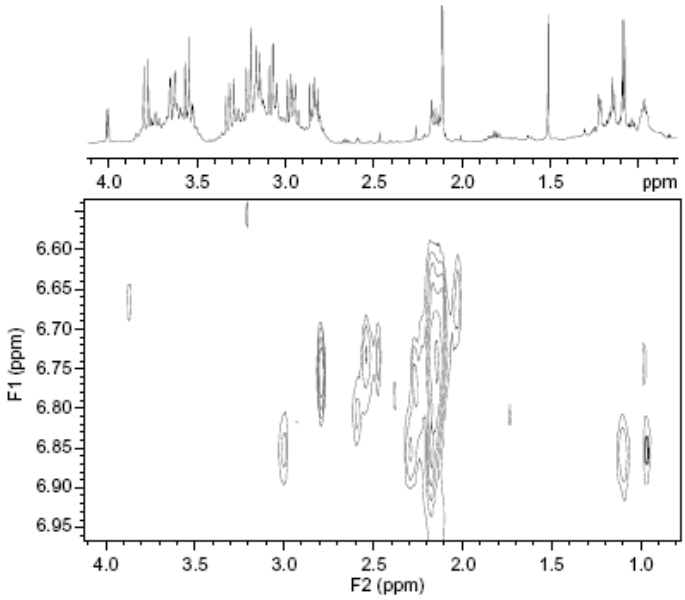

Figure 8. Homonuclear dipolar interactions in Pt/DVS-mes

STABILIZATION OF Pt/mes SOLUTIONS BY DVS AT DIFFERENT TIMES *(section 3.6)*

Stabilization at -40°C

In a typical experiment, a **Pt/mes** solution was kept at -40°C by a thermostat bath. When the temperature reached the desired value, a 5 mL portion of the solution (1.75 mg of Pt, $8.97 \cdot 10^{-3}$ mmol), was added to a large excess of 1,3-divinyl-1,1,3,3-tetramethyldisiloxane (DVS) (molar ratio DVS/Pt = 1000:1; 2.0 ml, 8.97 mmol) in a Schlenk tube (50 mL), at different times: 0, 30', 90', 120', 6 h, 24 h. The resulting thermally stable solutions were stirred at 25°C for 15 minutes. The solvent was removed under vacuum by keeping the solution at $5 \cdot 10^{-5}$ mBar for 30 minutes at 25°C. ^{1}H-NMR and DOSY spectra were recorded as usual (Figure 9).

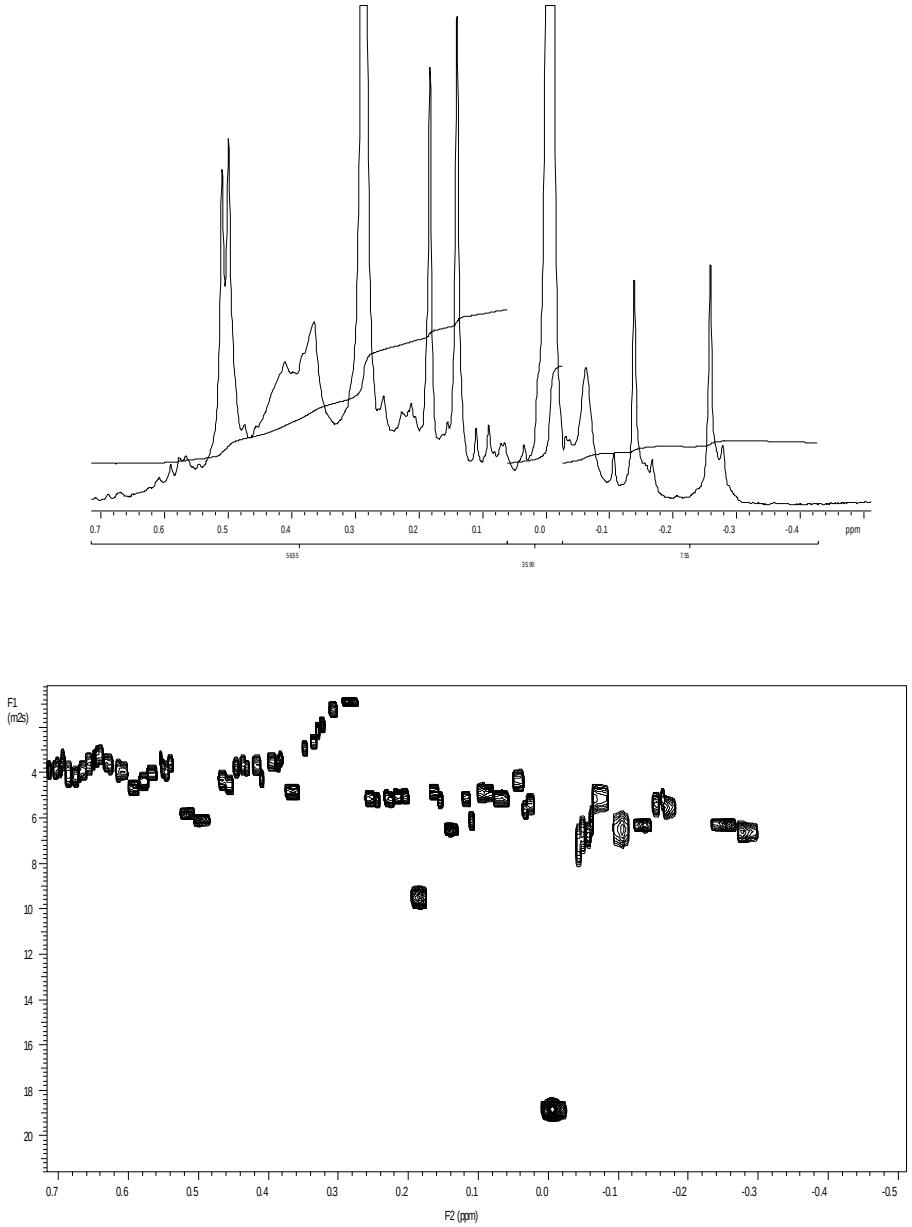

Figure 9. ^{1}H-NMR and DOSY spectrum of Pt(mes)/DVS at t = 0 (low chemical shifts)

Stabilization at 25°C

In a typical experiment, a **Pt/mes** solution was kept at 25°C by a thermostat bath. When the temperature reached the desired value, a 5 mL portion of the solution (1.75 mg of Pt, $8.97 \cdot 10^{-3}$ mmol), was added to a large excess of 1,3-divinyl-1,1,3,3-tetramethyldisiloxane (DVS) (molar ratio DVS/Pt = 1000:1; 2.0 ml, 8.97 mmol) in a Schlenk tube (50 mL), at different times: 0, 30', 90', 120', 240', 360'. The resulting thermally stable solutions were stirred at 25°C for 15 minutes. The solvent was removed under vacuum by keeping the solution at $5 \cdot 10^{-5}$ mBar for 30 minutes at

25°C. ^{1}H-NMR and DOSY spectra were recorded as usual (spectra of systems stabilized at 30', 90' and 120' are shown below, figures 10 - 12, respectively).

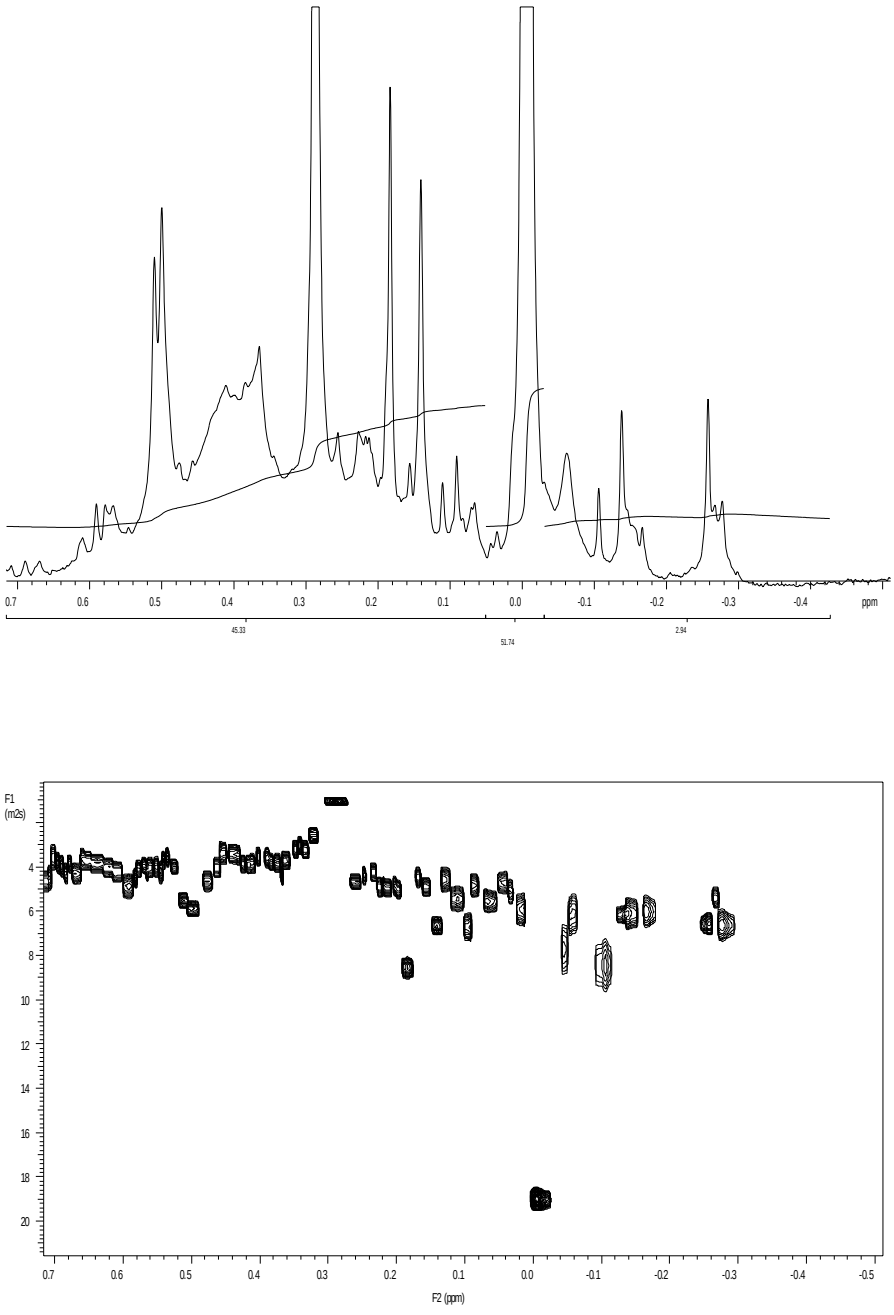

Figure 10. ^{1}H-NMR and DOSY spectrum of Pt(mes)/DVS at t = 30' (low chemical shifts)

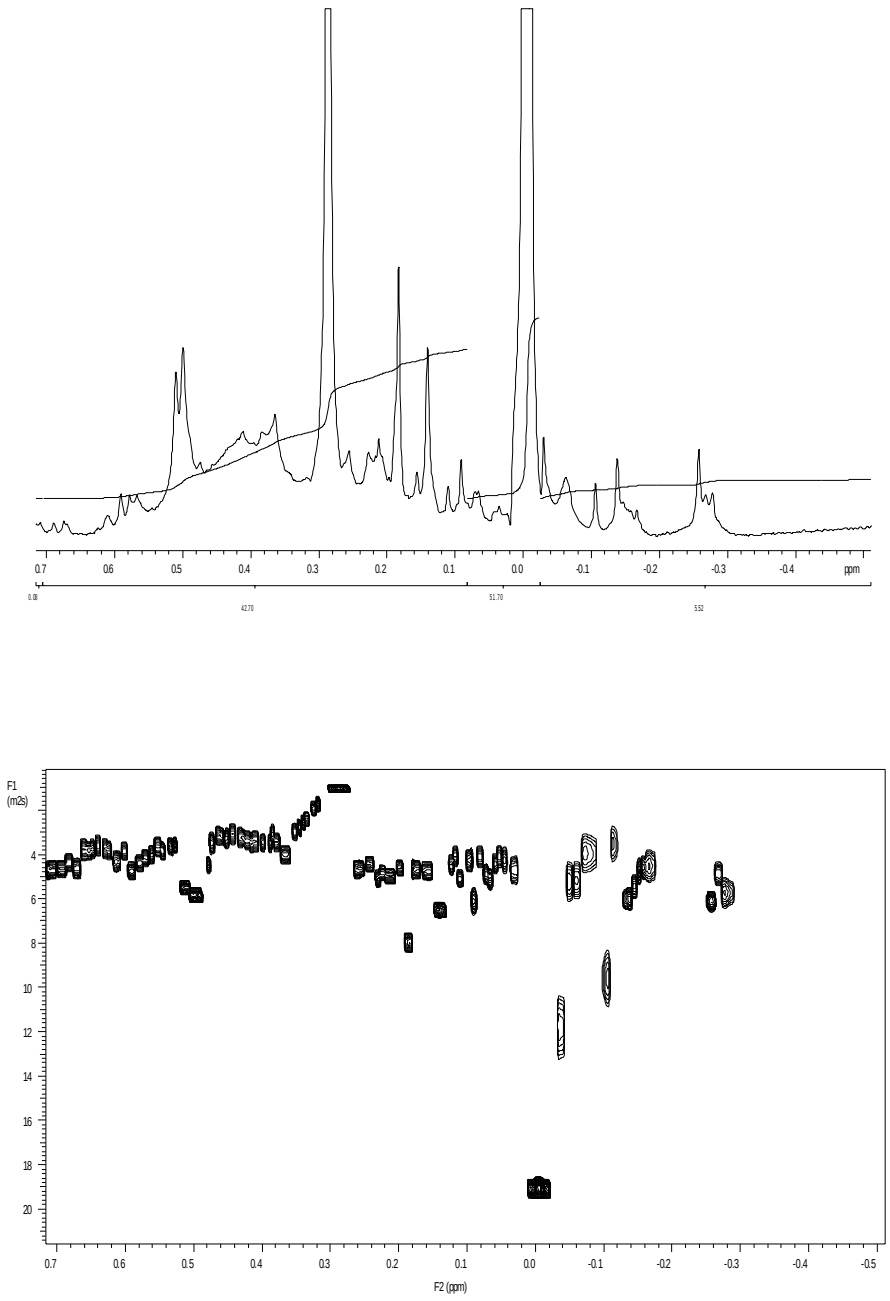

Figure 11. ^{1}H-NMR and DOSY spectrum of Pt(mes)/DVS at t = 90' (low chemical shifts)

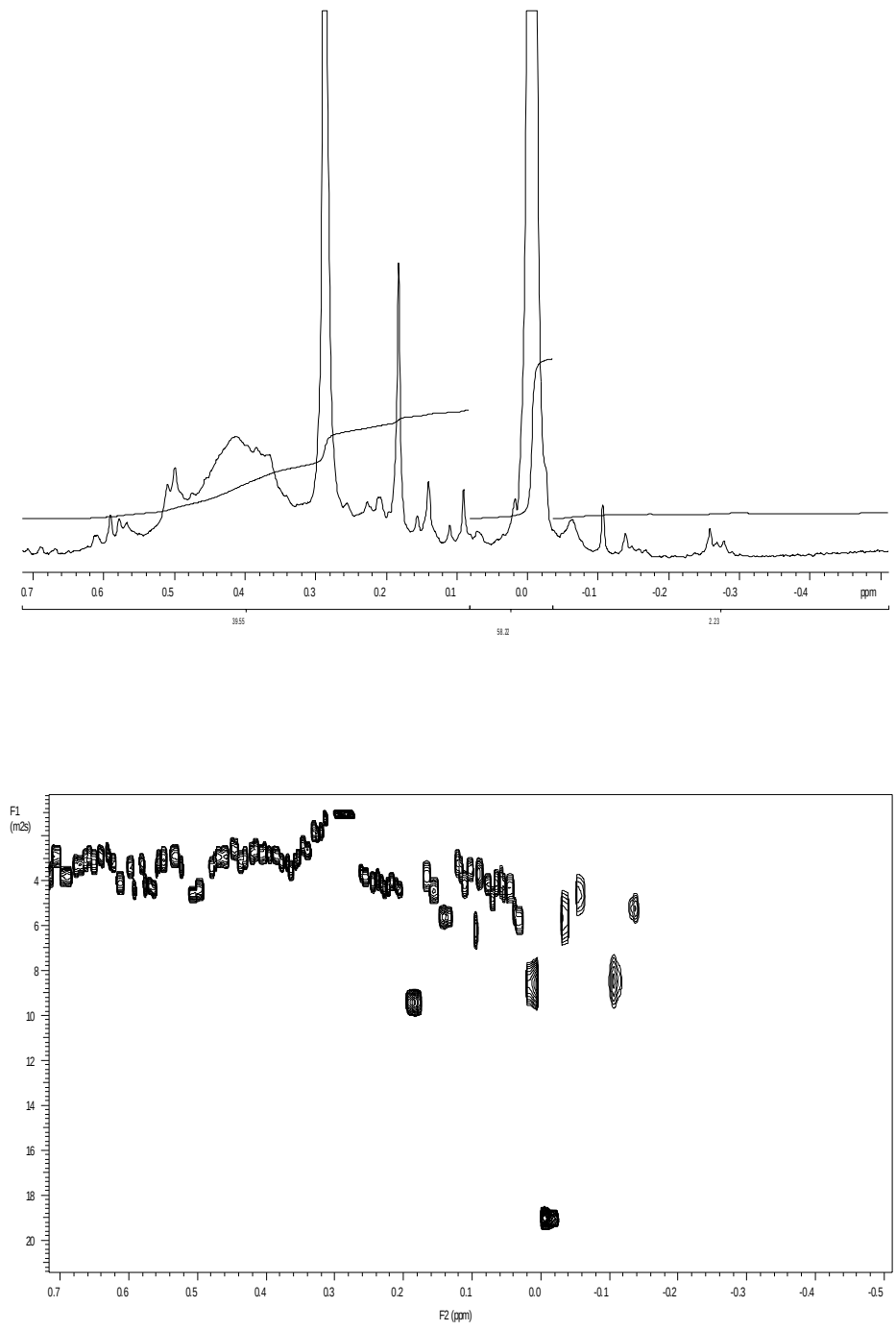

Figure 12. ^{1}H-NMR and DOSY spectrum of Pt(mes)/DVS at t = 120' (low chemical shifts)

CATALYTIC TESTS

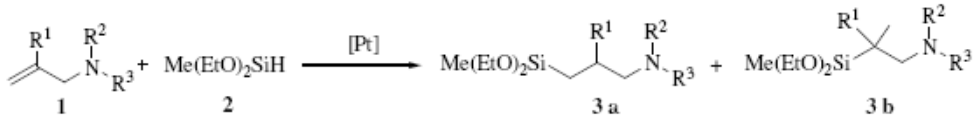

All catalytic reactions were carried out under Argon atmosphere in a Schlenk tube, with magnetic stirring. $5 \cdot 10^{-4}$ mg-atom of Pt catalysts (0.09 mL of **Pt/(DVS-mes)** solution, 1.2 mg/ml of Pt; 0.09 mL of Pt Karstedt catalyst, 1.2 mg/mL in Pt, obtained by dilution with xylene of the starting solution (2.2 % in Pt), 0.15 mg of platinum oxide hydrate, 81% in Pt) were introduced under argon, at room temperature. Subsequently, 5 mmoles of allylamine **1** (substrate/Pt molar ratio = 10000) and 5.3 mmoles of $(EtO)_2MeSiH$ (**2**, 0.85 mL, d = 0.83 g/mL, MW=108) were introduced. The mixture was kept at the given temperature, then analyzed by GLC.

EXPERIMENTAL SECTION OF CHAPTER 4

GENERAL

All operations involving the metal vapour synthesis (MVS) were performed under a dry argon atmosphere. The co-condensation of gold and the solvent was carried out in a static reactor. The solvated Au atom solutions were worked up under argon with use of standard Schlenk techniques. The amount of gold in these solutions was determined by atomic absorption spectrometry in an electrochemically heated graphite furnace with a Perkin-Elmer 4100ZL instrument. All reactant and reagents were purchased from Aldrich.

- Acetone was distilled over $KMnO_4$ and stored under argon.
- Cyclohexane was distilled over sodium and stored under argon.
- Toluene, water and ethanol were degassed and stored under argon before use.
- All other reactant and reagents were used as purchased.

PREPARATION OF Au/ac

(section 4.2)

Au vapour, generated by resistive heating of an alumina-covered tungsten crucible filled with Au chips (60 mg), was co-condensed with acetone (100 mL) in the reactor described above. The reactor chamber was warmed at the melting point of the solid matrix (- 50°C), and the resulting purple solution of **Au/ac** was siphoned and handled by Schlenk techniques. The content of the metal, evaluated by atomic absorption analysis (AAS), was 0.3 – 0.5 mg/mL. To obtain solution at various concentration, different amounts of metal and solvent were used, as for Platinum (see previous section).

PREPARATION OF Au/EtOH and Au/EtOH-H_2O

(section 4.3.6)

For preparation of **Au/EtOH** and **Au/EtOH-H_2O** the same experimental procedure as for **Au/ac** was used. Au vapour, generated by resistive heating of an alumina-covered tungsten crucible filled with Au chips (60 mg), was co-condensed with ethanol (100 mL) or a mixture 1:1 of ethanol and water (50 + 50 mL) in the reactor described above. The reactor chamber was warmed at the melting point of the solid matrix and the resulting purple solution was siphoned and handled by Schlenk techniques. The content of the metal, evaluated by atomic absorption analysis (AAS), was 0.3 – 0.5 mg/mL.

STABILIZATION OF ACETONE-SOLVATED Au ATOMS SOLUTIONS WITH DODECANETHIOL

(section 4.3)

In a typical experiment, **Au/ac** solution (10 mL, 15 μmol of Au) was added, at -50°C in a schlenk tube (50 mL), to a large excess (1 mL, 4 mmol) of dodecanethiol. After stirring at 25°C for 15 minutes, the solvent has been removed under vacuum, keeping the solution at $5 \cdot 10^{-5}$ mBar for 30 minutes at 25°C. Then, the concentrated solution was warmed to 60°C until the solution color changes (about 5 minutes). Subsequently, degassed ethanol was added under nitrogen in order to precipitate the capped Au nanoparticles. The solid was decanted or filtered under nitrogen, washed several times with ethanol and dried in vacuo. It can be redissolved in apolar solvents (toluene, chloroform, deuterated benzene) for characterization in solution and stored for indefinite time under inert atmosphere. The same procedure was used for the stabilization of **Au/EtOH** and **Au/EtOH-H_2O**. Representative ^{1}H-NMR, DOSY and Uv-vis spectra are reported below (Figure 13, 14 and 15 respectively).

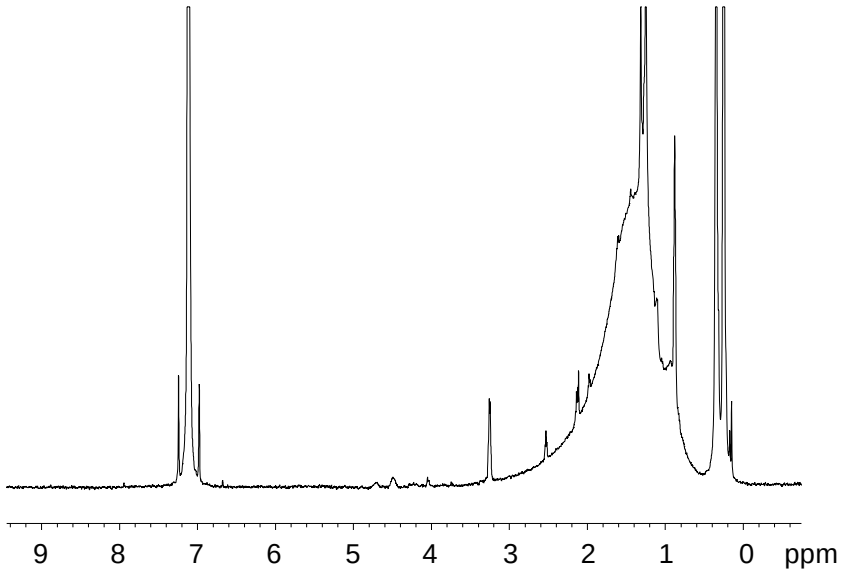

Figure 13. ^{1}H-NMR spectra in C_6D_6 of Au(ac)/DT

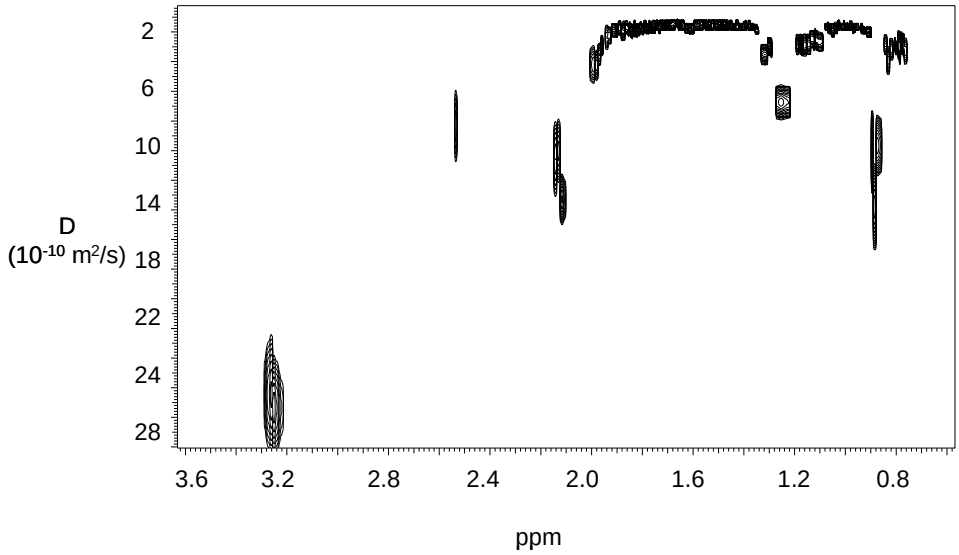

Figure 14. DOSY spectrum of Au(ac)/DT in C_6D_6

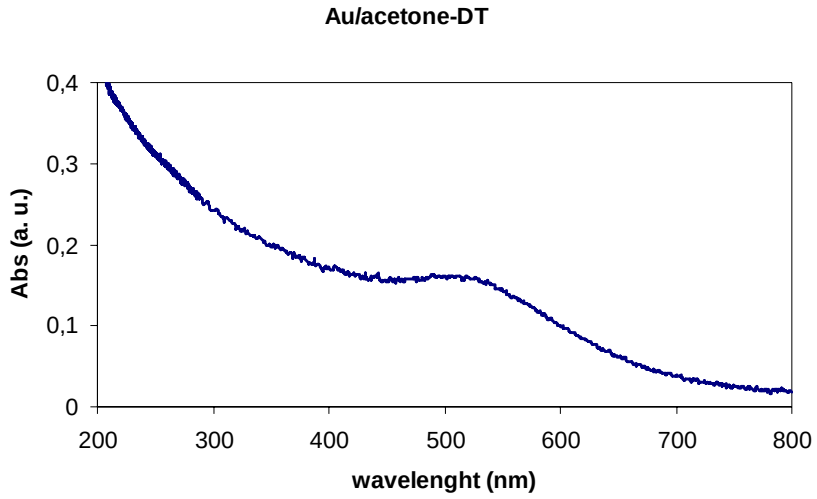

Figure 15. UV-Vis spectra of Au(ac)/DT NPs in toluene

PREPARATION OF NMR SAMPLES

As for Platinum (see previous section)

UV-VIS ANALYSIS

Stabilized gold nanoparticles, as dried solid products, were dissolved in degassed toluene (Au concentration = 10 mM). The obtained solutions were placed in a quartz cuvette, and Uv-vis spectra were recorded on a Perkin-Elmer spectrometer.

PREPARATION OF Au/DT BY ADDITION OF LIGAND TO SOLID MATRIX

Au vapour, generated by resistive heating of an alumina-covered tungsten crucible filled with Au chips (60 mg), was co-condensed with cyclohexane (100 mL). Before melting, a solution of dodecanthiol (10 mL, 40 mmol) in acetone (15 mL) were siphoned in the reactor. The solid was allowed to melt, by warming the reactor at room temperature and the solution was recovered as usual. The content of the metal, evaluated by atomic absorption analysis (AAS), was 1.0 mg/mL. Representative ^{1}H-NMR, DOSY and Uv-vis spectra are reported below (Figure 16 - 18).

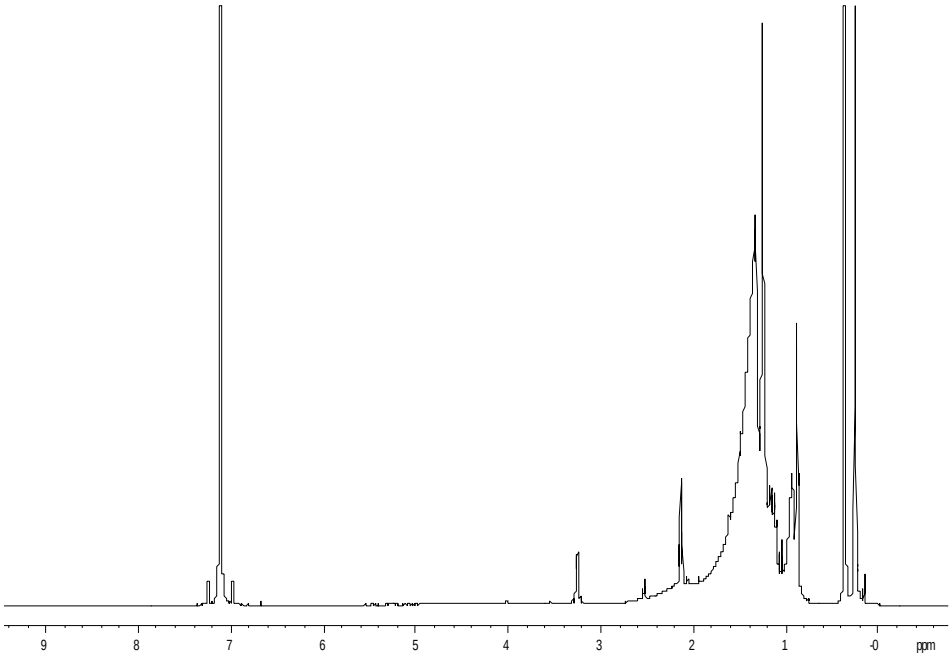

Figure 16. ^{1}H-NMR spectrum of Au/DT in C_6D_6

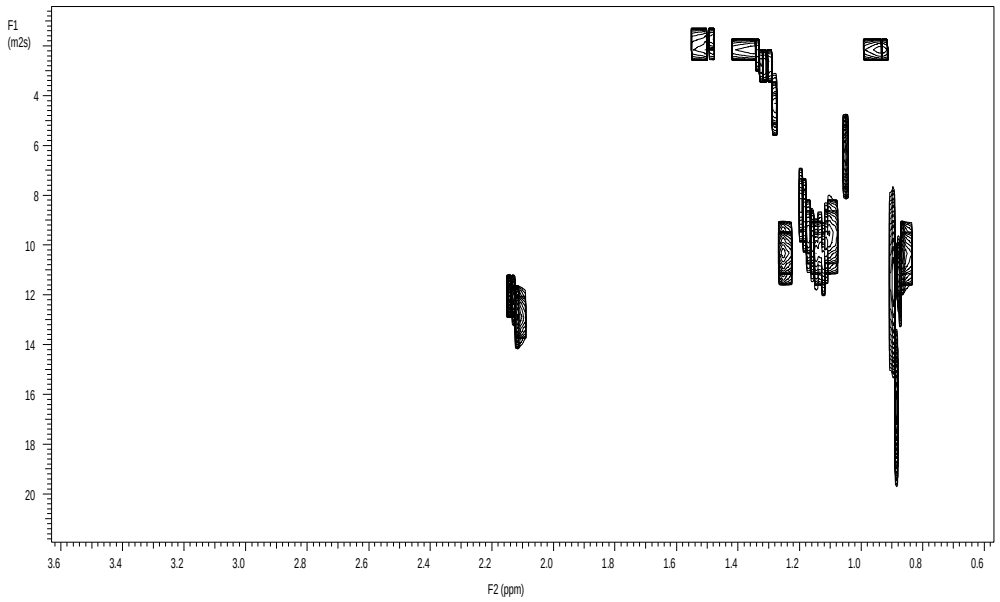

Figure 17. DOSY spectrum of Au/DT in C_6D_6

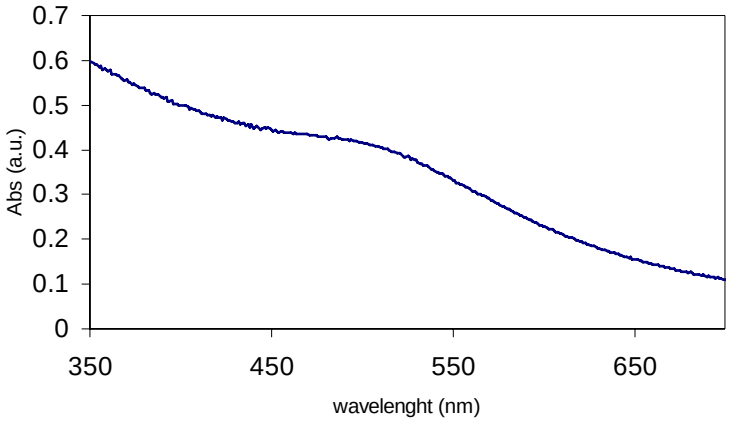

Figure 18. Uv-vis spectrum of Au/DT in toluene

PREPARATION OF Au/tBT BY CO-VAPORIZATION

Au vapour, generated by resistive heating of an alumina-covered tungsten crucible filled with Au chips (60 mg), was co-condensed with a mixture of cyclohexane and tert-butanethiol (100 mL, 9:1 volume). The reactor chamber was warmed at room temperature and the resulting brown solution was siphoned and handled by Schlenk techniques. The content of the metal, evaluated by atomic absorption analysis (AAS), was 1.0 mg/mL. By removal of excess ligand and solvent in vacuo, a brown powder was recovered, which can be completely dissolved in apolar solvents (toluene, chloroform) and partially dissolved in EtOH. The ethanol soluble and insoluble

fractions were characterized by ^{1}H-NMR, DOSY and Uv-vis spectra as usual (Figure 19 - 21).

a)

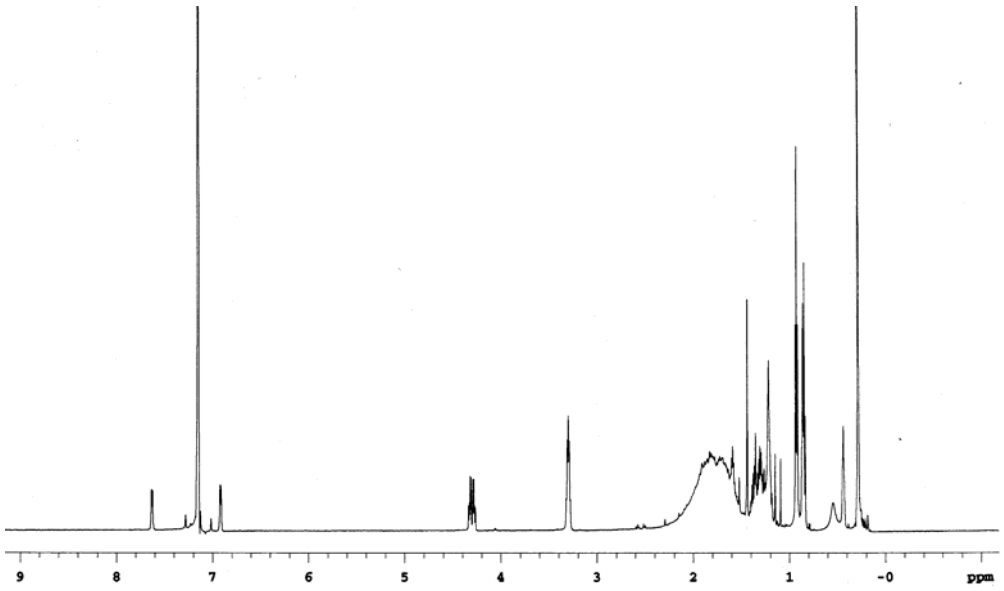

b)

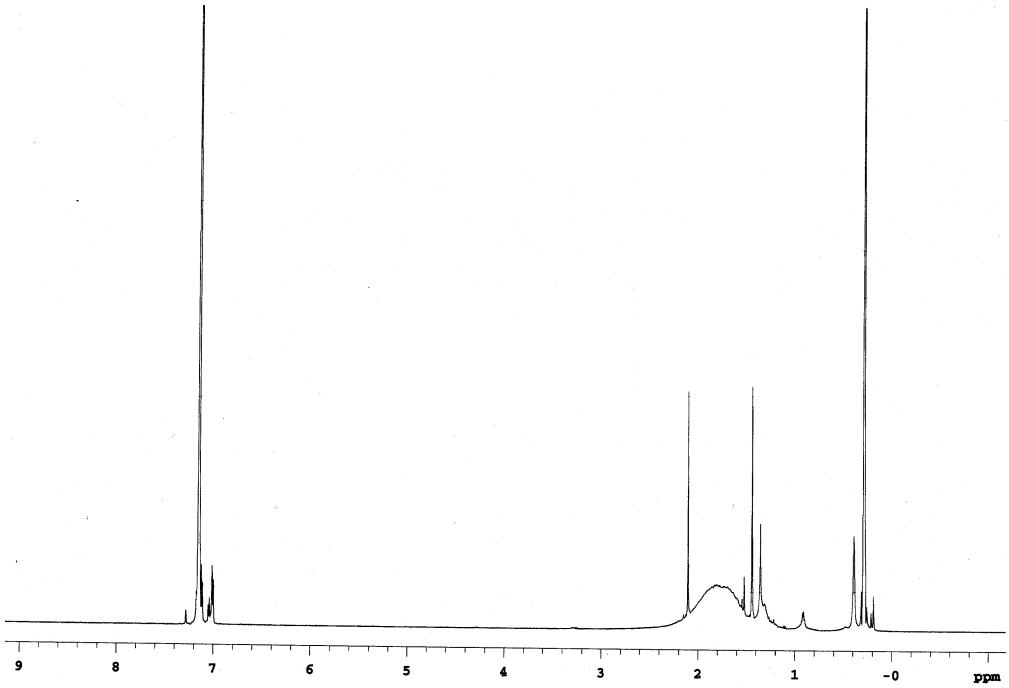

Figure 19. ^{1}H-NMR spectra of a) Au/tBT$_S$ and b) Au/tBT$_{NS}$ in C_6D_6

a)

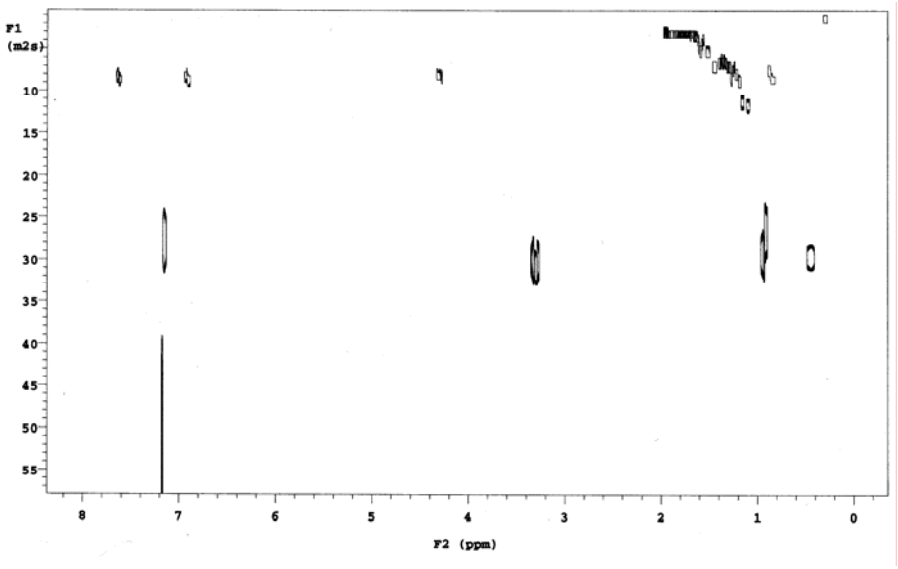

b)

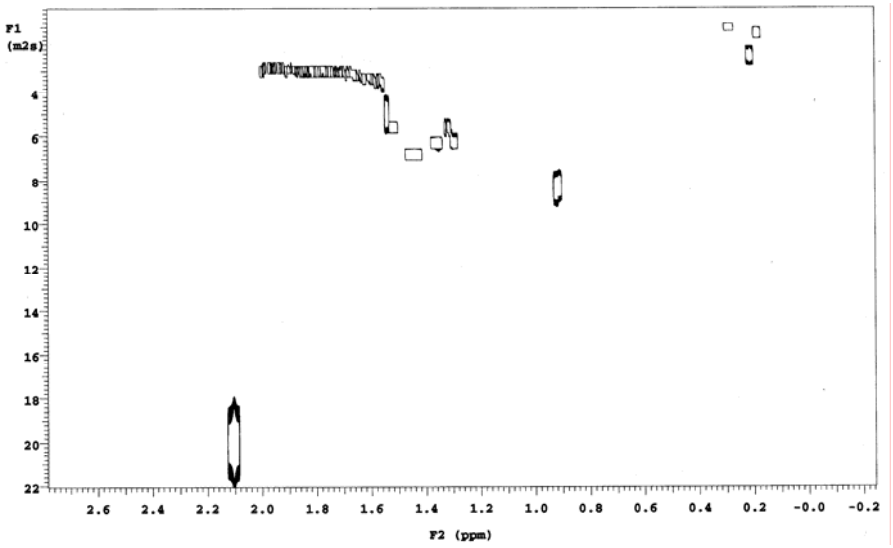

Figure 20. DOSY spectra of a) Au/tBT_S and b) Au/tBT_{NS} in C_6D_6

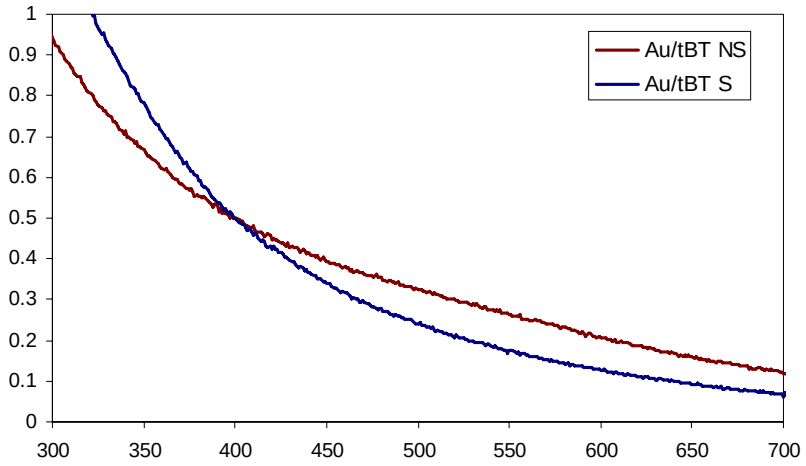

Figure 21. Uv-vis spectra of Au/tBT in toluene

THERMAL AND CHEMICAL TREATMENT OF STABILIZED AUNPS

Thermal treatment (general procedure. See Chapter 4 for more details)

Samples of stabilized Au nanoparticles were dissolved in toluene under nitrogen atmosphere, in a Schlenck tube (Au concentration = 10 mM) . In some cases, methyl-trioctylammonium Bromide (MTOAB) was added (1:1 mol with respect to metal). The solution was warmed in an oil bath at the given temperature for the given time. Then, the nanoparticles were precipitated, washed with ethanol and analyzed with ^{1}H-NMR, DOSY and Uv-vis as usual.

Deposition on inorganic support (general procedure. See Chapter 4 for more details)

A solution of stabilized Au nanoparticles in toluene was added dropwise to a magnetically stirred suspension of γ-Al_2O_3 (Al_2O_3/Au = 100 w/w) in the same solvent, under nitrogen. The suspension was stirred at room temperature overnight or until decoloration of the solution. For **Au/tBT**, the complete deposition of metal was confirmed by AAS analysis after dissolution of the solid in *aqua regia*.

Reaction with chemical reductants (general procedure. See Chapter 4 for more details)

Samples of stabilized Au nanoparticles were dissolved in toluene under nitrogen atmosphere, in a Schlenck tube (Au concentration = 10 mM). Then an excess of reductant (Et_3SiH, $NaBH_4$) was introduced. In some case the solution was warmed in an oil bath to the given temperature.

STABILIZATION OF ACETONE-SOLVATED Au ATOMS SOLUTIONS WITH DECYLAMINE

In a typical experiment, **Au/ac** solution (10 mL, 5 - 50 μmol of Au, depending on the concentration) was added, at room temperature in a schlenk tube (50 mL), to a large excess (1 mL, 5 mmol) of decylamine. After stirring at 25°C for 15 minutes, the solvent has been removed under vacuum, keeping the solution at $5 \cdot 10^{-5}$ mBar for 30 minutes at 25°C. Subsequently, degassed ethanol was added under nitrogen in order to precipitate the capped Au nanoparticles, except in those cases in which the solid precipitate spontaneously from acetone. The solid was decanted or filtered under nitrogen, washed several times with ethanol and dried in vacuo. It has been redissolved in apolar solvents (toluene, chloroform, deuterated benzene) for further studies.

PREPARATION OF Au/DA STABILIZED AT DIFFERENT TIMES

Samples of **Au/ac** solution (10 mL, 5 – 50 μmol Au) were kept at room temperature for the selected time, then added into an excess of decylamine (1 mL, 5 mmol). After stirring for 5 minutes at room temperature, the solvent was removed under vacuum and the solid precipitated by addition of ethanol, as usual and characterized by ^{1}H-NMR and DOSY spectra (Figure 22 - 25) and by HRTEM (see discussion in Chapter 4).

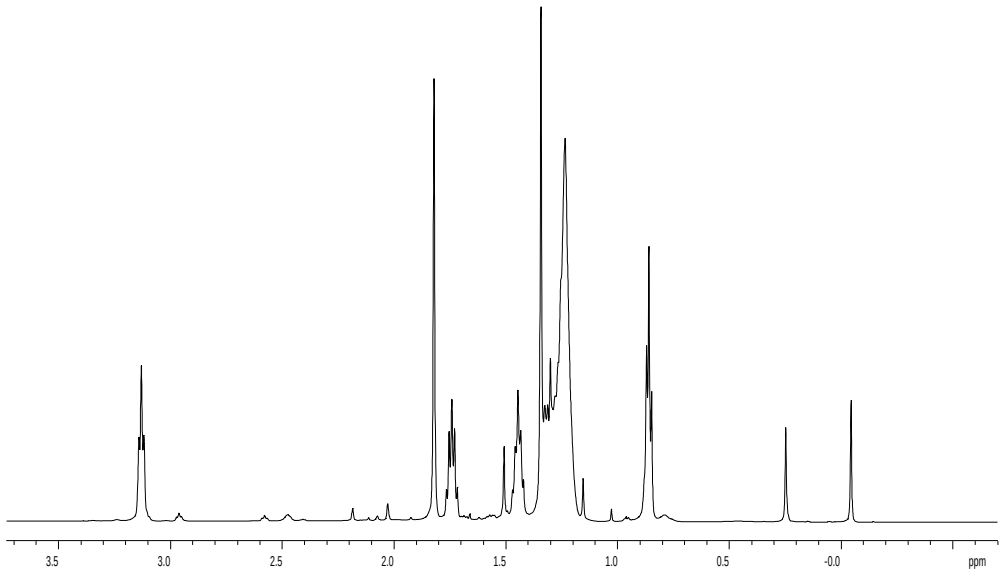

Figure 22. ^{1}H-NMR spectra of Au(ac)/DA in C_6D_6 (diluted solution, t = 0)

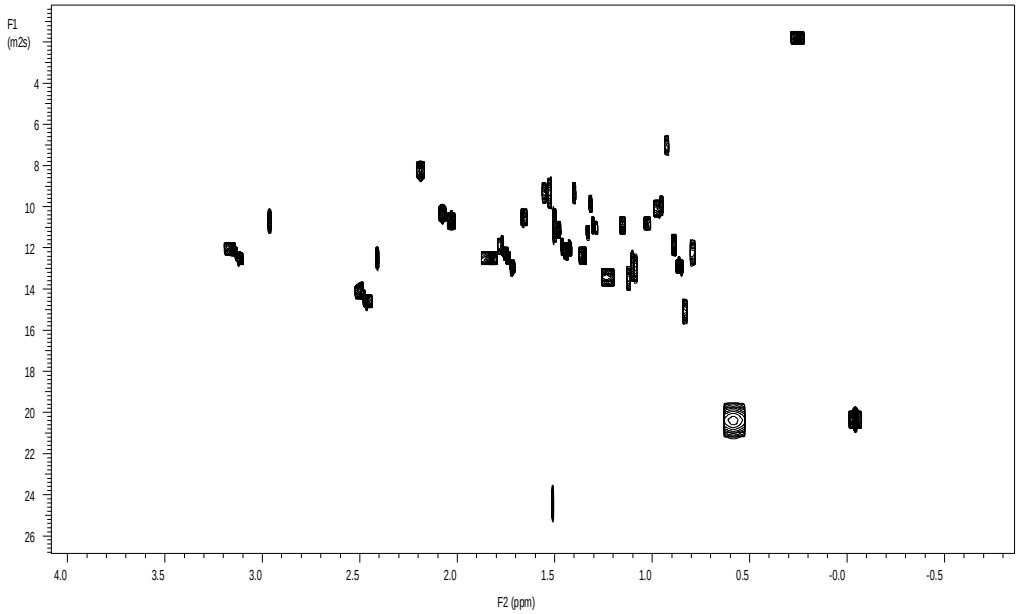

Figure 23. DOSY spectra of Au(ac)/DA in C_6D_6 (diluted solution, t = 0)

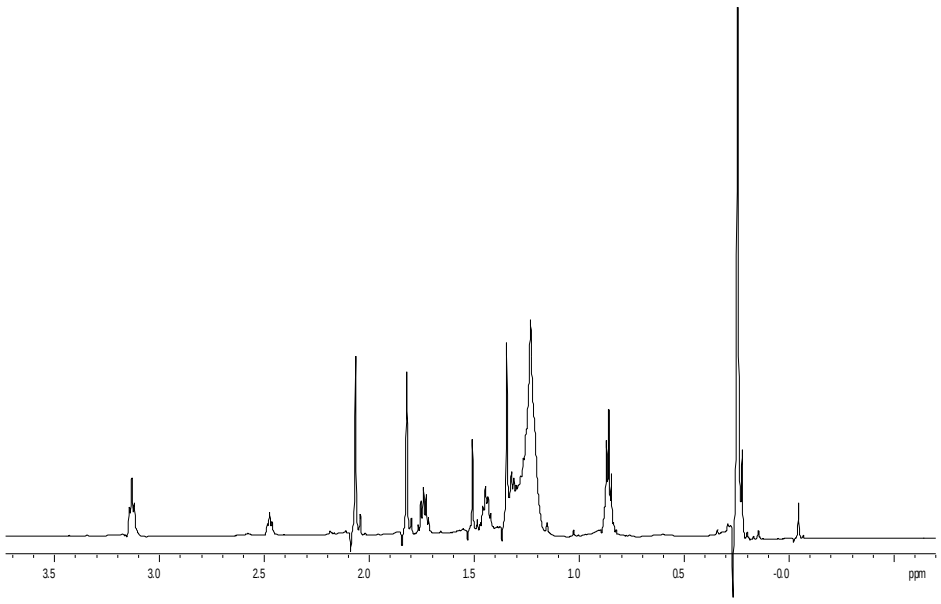

Figure 24. ^{1}H-NMR spectra of Au(ac)/DA in C_6D_6 (diluted solution, t = 24 h)

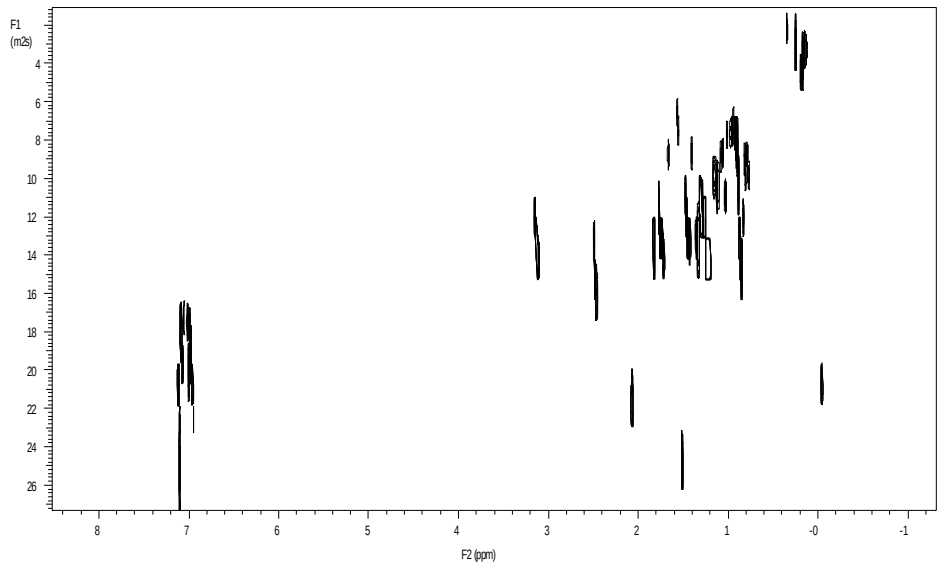

Figure 25. DOSY spectra of Au(ac)/DA in C_6D_6 (diluted solution, t = 24 h)

CATALYTIC TESTS

Alkyne hydrosilylation

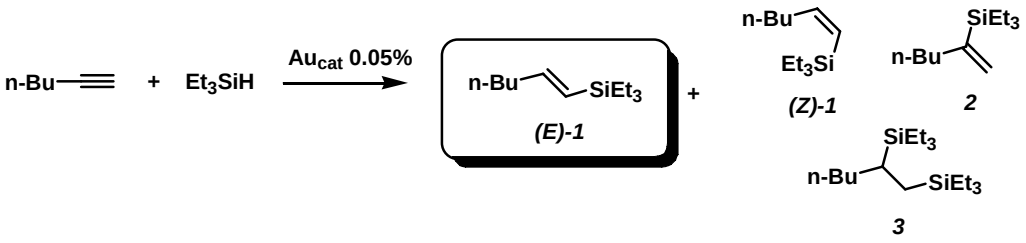

Catalytic runs have been carried out in Pyrex Carius tubes fitted with rotaflo taps. To the proper amount of Au catalyst (0.05 % mol with respect to silane) were added via syringe 8 mmol (0.91 mL) of 1-hexyne and 2 mmol of triethylsilane (0.32 mL). The suspension was stirred for a chosen time at the reported temperature, filtered on celite and the filtrate evaporated under vacuum to remove the excess 1-hexyne. The crude products were characterised by GC analysis.

Silane alcoholysis

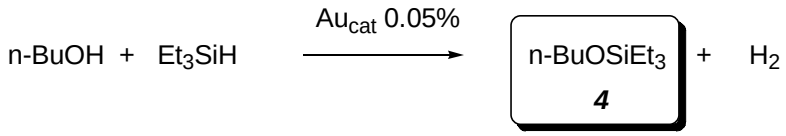

Catalytic runs have been carried out in Pyrex Carius tubes fitted with rotaflo taps. To the proper amount of Au catalyst (0.05 % mol with respect to silane) were added via syringe 2 mmol (0.18 mL) of n-butanol and 2 mmol of triethylsilane (0.32 mL). The suspension was stirred for a chosen time at the reported temperature and filtered on celite. The crude products were characterised by GC analysis.

LIST OF ACRONYMS AND ABBREVIATION USED IN THIS WORK

AAS	Atomic Absorption Spectroscopy
ac	acetone
AFM	Atomic Force Microscopy
AOT	sodium bis(2-ethylhexyl)sulfosuccinate
CAL	Cinnamaldehyde
CD	Chinchonidine
CNT	Classical Nucleation Theory
COD	1,5-cyclooctadiene
COT	1,3,5,7-cyclooctatetraene
CTAB	cetyltrimethylammonium bromide
Cy	Cyclohexyl
DA	Decylamine
dba	E,E-dibenzylidene acetone
DES	Diethyl sulfosuccinate
DHCIN	dihydrocinchonidine
DLS	Dynamic Light Scattering
DLVO	Derjaguin-Landau-Verwey-Overbeek (theory)
DMA	N,N-dimethyl aniline
DMAP	4-(dimethylamino)pyridine
DOCEA	(R)-dioctylcyclohexyl-1-ethylamine
DOS	Density of states
DOSY	Diffusion Ordered Spectroscopy
DT	Dodecanethiol
DVS	1,3-divinyl-1,1,3,3-tetramethyldisiloxane
DVTMDS	1,3-divinyl-1,1,3,3-tetramethyldisiloxane
EDS	Energy Dispersive X-ray Spectroscopy
ESI	Electrospray Ionization
EXAFS	Extended X-ray Absorption Fine Structure
FFT	Fast Fourier Transformation
FT	Fourier Transformation
GC	Gas Chromatography
gHSQC	gradient Heteronuclear Single Quantum Coherence
GLC	Gas-Liquid Chromatography
HMTS	heptamethyltrisiloxane

HOMO	Highest Occupied Molecular Orbital
HRTEM	High Resolution Transmission Electron Microscopy
ILT	Inverse Laplace Transformation
IR	Infrared Spectroscopy
IRAS	Infrared Reflection Absorption Spectroscopy
LDI	Laser Desorption Ionization
MALDI	Matrix Assisted Laser Desorption Ionization
MEK	methyl ethyl ketone
mes	mesitylene
MMFF	Molecular Mechanics Force Field
MMK	acetone
MO	Molecular Orbital
MPCs	Monolayer Protected Clusters
MS	Mass Spectrometry
MTOAB	methyltrioctylammonium Bromide
MVS	Metal Vapour Synthesis
nbn	norbornene
NMR	Nuclear Magnetic Resonance
NPs	Nanoparticles
PAMAM	Polyamidoamine
PDMP	Poly(dimethyl phosphazene)
PFGSE	Pulsed Field Gradient Spin Echo
PM3	Parametrized Model 3
PNIPAAm	poly(N-isopropylacrylamide)
PPPI	perfluorinated polyether-poly(propyleneimine)
PVA	Poly (vinyl alcohol)
PVE	Poly (methyl vinyl ether)
PVP	Poly (4-vinyl pyrrolydone)
ROE	Rotating frame Overhouser Enhancement
ROESY	Rotating frame Overhauser Effect Spectroscopy
SDS	sodium dodecyl sulphate
SEM	Scanning Electron Microscopy
SERS	Surface Enhanced Raman Spectroscopy
SMAD	Solvated Metal Atoms Dispersion
SPR	Surface Plasmon Resonance

STE	Stimulated Echo
STM	Scanning Tunnelling Microscopy
TA	Tartaric Acid
tBHP	tert-butyl hydroperoxyde
tBT	tert-butanethiol
TEM	Transmission Electron Microscopy
THF	Tetrahydrofuran
THPC	tetrakis(hydroxymethyl)phosphoniumchloride
TMNPs	Transition Metal Nanoarticles
TMS	Tetramethylsilane
TOAB	Tetraoctylammonium Bromide
TOCSY	Total Correlation Spectroscopy
TOF	Time Of Flight
tof	turnover frequency
TVCTS	1,3,5,7-tetravinyl-1,3,5,7-tetramethylciclotetrasiloxane
UV-Vis	Ultraviolet-visible spectroscopy
XANES	X-ray Absorption Near Edge Structure
XPS	X-ray Photoelectron Spectroscopy
XRD	X-ray Diffraction

LIST OF PUBLICATION RELATED TO THIS WORK

Papers on international journals

Claudio Evangelisti, Patrizio Raffa, Federica Balzano, Gloria Uccello Barretta, Giovanni Vitulli, Piero Salvadori "Size-Controlled Synthesis and NMR Characterization of Mesitylene-Vinylsiloxanes Stabilized Pt Nanoparticles in Solution" *J. of Nanosci. Nanotechnol.,* **2008**, *8*, 2096-2101

Gloria Uccello Barretta, Federica Balzano, Claudio Evangelisti, Patrizio Raffa, Alessandro Mandoli, Samuele Nazzi, Giovanni Vitulli "A New Platinum Vapour-Derived Very Efficient Hydrosilylation Catalyst: NMR Structural Investigation" *J. Organomet. Chem*., **2008**, *693*, 1276-1282

Raffa, P.; Evangelisti, C.; Vitulli, G.; Salvadori, P. "First Examples of Gold Nanoparticles Catalyzed Silanes Alcoholysis and Silylative Pinacol Coupling of Carbonyl Compounds" *Tetrahedron Lett.,* **2008***, 49,* 3221-3224 (article selected by the editorial board of Synfacts for its important insights, issue 2008/07 - 0772)*;*

Gloria Uccello Barretta, Claudio Evangelisti, Patrizio Raffa, Federica Balzano, Samuele Nazzi, Giovanni Vitulli, Piero Salvadori "The control of the growth of Pt clusters in solution: a way to prepare Pt particles of tailored size" *J. Organomet. Chem*., **2009,** *in press*

Claudio Evangelisti, Patrizio Raffa, Gloria Uccello Barretta, Giovanni Vitulli, Piero Salvadori "Generation of Gold Nanoparticles with tailored sizes by tuning their growth in solution" *manuscript in preparation*

Communications at International congresses and meetings

G. U. Barretta, C. Evangelisti, P. Raffa, P. Salvadori, G. Vitulli "Solvated Metal Atoms as source of metal nanoclusters: preparation and characterization" GSOMEN project first year meeting, Modena, 11 November **2005**

P. Raffa, C. Evangelisti, G. Vitulli, G. U. Barretta, P. Salvadori "Factors affecting the nucleation process and growth of metal atoms generated by vaporization of metals" GSOMEN project second year meeting, Berlin, 25 October **2006**

G. Vitulli, C. Evangelisti, P. Raffa, G. Uccello Barretta, G. Martra, S. Coluccia, P. Salvadori, "Chemistry change with size: nucleation and growth of metal atoms to particles of tailored dimensions" SAMIC 2006: From molecules to Nanosystems, Bressanone (BZ), 3-7 December **2006**

P. Raffa, C. Evangelisti, G. Vitulli, P. Salvadori, L. Bertinetti, G. Martra "Size-controlled Synthesis of Gold Nanoparticles and Their Application in Catalysis" VIII International Symposium on Catalysis Applied to Fine Chemicals (Cafc-8), Pallanza (VB), 16-20 September **2007**

C. Evangelisti; P. Raffa; G. Uccello Barretta; G. Martra; G. Vitulli; P. Salvadori "The control of the growth of metal clusters in solution: a way to prepare metal particles with tailored size" Nanotec 2009, Roma, 31 March - 3 April **2009**